BEHAVIOR OF HELICAL SOIL NAILS: AN EXPERIMENTAL AND THEORETICAL STUDY

Thesis submitted in fulfillment of the requirements for the Degree of

DOCTOR OF PHILOSOPHY

by

PANKAJ SHARMA

(176606)

DEPARTMENT OF CIVIL ENGINEERING

JAYPEE UNIVERSITY OF INFORMATION TECHNOLOGY

WAKNAGHAT, SOLAN-173234, HIMACHAL PRADESH, INDIA

September 2021

TABLE OF CONTENTS

DECLARATION BY THE SCHOLAR

I hereby declare that the work contained in the Ph.D. thesis entitled **"BEHAVIOR OF HELICAL SOIL NAILS: AN EXPERIMENTAL AND THEORETICAL STUDY"** submitted at **Jaypee University of Information Technology, Solan, India** is an authentic record of my work carried out under the supervision of **Dr. Ashok Kumar Gupta** and **Dr. Saurabh Rawat**. I have not submitted this work elsewhere for any other degree or diploma. I am fully responsible for the contents of my Ph.D. thesis.

Pankaj Sharma

Enrollment No.: 176606

Department of Civil Engineering

Jaypee University of Information Technology,

Solan-173234, Himachal Pradesh, India

Date: 28-06-2021

JAYPEE UNIVERSITY OF INFORMATION TECHNOLOGY

(Established by H.P. State Legislative vide Act No. 14 of 2002)
P.O. Waknaghat, Teh. Kandaghat, Distt. Solan - 173234 (H.P.) INDIA
Website: www.juit.ac.in
Phone No. (91) 01792-257999
Fax: +91-01792-245362

This is to certify that the work reported in the Ph.D. thesis entitled **"BEHAVIOR OF HELICAL SOIL NAILS: AN EXPERIMENTAL AND THEORETICAL STUDY",** submitted by **Pankaj Sharma** at **Jaypee University of Information Technology, Solan, India,** is a authentic record of his original work carried out under our supervision. This work has not been submitted elsewhere for any other degree or diploma.

Date:

Dr. Ashok Kumar Gupta
Dean, Academics and Research, JUIT and Professor, Department of Civil Engineering
Jaypee University of Information Technology, Solan, Himachal Pradesh, India

Dr. Saurabh Rawat
Assistant Professor, Senior Grade
Department of Civil Engineering
Jaypee University of Information Technology, Solan
Himachal Pradesh, India

ACKNOWLEDGEMENT

I would like to express my foremost gratitude and special appreciations to my Ph.D. supervisors ***Dr. Ashok Kumar Gupta*** *and* ***Dr. Saurabh Rawat*** *for their tremendous encouragement, unconditional support, and guidance through their enlightening views on several issues related to my research topic.* ***Dr. Ashok Kumar Gupta****, Dean, Academics and Research, Jaypee University of Information Technology (JUIT), Solan, Himachal Pradesh, India and Professor, Department of Civil Engineering, JUIT has always inspired me with his intelligence, perseverance and constructive criticism that has kept me going in the positive path of success throughout the entire course of my Ph.D.* ***Dr. Saurabh Rawat****, Assistant Professor, (Senior Grade), Jaypee University of Information Technology, Solan, Himachal Pradesh, India has always fortified me by his careful guidance and positive feedback during this entire study. They both have always supported and guided me to the right path, inspiring me for the successful completion of my research work.*

I gratefully acknowledge ***Jaypee University of Information Technology*** *for offering me scholarship and laboratory facilities to perform this research successfully.*

I would like to extend my foremost gratitude to ***Er. Manoj Sharma,*** *Head of Maintenance Department, JUIT, for the fabrication of the laboratory setup. It is my pleasure to acknowledge the timely help of the members of technical staff of the department, special thanks to* ***Mr.Jaswinder Deswal, Mr. Rajesh Sahu, Mr. Amar Bonsera, Mr.Pradeep Kumar,*** *and* ***Mr. Itesh Singh*** *for always providing the technical support whenever needed. I am grateful to* ***Dr.Preeti Pal and Mr. Ashwini Patiyal*** *for assisting me in mathematical modelling. I am also thankful to* ***Ms. Swati Sharma*** *for providing microscopic image of soil sample. I extend my sincere gratitude to* ***Mr.Sudheer Kumar Jala*** *for their valuable suggestions during the entire course of my Ph.D.*

I am also thankful to my DPMC members ***Prof. Sudhir Kumar, (HOD, BT&BI), JUIT, Prof. Rajiv Ganguly,*** *Professor, Department of Civil Engineering,* ***and Dr. Amardeep,*** *Assistant Professor, Department of Civil Engineering for their valuable suggestions throughout my research work. My heartfelt appreciation to* ***Prof****.* ***Ashish Kumar****,* ***HOD, Department of Civil Engineering****, for his co-operation, support and constant encouragement.*

Besides, I am also very thankful to my friends ***Dr. Anchal Sharma, Dr. Urvashi****, and* ***Dr. Charu Bhardwaj*** *for helping me in numerous ways over the last four years. I cannot forget the serenity of* ***my parents*** *throughout my research work. It is only because of their support, love, and blessings that I could overcome all frustrations and failures. All may not be mentioned, but no one is forgotten.*

Thanks to all of you!

Pankaj Sharma

LIST OF ABBREVIATIONS AND ACRONYMS

a	Adhesion
A_s	Surface area of nail
A_{helix}	Surface area of helical plate (mm^2);
A_{shaft}	Surface area of a shaft (mm^2)
C_u	Coefficient of uniformity
C_c	Coefficient of curvature
d	Shaft diameter of nail
d_m	Diameter of shaft in model
d_p	Diameter of shaft prototype
D_{50}	Average grain size
D_h	Helical diameter
G_s	Specific Gravity of soil
i	Angle of inclination
K_t	Capacity to the torque ratio
K_0	Coefficient of earth pressure at rest;
K_a	Coefficient of active earth pressure;
K_p	Coefficient of passive earth pressure;
$K^*, K_x{}^* K_s{}^*$	Modified earth pressure coefficient for first, second helix, and shaft respectively.
v	Poisson's Ratio
l	overall length
L	Effective length
δ_i	Interface friction angle
δ	Interaction Factor
Φ	Angle of internal friction

$\gamma_{d(max)}$	Maximum dry unit weight
$\gamma_{d(min)}$	Minimum dry unit weight
$f_\delta \langle(\delta i)\vert\Phi\rangle$	Ratio of Interface friction angle to angle of internal friction
R_D	Relative density
w_e	Effective radius of helix
τ	Pullout shear stress
(τ_T)	Torsional shearing stress
Q_u	Pullout capacity (kN);
$Qu_{(max.)}$	Maximum Pullout Capacity
T	Average installation torque (kN-m)
T_{max}	Maximum torque
P	Helical pitch
Z	Depth of uppermost helix below the ground surface
Z, Z_x, Z_s	Depth of the first helix, second helix, and shaft below the ground surface respectively
η	Efficiency
σ_n	Overburden pressure
σ'_v , σ'_{vx} , σ'_{vs}	Average effective vertical stress at first helix, second helix and shaft respectively.
q	Uniform surcharge;
γ	The dry unit weight of the soil;
$\boldsymbol{\delta}$	Angle of friction between the anchor material and the soil;
¥	Helix angle;
t_h	Thickness of helix;

LIST OF FIGURES

LIST OF TABLES

ABSTRACT

Helical soil nails are passive elements installed in the soil which attains its bond strength through skin friction and bearing from helices. The present study examines the behaviour of helical soil nail installed in cohesionless soil subjected to pullout force under varying parameters such as helical nail configuration (shaft diameter, helical diameter, helical pitch, number of helices), nail shaft types (roughness and stiffness), installation torque and overburden pressure. The installation torque and corresponding nail pullout capacity can be established using a torque correlation factor (K_t). K_t value decreases with increasing embedded nail area and is inversely proportional to the nail shaft diameter. From pullout tests result, it is found that for a model helical soil nail the pitch in the range of 24.5 to 35.5 mm shows better pullout capacity. Also, results shows that additional helices will only contribute to pullout capacity if located outside the region of soil mobilized in the failure mechanism of lower helix. Moreover, higher axial strains are found for hollow shaft a nail, which alters with increase in number of helices. Test results also indicate that various hollow shaft helical nails have nearly equal interaction friction angle to solid shaft helical soil nails with lesser shaft diameter. Therefore, it is concluded that solid shaft helical nails can be replaced by hollow nails without compromising on pullout capacity adding to reduction in construction cost.

The reinforcing action of soil nails is governed by its interaction with the surrounding soil generally investigated in terms of interface friction. The reported literature depicts that increase in interface friction enhances the reinforcing action of a soil nail. Thus, with the aim of utilizing additional interface friction from internal surface of a hollow pipe and bearing resistance from helical plates attached to it, the present work investigates the pullout behavior of newly developed open-ended pipe helical soil nails or hollow shaft helical soil nail. The study also examined the effect of soil plugging on pullout capacity. The test results indicate that soil plug contributes about 11.5% of the total mobilized skin friction during pullout. However, soil plug length is independent of number of helices. The installation and pullout characteristics are evaluated under varying surcharge pressures and inclinations of 0°,5°,10°,15°,20°,25°, and 30° with horizontal. During installation, the soil disturbances are also examined in terms of installation disturbance factor (IDF).

In field practices, helical soil nails are installed in groups with staggered or uniform spacing. However, among the few prevalent literatures on helical soil nails, study regarding the group effect of helical soil nail is non – existent. Thus, to evaluate and better comprehend the behaviour of helical soil nails in group, an experimental investigation is conducted on single and group of helical soil nail in sand. The group behavior is studied under two different configurations of staggered and uniform spacing. The earth pressures, torsional strains, and axial strains developed are also investigated. The tests results suggest optimized inclination range between 10° – 25° with horizontal showing low average IDF of 0.76, high torsional and axial strains. Helical soil nail group with staggered spacing revealed higher group efficiency, pullout resistance, and smaller installation torque in comparison to group with uniform spacing. Also, for uniform spacing, negative earth pressures along with large torsional strains and axial strains are also observed.

Further, theoretical models are developed to estimate the installation torque in cohesionless soil which is verified using laboratory tests result. Moreover, theoretical models are also developed to predict the pullout capacity of single and group of the helical nail with displacement. The theoretical models predict the pure-elastic and elastic-plastic behavior of different helical nails. The results are then compared with experimental results which are in good agreement with each other. Based on theoretical and experimental results an equations were developed to estimate the appropriate capacity-to-torque Ratio (K_t) for different diameters of helical nails. The theoretical and experimental result indicates that K_t will decrease with increases in the shaft of the helical nail.

KEYWORDS: Helical soil nail, torque correlation factor, hollow and solid shaft, pullout capacity, interaction factor, inclination angle, Group pullout capacity, Theoretical model.

CHAPTER 1

INTRODUCTION

CHAPTER 1
INTRODUCTION

1.1General

India is one of the fastest-growing economies in the world. India has retained its geographical diversity with The Northern Himalayan Mountains, Indo Gangetic Plains, The Desert, The Peninsular Plateau, and The Coastal Plains. Being one of the largest countries in the world, with a total area of 3.29 million km^2, accommodating a population of about 1.37 billion people. India has a huge construction activity in the region such as hydro-project construction, tunnel construction through the hilly region, and underground metro tunnel construction through loose soil, slope stabilization, excavations, cuts, and retaining walls. Due to these construction activities country require stabilization of slope or terrain in a different way. For stabilization of soil cohesive and frictional forces play an important role. The stabilization of strength characteristic of soil need to have increases cohesive and frictional forces. Various ground improvement techniques like chemical and mechanical ground stabilization, geo-grids, anchors, and soil nailing have been developed in history to fix these activities. This chapter provides a short description of soil nailing, one of the effective techniques for ground improvement of unstable slopes. Moreover, the chapter also covers the organization of the thesis.

1.2 DEFINITIONS OF SOIL NAILING

Under French National Project Clouterre [1], soil nailing is referred to as a passive inclusion of reinforcement in the soil to impart tensile strength. It is called passive element because it offers resistance from the passive region during ground movement in the active region which distinguishes the soil nail from the soil anchor. Soil nails are post-tensioned elements whereas soil anchors are pre-tensioned before installation. The soil nails are installed on the ground surface through drilling and strengthen with grouting to increase the in-situ shear strength of the soil or cuts. The tendons may be of either metallic or polymeric material and inserted into predrilled holes at 0-15-degree inclination with the horizontal, which mobilizes the friction along with the soil nail that provides stability to the soil slope.

1.2.1 BACKGROUND OF SOIL NAILING

The soil nailing technique was used firstly used to trigger an 18.3 m high cut-slope in sandy soil for a railway project near Versailles, France [2]. After the completion of the Versailles project, the soil nailing technique became very popular. The first research program, on soil nailing motivated by University of Karlsruhe in Germany that involved full-scale testing of experimental walls in partnership with a German contractor [3]. Jewell and Wroth [4] conducted a direct shear test of reinforced sand, studied the bond angle of friction between sand and reinforcement. The widely acceptable work on this field was presented by the Centre d'Enseignment et de Recherche en Mechanique des Sols (CERMES) in France. The English translation of various findings and suggestions of CERMES are given in FHWA [5] as Recommendations Clouterre I. Hereafter, the soil technique has been widely adopted by various countries in the world. The Geotechnical Engineering Office (GEO) of Hong Kong has broadly adopted this technology to stabilize the cuts and slopes due to the reason that the soil nailing technique shows good agreement with residual soil, which is commonly found in Hong Kong.

India is a developing country with geographical diversity, a large infrastructure of the road network, hydro-project, metro tunnel are on the way. In India, this technology is extensible in use like in Delhi metro tunnel construction, mitigation of mountain in Himachal Pradesh, Uttarakhand, Jammu and Kashmir, etc, and various other regions of the country. Various Universities of India working in the field of soil nailing technique to develop the design guideline for the Indian scenario for the time being work has been executed as per FHWA [5] guidelines.

1.2.2 LIMITATIONS OF CONVENTIONAL SOIL NAIL

Some of the potential limitations of conventional soil nails are described as follows:

- Conventional soil nail undergoes various problems during installation such as the settlement of soil mass during drilling of a borehole, dumping of excavated soil, placement or pumping of grout, maintains desirable grout pressure, etc.
- Unfavorable ground conditions can make the construction processes rather uneconomical and often difficult. The process of drilling during grouted soil nail installation often results in soil disturbances and release of stresses in the surrounding soil. This stress relief in surrounding soil

affects the pullout resistance of soil nail by making it independent of surcharge pressure, thereby making the pullout resistance reach only a limiting value. The stress release is further enhanced as grouting of drill hole is carried out. As the grouting is carried out at low pressure and is allowed to flow under gravity, air from the voids is replaced by grout which increases the soil disturbance. This compromises the structural integrity of nail and its compressive strength.

- Conventional soil nail criticized for the case of the cohesionless soil as pre drilled hole may collapse during construction.
- Subsequently, if cracking of grout occurs, it can lead to reduced interaction between soil nail tendon and surrounding soil. Moreover, cracking of grout can ultimately lead to breakage of soil nail.
- Ineffective for deep seated landslides due to difficulty in installation of long soil nail reinforcements.
- Conventional soil nails have always posed difficulties in construction with soil conditions consisting of silt, sand, gravels, cobbles, and boulders.
- A skilled contractor is required for construction of Conventional soil nail walls.

1.2.3 DEVELOPMENT OF HELICAL SOIL NAIL

Soil nailing becomes an important technique with time due to its fast execution and better placement in a congested area. Various researchers tried different the alternative of conventional soil nail to overcome the difficulties of installation [6, 7]. Using the concept of the helical pile in nailing this technique has been modified to a novel grout-free soil nailing technique termed helical soil nailing (HN). In helical soil nailing, a set of helices are attached to the nail shaft in such a way that it helps in installation with the least disturbance to the soil mass [8, 9]. The novel soil nailing technique imparts large pullout strength and efficiency because of the helices comparative of conventional soil nails [9]. The screw nails provided added advantages over conventional grouted nails as given below:

- Quicker installation and immediate reinforcement – Screw soil nails can be drilled into ground within a short period of time and soil reinforcement is available immediately upon installation.

- No requirement of specific equipment – Screw soil nails can be installed using simple drill motor with sufficient torque output attached to a backhoe, skid loader, or track hoe.
- Soil nailing using screw nails is more economical than conventional soil nails because stable soil condition which can withstand unsupported cut for 1 to 2 days is not required as screw nails are able to penetrate the ground at a rate compatible to the pitch of the helices.
- Screw nails can be used in soil conditions consisting of naturally cemented or dense sand, gravel, residual soils, weathered rock without unfavorable oriented joints or low shear strength, sand with some apparent cohesion due to capillary effects, stiff cohesive soils such as clayey or sandy silts and low plasticity clays that are not susceptible to creep.
- Screw soil nails eliminate building – up of pore water pressures, hence are also beneficial for construction in soil conditions below groundwater table.
- Screw soil nails are well suited for applications in rehabilitation of distressed retaining structures.

To study the various design parameter of soil nailing different experimental and theoretical study was conducted on conventional soil nailing [10-13]. Few researchers have conducted the experimental and numerical study of helical soil nails to understand the factors affecting the design parameter of nails [14-16]. Tokhi [14] and Sharma [15] investigate the effect of helix size, the number of helices, inter-helical spacing on the pullout capacity of HN under varying surcharge pressure, whereas Rawat [16] conducted experimental as well as numerical study via finite element method at a different angle of inclination.

The detailed investigation of the literature in the field of helical soil nailing reveals that various studies were conducted on keeping the shaft diameter constant [14-15], which is considered an important parameter during installation and pullout of the helical nail. Also, the study was conducted on variation in the number of helices and helical pitch up-to two in number [15]. Thus, previously published researches fail to explain the effect of the number of helix and pitch on pullout mechanism beyond published literature. The design parameter of HN works differently as compared to the conventional soil nail [14-16]. As per the best of the Author's understanding, there have been no studies exist to date to explain the mechanism of helical soil nail with different shaft diameter, shaft type (hollow and solid), surface roughness, multi-helices,

and different helix pitches. Besides, no investigation on the group pullout behavior of helical soil nail was conducted in the existing literature.

To bridge the research gap, an experimental and theoretical study was conducted on single and group helical soil nails with varying shaft diameter and shaft type respectively. To evaluate the research gap and objective for the present study, a detailed literature review has been studied to bridge the gap and new information has been generated in the field of soil nailing.

1.3 Thesis organization

This thesis contains six chapters as follows:

Chapter 1: *Introduction*. This chapter contains the background history of different types of nails and the organization of the thesis.

Chapter 2: *Literature Review*. The literature review presents the overview or summary of soil nailing investigated from field experience or published so far. The review presents different types of soil nails and their field applications. It gives an insight into previously presented experimental, theoretical, and numerical studies investigated to understand the pullout mechanism of the different soil nails. Based on the literature survey various research gaps are identified and present objectives of research work are made and presented in this chapter.

Chapter 3: *Experimental Program*. This chapter contains material and its properties used in the present study. The chapter provides a detailed description of the experimental setup and test procedure adopted for installation and pullout of the helical nail in the present study. A detail of the test setup and special gadget used in the laboratory tests is presented

Chapter 4: *Theoretical Modeling.* The chapter includes the details theoretical modeling of installation torque and pullout of helical soil nail using different mathematical model. The theoretical modeling was totally based upon the soil-nail interaction mechanisms of helical element, which is adopted for the validations of experimental result.

Chapter 5: *Results and discussions*. In this chapter, the experimental test data are presented, interpreted, and compared with different mathematical models used for installation and pullout of the helical nail. The laboratory tests are verified using mathematical models for

single and group pullout of the helical soil nail. The mathematical models include the effect of nail geometry, strength parameter of soil, and surcharge pressure.

Chapter 6: *Practical applications*. In this chapter, the practical application of soil nailing is presented for the site of the Kotropi landslide. The factor of safety is investigated by using the actual field shear strength parameter of soil for reinforced and unreinforced Kotropi soil slope.

Chapter 7: *Conclusion and Future Scope*. A summary and main conclusion derived from laboratory testing and theoretical analysis of single and group of the helical nail are made from this research project are presented. Suggestions are given for further work in the field of soil nailing.

CHAPTER 2
LITERATURE REVIEW

CHAPTER 2

LITERATURE REVIEW

2.1 GENERAL

Soil nailing is a ground improvement technique that is used to reinforce the soil mass. The soil nailing is a passive inclusion of steel bars at calculated spacing into the soil mass. The technique gets its popularity in Germany, France, and the United States soon after the 1960s when the New Austrian Tunneling Method implements the technique for rock excavation support [17-18]. With the passage of time, the application of soil techniques increases globally. This technique involves drilling of borehole into the soil slope and thus the placement of cement grout into the borehole. Then the tendon head fastens with a bearing plate along with shotcreting the wall face.

The important aspect of soil nailing is the soil-nail interaction which establishes the pullout resistance of a nail element. The soil-nail interaction mechanism depends upon various factors like nail geometry, soil type, and applied surcharge pressure. Hence, the soil-nail interaction alters with the change in such parameters. Thus, mechanisms of helical soil nails with variation in geometry, soil type, and varying surcharge pressure become complicated. To investigate the soil-nail interaction various researchers conducted laboratory, theoretical, numerical, and field studies on the different types of horizontal and vertical reinforcing elements [11-16].

This chapter includes a review of laboratory, theoretical, numerical, and field outcomes of soil nailing. This includes the basic mechanism of soil nails and the working of nail elements inside a soil slope. Moreover, the chapter incorporates the review of modern developments to overcome the drawback of conventional nailing techniques. Soil is a structural material that in the week in tension. To increase the tensile strength of soil a tensile member is suggested to install into the unstable soil. Thus, the overall shear strength of in-situ soil is increased by reinforcing action tensile members. A soil nail is defined as a passive inclusion due to its action within two zones of soil formed during failure.

The disturbance of unstable soil in the active segment tends to collapse which results in axial displacement alongside the soil nail which is positioned across the active-passive zone. Because of axial displacement in the active region, equal and opposite resistance forces have been generated in the passive region of the nail. Hence, nail members are called post-tensioned elements. Commonly used nail elements are conventional soil nails, fiber reinforced polymer materials nails, bamboo soil nails, Spiral soil nails, helical soil nails, etc. Based on

their working mechanism and methods of installation soil nails are classified mainly into two different categories. It includes grouted nails (or conventional nails) and driven nails [16-23]. To understand the interface friction of soil and reinforcing element the pullout study was carried out by different researchers as follow:

2.2 DESIGN OF SOIL NAIL

Soil nail wall systems are designed to fulfill the stability, service, and durability state during the design period. Several methods and philosophical designs investigated soil-nail interactions and reported that soil nails contribute to slope stability. Stocker et al 1989 estimated the stability using force equilibrium of small failure wedge considering the bilinear failure for a soil-nail structure. Gassler and Gudehus [24] suggested two-plane translational failures based on laboratory investigation which reported the least safety factor for different failure modes than better from a design point of view. Stocker and Riedinger [25] establish the two-wedge rigid body translational failure mechanism to estimate external stability and internal stability (i.e. pull out of the nail) under different forces. Juran et al [21] suggested a design step for the soil-nailed structures based on kinematical limit analysis, which includes resilience of global, local, facing stability, and nail force in each nail. The studies reported the significance of local stability of nails which are found more critical for a few cases in comparison to global stability. Thus, the majority of design approaches adopted multi-criteria approaches which assure global and local stability as well.

To design a soil nail system multiple failure modes are taken into considerations as shown in Fig.2.1. Thus, the soil nail design depends upon the strength parameter of soil, failure mechanism, pullout strength, and facing element. The collapse mechanism may be internal or external, while mixed failure includes the collapse of soil, nail, and facing simultaneously. To analyze the overall stability of the reinforced structure, the external failure modes are analyzed using limit-equilibrium methods (LEM). Moreover, the stability against the failure of soil nail structure is also analyzed using the LEM approach in bearing or sliding. The Internal and mixed failure include the tensile strength nail shaft, grout-nail bond, grout-soil bound, pullout strength, and nail head strength other than overall stability of soil nail structure [5, 19].

Besides, an internal failure is the failure of nail elements in active and passive segments of soil slope are designed using empirical methods. The limit analysis design methods have been extensible adopted by various researchers [16-26] also considers ultimate and serviceability limit state design principal for the reinforcement of soil slope. Based on the

field and laboratory testing Indian Road Congress (IRC) [26] recommends various guidelines for design principles using a limit state approach. In the limit state approach, the design load was calculated by multiplying specified load factors while resisting load was decreased by material factors. Moreover, for soil nail wall partial safety factor was considered to account for the effect of vibrations or disturbance. The analysis is adopted in two means Internal and external stability for different potential failure mechanisms [26]. The external stability deals with the stability of the reinforced soil wedge as a single unit, whereas internal stability includes the mechanisms of lateral pressure distributions. Further, the Indian Road Congress adopted FHWA, [5] for the application of soil nailing on the suggestions of the Indian Institute of Science, Bangalore. The limit equilibrium approaches didn't directly incorporate the effect of the magnitude of nail forces and facing materials. Thus, the design suffers various simplifications, assumptions, limitations, and drawbacks. Various methods recommend the soil nailing to increase the stability of soil mass, suggesting pullout strength as a controlling parameter. If the pullout strength of soil nail is found more the soil mass leads to an increase in internal stability (Fig.2.2) [5, 26]. Thus, the evaluation of pullout of nail experimentally becomes a predominant factor for the design of soil nail wall system.

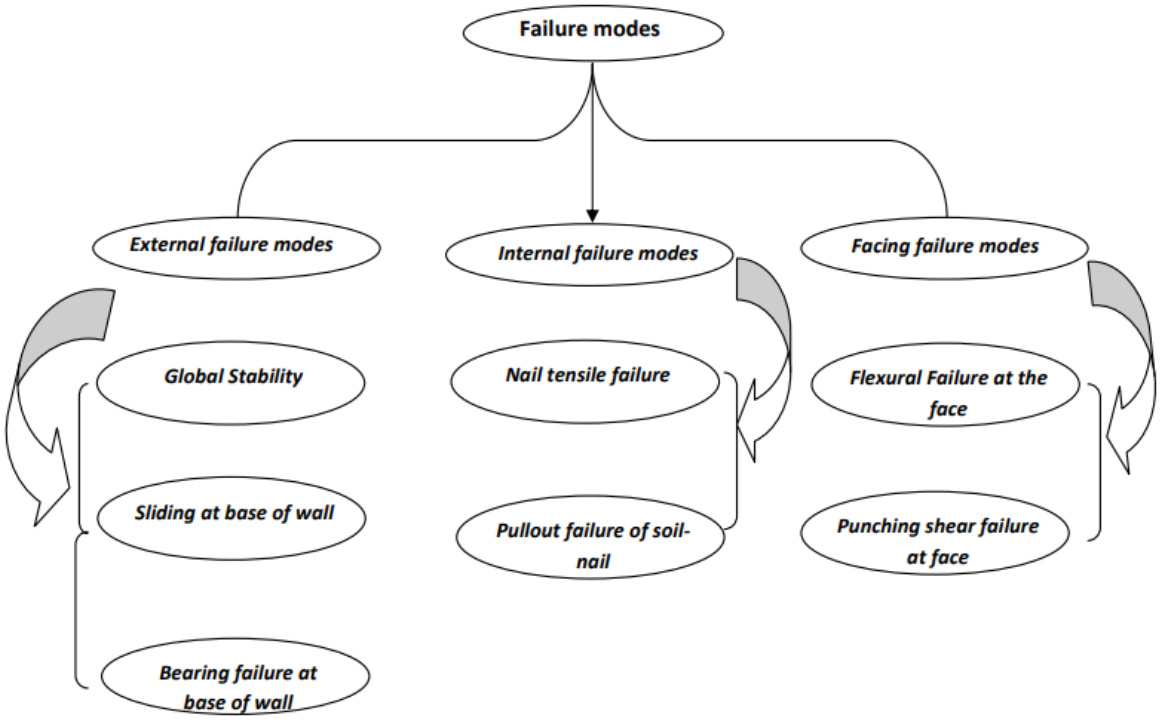

Fig.2. 1 Flow chart of failure modes of soil nailing system

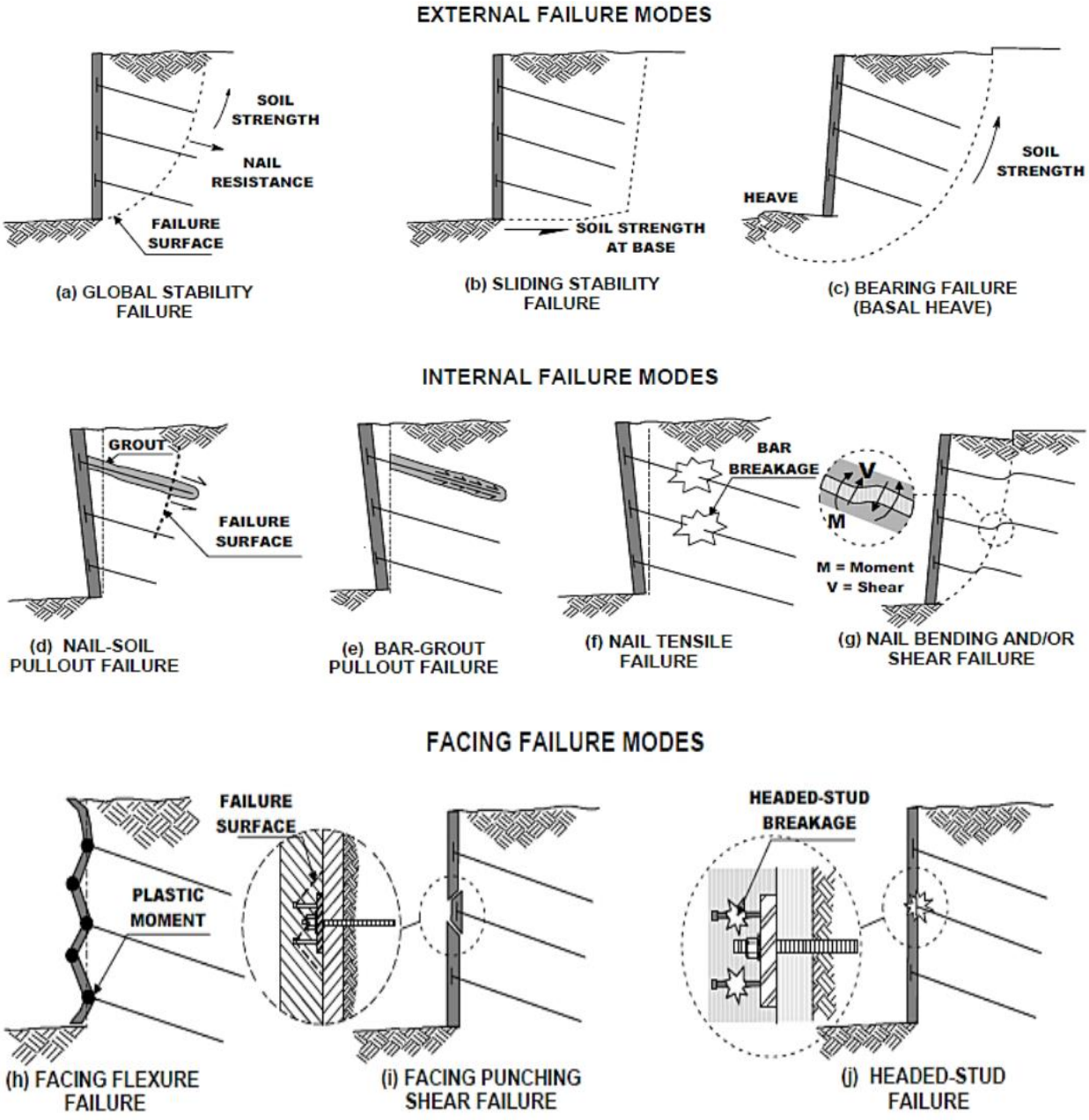

Fig.2. 2 Failures modes of a soil nail structure [19].

The conventional nails estimate the pullout resistance from the interface direct shear test. The interface shear strength is a prime factor for design perspective, which depends upon surface roughness, nail shaft, surface area, soil type, surcharge pressure, and its intensity [27-30]. Potyondy [27] studied the interface friction of different materials like steel, wood, and concrete. Each material was tested for both smooth and rough surfaces with different soil conditions, different water content, and varying normal load. Tests results reveal that change of skin friction depends upon the particle size of soil, water content, normal pressure, and type of surface. Jewell and Wroth [4] present the direct shear test (DST) as shown in Fig.2.3

adopted to estimate soil – soil and soil-nail interface friction angle between the interface with a change in shear stress under applied normal stress. The nail was placed in the shear box at an angle of 25° with the vertical in such a way that interface can yield peak resistance force during the shearing stage [3]. Jewell and Pedley (1990) reported strength deformation properties of soil-nail system. Moreover, Jewell and Pedley [31-31] investigate the geotechnical properties of soil nail wall system, study cover a range various angles (θ) of intersection between the nail and potential shear surface of soil (Fig.2.4). The study reported that most optimum angle for bending stiffness is equal to 0˚. Jewell and Pedley [31-32] adopted methods for slope stabilization using a unified design approach. The study reported that soil nails help to increase the interface shear strength of the soil-nail wall system under combined loading of shear and tension. The bending moment depends upon the shear force in the member.

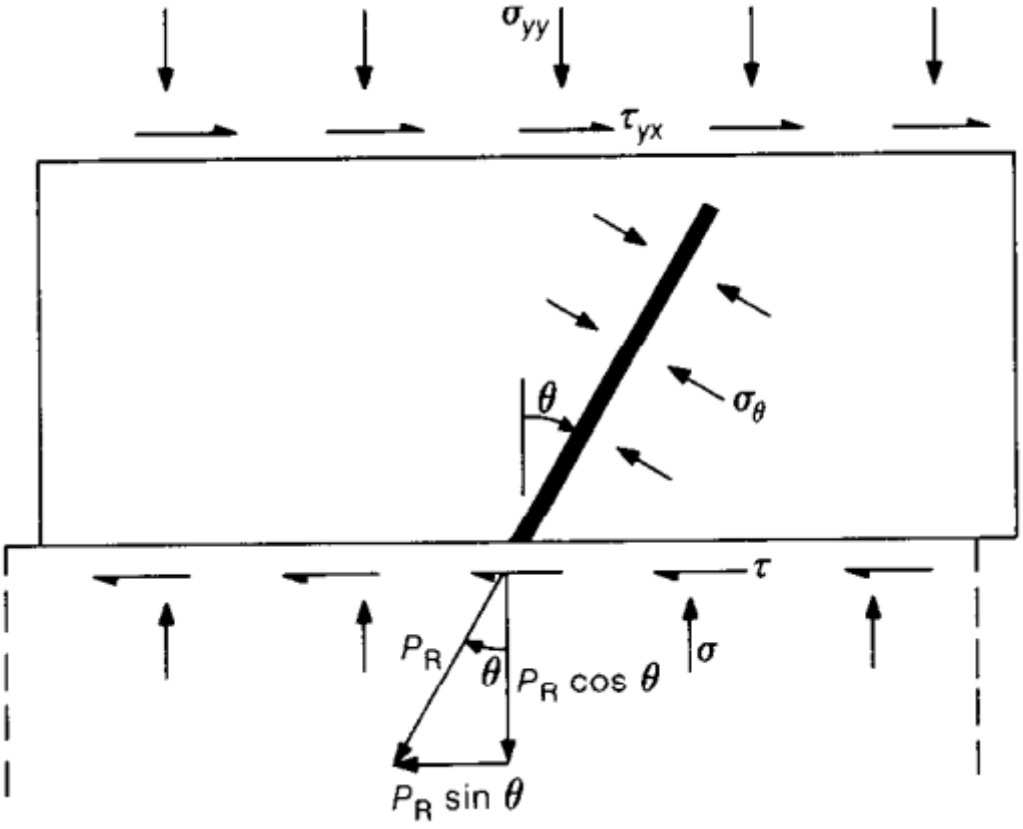

Fig.2. 3 Reinforced sand direct shear test (after Jewell and Wroth [4])

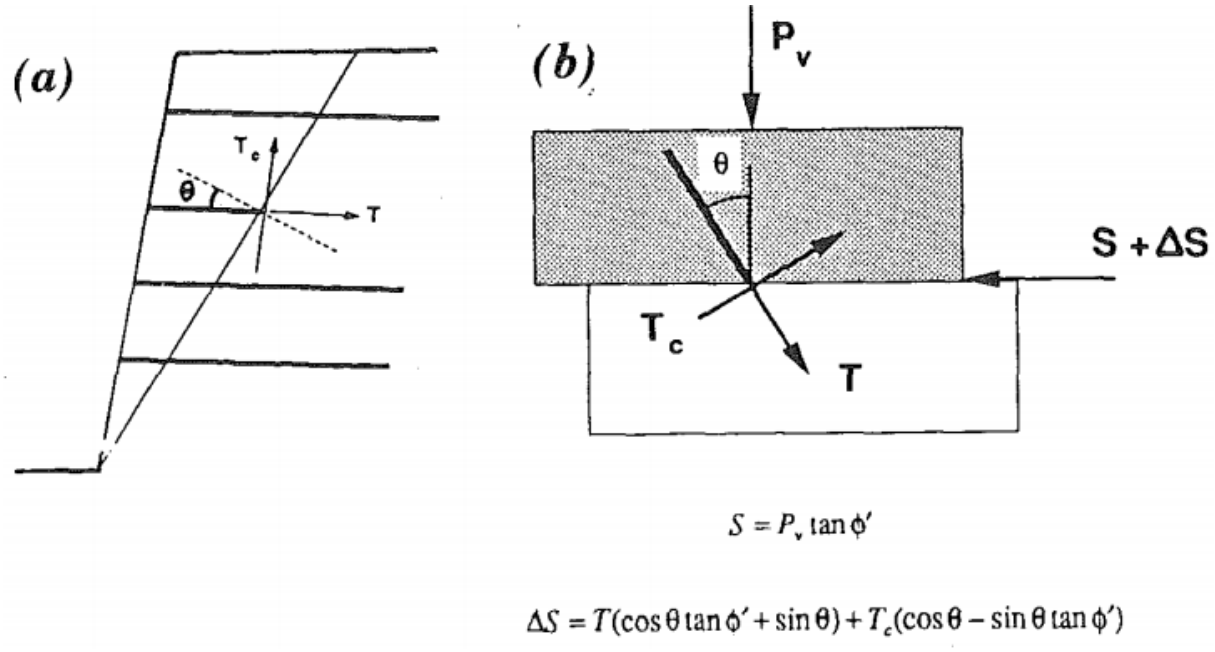

Fig.2. 4 Soil-nail shearing resistance inclined at angle with respect to shear surface [31].

Wang and Richwien [29] also evaluate mobilized friction between soil-nail interfaces, in which model is proposed for estimation of pullout strength from the interface direct shear tests. Liu et al [30] used the conventional direct shear test on the assembly of 50 mm aluminum rods with different diameters. The result concludes that the friction force can be eliminated if an upper section of the shear box is permitted to move freely in a perpendicular direction [30]. Shiu and Chang [33] inspected the effects of nail inclination using (FEM) finite element methods along with a strength reduction approach, further results are validated with the limit equilibrium approach. The study reported that nail inclination harms the reinforcing action of the nail. The reinforcing action of the nail increase slightly up to 10˚, with further inclination the reinforcing action starts decreasing. This is because the orientation and location of nails play a significant role in the force type which mobilized during failure. It is found that nail forces tend to endure transition from the tension force to compression force when the angle between normal to the slip surface and nail position vary from positive to negative as shown in Fig.2.5 [33-34].

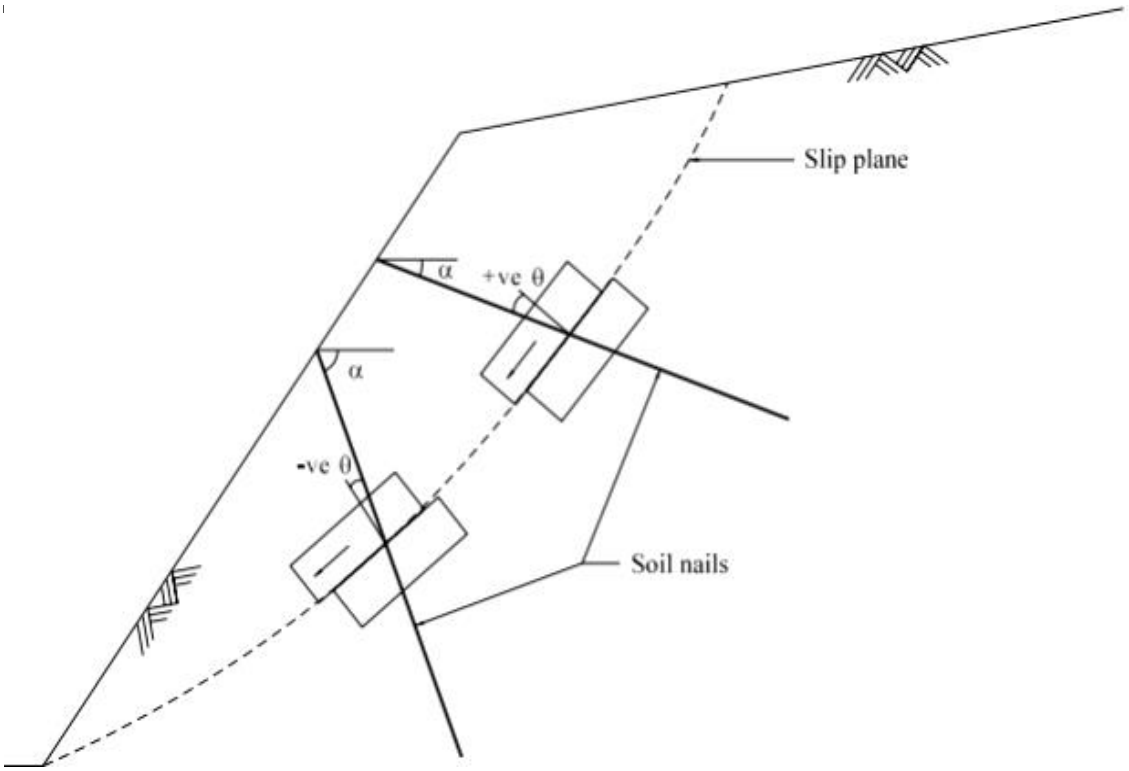

Fig.2. 5 Relationship between nail inclination and orientation [33]

The interface direct shear test is only simulating two-dimensional conditions, in which the rupture surface is already known and always horizontal in the shear test. This plane may be or maybe the direction of the weakest plane in the soil. There are stress concentrations at the boundary of the sample found to be non-uniform distribution on the rupture plane. Also, the area of the specimen under normal and shear loads does not remain uniform. Thus, the calculations of normal and shear stress made based on the constant nominal area of the specimen are inaccurate [35]. In the nutshell, the actual field conditions cannot be simulated accurately by the interface direct shear test. The test is simple and maybe adopted for quick estimation of interface friction of conventional soil nail and completely unsuitable for helical soil nail. Thus, to simulate the three-dimensional condition for conventional and helical soil nail pullout tests are found more suitable to estimate the interface friction angle between soil and nail [10-13].

2.3 PULLOUT CAPACITY

Helical soil nails are the latest type of soil nailing technique that mobilizes greater pullout resistance due to helices and facilitates easy quick installation with minimum soil disturbance [19]. The design procedure of the helical soil nail wall is not still well established to understand the fundamental mechanism of the helical nail. The pullout failure is an internal

failure mode that took place when the interface friction becomes inadequate [15-16]. To study the pullout capacity following are the analytical and experimental (laboratory and field) study conducted by the various researcher on different type of soil nail:

2.3.1 ANALYTICAL APPROACHES

Various researchers have estimated the pullout capacity of different soil-nail interfaces theoretically [20-39]. The maximum pullout strength of a soil-nail interface is the summation of entire shear forces mobilized beside specimen surface area. The various researchers suggested different equations for the estimation of pullout force are listed in Table 2.1. As per the field engineer and various researchers the factors that influence the pullout of soil nails are installation method, surcharge pressure, grout pressure, arching effect, nail geometry, nail roughness, soil dilation, water content, and shear strength parameter of soil. From the literature study, it is found that most of the pullout equations are dependent mainly on interface friction ($\tan(\ angle)$), nail geometry (p), adhesion between soil-nail (a), and normal stress (σ) acting on nail element (Table 2.1).

Table 2. 1 Review of different Pullout resistance estimation equations of soil nail

Authors	Equations
Potyondy [27]	$Q = f_c c' + \sigma_{n'} \tan(f_\phi \phi)\theta;$
Schlosser and Guilloux [36]	$Q = pc' + 2D_{eq}\, \sigma_v{}' \mu^*;$
Heymann et al. [37]	$Q = p(c' + \sigma_n{}' \tan(\phi');$
Jewell [32]	$Q = p\ (\sigma'_n f_c\ \tan(\phi);$
Mecsi [38]	$Q = p\ (\sigma'_n f_c\ \tan(\delta);$

The different analytical equations have their limitations which are improved later by the different researchers and field engineers. In this context, Luo et al. [40-41] anticipated an analytical model which includes the soil dilation effect during pull out of the soil nail. The study reported that the apparent coefficient of friction is inversely to overburden pressure.

Further, Zhou [13] investigated the load-transfer mechanism between soil-nail interfaces using the mathematical model. The model evaluates the shear stress along the soil-nail which includes the dilation effect and bending of the nail as well. Zhou [13] reported that nail elements in the passive zone of the slope are subjected to several forces. The normal stress is comprised of post-installation stress, stress due to soil dilation, and stress due to bending as shown in Fig.2.6.

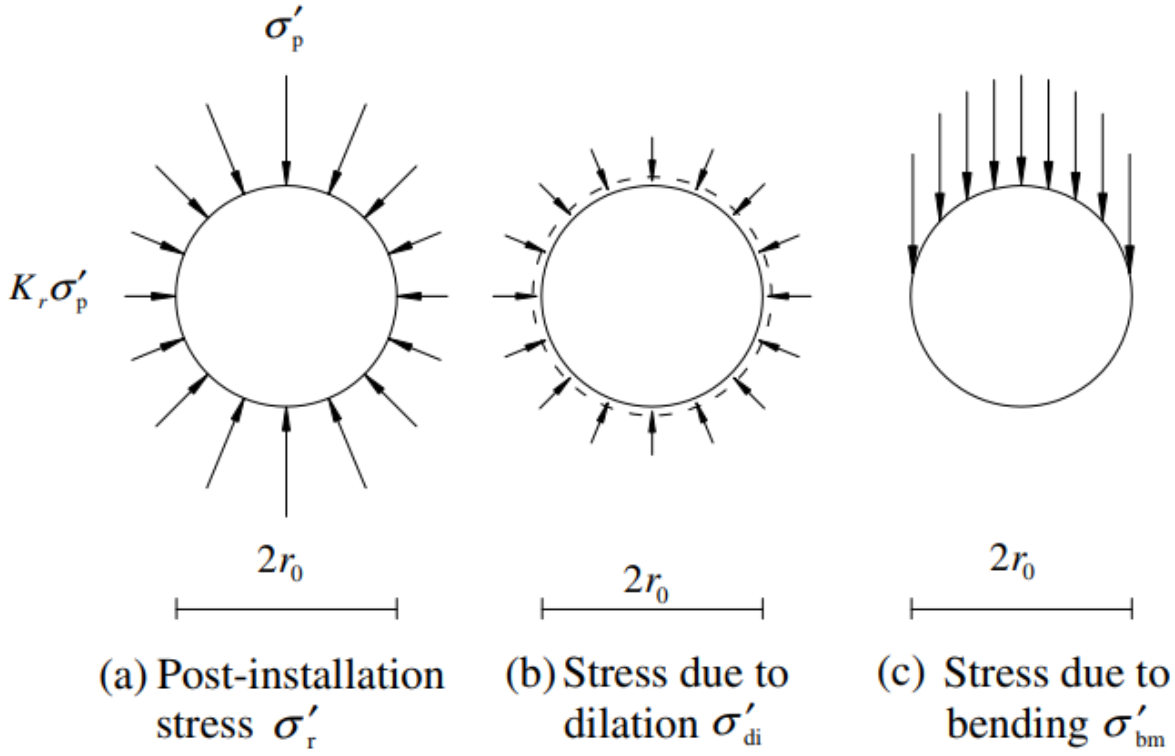

Fig.2. 6 Three normal stresses around the soil nail in the passive zone (Zhou [13])

The equilibrium equation of the soil nail for the elastic axial tension is given as in Eqn.2.1

$$\frac{d^2u}{dx^2} - \frac{2\pi r_o}{E_t A}\tau(x) = 0 \tag{2.1}$$

where,

E_t = combine elastic modulus of soil and grouted nail;

A= area of soil nail;

u = shear displacement;

$\tau(x)$ = shear stress;

The soil nail was considered as a beam in the analysis under axial and transverse loading. The various forces taken into account on the nail element for the analysis are shown in self-explanatory Fig.2.7. The equilibrium of moments of nail element due to vertical and horizontal forces subjected in the center of gravity of the end cross-sections of nail element [13]. Hence, the equilibrium equation for moments of nail element is given as Eqn. 2.2

$$\frac{dM}{dx} + N\frac{dy}{dx} - Q_V = 0 \tag{2.2}$$

where,

M = Moment;

N= Horizontal force;

Q_v = vertical force;

Using the differential equation of a beam in bending in Eqn.2.2 and ignoring small-angle $\boldsymbol{\delta}$ from the analysis and considering vertical force equal to normal force (i.e. $Q_n = \frac{dM}{dx}$), the resultant equation formed as Eqn.2.3

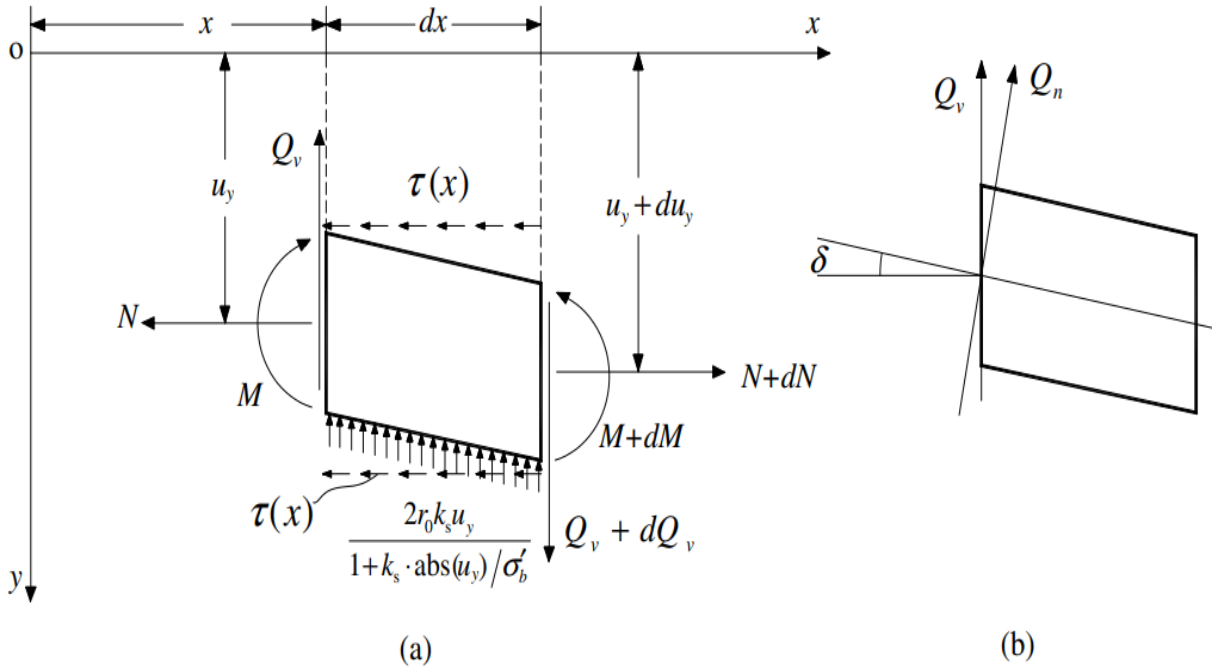

Fig.2. 7 Force in soil nail considered in the analysis (after Zhou [13])

$$\frac{d^4u}{dx^4} - E_tA\frac{d^2u_y}{dx^2}\frac{d\,u_a}{dx} - 2\pi r_o\frac{du_y}{dx}\tau(x) + \frac{2r_ok_su_y}{1+\frac{k_sabs(u_y)}{\sigma_b'}} = 0 \qquad (2.3)$$

where,

EI = Bending stiffness of nail element;

$\tau(x)$ = shear stress;

$Q_n = \frac{dM}{dx}$ = Normal force;

$M = EI\frac{d^2u_y}{dx^2}$ = Bending moment;

N= $E_tA = \frac{du_a}{dx}$ = Horizontal force;

Equation 2.3 can be solved using boundary conditions for the soil-nailing design problem. The suggested model then was verified with large-scale testing conducted by Pedley [42]. The study reported soil-nail interaction with large-scale shear box tests. The calculated results of shear force and bending moment are agreed well with experimental results observed data from Pedley [42] in Fig. 2.8 and Fig.2.9.

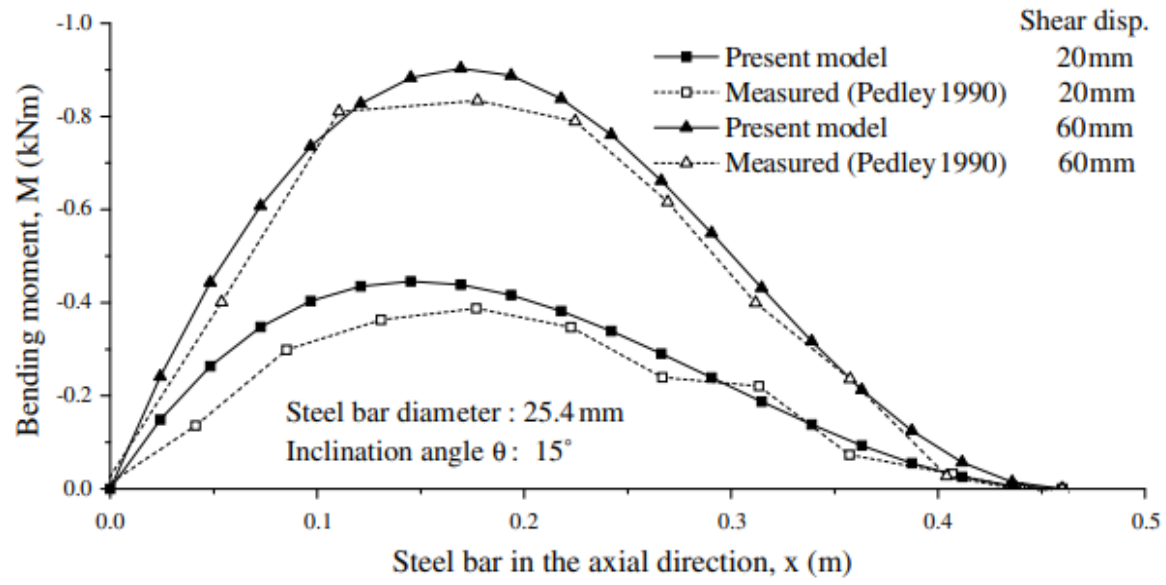

Fig.2. 8 Predicted and measured bending moment (Zhou [13])

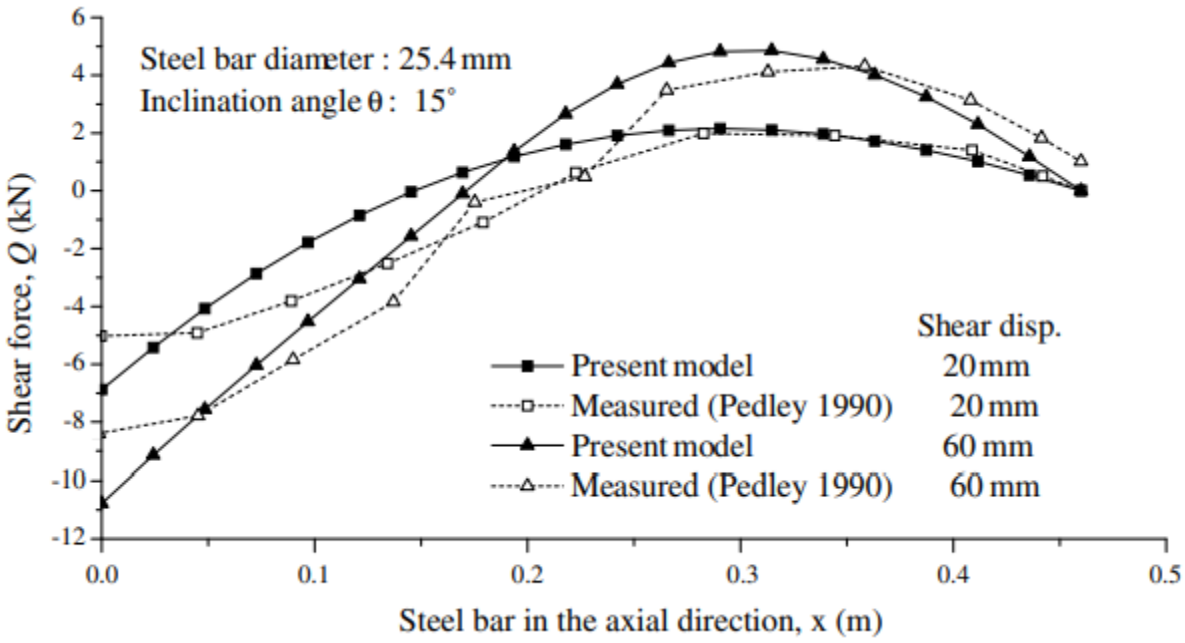

Fig.2. 9 Predicted and measured shear force (Zhou [13])

Moreover, Zhang [43] develop a pullout model using hyperbolic shear stress-strain correlations that describe the load-deformation behavior of grouted nails. The study includes the effect of surface roughness on the load-displacement behavior of nails. The mechanical model developed by Zhang [43] for the load-displacement of nail element as shown in Fig.2.10.

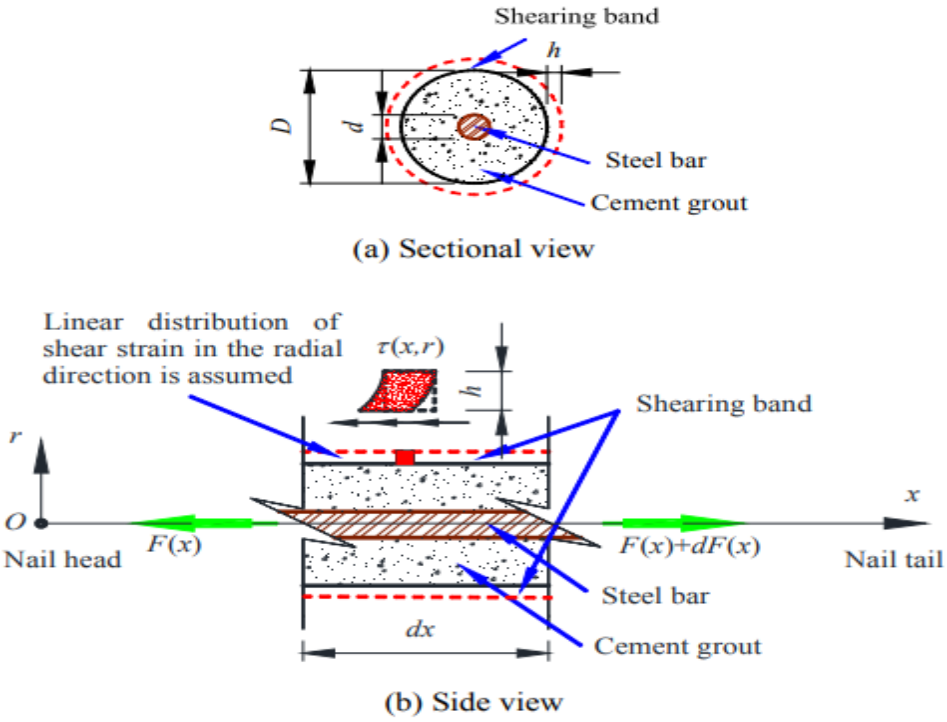

Fig.2. 10 Schematic illustration of pullout mechanism of a soil nail

Under various assumptions to maintain the analysis easy, the shearing band thickness was assumed to be uniformly distributed along the length. The axial displacement for the element is given as Eqn.2.4

$$u(x) = u_s(x,r)_{r=D/2} = -\int_{\frac{D}{2}}^{\left(\frac{D}{2}+h\right)} \gamma_s(x,r)dr \tag{2.4}$$

where x = distance from the nail head;

r = radial distance;

D = nail diameter with grout;

h = shearing band thickness;

γ_s(x, r) = shear strain in soil;

The hyperbolic model was adopted [43-45] to describe the stress-strain correlation. These types of problems can be solved by using non-linear governing equations. For the model formulation, the nail was taken as a tensile member in longitudinal equilibrium. Based on the

uni-axial equilibrium condition the derived differential equation leads to the following governing equation

$$\frac{d^2F}{dx^2} = \frac{4G_oF}{\pi^2\ \bar{E}\ D^3\tau^2{}_{ult}}\left[\frac{dF}{dx} + \pi D\tau_{ult}\right]^2 \tag{2.5}$$

F = force applied to nail in outward direction;

$\bar{E}$ = weighted Young's modulus of elasticity;

τ_{ult} = ultimate asymptotic value of shear stress;

G_o = initial shear modulus;

D = combine diameter of the nail with grout;

To solve the various differential equation of second-order the specific boundary conditions are applied to the governing equation. Thus, the pullout load-displacement curves for a different nail with surface roughness can be determined from the correlation. The results predicted by models are then compared to the experimental data of Chu and Yin [46, 47]. The hyperbolic load-displacement model predicts the pre-failure stage of the nail, which is consistently satisfying the result obtained from laboratory tests as shown in Fig.2.11**.** The test results for soil nails with regular and irregular surface roughness are in good agreement with theoretically calculated results.

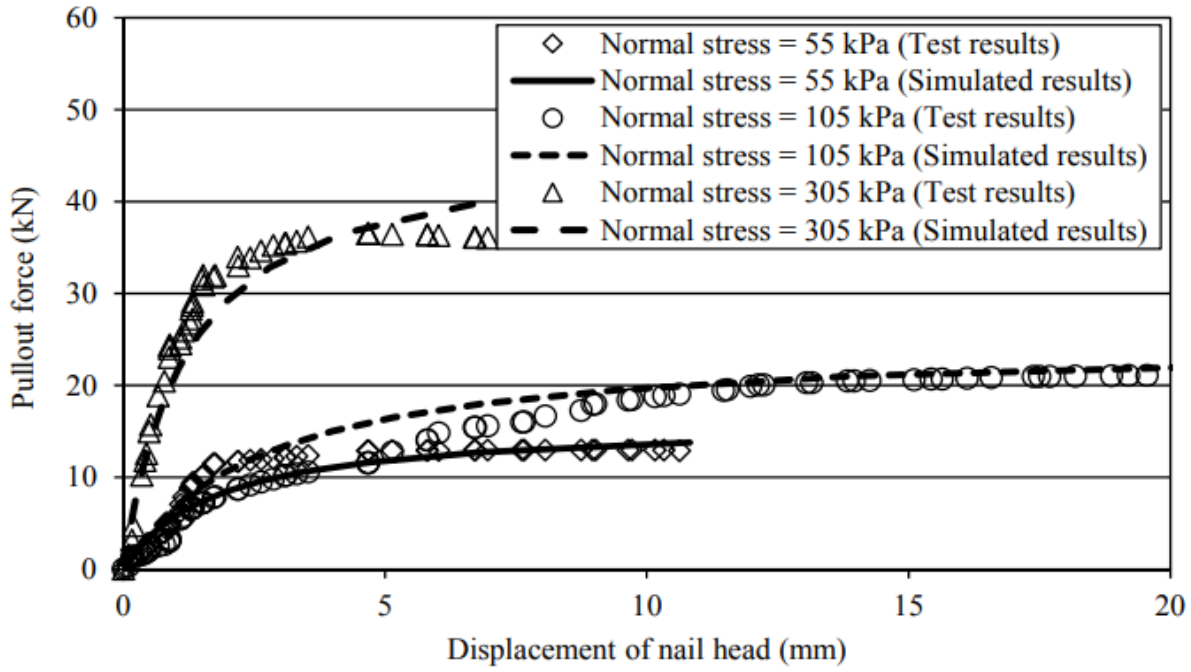

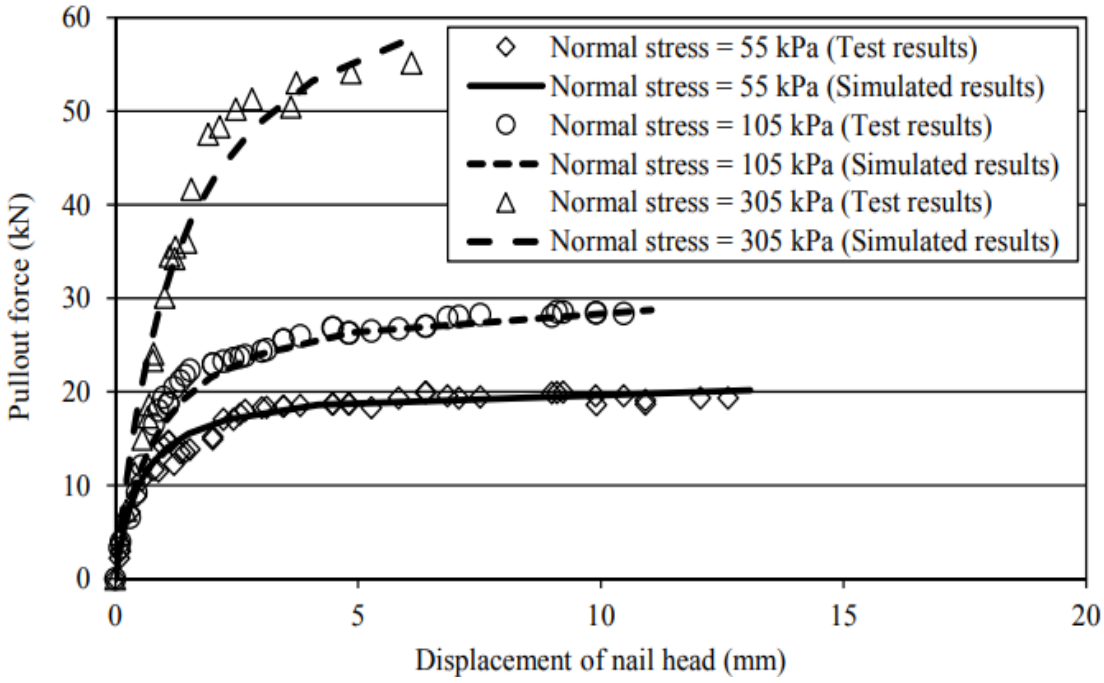

(b)

Fig.2. 11 Comparison between estimated and test results a) Soil nails with regular surface roughness. b) Soil nails with irregular surface roughness (Zhang [43])

Zhang [43] reported only the pre-failure behavior and effect of surface roughness of conventional soil nails. In further continuation of this work, a detailed study of nail roughness with surcharge pressure has been conducted by Sharma et al. [48], in which the study elaborated the pre-peak and post-peak behavior of soil nails. Sharma [48] adopted the Zhang [43] model for the pre-peak stage, whereas for the post-peak stage the model adopted for the study described by Srivastav and Basudhar [49] for soil-geosynthetics interfaces. The method enlightens a residual factor (R) for post-peak stress-displacement behavior of nail is given as in Eqn.2.6

$$R = \frac{\tau_p - \tau}{\tau_p - \tau_r} \tag{2.6}$$

where,

τ_p = peak interface shear strength;

τ_r = residual interface shear strength (Sharma et al.2019)

τ = initial shear strength

R= residual factor

The change in residual factor concerning nail displacement is given as Eqn. 2.7

$$R = 1 - e^{a(u_p)b} \tag{2.7}$$

where,

a and b = fitting parameters [48];

u_p = pullout displacement in the plastic stage;

The theoretical and experimental results are in good agreement with each other as shown in Fig.2.12. Moreover, the surface roughness, relative density, and surcharge pressure are directly propositional to the pullout strength. The various analytical study [24-34] under predict the result even follow the same trend this is because the analytical study not able to incorporate the effect of drilling or drilling speed, also not able to simulate the three-dimensional condition. The analytical model is primarily based upon the two-dimensional conditions of forces thus calculated results undergo various assumptions. Thus, to understand the pullout behavior of soil nails various laboratory and field studies were conducted by different researchers [35- 48].

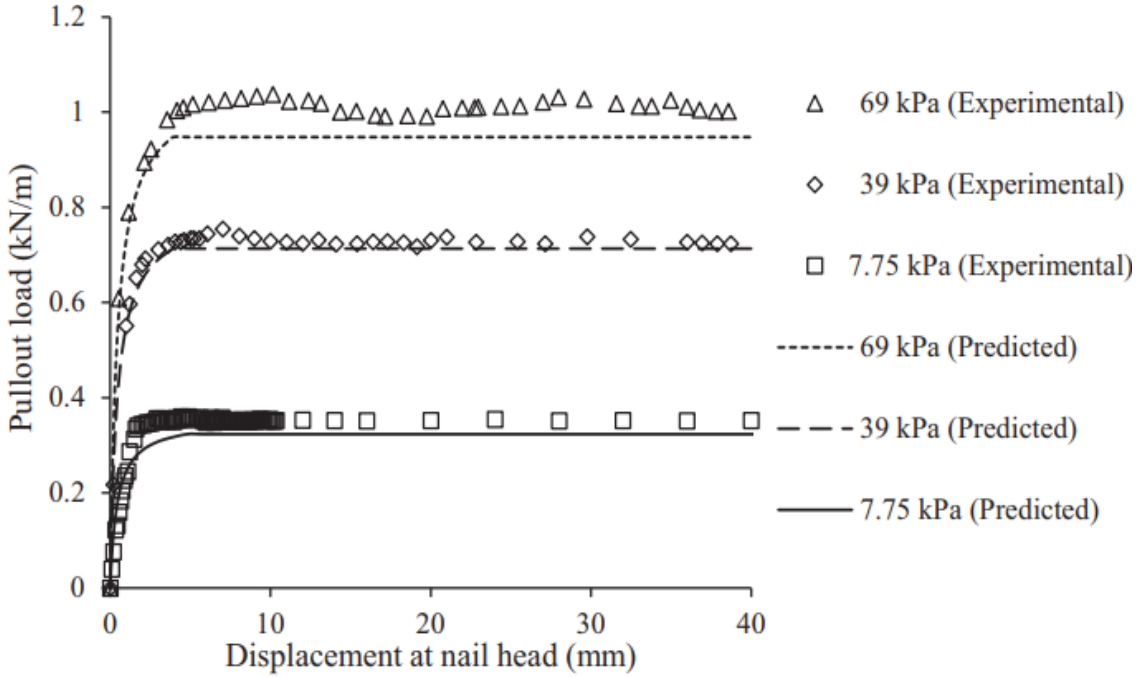

Fig.2. 12 Experimental and predicted load-displacement curves of smooth surface nail [48]

2.3.2 LABORATORY AND FIELD TESTING

Laboratory pullout testing provides more realistic conditions that incorporate the effect of uncertain factors from the soil mass. The pullout tests with displacement-controlled rate simulate the more realistic condition of the soil nail system to know the pre-peak and

post-peak stage behavior. To evaluate laboratory pullout behavior of soil nail Tei [50] conducted a pullout test in a test box as shown in Fig.2.13. The length**X** width**X** height of tank was adopted 254mm **X** 153 mm **X** 202 mm respectively. The investigation was conducted to estimate the effect of embedded length, shaft diameter, surface roughness, and stiffness on the pullout behavior of nail elements in sandy soil. The study reported that axial stress during pullout is directly propositional along the nail length. Moreover, the study reported that surface roughness significantly increases the pullout strength of the nail. Milligan and Tei [51] conducted a laboratory study on flexible and stiff elements. The study reported that friction co-efficient between stiff rough nails is affected by the angle of internal friction, soil dilation, soil stiffness, and the ratio of shaft diameter to mean grain size of soil [50]. The study suggests restricting the use of extensible and smooth nails as well for the in-situ condition. Franzen [52] conducted an experimental study using a pullout box having a size of 4000 mm **X** 2000mm **X** 1500 mm. The different types of nails are ribbed bar, angle bar, round steel bar, and expansion nail under different surcharge pressure of 25 kPa, 37.5 kPa, 75 kPa, and 125 kPa [50].

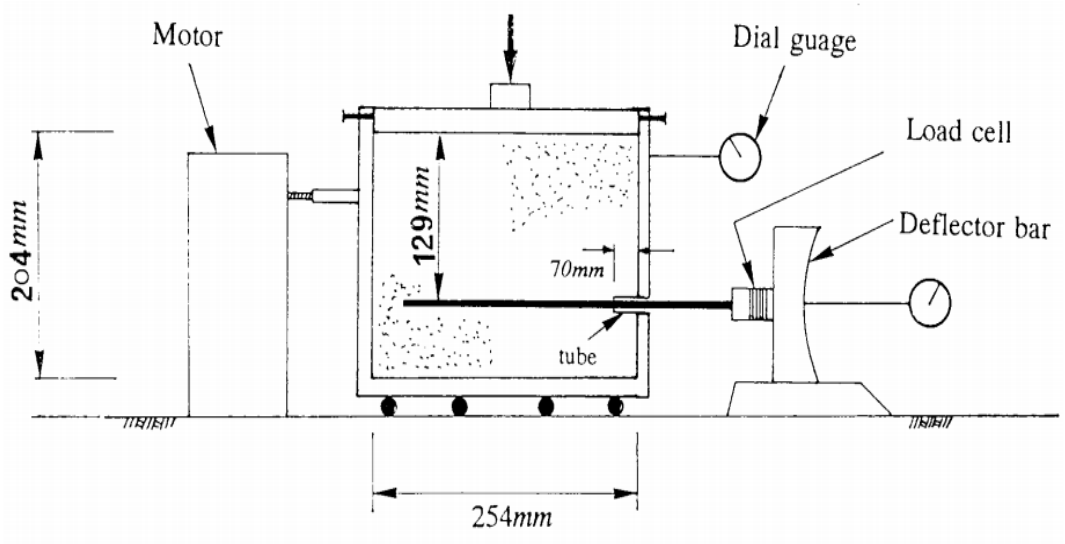

Fig.2. 13 Pullout setup Tei [50]

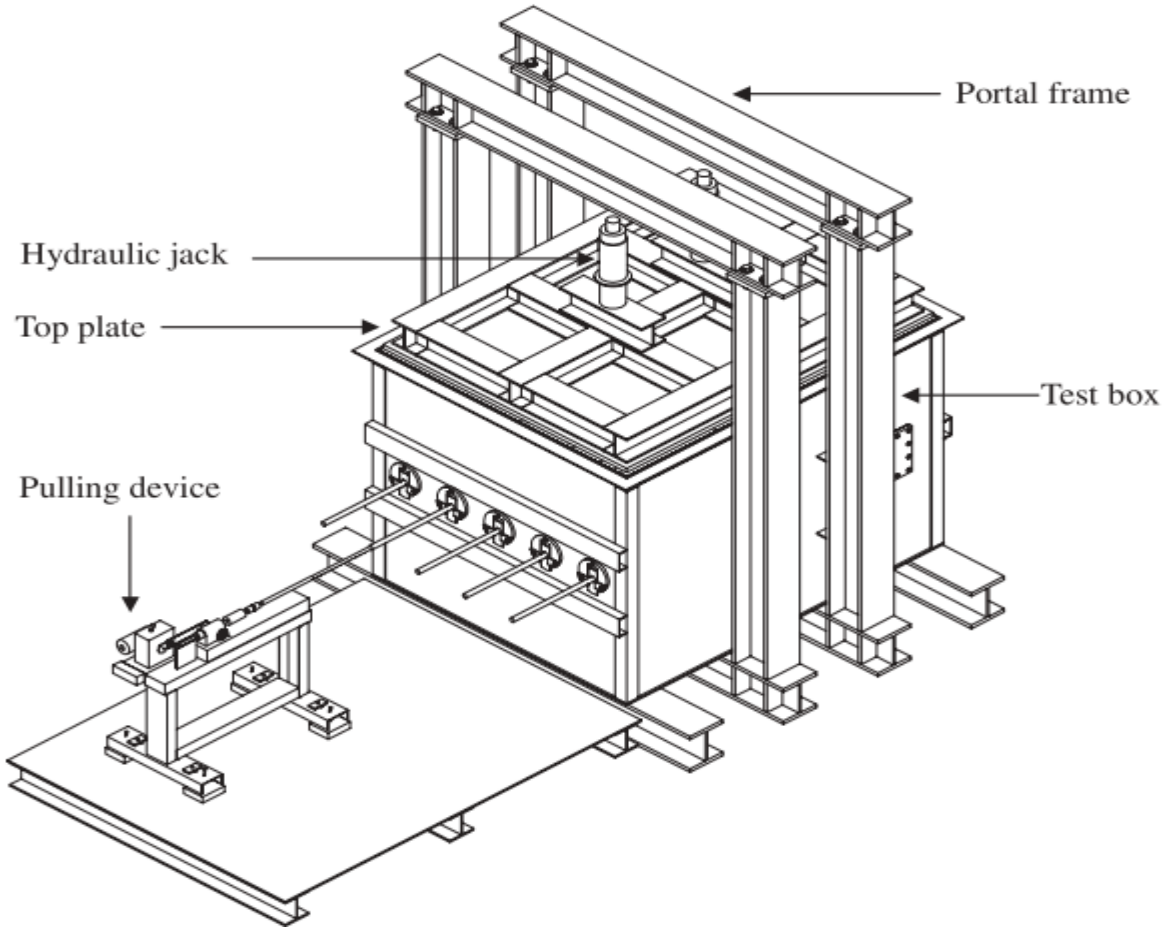

Fig.2. 14 Large scale laboratory Pullout test setup Junaideen et al. [53]

The results suggest that shaft roughness, the surface area of the nail, surcharge pressure, and relative density play an important role in resisting outward pullout force. The maximum pullout force for driven nails is found to be 50% more than jacked nails, while the plastic state of pullout force was found free of installation method. Fig.2.14 shows the experimental setup of Junaideen et al. [53] used for the testing of nail elements in loose fills. The dimension of the test tank was taken 2 m **X** 1.6 m **X** 1. 4 m and the safe surcharge pressure carrying capacity of setup were up to 150kPa that represent the 7 m of fill height in the field. The pullout test was conducted on varying surcharge pressure of 12 kPa, 45.5 kPa, 73.5 kPa, and 109.5 kPa respectively [53]. The strain rate of the device was 1.3 mm/min at which the entire testing program was accomplished. The specimens tested are with the ribbed shaft, knurled tube, and smooth surface under varying overburden pressure. The nail specimens used by Junaideen et al. [53] are shown in Fig.2.15.

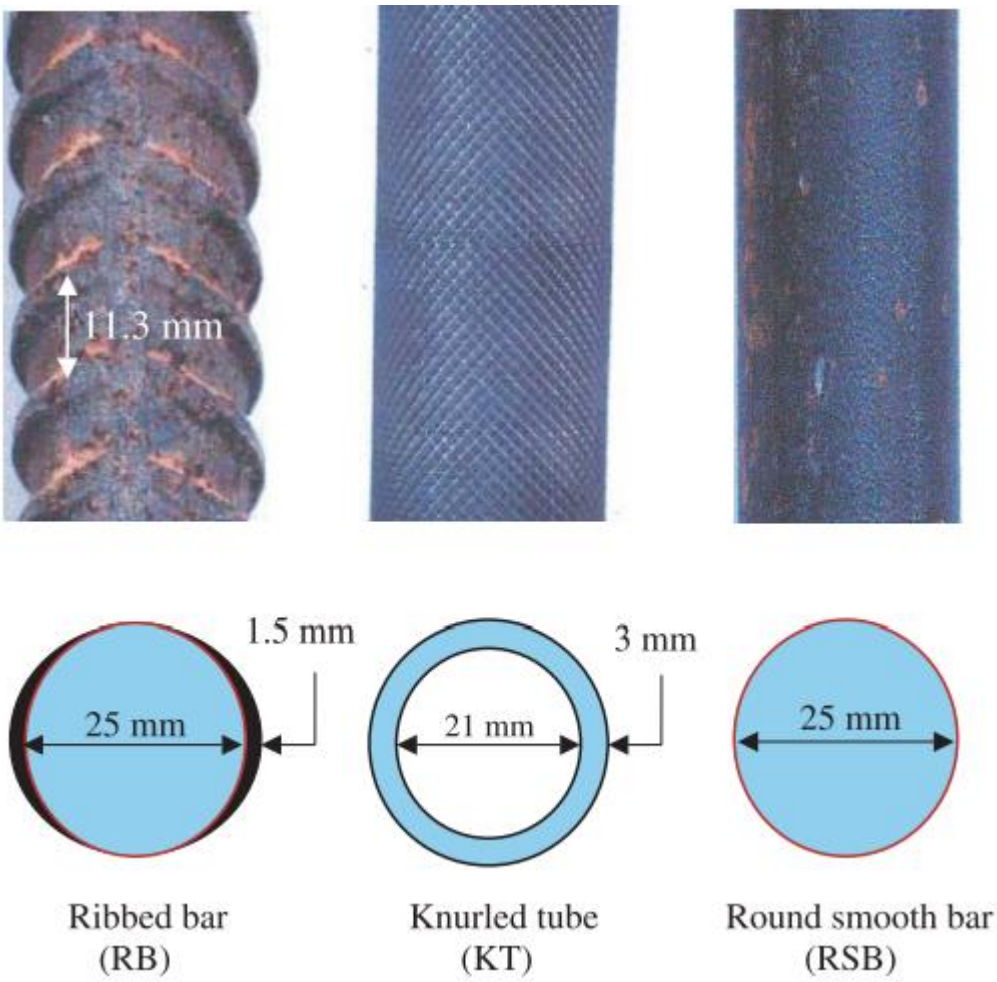

Fig.2. 15 Nail specimens used by Junaideen et al. [53]

The test tank has five openings on its front wall which allows the pulling of the nail. The number of nails and size of the opening was design in such a way that the influence of the boundary and scale was limited. For the no influence of consecutive elements the center to center spacing was taken two to five times the diameter of the element [54]. Junaideen et al. [53] adopted the spacing 10 times the shaft diameter of the nail, which is more satisfactory than required. Junaideen et al. [53] tested 25 mm diameter bars, for the first case one smooth round and two ribbed bars were examined. The imposed varying pressure used by Junaideen et al. [53] for the first case was 12kPa, 51.5kPa, 66.5kPa, and 91.5kPa respectively. The test results for the first case are presented in Fig.2.16. In another trial (i.e. case 2), total 5 number of the nail was tested in which two nail elements are of ribbed and knurled tubes while one is the round nail of smooth surface. The tests were conducted on imposed varying pressure of 12.0, 45.5, 73.5, and 109.5 kPa respectively. As the force was applied to the nail head the buried length of the nail element reduce with pullout displacement, resulting in pullout force,

and peaking pullout force was calculated along the length. The variations of pullout force along the different nail specimens along the length for the second case are shown in Fig.2.17.

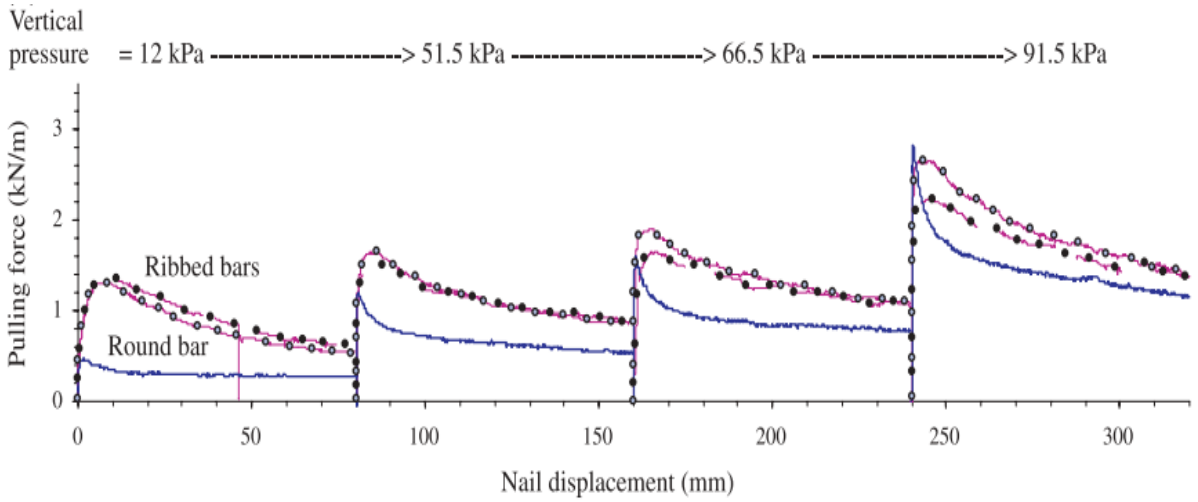

Fig.2. 16 Pullout load-displacement curves for ribbed and round bars (Junaideen et al. [53])

As evident from Fig.2.16 and Fig.2.17, test results show the different peaks for different specimens followed by a change in pullout force. This shows that pulling force mobilizes uniform shear stress alongside nail length with a change in pullout displacement. The axial force decreases with pullout displacement of the nail shaft. Tests results show that ribbed nails higher resistance because of ribs, while a round bar with a smooth surface shows relatively lower pullout resistance. The reveals that the normal stress on the nail increases because of the contractive tendency of the soil in the pre-peak states while decreases due to the arching effect of the soil. The decrease in pullout force in the plastic state is because of the reduction in normal stress acting on the nail element. In the traditional method of analysis, the effect of variation of normal stress during pullout was ignored previously. In this context, the revised parameter was suggested by incorporating the effect of normal stress interims of interface friction angle and adhesion. The ribs have a significant influence on the pullout resistance. Thus, the roughness of nails increases the pullout force, while the effect of overburden is negligible on pullout force. Also, the axial strain was found directly propositional to the axial force. The study also measures the change in vertical pressures during pullout testing using an earth pressure cell installed at 50mm fill above the nail.

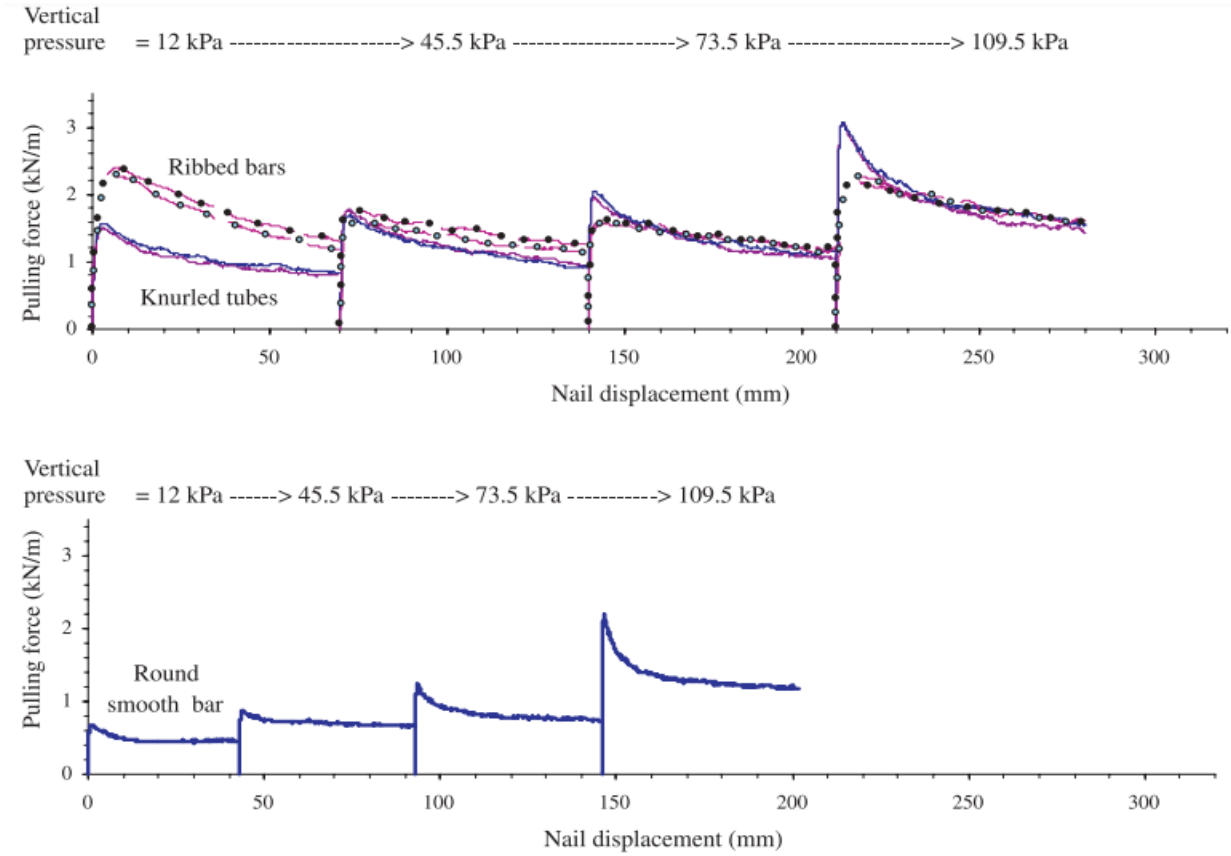

Fig.2. 17 Pullout load-displacement curves for ribbed, knurled tubes and round nail

The variation of vertical pressure inside soil mass during pullout of the different nails (case 2) is given in Fig.2.18.The vertical pressures distribution is found to uniform along the nail shaft, the vertical pressure is found to be decreased in a plastic stage. The tests were also conducted at different speeds in a saturated soil sample to investigate the effect of pulling rate on load-displacement behavior. The result shows that the linear, longitudinal stress and pore pressures establish changes in effective stress in the different interfaces.

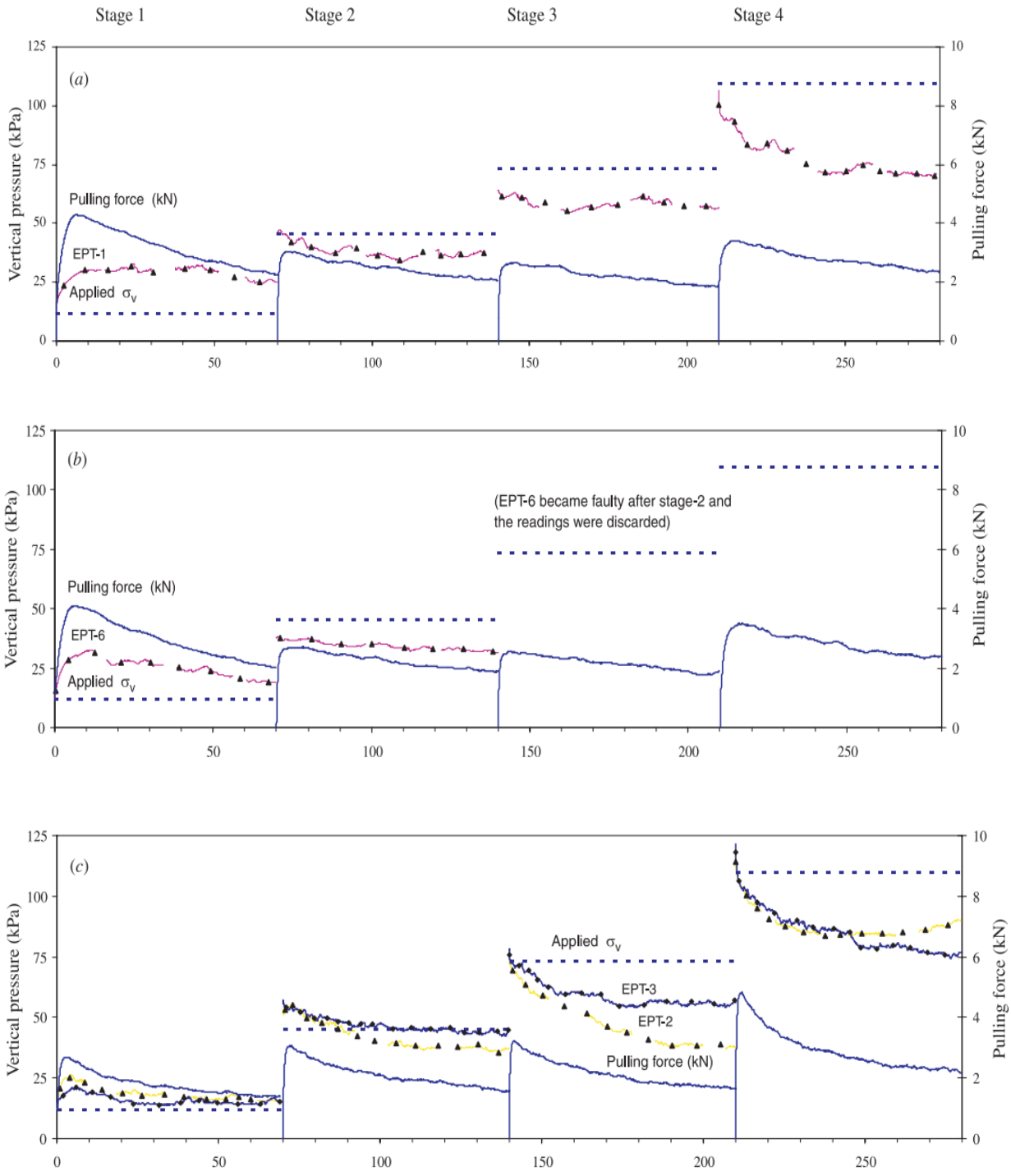
Stage 1
Stage 2
Stage 3
Stage 4
(a)
Vertical pressure (kPa)
Pulling force (kN)
Pulling force (kN)
EPT-1
Applied σv
(b)
(EPT-6 became faulty after stage-2 and the readings were discarded)
Pulling force (kN)
EPT-6
Applied σv
(c)
Applied σv
EPT-3
EPT-2
Pulling force (kN)

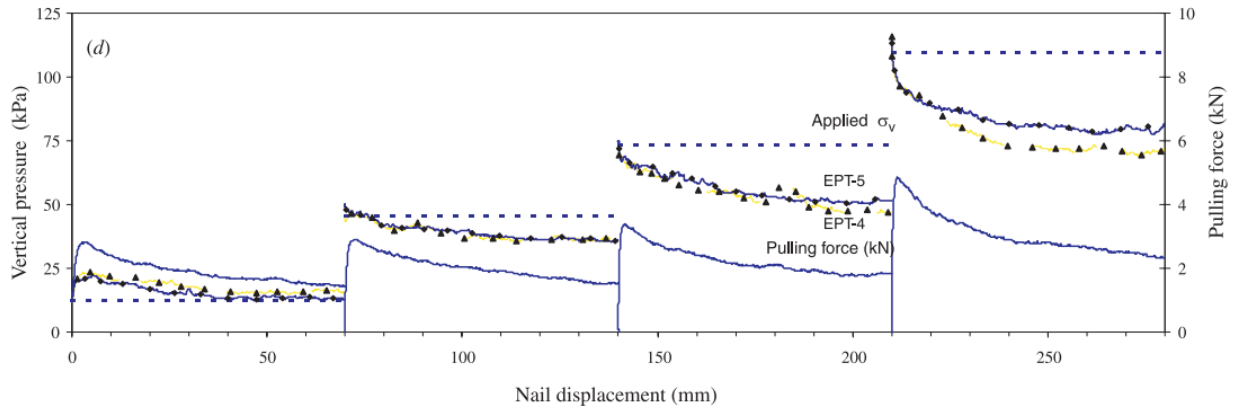

Fig.2. 18 Variation of vertical pressure inside soil mass during pullout of the different nail (case 2): ribbed bar 1; (b) ribbed bar 2; (c) knurled tube 1; (d) knurled tube 2 [53]

Chu and Yin, [46] investigated the load-displacement of behavior of grouted nail in completely decomposed granite using the laboratory set as shown in Fig.2.19. The study investigated the interface friction of decomposed granite and grouted nail. Further, Chu and Yin, [47] investigated the shear stress-displacement behavior and peak shear strength between the interfaces. The study also compared the results obtained from pullout testing with large-size direct shear test. The test results show the shear stress–displacement performance of both soil-grout and soil–soil interface is similar for different pullout tests.

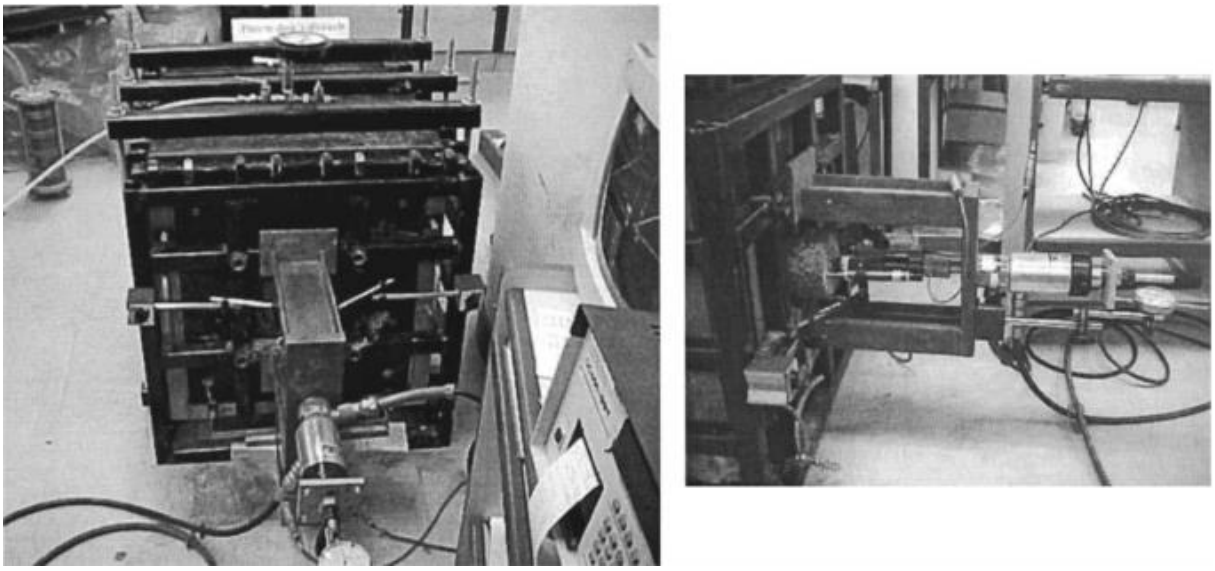

Fig.2. 19 laboratory pullout test apparatus [46, 47]

Yin and Su [55] conducted a pullout test using a model test tank on a short length nail, to investigate the effect of various parameters like surcharge pressure, degree of saturation, grouting pressure, and soil dilatancy. The setup was maintained in such a way that the soil properties and stresses are uniform and isotropic in all directions. The test box was designed

in such a way that there should be no boundary effects and the size selected should be optimum. To ensure the size of the tank the stress distribution was studied in ABAQUS6.3-1 which works on the finite element model.

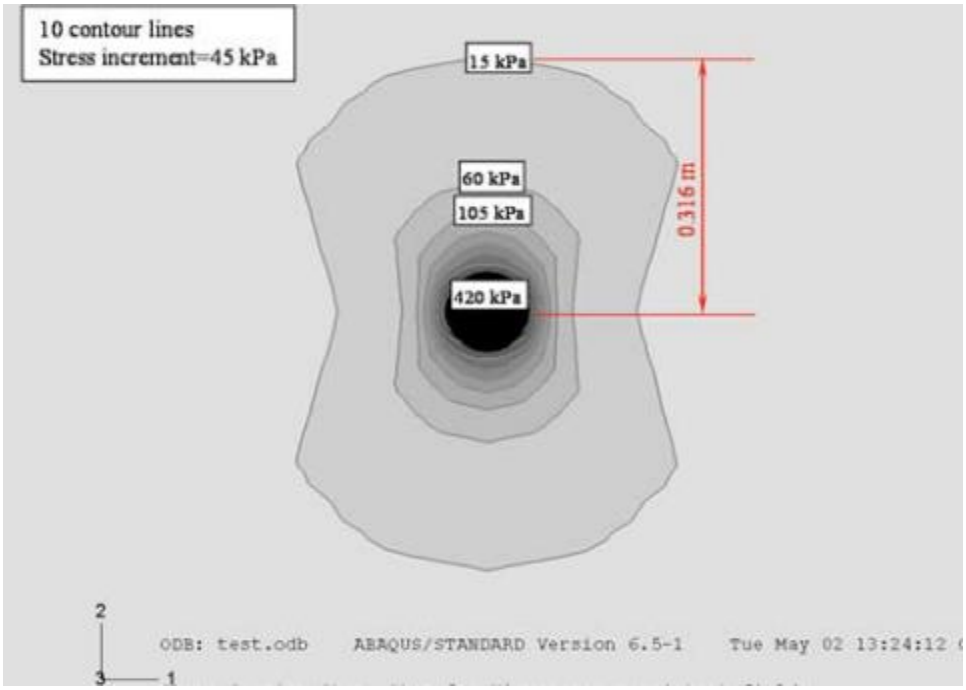

Fig.2. 20 Stress distribution in the test box

The model used for the analysis was Mohr-Coulomb, the result shows that the influence of stresses varies up to 300mm to 400 mm about the fringe of the nail as shown in Fig.2.20. Thus, the effective dimension of the tank was adopted by Yin and Su [55] is 1 m **X** 0.6 m **X** 0.83 m (length **X** width **X** height). The surcharge pressure was applied to the sample using a rubber diaphragm also a wooden board was placed along with a diaphragm to distribute equal stress. The thickness of steel plate is 8 mm for the fabrication of test tank. The installation of the nail a hole was positioned near the center of the front plate that was covered by a thin rubber membrane. Before placing the nail, a drilling operation was made using a drilling machine as shown in Fig.2.21. For the measurement of applied pressure in soil mass pressure, a dial gauge was used while the volume changes meter the compression of soil sample expansion. The other peripherals used during testing were linear variable differential transformers (LVDT), Load cell, hydraulic jack, soil moisture probes, pore-water pressure transducers, strain gauges, and data logger.

Fig.2. 21 Drilling machine Yin and Su [55]

The laboratory pullout setup of Yin and Su [55] is shown in Fig. 2.22. The pullout setup was accomplished with a hydraulic jack alongside the reaction frame on the front plate of the tank. To record the pull or drag out strength and displacement, a load cell and two LVDT were used respectively. The grouting pressure adopted for the execution of nailing operations were 0, 80, and 130 kPa under the surcharge pressure of 80 and 200 kPa. Moreover, a submerged test without grouting pressure was conducted under a surcharge pressure of 300kPa. The variation of earth pressure during placing and pullout of soil nail was monitored by using an earth pressure cell. The placement of cell and layout of setup has been shown in Fig.2.23. From the test result, the ratio of pullout force to the lateral surface area of nail yields the pullout shear stress. The average shear stress was then plotted against pullout displacement, which is more reliable to stress around the nail. As evident from Fig.2.24, the average shear stress rises with displacement up to the highest value, and then gradually starts decreasing with further displacement. A similar trend was followed by average effective earth pressure with displacement for submerging soil samples.

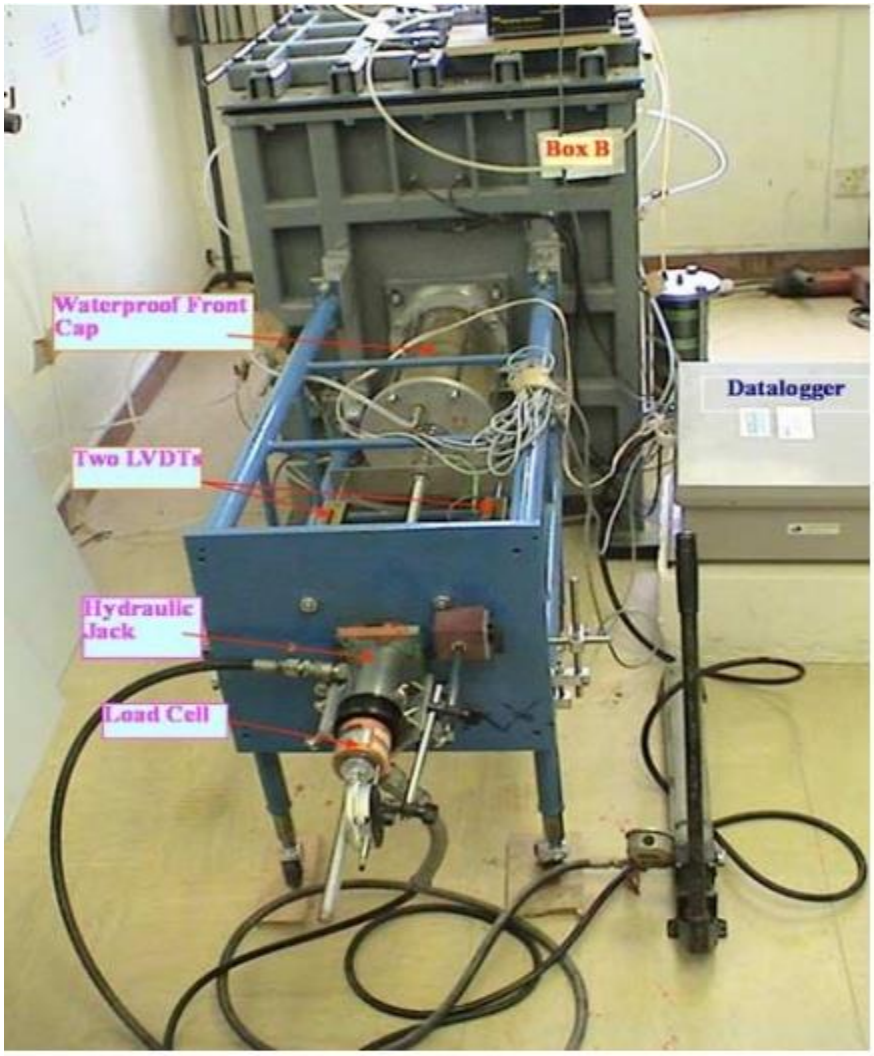

Fig.2. 22 laboratory pullout setup of Yin and Su [55]

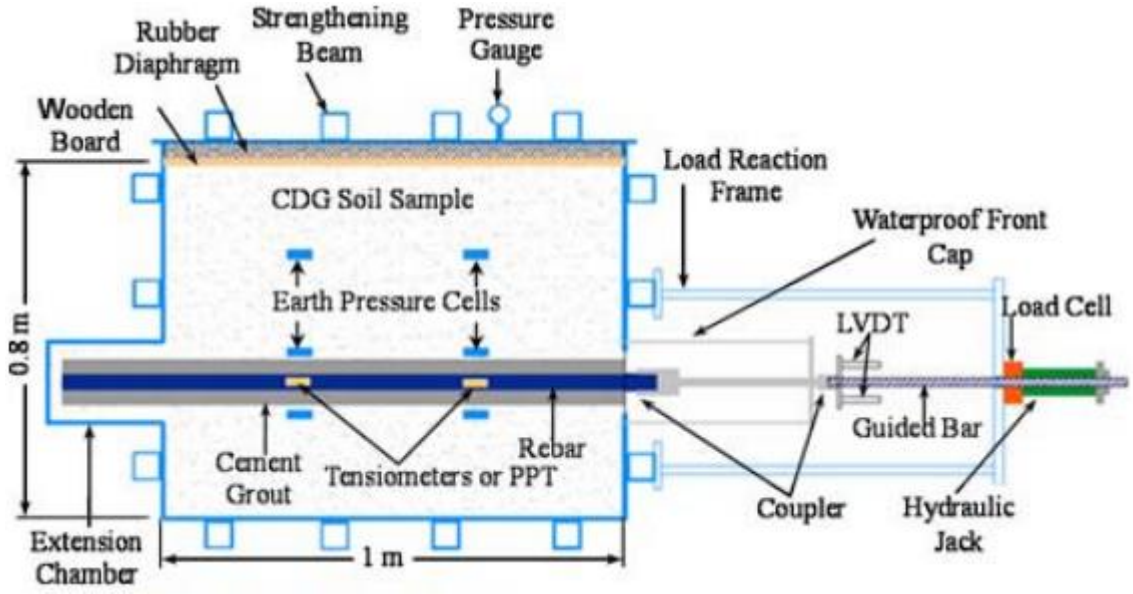

Fig.2. 23 Layout of testing setup [55]

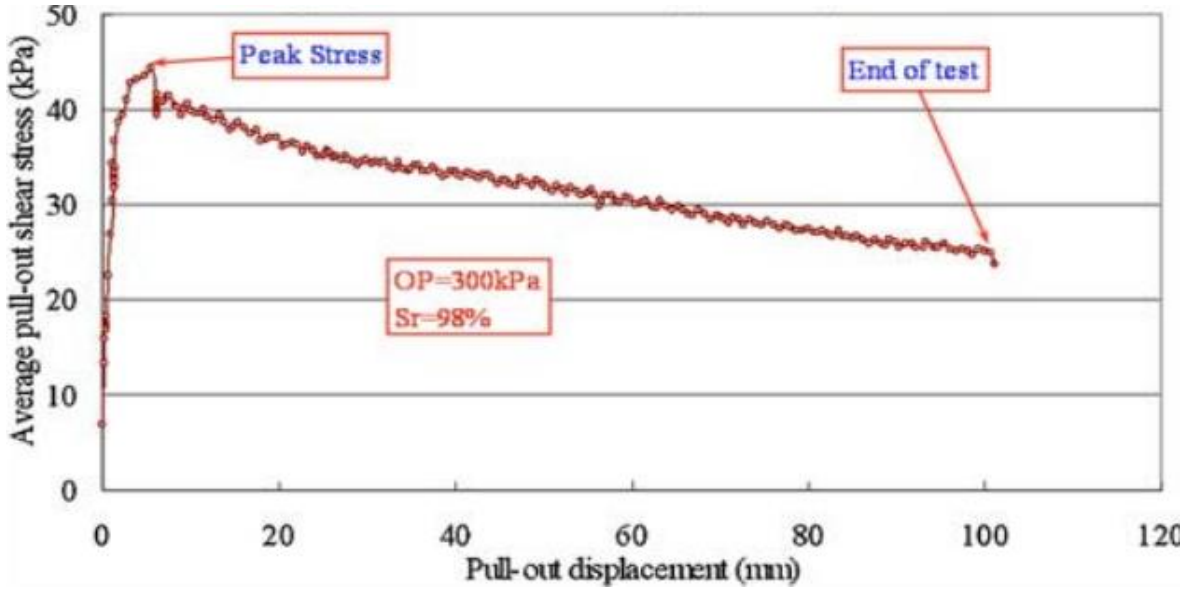

Fig.2. 24 Variation of average pull-out shear stress with pull-out displacement [55]

Yin and Zhou [56] use the same apparatus for the pullout testing of absolutely decomposed granite soil under combine stresses of grouting and overburden. The study reported that overburden and grouting pressure have an interactional influence on the resistance capacity of the fastening element. The result obtained from the experimental test of peak and residual shear strength is plotted against overburden pressure is given in Fig.2.25.

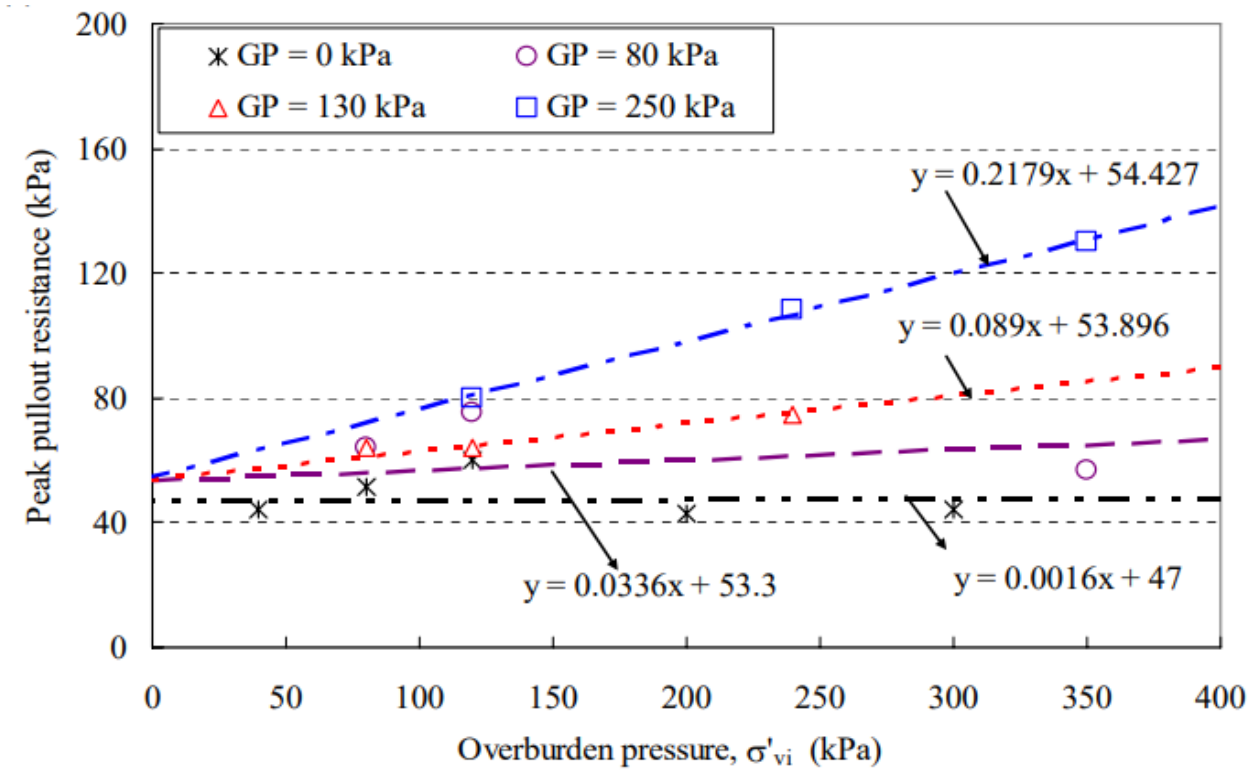

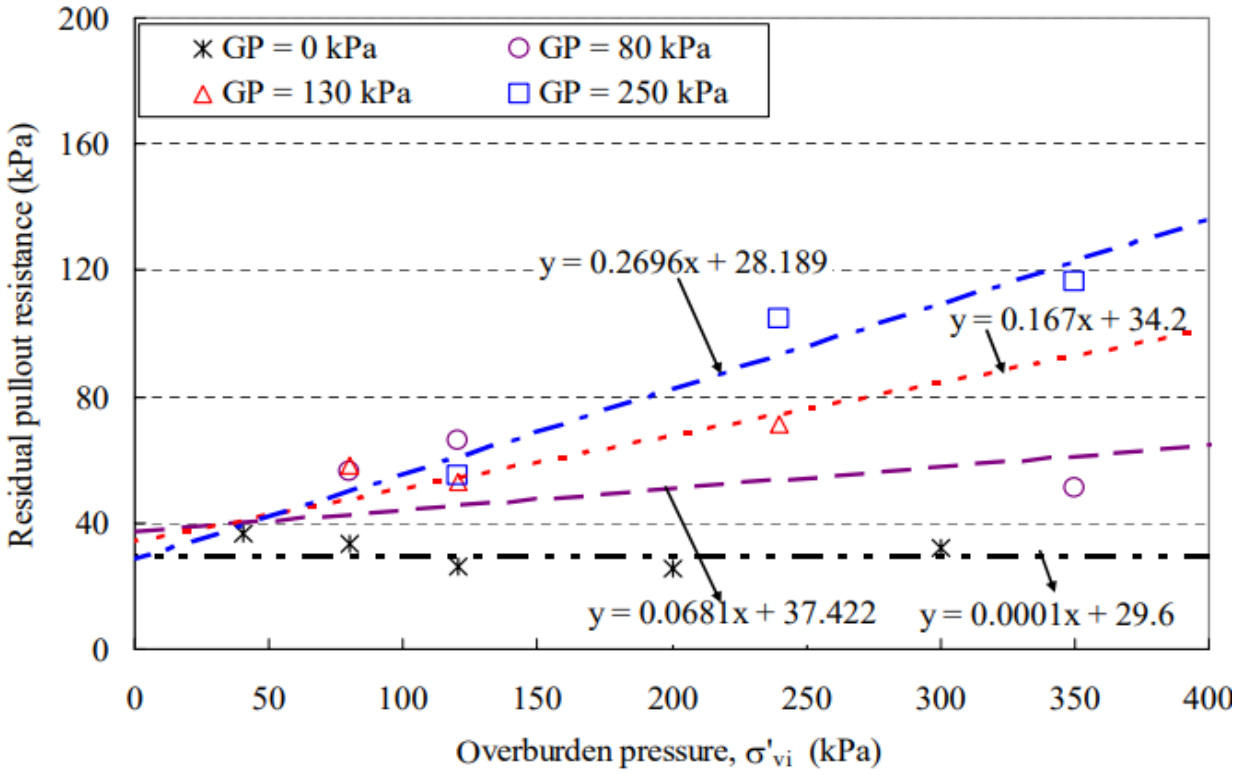

(b)

Fig.2. 25 Different interface shear strengths under different grouting pressures: interface shear stress at peak stage (b) interface shear stress at the residual stage with overburden pressure [56].

A linear relationship has been developed between shear strength and overburden pressure with different equations and different interfaces. From the test results, a generalized equation has been proposed for the calculation of pullout resistance incorporating the surcharge pressure and grouting pressure as Eqn.2.8.

$$\tau^{-} = c_G'(p_G) + \sigma_v'\mu_G'(p_G) \quad (2.8)$$

τ^{-} is average shear stress; c_G' fitting parameter value when overburden stress is zero; p_G is grouting pressure; σ_v' is overburden stress; μ_G' is the slope of the line.

Gurpersaud et al [57] performed a pullout test on horizontal, vertical, and at an inclination of 15˚ with vertical to the test box. The study incorporates the matric suction effect, which is generally ignored in the pullout study. Gurpersaud et al [57] inspected the effect of matric suction on the uplift capacity of reinforced element fixed in saturated and unsaturated sand. The internal dimension of the tank was 1.5 m **X** 1.2m **X** 1.1m, set along with plumbing fixtures to simulate the saturated and unsaturated soil conditions. For the transportation of water to desired location perforated pipes are attached at the bottom of the test tank. Details of laboratory pullout setup of soil nail are presented in Fig.2.26. The sand sample was compacted using a 6.5kg compactor layer by layer having a thickness of 150 mm. Gurpersaud

et al [57] used drilling machine for drilling holes for the placement of nail and grout. The grouted depth of the nail was 800 mm from the top surface. The pullout tests were conducted using force-controlled loading of 1 mm/min.

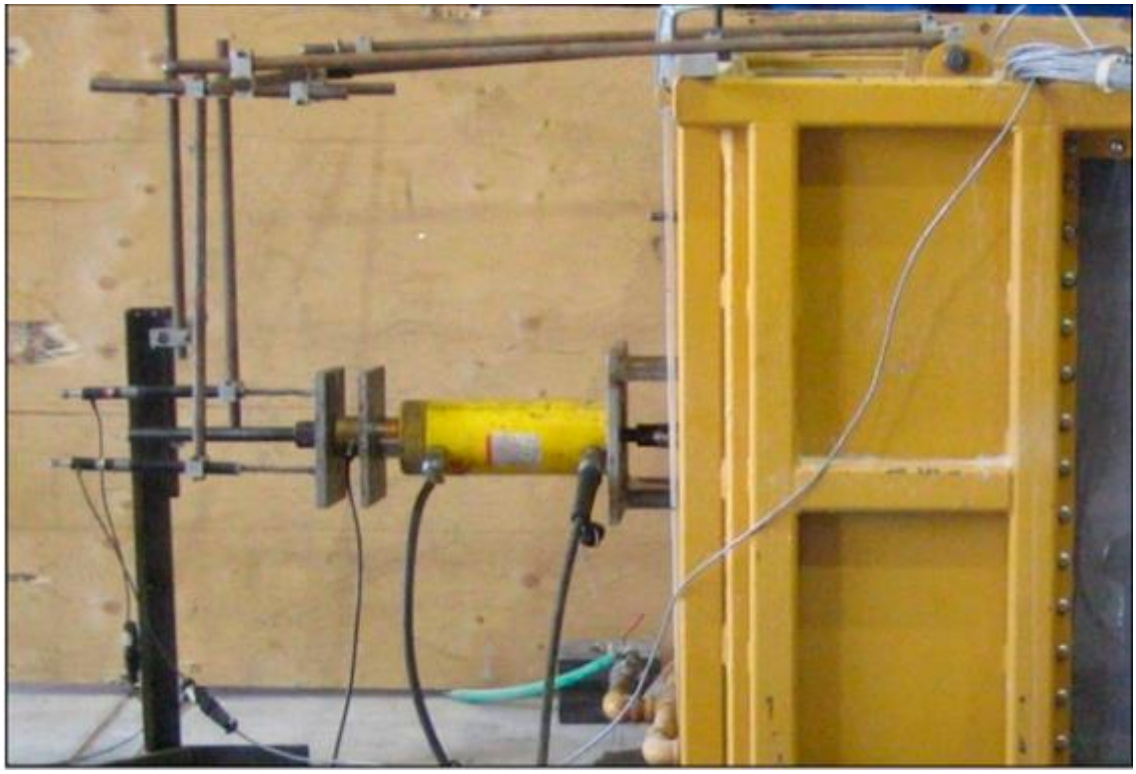

Fig.2. 26 Pullout testing of soil nails at 90˚ to vertical (Gurpersaud et al. [57])

Gurpersaud et al [57] reported pullout capacity of the nail element is directly proportionate up to the air-entry value, beyond this point the pullout behavior of the nail becomes non-linear. The estimated value of pullout resistance of soil nail for compacted unsaturated sand was 1.7 times greater than saturated sand. The semi-empirical method is suggested to estimate the pullout capacity corresponding to matric-suction and interface shear strength parameters. The measured value is in good agreement with the experimental and data available in the literature.

Stephens et al. [58] examine the performance of twisted square helical shape hollow steel pipes called spiral nails as shown in Fig.2.27. Soil nailing is driven into soil mass without cement grout to develop a bond with the soil to provide internal stability. Stephens et al. 2013 suggest spiral nail reinforcement design to increases the factor of safety of the soil-nail system. In this project, the performance of the spiral nail soil nails to check the applicability of existing design methods. The study explains the methods of design, construction, soil type, instrumentation, and load-displacement behavior of these types of nails. The load-displacement data is measured and calculated to offer equivalent bond stress.

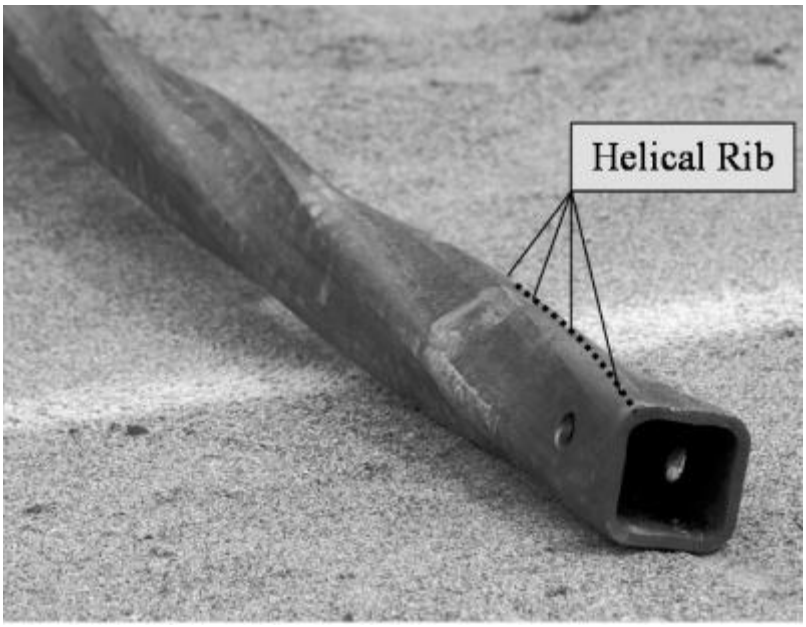

Fig.2. 27 Spiral nail

Ye et al. [59] conducted a model test for a new type of developed conventional nail, the outcomes of that were judge against the 3-D simulation via finite element method. The pullout tests were conducted to evaluate the shape angle and friction coefficients using a physical tank having a dimension of 0.6m **X** 0.73m **X** 1m. The plan of the model test of Ye et al. [59] is shown in Fig.2.28. The physical model was used for testing is presented in self-explanatory Fig.2.29. The pullout mechanisms of newly developed soil nails were then analyzed which show constructive influence on the pullout capacity of the nail. The study suggested compaction-grouted nail consistently increases the pullout force with no yield force with change in displacement. Due to which the stability of geo-structure increases resulting in nail reveal high pullout capacity. The amount of cement used for grouting was found to decrease compared to conventional nails. The laboratory results were verified by using numerical methods, which are found in good agreement with each other. Moreover, the study confirms that the finest approach for increasing pull-out force is by increase the diameter of cement bulk than increasing the nail length.

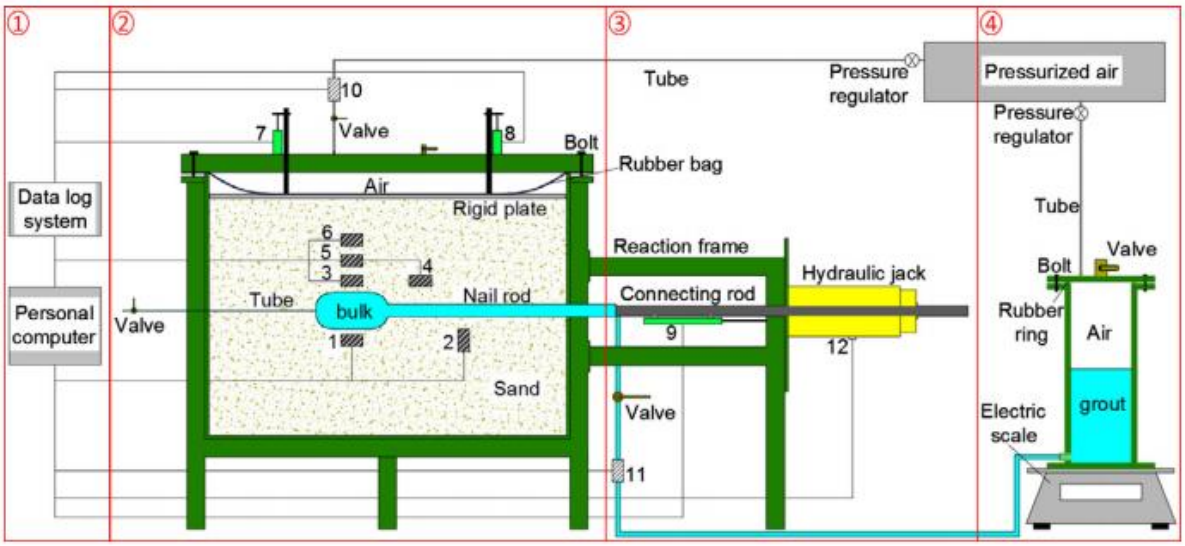

Fig.2. 28 Schematic layout of the model test (Ye et al. [59])

Fig.2. 29 The laboratory pull-out system (Ye et al. [59])

Kwong and Lee [60] conducted a field study on soil nailing subjected to rise in groundwater table artificially by injecting water using pipes as shown in Fig.2.30. The test was conducted at a very steep angle of 55° in volcanic soil for a height of 10 m. A total nine number of conventional nails were installed at 15° inclinations with horizontal. The soil nails were fastening along with strain gauges, inclinometers, piezometers, settlement prisms, etc. The load-displacement study of soil nails for the soil slope having a high-water table. The test results show calculated load for a reinforcing element was found lesser than the expected load. Finding suggests that economy can be achieved if mobilization of force was measured in schedule design. The field results were validated using finite element analysis by simulating the field conditions.

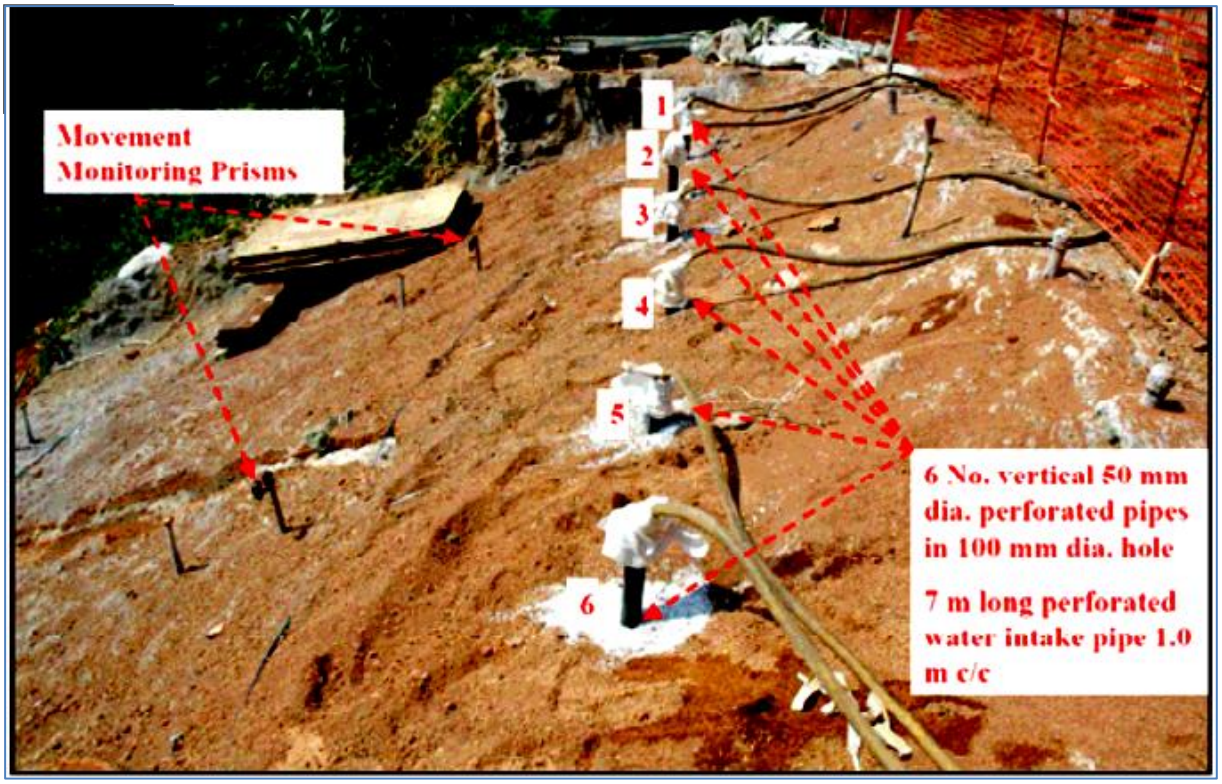

Fig.2. 30 Water intake pipes installed [60]

Zhang et al. [61] conducted 167 in-situ tests on completely decomposed granite soil from the landslip, preventive measures plans are collected (Fig.2.31). The in-situ tests results are then interrelated and compared with theoretical results. The variability due to surcharge pressure, soil suction, soil dilatancy, and grout-length are then estimated. To execute the nailing operation the slope was drilled with a 100 mm diameter hole having spaced 1 to 2 m in all directions. From the test result, Zhang et al. [61] reported that pullout capacity is independent to the surcharge pressure. Also, the in-situ results found a discrepancy with calculated values. As evident from Fig.2.32, bond stress changes with pullout displacement of the soil-nail interface. Tests results observed that stress yielding continue along with displacement up to 10 mm.

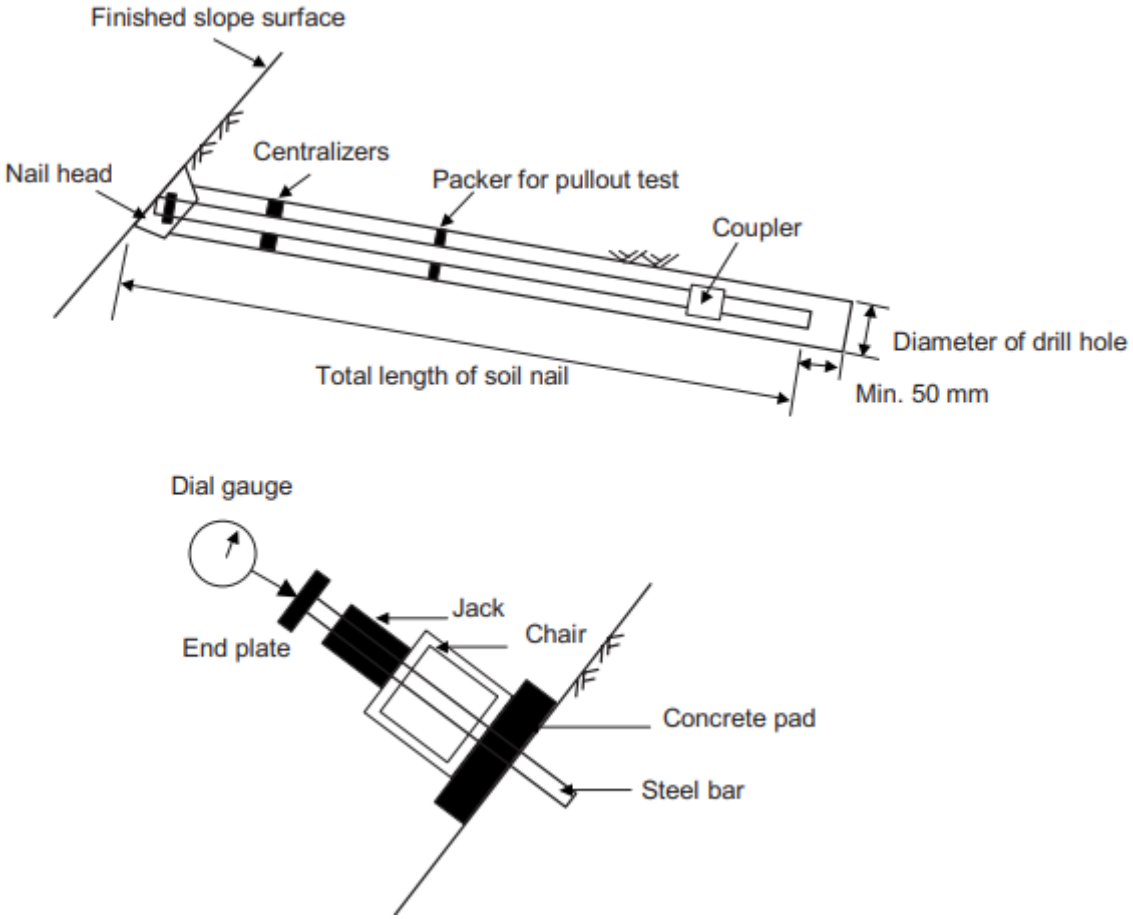

Fig.2. 31 Typical soil nails in cut slope and field pullout-test arrangement (Zhang et al. [61])

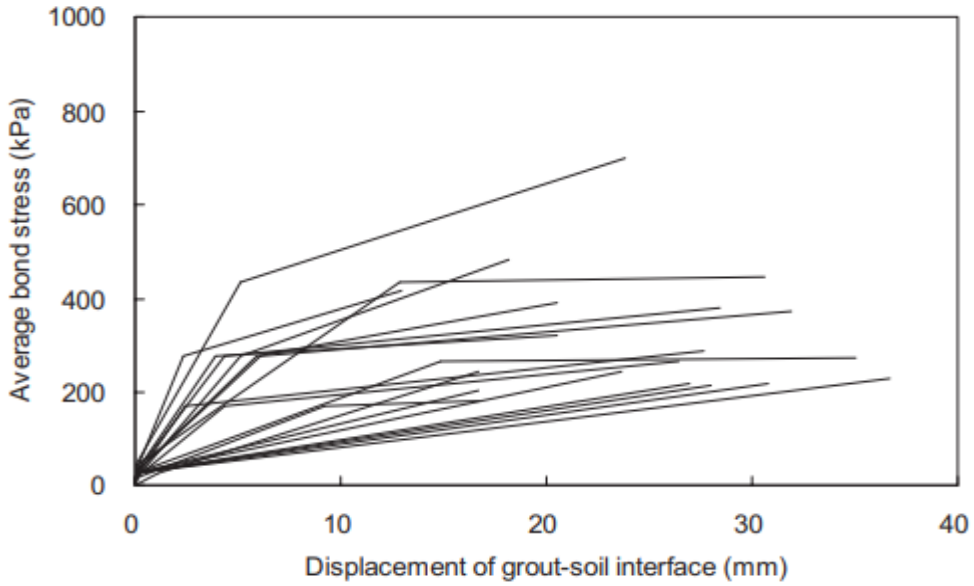

Fig.2. 32 Bond stress-displacement (Zhang et al. [61])

Babu [62] conducted a field studies on the stabilization of vertical cut using soil-nailing technique as shown in Fig.2.33. The stability of soil nailing system found to be increased

using reinforcing action of soil nailing. The investigation reveals that soil stability of a slope can be improved by soil nailing significantly.

Fig.2. 33 Soil Nailed Wall [62]

Babu and Singh [63] conducted a field to investigate the pullout strength of soil nails in the field and to verify the previously published analytical and laboratory studies. To perform the field test a local site of 10 m height was excavated vertical and conducted the three field tests as shown in Fig.2.34. The tests were divided into two groups: the first group accompanies nails with the same condition, geometric configuration, and installation methods, while the second group accompanist nails with different conditions geometric configuration like diameter, length, etc.

Fig.2. 34 Field pullout test [63]

Results obtained from the field test are present in Fig.2.35. The study reported pullout strength at the relatively small displacement of 10 mm and observe that pullout force comes into play and offers resistance force when there is any displacement in the soil mass. Also, the force-displacement response of the in-situ pullout test can be generalized to manifest the elasto-plastic relationship of the soil-nail interface. Thus, the force-displacement relationship can be used for the estimation of the shear modulus of the interface. Based to field experience analytical models can develop to estimate the interaction behavior of the soil-nail element. Moreover, field tests also able to drive the shear stiffness with the soil-nail element.

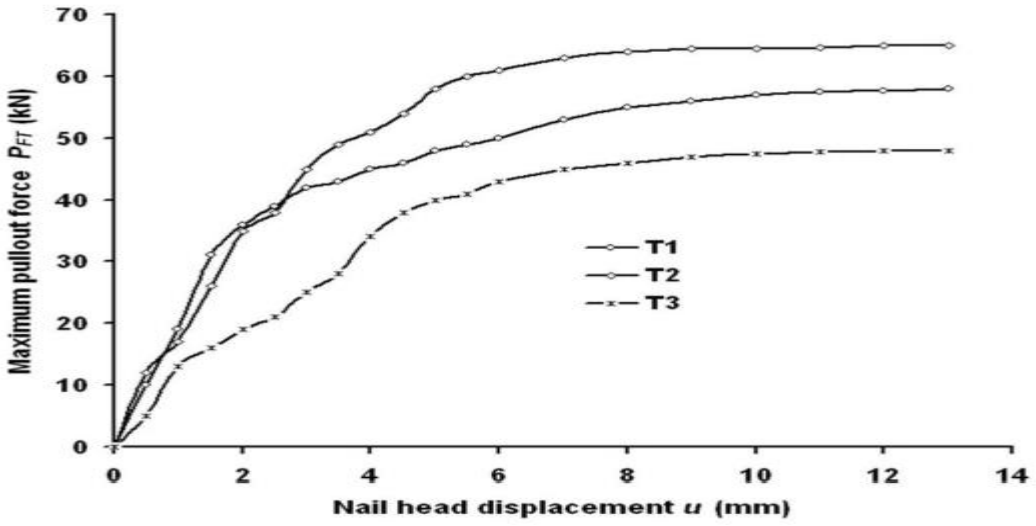

Fig.2. 35 Variation of pullout force with displacement [63]

Zhu et al. [64] studied the applicability of Glass fiber–reinforced polymer (GFRP) soil nails using two field pullout tests as shown in Fig.2.36.

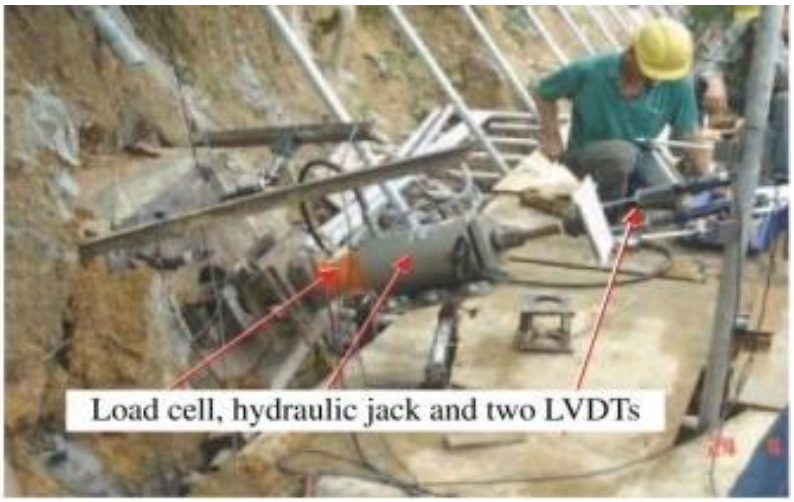

Fig.2. 36 Field pullout test GFRP soil nails [64]

The load-transfer mechanism of polymer nail was compared with steel nail, which has a definite difference. Based on results, a hyperbolic shear stress-strain model was developed to estimate the pullout of glass fiber–reinforced polymer nail. Based on a parametric study of GFRP soil nail recommend that fiber nail impart less strength than steel nails but follows the similar trend.

Cheng et al. [65] conducted laboratory and in-situ tests of different site conditions with different nails. To avoid the corrosion problem of steel, the glass and carbon fiber reinforced polymer (GFRP &CFRP) were studied as an alternative to the steel nail. The study suggests from the test results that fiber reinforced polymer is much lighter than the steel nail and can be used as an alternative for the sites where steel nails have difficult access. Also, GFRP nails are preferred over CFRP nails for normal applicability. Yu et al. [66] conducted a non-destructive laboratory and in-situ investigation to evaluate the integrity of nail elements. The study estimates the grouted ratio and installation length of nail elements using longitudinal waves. The study investigated the partially and fully grouted nail length. The measurement system was developed to determine reflected waves using longitudinal waves as shown in Fig.2.37. The hammer and an accelerometer were used for the creation and measurement of waves. The test results show that the speed of the wave was remaining the same for grouted steel bars in air and soil respectively. The wave velocity of grouted steel bar decreases with an increase in the grouted ratio. The study suggests that velocity and the

grouted ratio can be a functional indicator for evaluating the integrity of soil nails with different embedment lengths.

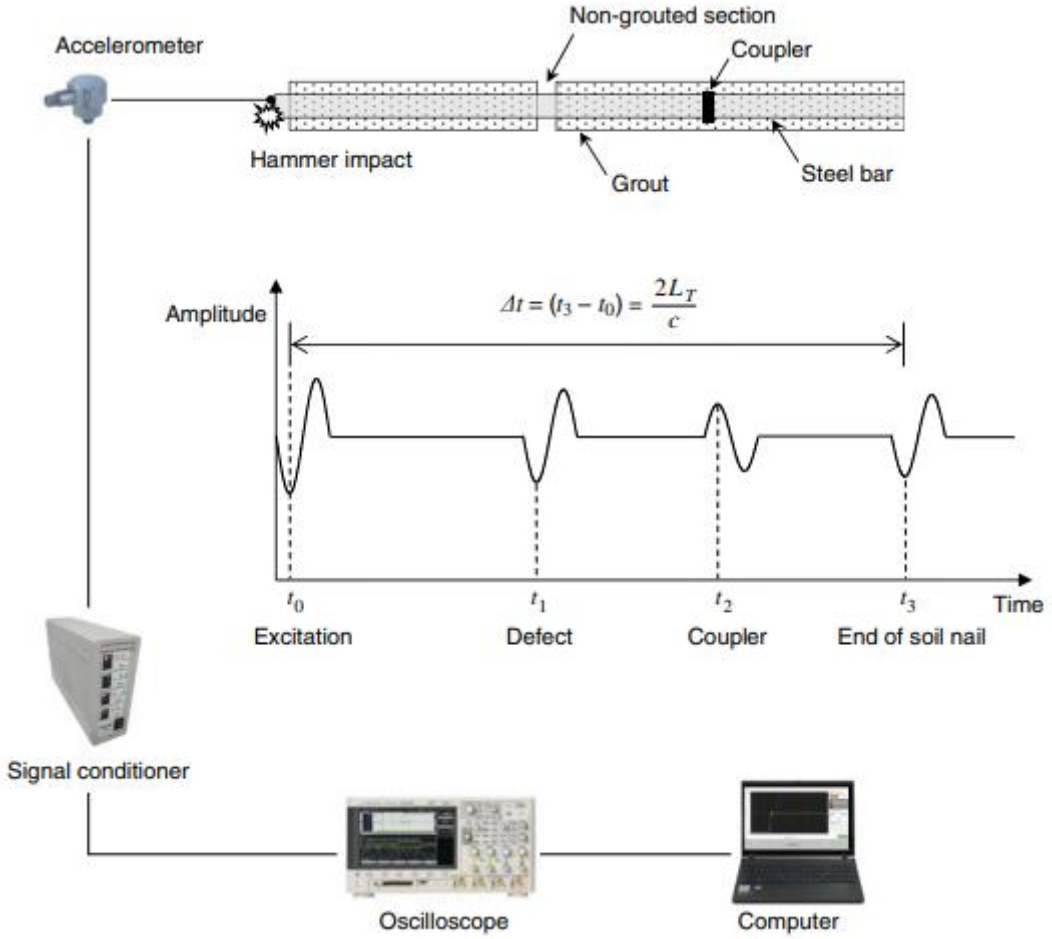

Fig.2. 37 Schematic diagram of the measurement system of longitudinal wave velocity [66]

Ye et al. [67] investigated the negative or unconstructive influence of installation on the actions of a compacted-grouted reinforcement in sandy soil. To encase an injection hole in this study a rubber membrane was used with a diameter of 50 mm. The dimension of tank box was 1**X** 0.8 **X** 0.600 mm respectively. A grout bulb was formed between the nail and membrane which provide the pullout force. The two laboratory test was conducted to such nail with a predrilled hole to study the effect of the installation methods. The details of the model test are shown in Fig.2.38. The test results compared and conclusions were drawn that installation methods had a slight impact on the mass of grout, while the grout bulb showed difference with soil conditions. The drilling show stress release and the release rate propagation with distance. The pullout force of a predrilled test is much smaller than an embedded test, which shows a significant difference at high pressure [67]. Thus, the bond strength of the embedded nail was significantly increased with pullout displacement as shown

in Fig.2.39. Moayed and Namaei [68] investigate the effect of overburden to pullout strength for the in-situ condition in Tehran. Total 42 field tests were conducted in three different types of coarse grain and one of fine-grained soil. Tests indicate that bond resistance increases with the overburden pressure in cohesionless soil, while it has a negligible effect on fine-grained soil. Bayesteh et al. [69] carried out a field study for anchorage applications in problematic soil. For the improvement of soil, hollow bars are used as a low-cost technique in loose sand. The result indicates that hollow nails showed higher resistance than the strand bars.

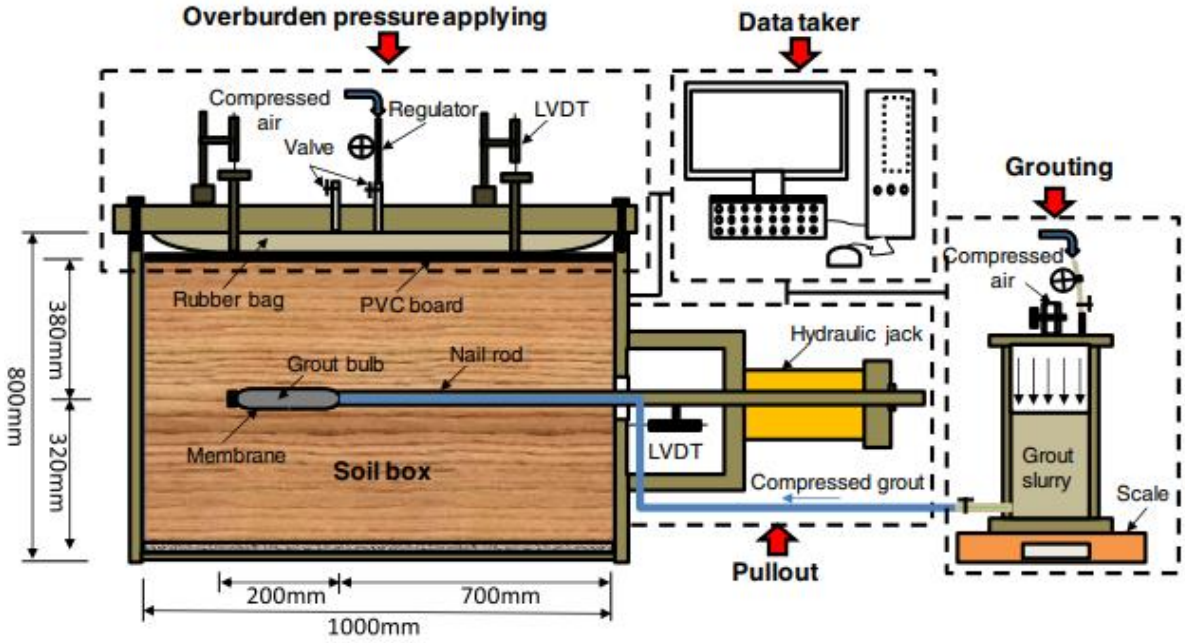

Fig.2. 38 Setup of the model test [67]

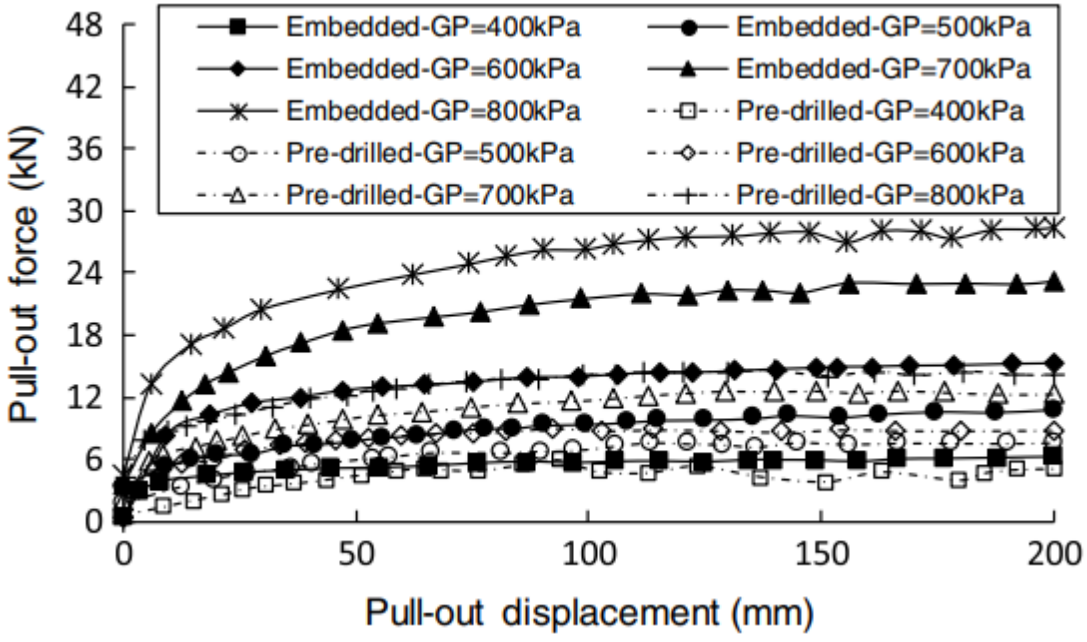

Fig.2. 39 Pullout force-displacement [68]

Table 2. 2 Summary of the pull-out capacity model tests in literature

Author	Year	Pullout dimension(m)	Instruments	Nails	Parameters Investigated	Inclination	Conclusions
Tei	1993	0.254 **X** 0.153 **X** 0.202	1) Data monitoring and logging system, 2) Model box with overburden pressure application system, 3) Pull -out system	Conventional nail	Embedded length, shaft diameter, surface roughness, and stiffness	0°	The study was conducted to inspect the interaction mechanism of soil and nail. The study investigated the bond friction smooth and rough surface of nail.
Junaideen et al.	2004	2**X**1.6 **X** 1.4	1) Data monitoring system, 2) Model box, 3) Pull -out system 4) Grouting system	Single, grouted nail	Roughness of the nails, overburden pressure	0°	The test determines the load-displacement characteristics of conventional nails for the pre-peak and post-peak shearing state. The test results also show that the normal stress acting on the nail changes because of the volume-change tendency and arching effect of the soil being sheared around the nail. The post-peak decrease in the

						pullout force is mainly due to the reduction in the normal stress caused by the arching effect of soil around the nail.
Chu et al.	2005	0.7 **X** 0.56 **X** 0.605	1) Data logging device, 2) Model tank with pressure application system, 3) Pull -out system 4) Grouting system	Single, grouted nail	Saturation ratio, overburden pressure	0° The shear stress–displacement behavior and ultimate shear strength at the interface between the cement–grout nail and decomposed granite soil.
Pradhan et al.	2006	2 **X** 1.6 **X** 1.4	1) Loading frame consists of two hydraulic jacks on steel plate. 2) LVDT 3) Pull out device 4) Drilling and grouting by hand auger	Convention al nail	Effect of retained dilatancy on loose soil. Different overburden pressure	0° A numerical model was developed to simulate the pullout force in soil nails. It has been shown that a simple that a simple one dimensional spring model can be used to simulate the pull-out load displacement relationship nails [70].
Y. Jian Hua &S.Li Jun	2006	1 **X** 0.6 **X** 0.83	1 Rubber diaphragm 2 Strengthening Beam 3 Pressure Gauge	Convention al nail	Degree of saturation, Cement	0° The paper presents details of the new pull out tests are presented and discussed.

			4 Wooden Plate 5 Tensiometers 6 Rebar 7 Cement grout 8 External chamber 9 Earth preassure cell 10 LVDT 11 Coupler 12 Load cell 13 Guided bar Hydraulic jack 14 Load reaction frame 15 Brim Stiffener		pressure grouting , Overburden pressure, Interface shear dilation, Roughness of the hole surface		
Su et al.	2008	1 **X** 0.6 **X** 0.83	1)Pull -out system 2) Grouting system 3) Overburden application system	Convention al nail	Overburden pressure	0°	Concluded that the installation process of nail induced considerable vertical stress changes in soil around the soil nails and that the soil nail pull-out shear resistance is independent of the overburden

							pressure.
Gurpersaud et. al.	2013	1.5 x 1.2 x 1.1	1) LVDT 2) Computer with logger 3) Load cell 4) Hydraulic pump	Conventional nail	Capacity of grouted soil nail in saturated and unsaturated soil environments	0°	A comprehensive experimental program was undertaken to determine the pull-out capacity of soil nails in both saturated and unsaturated compacted sand. The pull-out capacity of soil nails under unsaturated conditions increases almost linearly up to the air-entry value. There is a non-linear behaviour in the pull-out capacity beyond the air-entry value.
Xinyu et.al.	2017	0.6 **X** 0.73 **X** 1	1) Data monitoring and logging system, 2) Model box with overburden pressure application system, 3) Pull -out system 4) Grouting system	Compacted grouted soil nails.	Shape angle, Friction Coefficients (ABAQUS)	0°	The shape angle and friction coefficient affect the increase in the total pull out force of the soil nail.

			5) Transducers for earth pressure , tensiometers, volumetric water content 6) Pressure transducers 7) Force transducer 8) Bolt 9) Connecting rod 10) Hydraulic jack			
Ye et al.	2020	1 **X** 0.8 **X** 0.6	1) Data monitoring and logging system, 2) Model box with overburden pressure application system, 3) Pull -out system 4) Grouting system	Grouted soil nails.	Installation methods, lower soil densification, dilation, and squeeze effect	0° The pullout force of a post placed soil nail experiences a slower increase rate with an increase in the grouting pressure, which results in a lower efficiency of the increasing pullout force .

2.3.3 NUMERICAL MODELING

Numerical modeling techniques are broadly adopted to understand the interaction mechanism, stress distribution, and serviceability of soil and nail element. Based on laboratory and field test numerical models are established to evaluate the pullout test of soil nails. To explore the numerical analysis for pullout behavior of nails various parametric studies were carried out by various researchers [71-77]. Shafiee [71] conducted the first numerical study using a finite element program. This includes various factors like friction angle, adhesive force, and installation angle for the theoretical estimation of resistance force. Smith and Su [72] reported a three-dimension numerical study by the finite element method, which investigates the interaction mechanism of the nail and studies the failure mechanisms (internal and overall) of nail structure. Babu et al. [73] examine the installation methods effect, facing type, facing stiffness, and inclination angle using numerical simulations by FLAC. Babu and Singh [74] investigate the use of plate and geo-grid element to simulating soil nails using PLAXIS 2D. Finding suggests a plate element to simulate nail element in comparison to geo-grid. Singh and Babu [75] studied different soil models like the hardening model and Mohr-Coulomb to simulate the field condition response of conventional soil. Zhou et al. [76] developed a plane–strain numerical model to present a loose soil fill under overburden pressure for back analysis of the in-situ test. The analysis was carried out incorporating the various parameters like water content, surcharge loading, and displacement after application of overburden pressure. The model parameter includes the hydraulic and mechanical properties of soil slope obtained from test results. The model developed was simple and the result estimated from it is in close agreement with laboratory and in-situ tests results of allocation of nail forces under different overburden pressure as shown in Fig.2.40. The study suggests that nail elements are capable of increase the overall stability of loose soil under applied pressure. On another hand, lesser nail forces mobilized near the nail head indicate that the grillage system has a beneficial effect at the slope for the pressures range from 30 to 72 kPa.

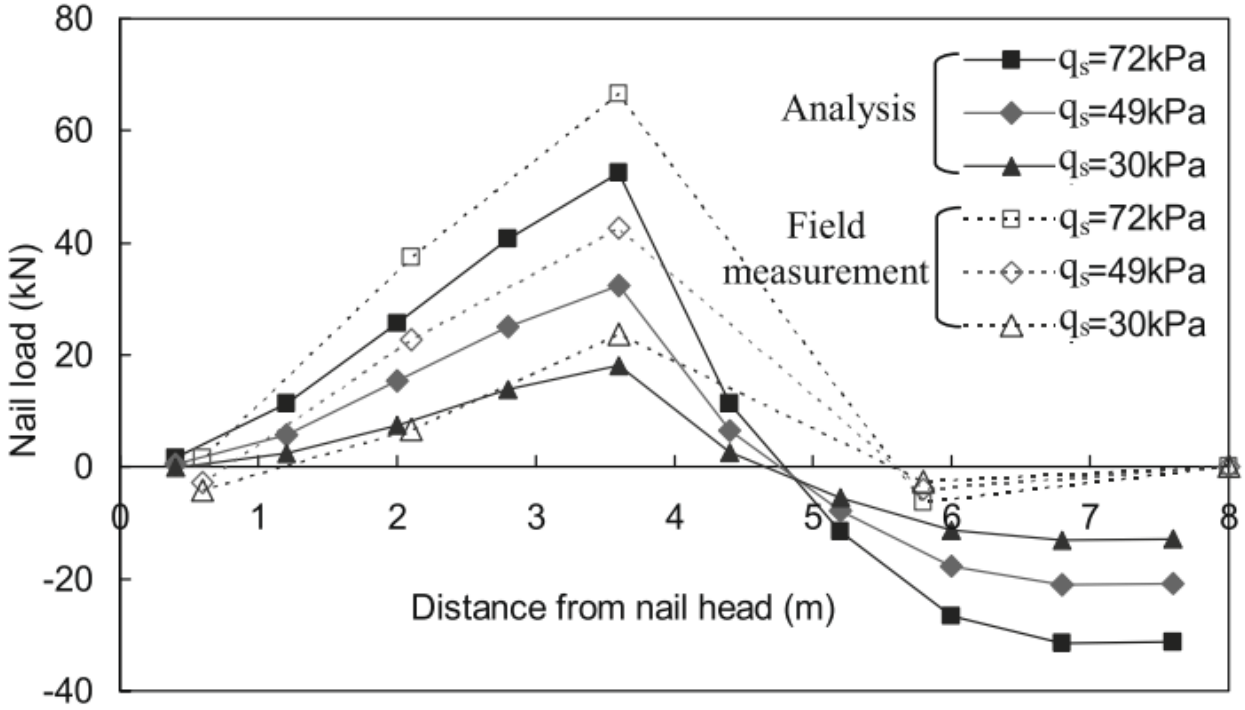

Fig.2. 40 Distribution of nail loads during the surcharge process [76]

Su et al. [77] established a three-dimensional finite element model for replicating soil nail pullout test. The finite element model results were compared with the experimental results. The average pull-out shear stress and stress variation were in very good agreement with experimental and simulated results. The model includes the effect of overburden and dilation angle for force-displacement study. Moreover, the result also predicts that with an increase in dilation angle of the shearing zone resisting force also increased. The investigation indicated that constrained dilatancy of interface contributed play significant role in peak load-displacement capacity. Sharma and Ramakrishnan [78] investigated soil-nail interaction and back analysis of the pull-out resistance of nails using (FEM) Finite Element Analysis using PLAXIS 2D. It is observed that the pull-out resistance of the nail depends upon the depth of the nail, which is validated using Limit Equilibrium Analysis. Moreover, the study also reported seismic analysis for a nail with reduced nail length, results observed a slight percentage increase in the serviceability conditions like horizontal deformation. Rawat S, Gupta AK [16] investigated the slope stability analysis of soil nails using limit equilibrium (LEM) and finite element methods (FEM). The program used for the analysis is SLOPE/W and PLAXIS 2D respectively. The slope angle was adopted for the analyses are 45˚ and 60˚, which strengthen using nail element at inclinations of 0, 15, and 30 respectively. The slope angle and inclinations are taken from the horizontal. Comparisons have been made using these two methods on stability parameters. The factor of safety using the SLOPE/W (LEM)

method is found to be more than the finite element method. Rawat [16] conducted a similar study using Plaxis 3D (FEM) and the results are then compared with experimental results. The study suggested that the failure mechanism for different slopes is found similar. However, the peak load carrying capacity of the different slopes is found different. The tests result shows that soil slope of 45˚ with nail inclination of 0˚ show maximum resistance in load-bearing.

2.3.4 INSTALLATION AND PULLOUT CAPACITIES OF HELICAL PILES/ ANCHOR

The conventional soil nail undergoes a problem in installation due to drilling of soil slope which creates a large disturbance to the soil mass. The techniques acquire the influence of helical anchors which is seen as an innovative alternative for the installation of the nail which also leads to an increase in pullout strength. Various researchers reported the installation and pullout capacity helical anchor [59-69]. Mitsch and Clemence [79] examine the uplift capacity of helical anchors in fields and laboratories. The study monitors the uplift load-displacement of helical anchor and deflections of the soil mass. The results indicate that the cylindrical soil failure surface develops beyond the crown plate during the pullout. Above the top helix is the failure surface dependent on the depth anchor. Hoyt and Clemence [80] investigate the methods of uplift capacity i.e. cylindrical shear and individual bearing and develop a correlation between uplift capacity and installation torque.

$$Q_u = K_t T \tag{2.9}$$

where,

K_t = empirical factor;

Q_u= Pullout capacity (kN)

T = Average installation torque (kN-m)

The study suggested empirical factors for a different type of nail shaft which helps in the estimation of installation torque and pullout capacity when one of the parameters is unknown. Ghaly et al. [81] investigated the performance of single pitch and multi-pitch screw anchors with different geometric arrangements. Further, the study investigated the analytical and laboratory study on installation torque of screw anchors [82]. The examination reveals that estimated and measured results are found in reasonable agreement with each other [82]. Ghaly and Clemence [83] conducted the pullout test of helical anchors under different inclination angles. From test results, rupture surface is found unsymmetrical and have a very complex nature, and can be present by logarithmic spiral curves. The theoretical and experimental

results show reasonable agreement with each other. Tsuha and Aoki [84] investigated the relationship between installation torque and uplift capacity deep helical piles in sandy soil using centrifuge and direct shear interface tests. From the field and laboratory tests, it was observed that the torque correlation factor (K_t) is inversely propositional to nail dimensions moreover the torque correlation factor increases with the angle of internal friction [84-86]. Lutenegger [87] investigate the installation disturbance of helical anchor and found that multi-helical anchor creates more disturbance than the single helix. Sakr [88] develop a theoretical model to predict the installation torque of sand soil to install a helical pile. The calculated torque is then compared with measured installation torque from different in-situ conditions. The study also investigates the factors that affect the installation like the water table, pile geometry, soil properties, and installation methods. A relationship has been established between uplift capacity and installation torque, which reveal torque factor depends upon the load path. Schiavon et al. [89] simulate the behavior of helical anchors in cohesionless soil using centrifuge modeling. To evaluate the scale effect on plate anchors and helical anchors, the study suggests the effect of grain size on the uplift capacity of cohesionless soil. The study shows no scale effect for models having a ratio of effective radius to average grain size greater than 58. Kwona et al. [90] investigate the pullout behavior of helical anchors with different inclination using Eulerian-Lagrangian (CEL) analyses. The helical anchors have a different number of a helix having equal and unequal in size with single, double, and triple helices. The findings suggest that pullout capacity remained almost unchanged up to 60° and then starts decreasing with further increase in inclination and found least at 90°. Pandey and Chauhan [91] attempted to evaluate the peak pullout capacity of the vertical helical anchor embedded in clay with varying configurations using limit equilibrium and finite element methods. The development of failure surfaces has been observed with the change in installation depth of single helix anchors, while for multi-helices the interference of failure surfaces was observed with variation in S/D ratio.

Perko [9] and FSI [8] published a convenient guide to design and install helical piles and anchors respectively, it includes detailed evaluations of installation, and pullout of helical pile anchors. It contains information regarding installation procedures and the basic installation equipment uses for the installations. The study reported the geotechnical aspects and influence of soil properties on the design and application of helical piles. It also includes the effect of geometric configurations on the bearing capacity of the helical pile. The individual bearing and cylindrical shear are the methods of determining the bearing capacity

of helical pile/ anchors are also elaborated in detail. In the cylindrical shear method, the helices act as a single semi-rigid block having a diameter nearly equal to the bigger most diameters [8, 9]. The failure is said to be cylindrical when inter-helices spacing is less than 3 times the diameters of leading helices, while for spacing more than the prior condition the failure is called individual bearing failure. The individual bearing capacity of the helical pile [9] is given as in Eqn. 2.10. While the ultimate bearing capacity of the helical pile [9] is given as in Eqn. 2.11.

$$P_u = \sum_n q_{ult} A_n + \alpha H(\pi d) \tag{2.10}$$

$$P_u = \sum_n q_{ult} A_1 + T(n-1)s\pi D_{avg.} + \alpha H(\pi d) \tag{2.11}$$

where,

q_{ult} is maximum bearing pressure;
A_n is the nth area of the plate;
α is adhesion between interface;
H is the length of pile/anchors;
d is shaft diameter;
A_1 is an area of bigger helix;
T is the shear strength of soil;
(n-1) length of soil mass between helices;
The Cylindrical shear failure and individual bearing failure for helical anchors are given in Fig. 2.41 respectively.

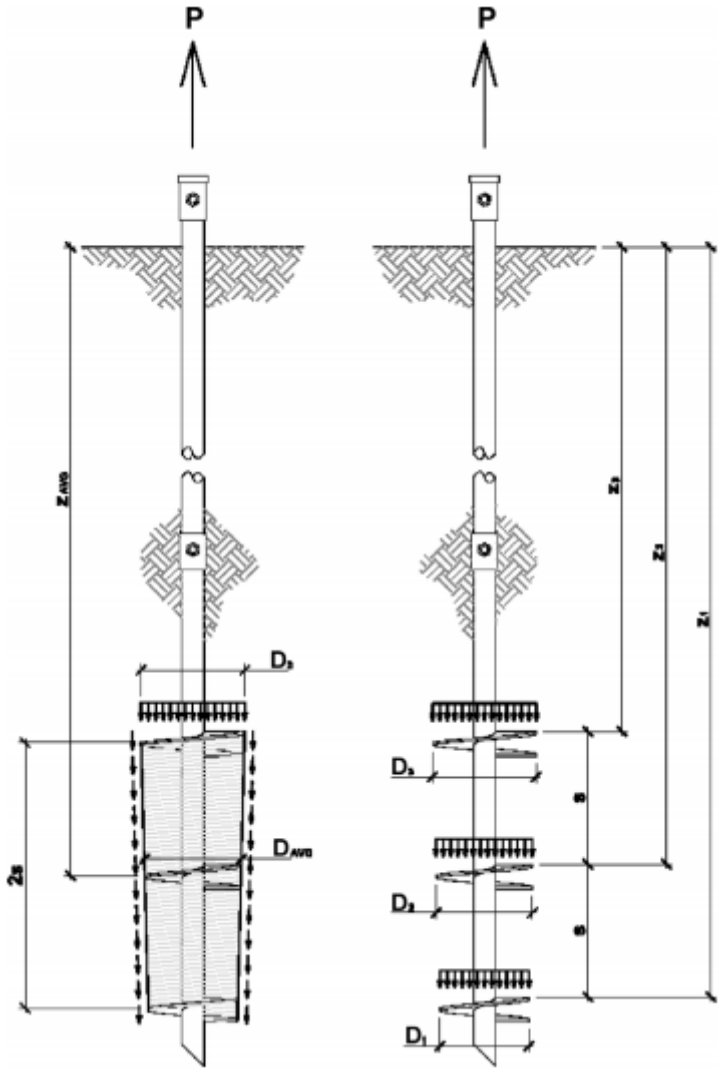

Fig.2. 41 Cylindrical shear and individual bearing methods for helical anchors (Perko [9])

Perko [9] and FSI [8] suggested the Capacity-to-Torque Ratio (kt) for helical piles and anchors. Perko [9] reported kt values for 114mm, 152 mm, and 254 mm diameter shaft equal to 18m-1, 14m-1, and 9m-1 respectively. Whether as per FSI [8], reported kt values for 3.81 cm to 9 cm to vary from 32.8 m-1 to 23.33 m-1 respectively. From both design guides (Perko [9] and FSI [8]), clean that capacity-to-torque ratio is inversely propositional to the effective shaft diameter. FSI [8] suggests various guidelines for the performance of the helical element. Helices are an important part of a helical element which helps in installation with the least disturbance with bearing resistance. The helical geometry affects the rate of penetration, soil disturbance, and capacity to torque correlation. Due to poorly-formed helices soil disturbs significantly with augering effect. The true shape or poorly-formed helices are shown in

Fig.2.42. A true helix is defined as a helix having a three-dimensional curve that sweeps around an axis where the radial line remains perpendicular to the axis.

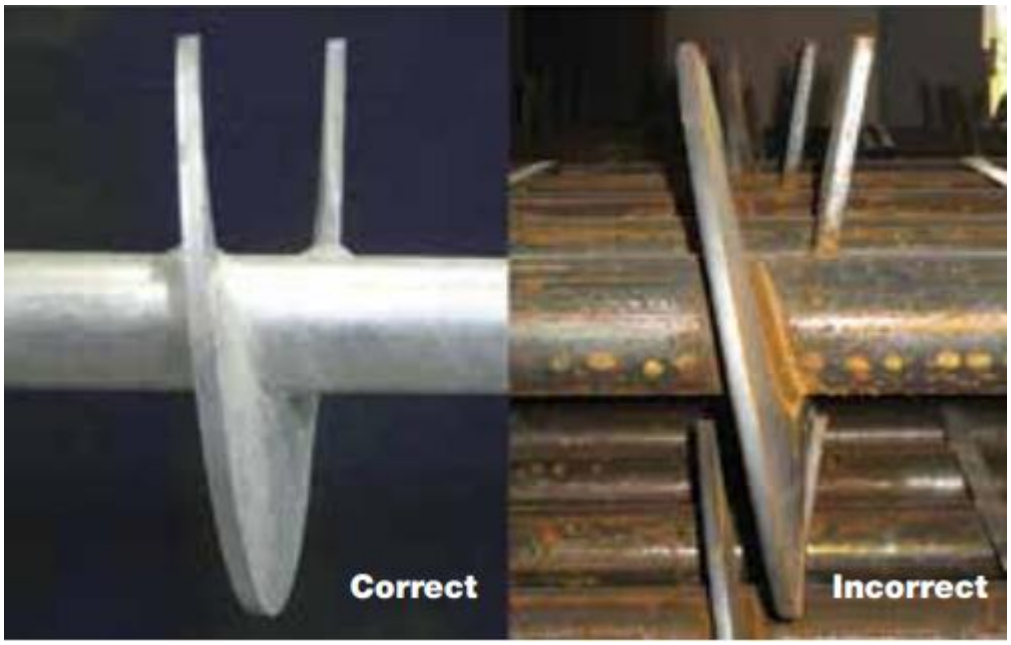

Fig.2. 42 True shape and Poorly-formed of helices

FSI [8] suggests the helical spacing between two helices varies 2.4 to 3.6 times the previous helix, while the diameter of the helices plate varies from 6 inches to 16 inches. Most of the piles are generally spaced three times diameters to prevent one plate from contributing stress to the bearing soil of the nearby plate. For such conditions, the bulb formed around helices will not intersect each other and each helical plate acts independently in bearing along the shaft as shown in Fig.2.43. The helical element i.e. pile/anchor comprises of round or square solid shaft used for the tension applications. For vertical compressive load square shaft helical are preferred over round shaft by the manufacturers. There is diverse suggestion amongst design and industrial professionals for applications of square and round shaft helical products. To resist both tension and compressive load hollow shaft is preferred over a solid shaft for the helical product. The hollow and solid shafts are as shown in Fig.2.44

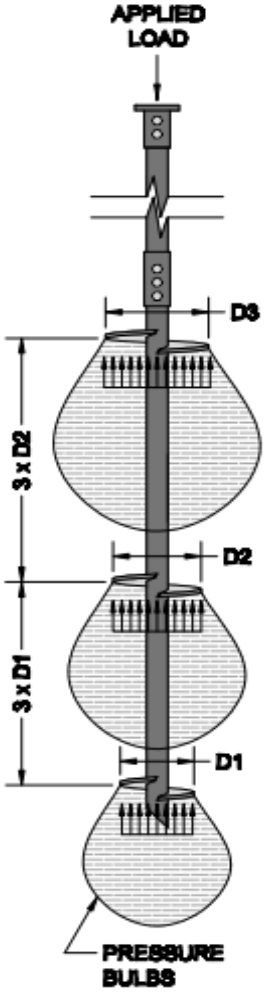

Fig.2. 43 Helix plate spacing with bulbs of significant stress influence (FSI, [8])

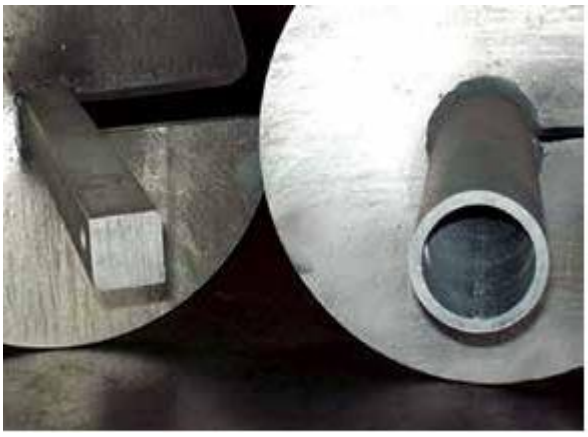

Fig.2. 44 Round shaft and Square shaft (FSI, [8])

FSI Engineering Department, 2014 suggests hollow round shafts are suitable for compression while the solid square shaft is beneficial for tension applications. Perko, [9] mentions the plugging study of hollow shaft helical pile/anchor. As hollow shaft helical pile/anchor move

forward into the soil mass it becomes plugged within a few feet of installation. Fig.2.45 shows the photograph of the end of the hollow shaft helical pile.

Fig.2. 45 Plugged end of a typical helical pile (Perko, [9])

Perko, [9] reported the soil plug expands up to some length in shaft diameter the remaining shaft remains empty. Owing to the compression of the material plugging the end of helical items, the area of helical items considered as the full area for the calculations of bearing capacity. FSI, [8] didn't report anything about soil plugging of hollow shaft helical items. Various researchers reported the plugging effect of open-ended piles/anchors [92-95]. Gudavalli et.al [92] studied the degree of soil plugging during installation of the pile that affects the ultimate capacity of open-ended pipe piles. The in-situ testing was conducted on dense sandy soils to measure the plug lengths at the final installation. The results reported that unit skin friction and unit end bearing values is directly proportional to the end bearing factor. Ko and Jeong [93] conducted full-scale testing of open-ended piles installed in cohesionless soil. The research investigates the plugging effect of open-ended piles which includes both dynamic and static axial compression load tests and measures the outer and inner shaft resistances acting on the piles. The plugging effect of open-ended piles may be classified into three conditions: unplugged; partially plugged; and fully plugged, as shown in Fig.2.46. Soil plug development can be quantified by measuring the soil plug height and calculating the PLR (plug length ratio) and IFR (increment fill ratio) during the pile driving process [92-95]. The PLR(plug length ratio) is defined as the proportion of the soil plug length to the

penetration depth at the end of pile driving, while IFR (increment fill ratio) can be defined as the ratio of the increase in the soil plug to the increment of pile depth during pile driving.

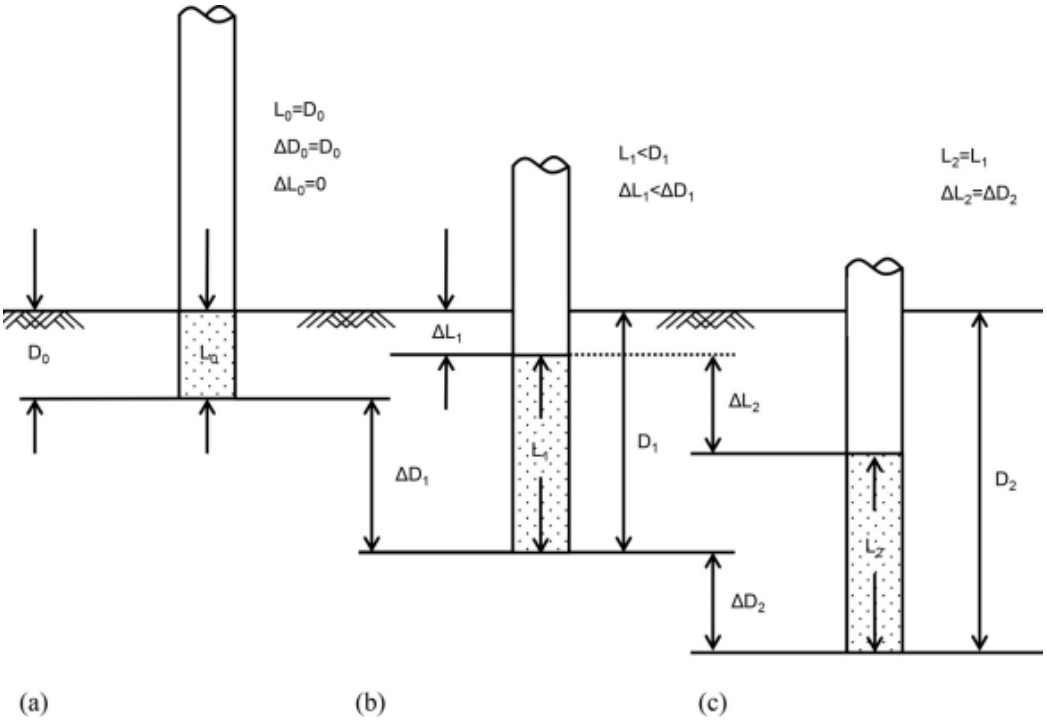

Fig.2. 46 Conditions of plugging effect unplugged; (b) partially plugged; (c) fully plugged [95].

The effect of the results of the standard penetration test (SPT) and IFR (increment fill ratio) on the installation plug resistance is investigated in Fig.2.47. The test results show that IFR is directly proportional to the N-value of SPT and inversely proportional to apart from of soil conditions. Moreover, the test result suggests that the SPT is extremely associated with the IFR. The finding shows that the inner shaft resistance was mostly mobilized near the pile tip and nearly 18%–34% of the entire plug length. Also, it is found that lower portion geometry significantly influences the soil plugging and inner shaft resistance as well. Besides, it can be also verified that the proportion of inner shaft resistance plus annulus load resistance to total resistance was declined with increasing pile diameters. Also, observed that the SPT linearly inversely proportional to the pile inner diameter indicating that the plugging depends upon the inner shaft resistance. Han et al. [95] evaluate the load response of closed-ended and open-ended pipe piles installed in gravelly sand (Fig.2.48). The test was conducted by the maintained static load on closed-ended and open-ended pipe piles installed along side gravelly profile [95].

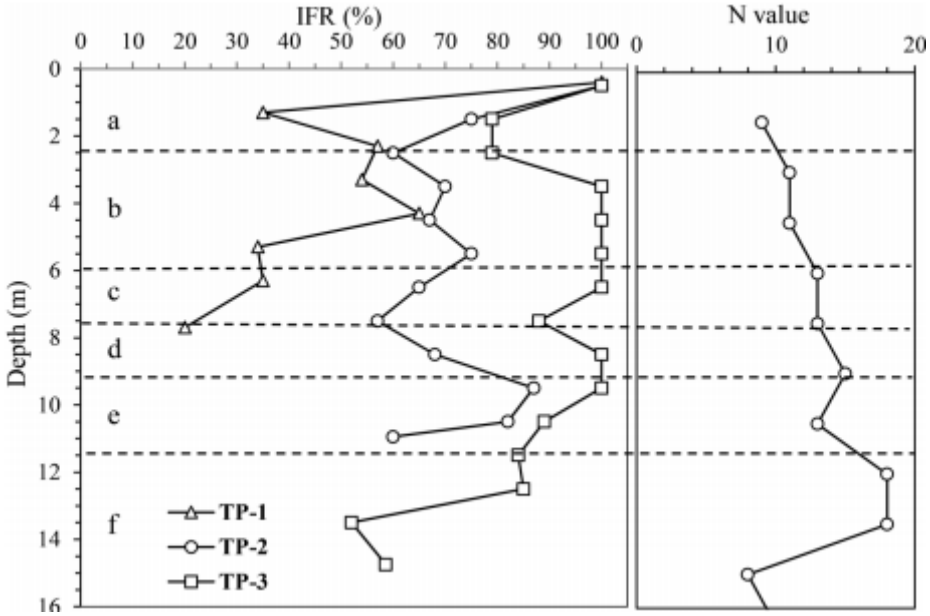

Fig.2. 47 Variation of IFR with N value [94]

The cone penetration tests and standard penetration tests (SPTs) were conducted in the laboratory and field as well at different depths of soil. The piles are installed inside the soil mass instrumented along with strain gauges. The open-ended test pile was fabricated double-wall which allows separation for the measurements of the inner and outer shaft resistances.

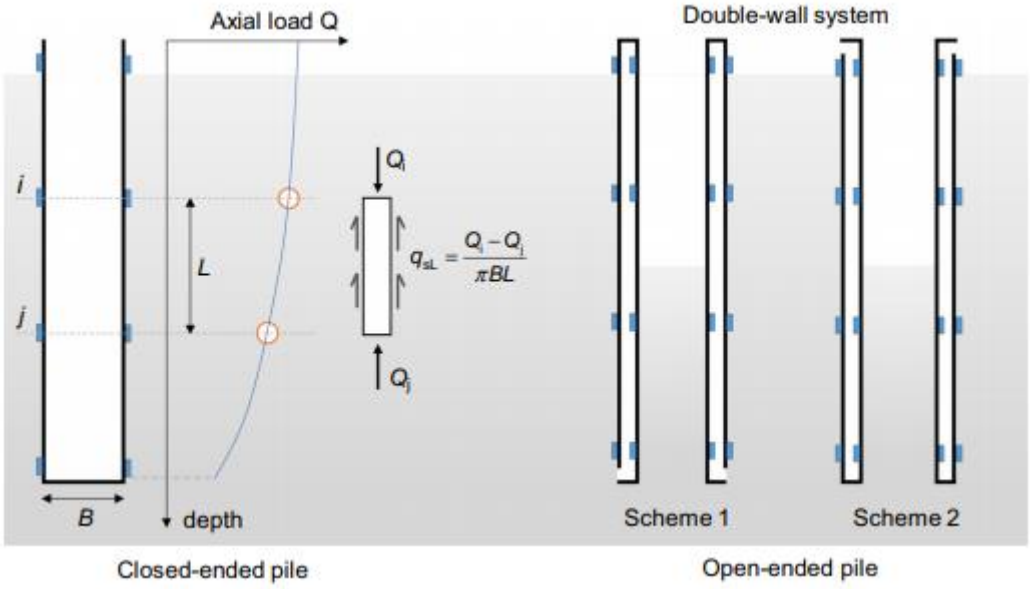

Fig.2. 48 Closed-ended and Open-ended pipe piles [95]

The study evaluates the comparison between solid and hollow-ended pipe piles in terms of load response, driving resistance, base resistances, and profiles of the unit shaft. The CPT-based pile design evaluated through a layer-by-layer evaluation of the predictable resistances

compared to static load tests. Han et al. [95] present the load–settlement curve for closed-ended and open-ended pipe piles (Fig.2.50). The load transfer- unit shaft resistance was achieved from the static load test [94-95].The resistance of the test pile was measured using cone penetration test and then compared with static load test. The results show that plug resistance increased very slowly initially and increased significantly after displacement accomplished 30 mm. Further with pile movement, the plug densified due to resisting force the plug resistance builds up.

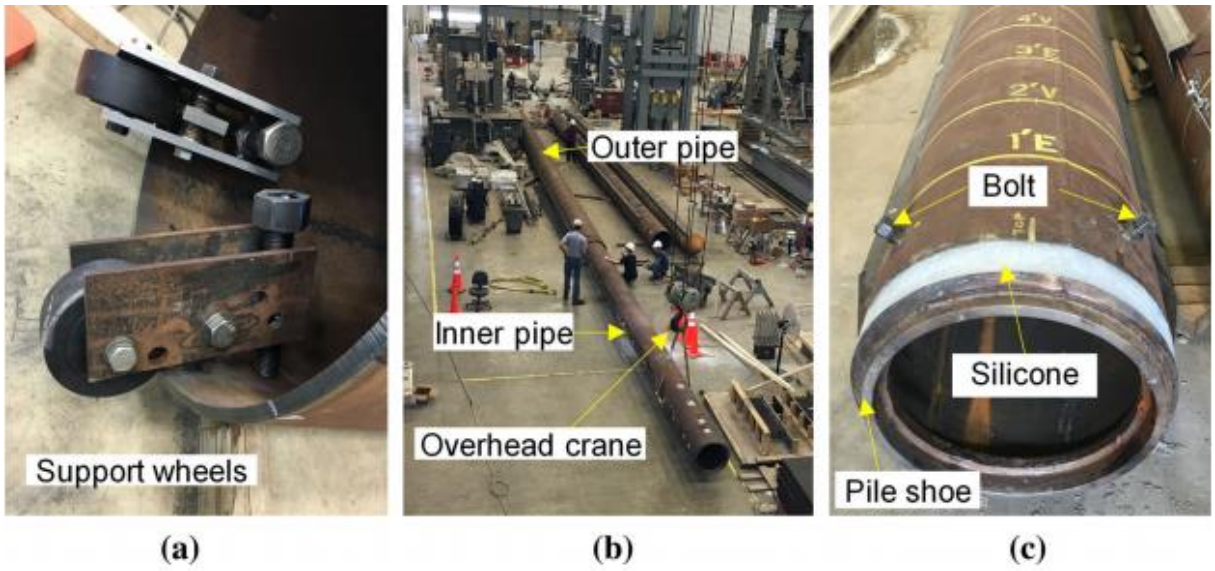

Fig.2. 49 The open-ended test pile: two support wheels attached to the top of the inner pipe; (b) sliding of the inner pipe into the outer pipe with the assistance of the overhead crane; (c) details at the base of the open-ended test pile [94-95].

Using the concept of helical anchors in conventional nailing techniques evolve an updated type of nail called helical soil nail. The helical anchors are different from the helical nail from the application and working point of view. The helical pile/anchor is installed vertically, while helical soil nails are installed horizontally and the distribution of confining soil stresses is not similar for both types of elements, resulting in failure mechanisms for both cases become different (Fig.2.50). From Fig.2.50, evident that soil nail is a passive element that acts as a fastener between two zones (active and passive) of soil slope during soil deformation. As the soil mass deforms in the active section, resulting there is generation of tension force in the passive section. In other words, the deformation of soil mass in the active region is the action over the nail, while resistance force in the passive region against the deformation is considered as a reaction due to soil nail interaction. Thus, soil nails are post-tensioned elements requiring soil movement for mobilization of reinforcing action, while helical

anchors/piles which are pre-tensioned elements. Alternatively, helical piles/anchors principally act within the active earth pressure zone during failure [8-9]. The difference between helical soil nails and helical piles/anchors is clear from Fig.2.50 (a, b). Moreover, the pullout mechanism of the helical nail is different from the helical piles/anchors. However, the pullout resistance of helical nails can be realized to enhance by utilizing the helices for easy installation and additional bearing resistance [96-102]. The pullout is considered a vital parameter for the design of soil nail walls. Few researchers investigate the effect of overburden, nail length, and surface of the shaft on the pullout-resistance of the helical nail (HN) [14-16, 96-102]. The study reported that the performance of a helical nail is superior to the conventional nail.

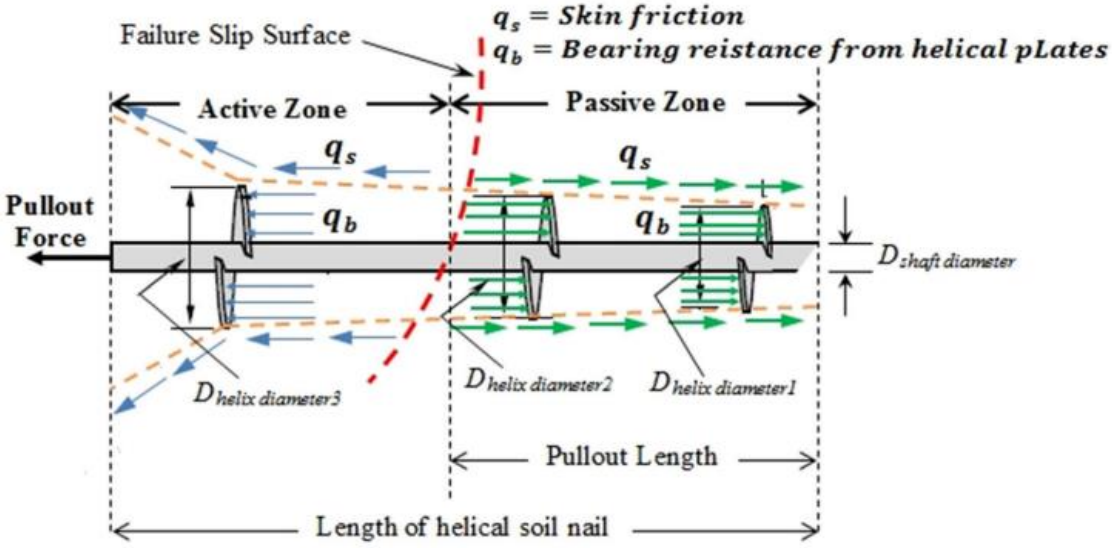

(a)

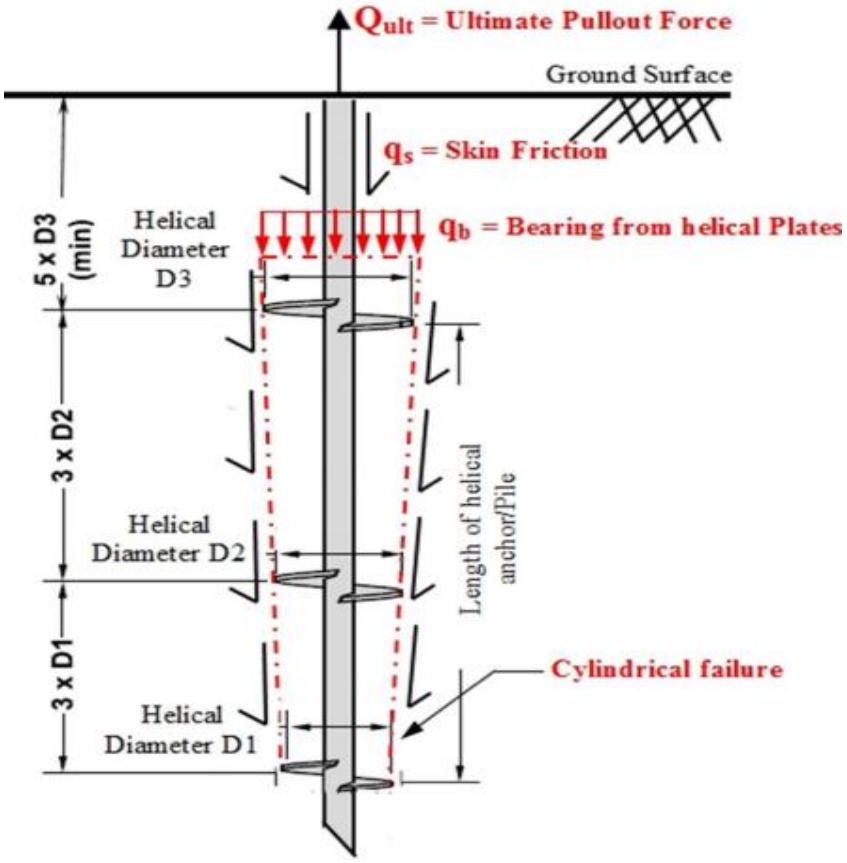

(b)

Fig.2. 50 (a) Load transfer mechanism helical soil nails (b) helical anchor/pile [96]

2.3.5 PREVIOUS STUDIES ON HELICAL SOIL NAIL

Tokhi [14] conducted an experimental study on a novel screw soil nail as shown in Fig.2.51. The study investigated the parameters like water content, shear strength, and maximum and minimum density and grain size analysis. The particle size distribution curve reveals that the soil is fine sand. The direct shear tests were conducted to determine the strength parameter of the soil sample under varying normal pressure ranging from 25 to 100 kPa. The angle of internal friction for the soil sample was found to be 36˚. The dilation effect in the study was considered negligible in the study. The study was conducted to incorporate the installation difficulties of conventional soil nail-like improper drilling, the existence of cavities, improper grouting pressure, etc. Tokhi [14] develop screw soil nails by considering the design philosophy that allows the easy installation of nails such that increase the soil-nail bond strength. The screw nail offers the controlled installation torque and penetration rate, thus can be successfully adopted for retaining structures and earthwork. The main purpose of

introducing screw soil nails is to increase the soil-nail interaction without compromising the pullout capacity and to reduce the soil disturbance.

Fig.2. 51 Screw nail (after Tokhi [14])

The goal of this study was to investigate the fundamental mechanism of news multi-plate helical soil nails in loose sand. The study investigates the fundamental interface mechanism of screw soil nails and has made attempts to describe the failure zones of sandy soil using a color band using a fabricated pullout box as shown in Fig.2.52. The dimension of the test tank was adopted as 1.5 m **X** 1 m **X** 1 m, which is fastened with frame assembly using bolts joints. The tank opening was located in the front plate of the tank with a 150 mm diameter of the hole. The surcharge pressure was applied to the soil sample with help of a pneumatic jack. The controlled pullout rate of the nail actuator was maintained as 2 mm/ min. The load-displacement curves for different overburden i.e. 20 kPa, 35 kPa, and 75 kPa were observed as 16 kN, 19 kN, and 24 kN respectively, beyond displacement less than 30 mm. The test results reveal that an optimal shear mechanism was developed due to high soil-nail adherence. Due to substantial soil-nail bond strength, the helical soil nails are highly suitable for the earthquake-prone region. Moreover, the results indicate that the pullout capacity of screw nails is significantly greater than grouted nails. The effect of geometry configuration of screw nail specimens' creates different soil stresses around the screw nail. Moreover, the laboratory test reveals that contrary to the grouted nail the pullout capacity depends on the surcharge pressure. The study also observes the in-situ stresses of soil during pullout of soil screw soil nail. The vertical load cells were placed at 100 mm over the bottom of the tank, while horizontal cells were located about 400 mm from the base of the tank respectively [14]. The observed in-situ stresses are then plotted against time. The positive value shows the tension while the negative value represents the compression. The stress distribution behavior of screw

nails is found un-symmetrical in mutually perpendicular directions. The stress distributions were significantly increased with increases in compression.

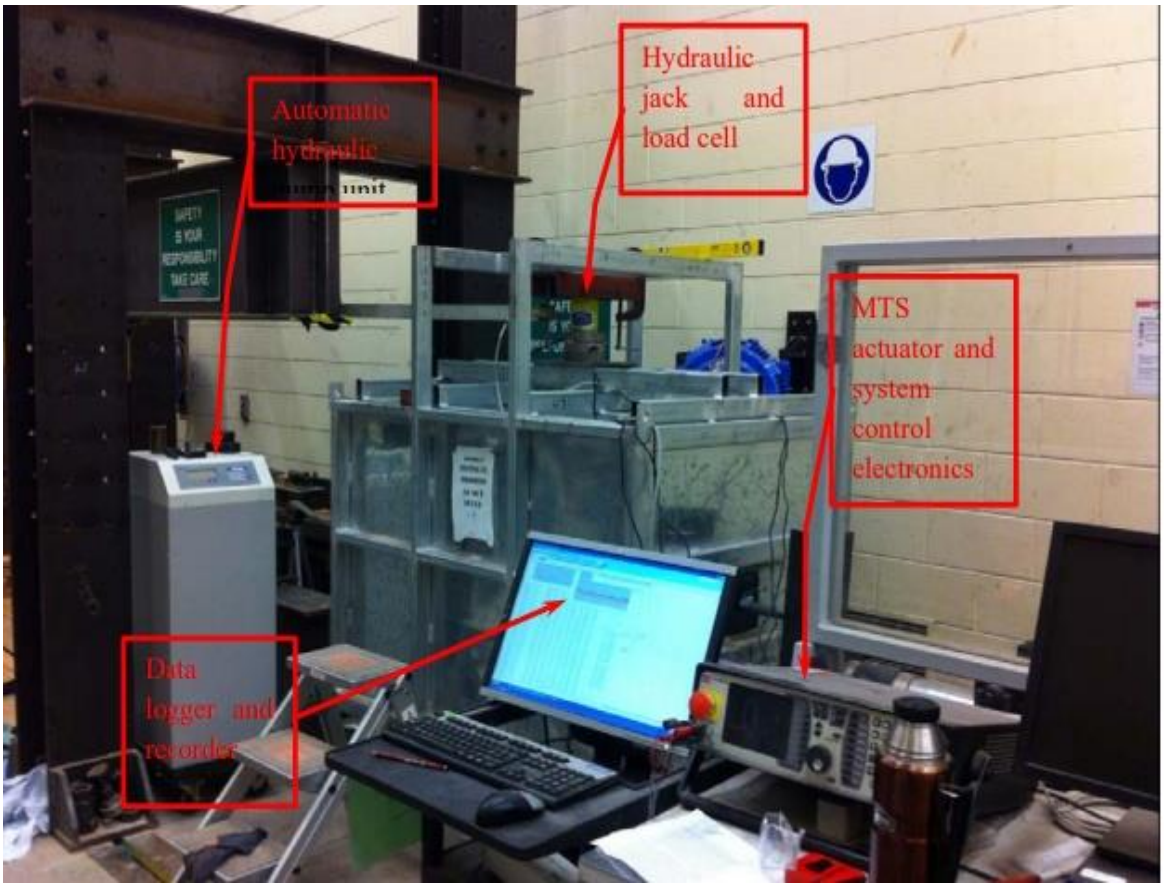

Fig.2. 52 Laboratory testing apparatus and set up (after Tokhi [14])

Estimation of the pullout strength for the screw soil nail when compared with a conventional nail which shows better performance of screw nail. This may be due to fact that helical soil nails improve the soil around the helices in dense soil, resulting in actual failure surface shift deeper into the surrounding soil. It is also clearly declared that pullout capacity does not only depend upon soil nail but also depends upon the shear strength parameter of soil. The test results predicted that a failure plane expands to a definite radial path from the soil–nail interface, and follows the Mohr-Coulomb failure condition [14]. The laboratory tests are validated by using FEM analysis, which depicted a similar failure mechanism with plastic strain generated primarily following each helical plate [14-16]

Sharma et al. [15] investigated the installation torque and pullout capacity of helical soil nails in dry dense sandy soil. The study was conducted by varying numbers of helices, helical pitch, and surface type. Laboratory testing apparatus used by Sharma et al. [15] is shown in Fig. 2.63. The pullout test setup of was designed and developed by the Council of Scientific

and Industrial Research – Central Building Research Institute (CSIR–CBRI), Roorkee, India. The pullout setup contains four major parts i.e. pullout machine, test box, overburden pressure application system, and data logger. The pullout machine of anchors and soil nails enables to pull of the soil nails at a controlled displacement rate. The maximum and minimum strain rates of the device were given as 70 mm and 0.7 mm/min respectively. The least count of strain rate of the device was given as 0.01 mm/min. The peak pullout capacity of the machine is 45 kN with a least count of 0.01 kN [15]. The machine was able to drive and pull the helical soil. Further, nail allows the measurement of installation length and pullout displacement of nail during the operation using linear variable displacement transducer (LVDT). The tank size adopted by Sharma et al. [15] was given as 2 m **X**1.5 m **X**1m. The test tank was made up of solid steel boundaries as shown in self-explanatory Fig.2.53. The study adopted the minimum tank dimension size 10 times greater than the maximum size of helices to make the side effect insignificant. The overburden pressure application system includes 3 hydraulic jacks placed over the 25 mm thick steel plate, which is placed over the soil sample to distribute the equal surcharge pressure to the sample. The jack applied the pressure by a mean of reaction against the portal frame. The study was conducted over river sand which is classified as poorly graded sand. The nail diameter was adopted in the study was 16 mm, which is obtained by scaling down the peak field nail diameter by 5.55. The overall and effective length was 1124 mm and 900 mm respectively. Moreover, the study satisfies the condition for no scale effect as per the previous literature. The study was conducted over the nail with single and double helices with smooth and rough shaft surfaces. The sand mediums were filled in the tank in sequence of 50 mm elevation to achieve the relative density of 75%. The soil sample was left untouched for 24hours to attain initial stress after the application of load over the sample. Then the soil nails were driven into the soil mass with an installation speed of 1 to 1.5 rpm for different nail samples. Similarly, after installation the nail was again left for 24 hours then the operation of pullout was performed. The tests were repeated over different nail specimens under varying pressure. The load-displacement data were recorded in the data logger up to 60 mm pullout displacement. The study found no peak point in load-displacement curves for different specimens, thus adopted the peak pullout capacity at a spot beyond which the proportion of change in pullout resistance to change in displacement becomes minimum. Tests results reveal that roughness of the surface significantly influences the ultimate pullout resistance capacity of the helical nail. The maximum pullout load was found in a linear relationship with increases in surcharge pressure. Moreover, helical nail with unequal

diameters keeping other geometry of nail constant shows higher pullout capacity to the nail with a uniform diameter. The position of the helices and inter-helices spacing of nails play a significant role in the pullout capacity of the helical soil nail.

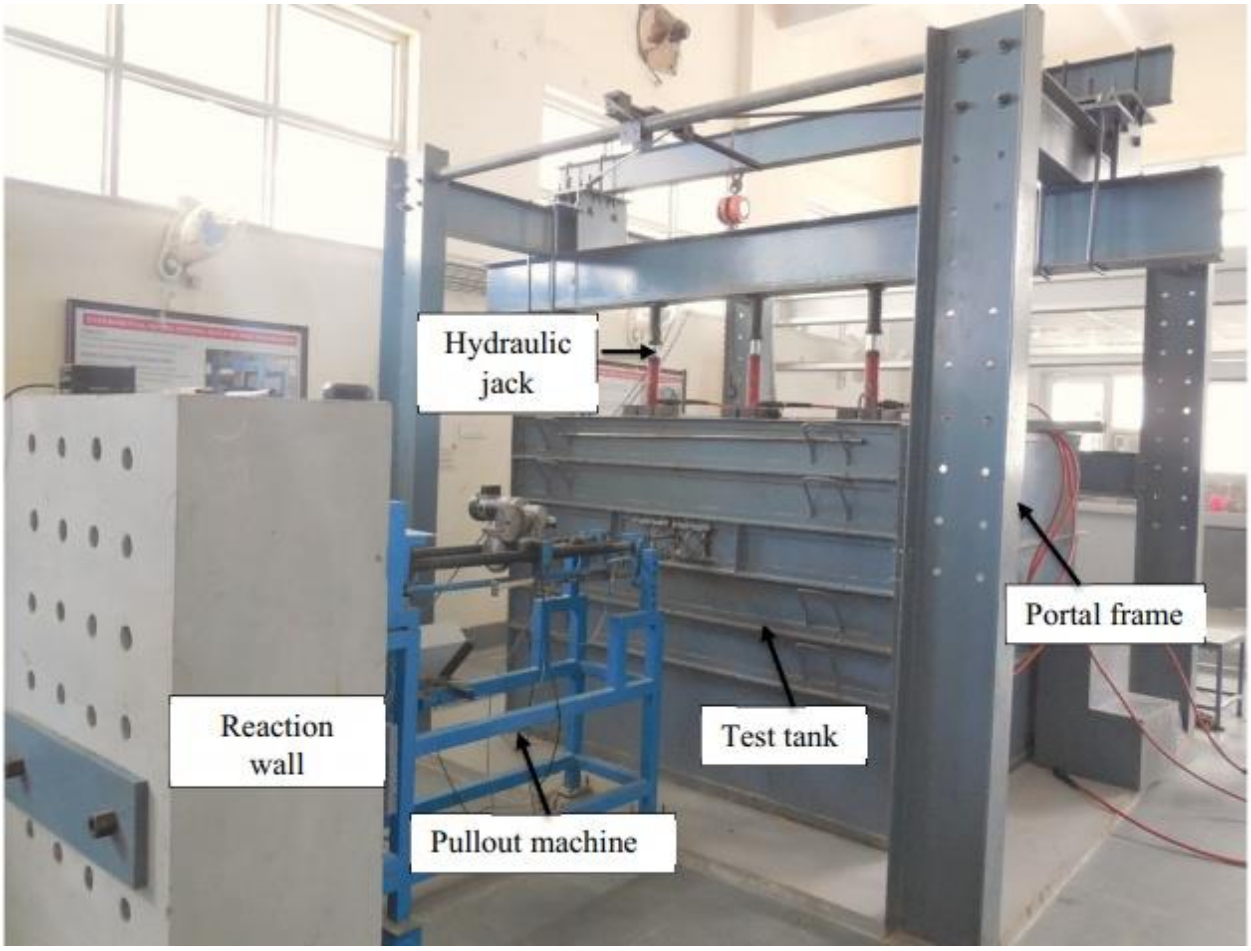

Fig.2. 53 Laboratory testing apparatus (after Sharma et al. [15])

The study reported that roughness of nail increase the pullout capacity of nail. The mobilization and the interlocking of soil particles are leading shearing mechanisms for rough nail which dependable for the mobilization of higher pullout strength. Sharma et al. [39] investigates the influence of static and seismic conditions on soil nail structure. Based on experimental tests a pullout capacity equation has been developed which afterward adopted for the stability analysis of soil nail wall structure. The different geometric and soil parameters are evaluated for static and seismic conditions. The factor of safety (FOS) predicted by using theoretical and experimental base are lower than the FOS obtained using pseudo-static and pseudo-dynamic values.

Rawat and Gupta, [103-107] investigated the behavior of modern screw nails as shown in Fig.2.54 The model nail specimen of the nail has been tested at a slope angle of 45˚ and 90˚ with horizontal. The size of the model test tank is made up of perspex sheets having a dimension 0.6m**X**0.94 m**X**0.96 m. Artificial soil slopes were developed using the sand raining technique to achieve a unit density of 16.5 kN/m3 for each slope.

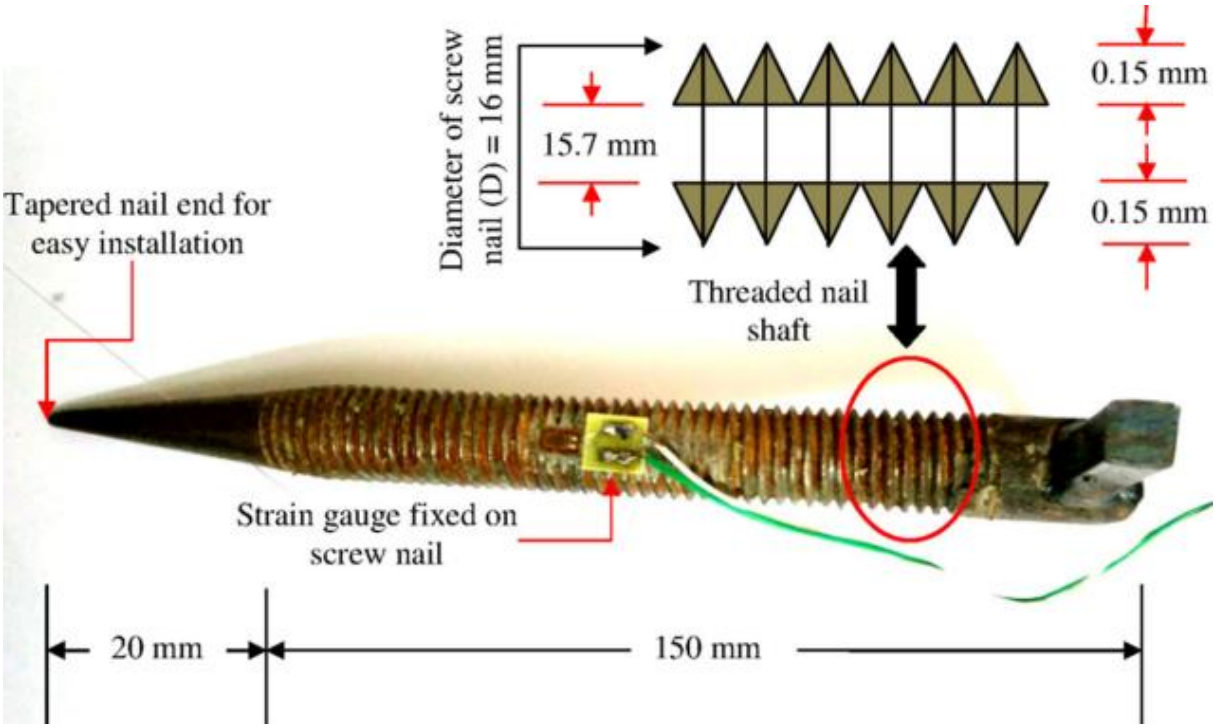

Fig.2. 54 Screw nails [16]

The modeled screw nails were tested under Universal Testing Machine (UTM) with increasing surcharge load at slope crown. The distribution of pressure ensured uniform throughout the soil sample. The test result yield load-settlement along with strains generated in the nail element during testing values on the soil slope. It is found that with an increase in the surcharge pressure shear strength of soil slope is mobilized resulting formation of slip circle occurs towards slope face. The local cracks were found to develop on weaker zones of the slope. Due application of surcharge pressure shows mobilization of interface shear force between the two interfaces, reveals the load-transfer mechanism of the soil-nail system. In addition, a factor of safety of soil nail system has also been evaluating using limit equilibrium methods (LEM) (Slope/W). Further tests are evaluated using finite element (FEM) (Plaxis 2D) to evaluate the load-displacement characteristics of volumetric deformations, potential slip surfaces, and factor of safety of screw nail. The laboratory test results are in good

agreement with LEM and FEM methods. Rawat et al. [105] investigated the pullout behavior of helical nail assuming circular discs as helical plate using finite element analysis using Abaqus/Explicit routine. A soil nail may be located at diverse angles with horizontal within the soil mass. The different helical nail shaft diameters were simulated using FEM analysis. The specimens with different helix diameter to shaft ratio were simulated by using Plaxis 2D. The study assumes the circular disc as a helical plate. The tests were simulated for an overburden pressure of 20kPa on a soil sample [103-107]. The general model of screw nail was simulated in the analysis is shown in Fig.2.55

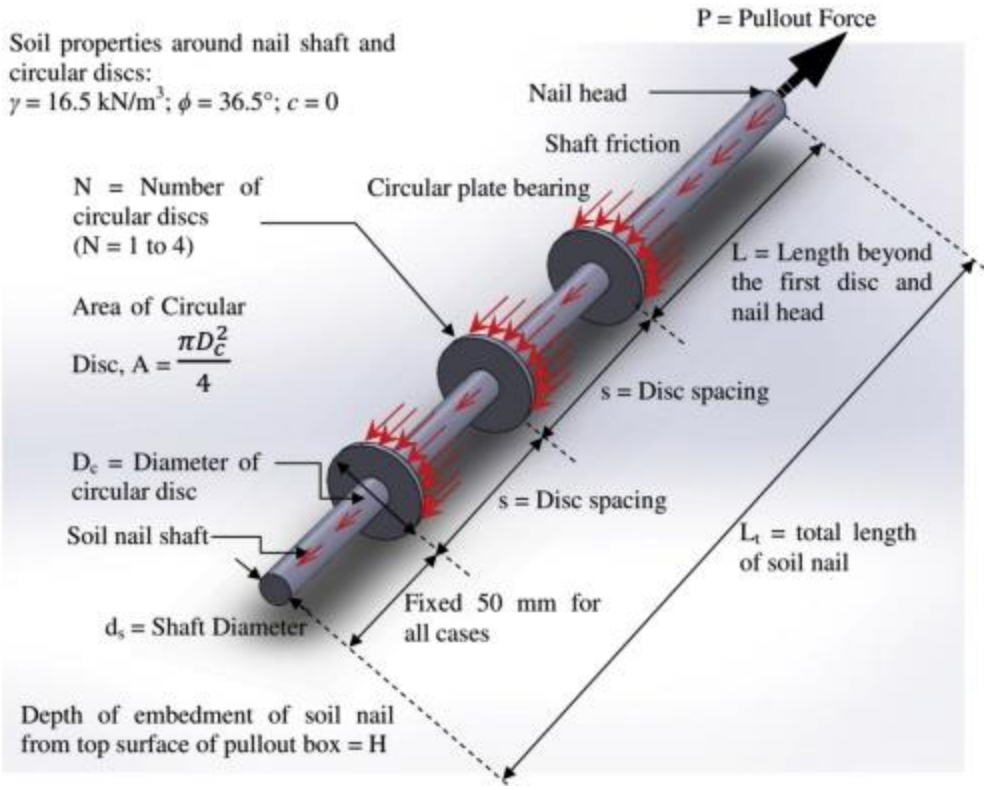

Fig.2. 55 Model of screw nails [106]

Results show that the shear-stresses produce around the soil-nail interface throughout its anchorage length. The shear stresses are transferred as mobilized tensile forces in the nail shaft. A total of 67 simulations tests programs were run with varying geometric configurations by keeping the surcharge pressure constant of 20kPa on the nail. The pullout load-displacement, failure mechanism, and soil stresses were investigated in the soil mass. Moreover, the various dimensionless factors like embedment ratio, diameter ratio, anchorage length ratio, etc were also studied. The test results indicate that the pullout capacity found increases significantly with the addition of circular discs to the nail shaft. Also, with additions

of discs pullout capacity increases significantly because of bearing resistance offered circular disc. Rawat and Gupta [107] investigated the failure surfaces for different helical soil nail along with the pullout mechanisms. The result shows that pullout capacity is directly proportional to number of helical plates. The ratio of plate spacing to the plate diameter ($\frac{s}{D_h}$) are found directly proportional to the pullout capacity up to a peak value. The test result shows that as ($\frac{s}{D_h}$) ratio increases beyond 3 the failure envelope changes from cylindrical shear failure to individual plate failure. The plate starts acting independently without disturbing inter-helical soil as shown in Fig.2.56.

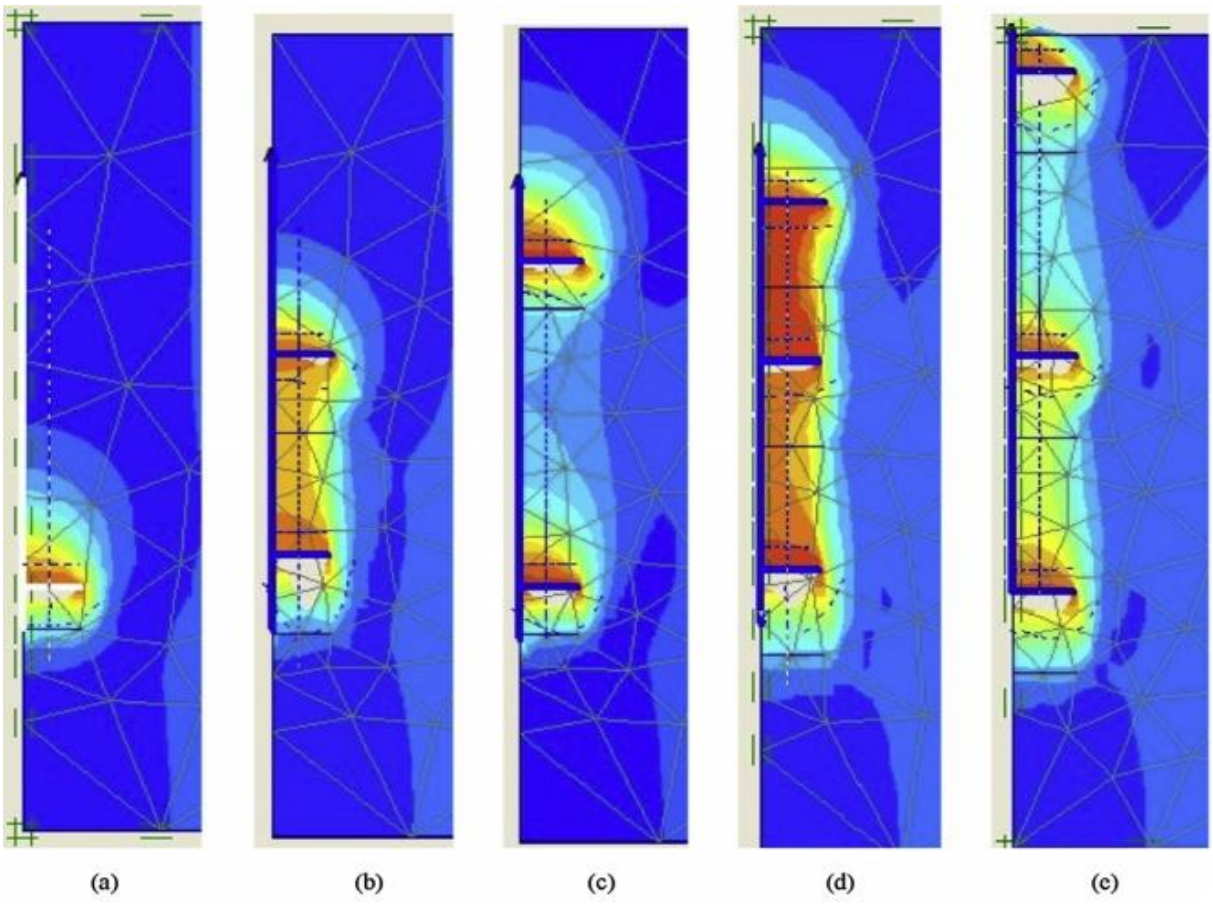

Fig.2. 56 Failure mechanism with different spacings of helical plates: 1-H; (b) 2-H at $\frac{s}{D_h}$=1.5; (c) 2-H at $\frac{s}{D_h}$ =3.5; (d) 3-H at $\frac{s}{D_h}$ =1.5; and (e) 3-H at $\frac{s}{D_h}$ =3.5 [107]

Table 2. 3 Summary of the pull-out capacity of helical soil nail model tests

Author	Year	Pullout dimension(m)	Instruments	Nails	Parameters Investigated	Inclination	Conclusions
Tokhi	2016	1.5 **X** 1 **X** 1	1) Data monitoring and logging system, 2) Model box with overburden pressure application system, 3) Pull -out system	Helical soil nail and grouted nail	Number of helices, overburden pressure, and bending stresses	0º	Pullout capacity of helical soil is considerably high than conventional soil nail.
Sharma et al.	2017	2**X**1.5 **X** 1	1) Data monitoring and logging system, 2) Model box with overburden pressure application system, 3) Installation torque 4) Pull -out system	Helical soil nail	Roughness of the nails, overburden pressure, number of helices	0º	A helical soil nail with double helices of unequal diameter show higher pullout capacity than nail having double helices with same diameter.

2.3.6 RESEARCH GAPS

Based on the elaborative literature study on conventional and helical soil nails, the following research gaps were found that lead to the establishment of the objective of the present study.

Research Gap 1: Effect of shaft diameter and shaft type (solid and hollow) on installation torque and pullout capacity

Based on the literature survey investigated to date as per the best of author knowledge, there is not even a single study that investigates the installation torque and pullout capacity of the helical nail with a varying shaft diameter of the nail. Moreover, the nail studied till date is with solid shaft only. No such study was carried by any researcher on hollow shaft helical soil nail and plugging effect of hollow nail. Moreover, previously available studies didn't explain the critical helical pitch and number of helices for a helical soil nail.

Research Gap 2: Group pullout of helical soil nail

The available studies on helical soil nails are mainly explaining the effect of influencing parameters on individual helical soil nails. The single and group nail behaves differently inside a soil mass with varying conditions. Keeping the research gap in mind present study feels the need to frame the objective to investigate the group pullout capacity of helical soil nail to simulate actual condition.

Research Gap 3: Requirement of analytical study of helical soil nail

Insufficient laboratory and numerical investigation are published by a few researchers to investigate the pullout study of the helical soil nails. To predict more close results of critical pullout resistance or reliable result from the design point of view, an analytical study has also been found essential. Therefore, considering the influence of geometric configuration of nails and soil properties an analytical study is beneficial for the design or execution purpose of the helical soil nail.

2.3.7 OBJECTIVES OF RESEARCH WORK

Following objectives are framed for present research work on basis of literature survey and research gaps:

Objective I

To investigate the installation torque and pullout capacity of hollow and solid shaft helical soil nail along with varying configuration namely nail diameter, helices pitch, helix diameter, helix spacing, nail plugging, and nail inclination using displacement-controlled pullout device.

Objective II

Investigation of installation torque and pullout capacity of group helical soil nail with different Spacing arrangement.

Objective III

Theoretical modelling of installation & pull-out capacity of helical soil nails

Objective IV

To examine the field application of helical soil nail as a landslide mitigation potential measure: A Case study

CHAPTER-3

EXPERIMENTAL PROGRAM

CHAPTER 3

EXPERIMENTAL PROGRAM

3.1 General

The chapter contains the details of the experimental setup, materials, and methods adopted in the present study. The chapter also contains fabrication of laboratory setup, nail, and instrumentation used during the testing. Detailed procedures of installation and displacement-controlled pullout test along with the testing program are also elaborated. Moreover, the chapter also presents the installation torque, pullout capacity of single, and group of helical soil nails.

3.2 Basic Assumptions and Limitations of the present study

- The present solution is valid for only dry, isotropic, and homogeneous *cohesionless soil*.
- The study was not conducted for the *saturated soil* sample.
- The effect of dynamic or cyclic loading was not taken into account. The results are valid for static conditions only.
- In theoretical modelling, the effect of *displacement rate* and *revolution rate* was not incorporated.

3.3 Material

The materials used in the current study are briefly described in the following subsections.

3.3.1 SOIL SAMPLE

The river sand was collected from a stream of Satluj river close to Bilaspur (H.P.) India. The cohesionless soil contains angular, rounded to sub-rounded particles in it as shown in Fig.3.1. As per IS: 2720 – 4 (1985) [108] the soil sample is classified as poorly graded sand (SP) as shown in Fig.3.1. The maximum dry unit weight and optimum moisture content were calculated using a light compaction test as per IS 2720-7 (BIS 1983) [109] as shown in Fig 3.2. Also, Field unit weight was measured in a loose state using the core cutter method as per IS 2720-1975/88 (Part XXIX) [110]. Moreover, as per IS 2720-13 (BIS 1986a) [111] the angle of internal friction was calculated as 37.9º as shown in Fig.3.3. The fundamental properties of the soil sample are listed in Table 3.1.

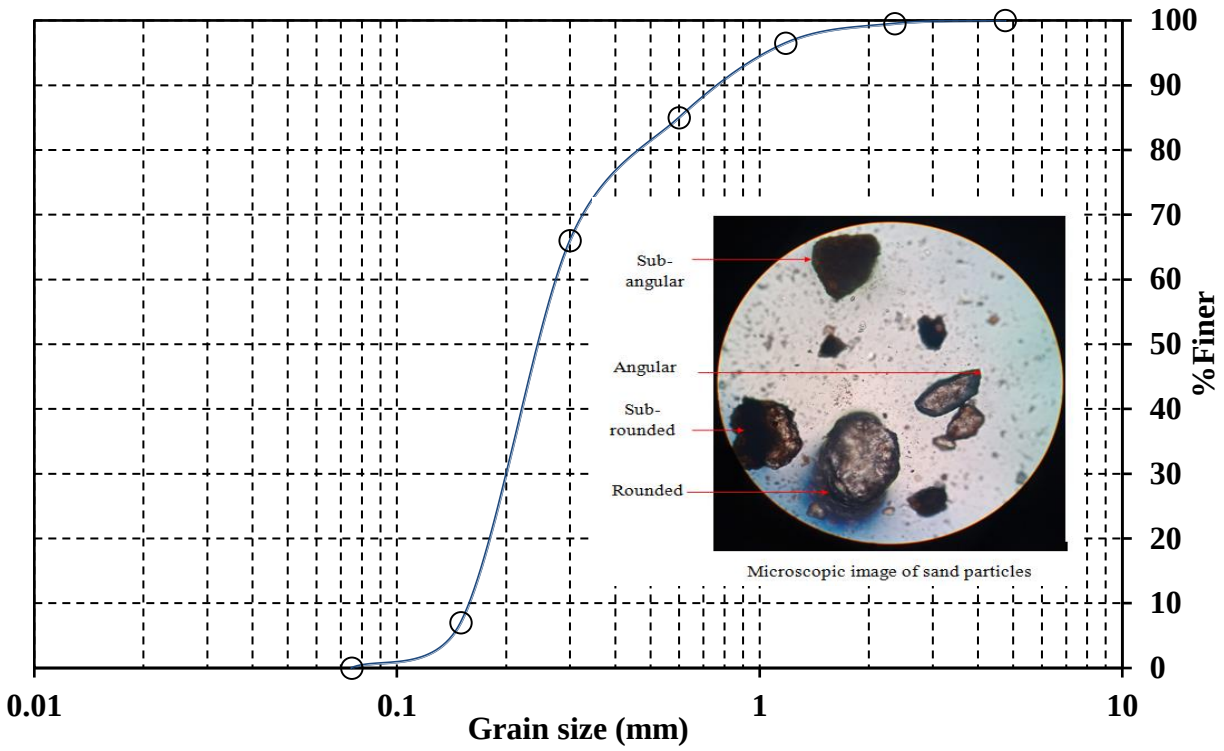

Clay	Silt	Sand	Gravel

Note: D_{50}, average grain size. D_{10}, D_{30}, and D_{60} are the soil grains diameter where 10%, 30%, and 60% of the particles are finer than this size respectively

Fig.3. 1 Particle size distribution of soil sample

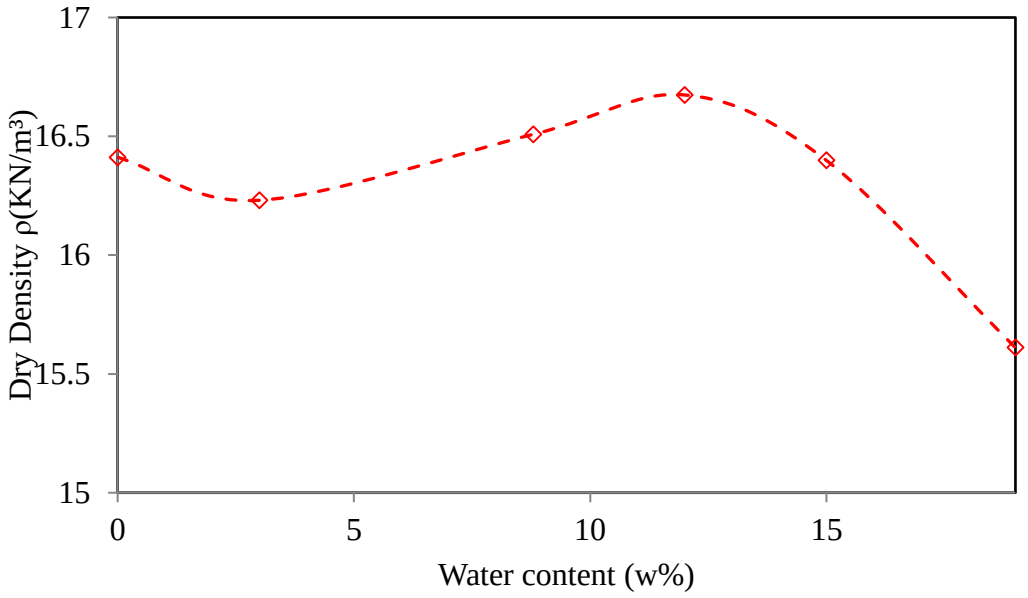

Fig.3. 2 Maximum dry density with water content

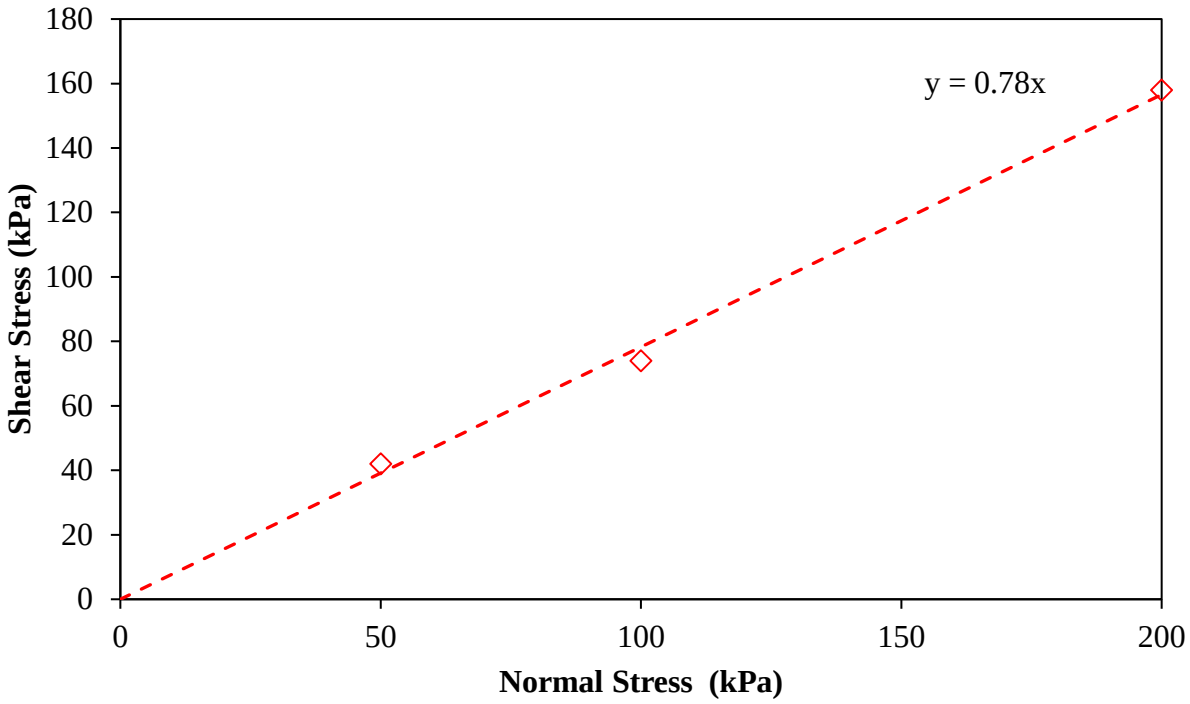

Fig.3. 3 Variation of shear stress against normal stress

Table 3. 1 Fundamental properties of the soil sample

Property	Value
Specific Gravity, G_s	2.72
D_{60} (mm)	0.28
Average grain size, D_{50} (mm)	0.25
D_{30} (mm)	0.21
Effective size D_{10} (mm)	0.16
Coefficient of uniformity, C_u	1.75
Coefficient of curvature, C_c	1
Friction angle from the direct shear test, Φ (º)	37.9 º
Maximum dry unit weight, $\gamma_{d(max)}$ (kN/m³)	16.87
Minimum dry unit weight, $\gamma_{d(min)}$ (kN/m³)	13.13
Relative density, (R_D)	86.4%

3.3.2 INTERFACE DIRECT SHEAR TEST

The interface direct shear test was adopted for the rough assessment of friction angle between soil–nail interfaces. Usually, interface direct shear test was preferred for fast calculation of soil–nail interface friction. Previous studies [4,29] have recommended that interface-friction among soil and nail interface can be precisely measured through a direct shear device. Thus, in the present study direct shear box of size 60 mm **X** 60 mm was employed to examine the soil–soil and soil–nail interface friction values. To evaluate the soil-nail interface friction, furnish a well-documented draft that recommends the nail location in the region of incremental tensile strains developed in the soil during shearing. The incremental tensile strains can be attained by adjusting the nail element at an inclination of 25˚ (θ = 25) from the perpendicular directions (Fig.3.4a). The interface direct shear test was conducted at a strain rate of 1 mm/ min. However, the interface direct shear test is only simulating two-dimensional conditions, in which the rupture surface is already known and always horizontal in the shear test. This rupture plane may or may not be the direction of the weakest plane in the soil, thus it may reveal wrong results. There are stress concentrations at the boundary of the sample found to be non-uniform distribution on the rupture plane. Also, the area of the specimen under normal and shear loads does not remain uniform. Thus, the calculations of normal and shear stress made based on the constant nominal area of the specimen are inaccurate [13,77]. In the nutshell, the actual field conditions cannot be simulated accurately by the interface direct shear test. The test is simple and may be adopted for quick estimation of interface friction of conventional soil nail and completely unsuitable for helical soil nail. Thus, to simulate the three-dimensional condition for conventional and helical soil nail pullout tests is found more suitable to estimate the interface friction angle between soil and nail [13, 77]. The outcomes of unreinforced and reinforced direct shear tests of different types of interface are presented in Fig.3.4b. Evident, from Fig.3.4b the shear strength parameters of soil–soil and soil-nail interfaces. The soil–soil interface reveals a higher Mohr-Coulomb failure envelops in comparison to different soil-nail (soil–solid rough shaft; soil–solid smooth shaft, and soil–hollow smooth shaft) interfaces. The tests result in a show that soil–nail interface will mobilize before the soil-soil interface during failure. Evident from Fig.3.4b that with the

addition of reinforcing element the normal stress increases resulting increase in overall shearing strength which reveal Eqn. (3.1) as:

$$\tau_{\text{reinforcement}} = \frac{P}{A_S}(\cos\theta \tan\phi + \sin\theta) \tag{3.1}$$

The additional shearing strength is due to the mobilized friction angle (ϕ) represented by the 'tanϕ' component in Eqn.3.1.The mobilized angle of internal friction of soil sample was found equal to ϕ = 38°, while from the different interface the soil–solid nail with rough surface mobilized at interface friction (δ_i) of δ_i = 31°. Thus, an increase in shear strength is because of nail element mobilizes interface friction and adhesion components so rising the ultimate strength of the composite soil. The mobilized shear strength for each solid and hollow bar in the soil medium is mobilized at δ_i = 19°. However, the adhesion obtained for the solid bar is found to be more comparative to the hollow shaft, resulting in shear strength offered by solid nail found to be more comparative to hollow nail. In addition, evident that as the surface roughness increases the interface friction also increases while adhesion is found to decrease. Reinforced soil under shearing state reduces the interface friction angle enables early mobilization of nail forces which produce additional shearing resistance, increasing the ultimate shear strength of the soil. For unreinforced soil (soil only) the mobilization of peak angle of internal friction will occur rapidly under low tensile strains resulting in soil failure. For the simplification, the mobilization of stresses in the soil-nail interface is calculated with a dimensional less factor termed as interface reduction factor (f_δ). The interface reduction factor is equal to the ratio of friction angle (δ_i^o) between the interfaces to the angle of internal friction of soil (ϕ°). For f_δ < 0.5 and f_δ > 0.8 is considered as smooth and rough surface respectively. The interface reduction factor found for the different interfaces is given in Table 3.2. Evident from Table 3.2, the interface reduction factor for smooth as well as rough shaft are in the suggested limit by Wang and Richwien [29]). Evident that f_δ values for the rough and smooth shaft (solid and hollow) are within the suggested limits. Clear that different solid and hollow nail shafts in the soil are adopted, the shearing is allowed by the reinforcement up to 50% of frictional resistance of soil is mobilized. In addition, also clear that shaft roughness increases the soil-nail interaction.

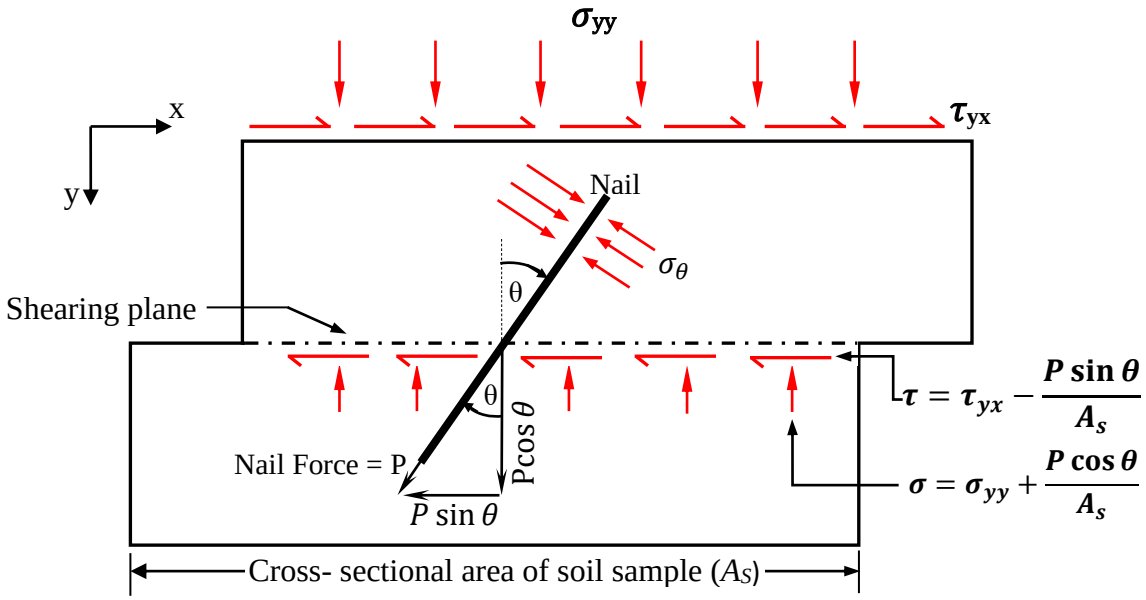

(a)

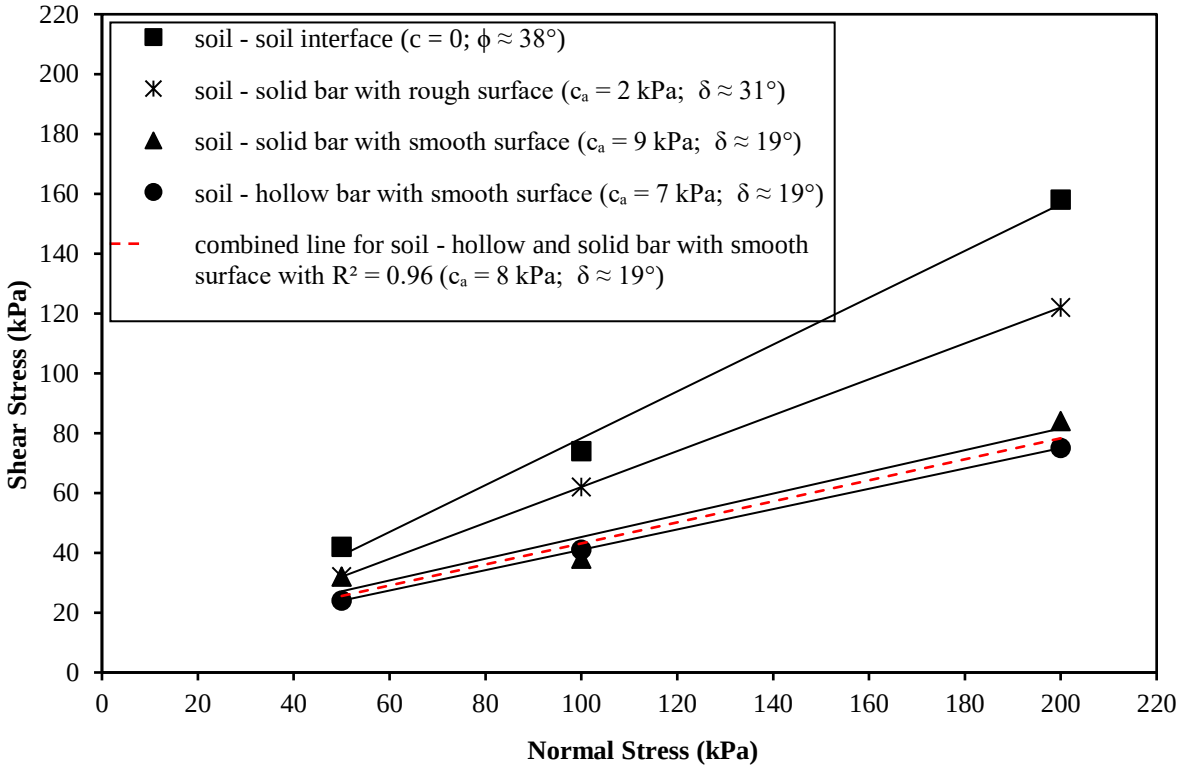

Fig.3. 4 ***(a)*** Direct shear test for soil nail reinforced sand ***(b)*** Shear strength parameters.

Table 3. 2 Interaction of different soil nail interfaces from direct shear test.

Type of interface	Interface reduction factor $f_\delta = \frac{\delta_i}{\phi}$
Soil- solid shaft with Rough surface	0.82
Soil- Solid shaft with smooth surface	0.50
Soil-pipe shaft with smooth surface	0.49

3.4 Scaling and fabrication of helical soil nails

The phenomenon of scale effect could distress the laboratory test results of the helical soil nails in cohesionless soil. The scale effect is explained based on two mechanisms: i) Influence of mean particle-size on nail shaft and ii) Influence of mean particle-size on helical bearing [89]. No scale effect is observed on nail shaft if the proportion of least shaft diameter (d) to mean grain size of soil (D_{50}) satisfies the given Eqn. (3.2) as:

$$\frac{d}{D_{50}} > 30 - 50 \tag{3.2}$$

Eqn.3.2 is only appropriate for the nail shaft, while for the helical plate the scale effects are more often associated with the effective radius of a helix (w_s), which is calculated as Eqn. (3.3)

$$w_s = \frac{D_h - d}{2} \tag{3.3}$$

Thus, for no scale effect on helical plate resistance, Schiavon et al. [89] recommended that the proportion of effective radius of a helix (w_s) to mean grain size of soil (D_{50}) is given by Eqn. (3.4) as:

$$\frac{w_s}{D_{50}} > 58 \tag{3.4}$$

For a helical element, no scale effect is observed if satisfies Eqn.3.2 and Eqn.3.4. Thus, for fabrication of helical soil nails in the present study with D_{50} of used soil as 0.25 mm, minimum shaft diameter comes out to be 12 mm such that d/D_{50} = 48 which lies within the range 30 – 50

(Eqn. (3.2)). Similarly, the diameter of helices is adopted such that for a 12 mm nail shaft, the effective radius of helix (w_s = 0.5(48 - 12)) is 18 mm, and the corresponding w_s/D_{50} ratio is 72, which is greater than 58 as per Eqn. (3.4). Similarly, the norm is also holding true for the rest of model shaft diameter of nail. Thus, the present study satisfying both the norms and it is assumed that the model test results have found no scale effect.

Deardorff et al. [112] and Perko,[9] suggested helical soil nail shaft and helical plate diameters for in-situ soil in the range of 38.1 mm to 88.9 mm and 152.4 mm to 355.6 mm respectively. The helix to shaft diameter ratio was fixed as 4 and 6 [8-9].To study the behavior of helical soil nails Rotte and Viswanadham [113] adopted a scale factor (k) of 5 to reduce the prototype soil nail size to obtain the model helical soil nail size as given in Eqn. (3.5)

$$d_m = \frac{d_p}{k} \tag{3.5}$$

where, d_m = model nail shaft diameter;

d_p = Prototype nail shaft diameter.

In the present study, various field diameters are scale down to model shaft diameter using a scale factor (k) of 5. In order to satisfy the conditions of no scale effect (i.e. Eqn.3.2 and 3.4) the scale factor (k) adopted equal to 5 as shown in Table 3.3. The model shaft diameters adopted in the present study are 12 mm, 14 mm, 16 mm, and 18 mm, respectively. In this study, hollow and solid two different shafts of helical soil nail were used to investigate the influence of varying parameters of the helical soil nail. The outer shaft diameter of both solid and hollow shaft was the same, while for hollow shafts helical soil nail the inner shaft diameter was taken as outer shaft diameter (d_0) – 4 mm thickness (t). The thickness of the hollow shaft wall was 2 mm and the weight of the hollow shaft nail was three times lesser than the solid shaft, while the outer diameter is constant for each case. The hollow shaft soil nail also allows the soil to move inside the shaft pipe. Hence, hollow shaft helical soil nail was also known as open-ended pipe helical soil nail. The diameter of the single and multi-helical plate varies from 48 mm to 96 mm. The thickness of helices was adopted 8 mm, while pitch varies from 24.5 mm to 41 mm. The full length of the model soil nail shaft was 1000 mm, while effective/installation nail length was l_e = 0.7H where, H = soil sample height (as per FHWA). The soil sample height in the present study

was 1000 mm, the thus effective length of the nail was 700 mm, and the additional nail length of 300 mm was used for fastening purposes of the soil nail. Perko, [9] and FSI, [8] reported that closely spaced helices $\left[\text{i.e.}\frac{\text{helical spacing(s)}}{\text{helical diameter }(D_h)} \leq 3\right]$ act as a single unit, and cylindrical shear failure is observed in the region of the helices, while the broadly spaced helices act separately$\left[\text{ i.e.}\frac{\text{helical spacing(s)}}{\text{helical diameter }(D_h)} > 3\right]$ and individual shear failure was observed. Thus, evident that change between cylindrical and individual shear failure occurs at a helical spacing of $2.5(D_h)$ to $3.5(D_h)$, where (D_h) is the diameter of the leading helical plate. Perko, [9] and FSI, [8] suggested the helical plate spacing of $3(D_h)$ for best results $\left[\text{i.e.}\frac{(s)}{(D_h)} = 3\right]$. Thus, in the present study helical plate spacing was adopted equal to three times the leading helical diameter. Also, the nail was beveled from the apex at an angle of 30° to facilitate easy installation along with placement of the first helix at 20 mm from the nail crown. The nail shafts adopted in the study are of circular cross-section and have smooth as well as rough surfaces. The HN specimens are made up of mild steel as shown in Fig.3.5.

3.4.1 ELASTIC MODULUS OF NAIL

The helical soil nails were fabricated by Regional Facility Centre, Solan (H.P) India. The industry reported the elastic modulus value for both solid and hollow shaft equal to 210GPa and 140GPa respectively.

Table 3. 3 Recommendation for no Scale effect for Model and Prototype

Sr. No.	Nail Identification with shaft type	Least Shaft Diameter (d) adopted (mm)				Helix Diameter, (D_h) (mm); D_h > 3d		Inter – helical spacing (s) (s/D_h = 3)		Pitch of helix (mm)		Number of Helices		Length of helical nail (mm) (Adopted L/H = 0.9)		For no scale effect			
																d/D_{50}		W_R/D_{50}	
		Model		Prototype		Model	Prototype	Model	Prototype	Model	Prototype	Model	Prototype	Model	Prototype	Model	Prototype	Model	Prototype
Individual Helical soil nail																			
1	Solid Shaft	16		80		64	320	192	960	15	76	3	3	900	3650	64	> 30 - 50	160	>58
						90	400	270	1200										
						96	480	288	1440										
2	Hollow Shaft	d_i	d_0	d_i	d_0	64	320	192	960	15	76	3	3	900	3650				
		12	16	60	80	90	400	270	1200										
						96	480	288	1440										

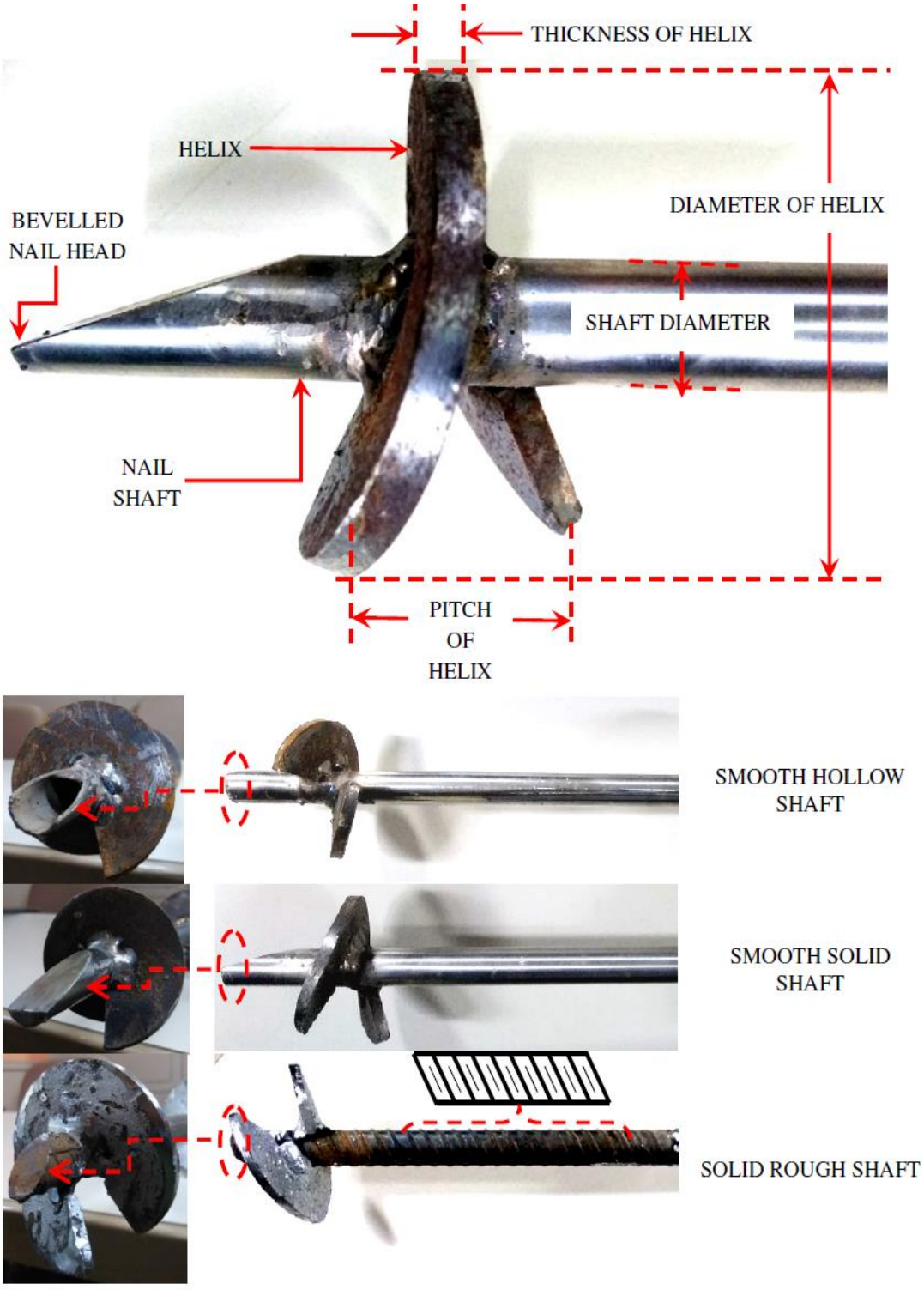

Fig.3. 5 Helical soil nails

3.5 Physical Model setup

The model setup of the pullout apparatus is designed and fabricated at the Jaypee University of Information Technology, Solan (H.P.) India (JUIT). The schematic diagram of the test setup is shown in self-explanatory Fig.3.6. The laboratory test apparatus comprises four main units: Installation and pullout device, surcharge application system, test tank, and Universal Data Acquisition System (UDAS).

3.5.1 INSTALLATION AND PULLOUT DEVICE

The installation and pullout operation of helical soil nails (HN) is conducted by the installation and pullout device, which includes two three-phase induction motors having 0.5 (horsepower) HP capacity. The first induction motor maintains a uniform rotation rate, while the other motor facilitates forward and backward movement of helical soil nails. The three-phase induction motor for installation consists of a driving head for providing the required torque and adapter to hold variable shaft diameter of HN. Each motor is coupled together to deliver installation torque and crowd force for the installation of HN in the test tank. For pullout operation, the alignment of the drive head is being locked and locating the device in the reverse way to cause the pullout of the nail. A load cell assembly was inserted among two motors that are further coupled to calibrated torque and pullout meter. The maximum pullout and installation capacity of the machine is 50 kN and 2 kN-m respectively (Fig.3.6). The least count of installation torque and pullout capacity was 0.001kN-m and 0.01kN respectively. The controlled pullout displacement rate of the device varies from 1 mm/ min (minimum) and 10 mm/min (maximum) [5]. The apparatus is also suitable for performing operations for nail inclination between 0˚ and 30˚ with horizontal. The production of apparatus has been as per specifications for field installation and pullout of helical soil nails. The device can revolve the nail under a variable revolution rate of 10 to 20 rpm installation rate. In the present study, the revolution rate was maintained at 10 rpm during the testing [96-100].

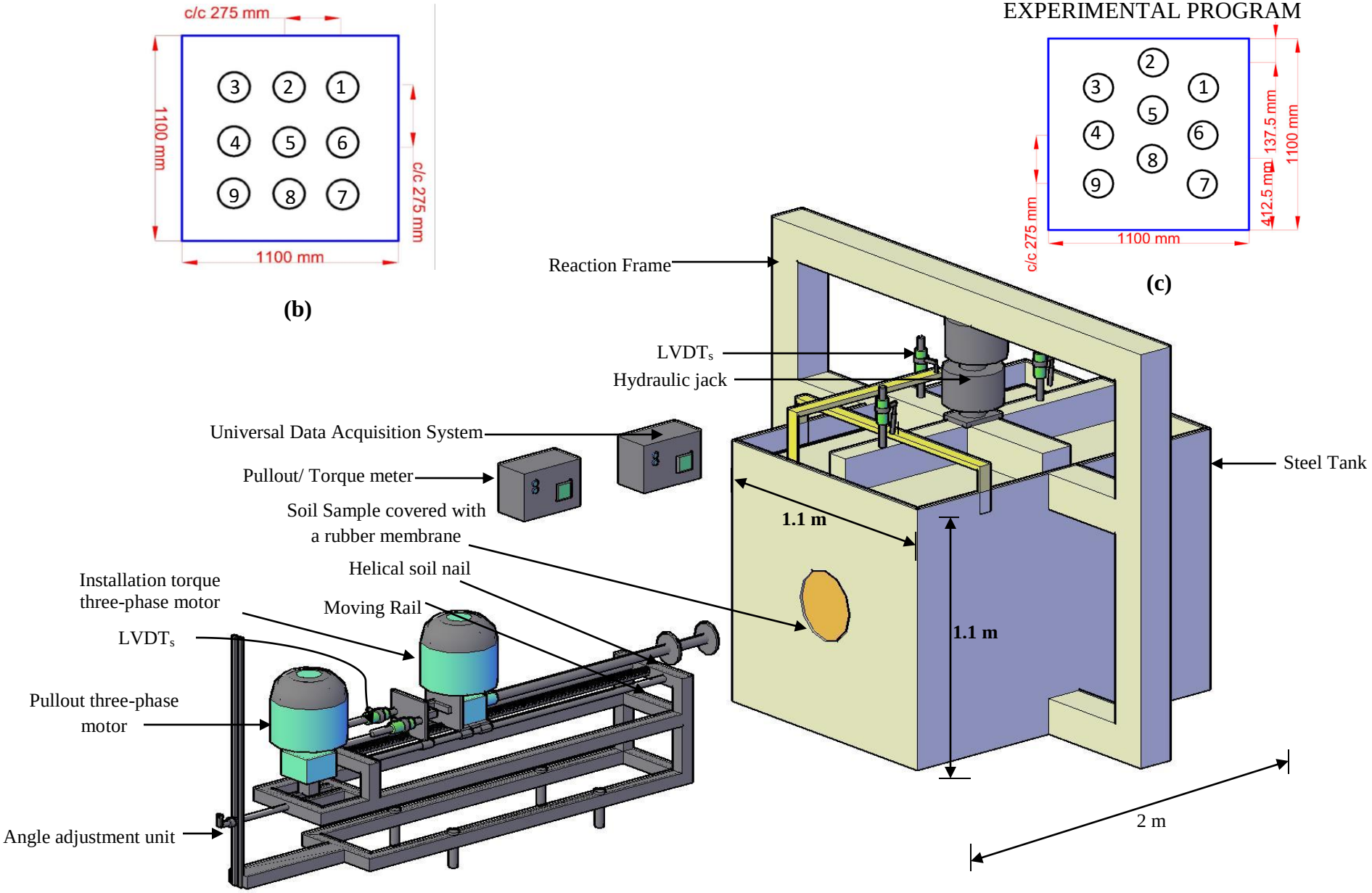

Fig.3. 6 Pullout system for soil nail (b) Group cap with uniform centre to centre spacing (c) Group cap with uniform centre to centre

The installation torque and pullout force were recorded and displayed by a torque/pullout meter (Fig.3.7) in real-time for the entire testing. The apparatus is licensed and Calibrated by the National Accreditation Board for Testing and Calibration Laboratories (NABL), New Delhi, India.

Fig.3. 7 Torque/Pullout meter

3.5.2 SURCHARGE APPLICATION SYSTEM

In the present study, a stainless-steel plate of 10 mm thickness was positioned as top cover to apply uniform pressure on the soil. The plate was stiffened with two I-sections laterally and longitudinally to avoid the deflection of the plate. A hydraulic jack having a capacity of 65 tons was used against a steel reaction frame for applying overburden pressure. The applied overburden pressures were estimated by load cell and recorded by data logger respectively. The different overburden pressures are selected for the investigation of installation torque and pullout of helical soil nail are 5 kPa, 12.5 kPa, 25 kPa, and 50 kPa respectively. The soil sample was left undisturbed for 24 hours such that it accomplishes stable stress conditions after initial consolidation. Though, the hydraulic jack was used for the continuous load application for long periods during testing imposed a limit of applying the highest surcharge pressure of 55 kPa only. The overburden pressure is considered as one of predominant factor which affects the pullout

strength of soil nail. Various researchers reported that pullout resistance is considerably reduced by the phenomena of arching action of soil under very high surcharge pressure as compared to rise in pullout capacity owing to soil dilatancy (GEO, [34]; 114-115). Hence, Geo [34] suggested an upper limit of surcharge pressure of 300 kPa for the estimation of pullout capacity in conventional nails. In view of this suggestion, various investigators adopted different ranges of surcharge pressure during model testing of conventional and helical soil nails as given in Table 3.4. Pradhan et al [70] and Junaideen et al. [10] conducted the model testing of grouted soil nails under an overburden pressure of 150 kPa to model a fill height of 6 – 7m. Thus, in the present research, a low confining stress corresponding to a fill height of 2 m is considered while testing pullout of helical soil nails under a maximum overburden of 50 kPa. To ensure the uniform load-transferring from top to bottom with load-steel model interfering, the reaction frame was designed as per IS 800:2007. As per IS 800:2007, the applied pressure will transmit from top to bottom without any disturbance if the deflection of beam's not exceeded than span (*l*)/250 [116].

Table 3. 4 Overburden pressure range adopted by various researchers during model testing of soil nails

S. No.	Overburden Range	Reference
1	5 to 25kPa,	[Tokhi,[14]]
2	5.6 to22.7kPa	[Milligan GWE, Tei K [51]]
3	40 to 300 kPa	[Su et al. [12]]
4	7.75 to 99 kPa	[15]
5	0-150 kPa	[70]

The reaction beam is welded to each side of the frame, hence as per IS 800:2007 the beam act as a fixed beam. The deflection calculation for load-transferring from soil sample has been given as follow:

The peak pressure adopted in the present study was 50 kPa

Thus, the applied maximum load over soil sample = Area X pressure i.e. (1.1 X 2) X 50 = 110 kN.

Hence, the design load is 110kN.

Factored load as per IS: [116] is 1.5**X** Design Load ≈ 165 kN

From bending equation:

$M = \frac{\sigma I}{Y} = \sigma Z;\ \left(\frac{I}{Y} \text{ is equal to section modulus (Z)}\right)$ (3.6)

M is calculated bending moment for the section;

I = moment of Inertia;

σ = permissible bending stress $=0.66 f_y \left(f_y \text{ is yield stress of steel} = 250 N/mm^2\right)$ = 165 N/ mm²;

Y is a vertical distance away from the neutral axis;

The hydraulic jack applies force to the reaction frame and acts as a point load at the mid-point of the fixed beam from a downward direction. The arrangement of the hydraulic jack and fixed beam is given in Fig.3.8a. Using Slope- deflection method, the maximum bending moment has been estimated for Fixed-beam as given below:

Step-1: Fixed end Moment:

$M_{Fab} = + Fab^2/l^2 = 44$ kN-m; (3.7)

$M_{Fba} = - Fab^2/l^2 = - 44$ kN-m (3.8)

Sign (positive (+) and negative (+)) represent direction of moment; F is point load = 165kN;

a and b is the length of span between support and point load; *l* is span length = 2.10m;

Step-2: Slope Deflection Equations:

$M_{ab} = M_{Fab} + \frac{2EI}{L}(2\emptyset_A + \emptyset_b - \frac{3\Delta}{L})$; (3.9)

where $\emptyset_A$ and $\emptyset_b$ are the slope at ends A and B respectively;

Δ is settlement at ends A and B;

Due to welded joint both A and B support act as fixed, hence $\emptyset_A$, $\emptyset_b$ and Δ is equal to zero.

Therefore, fixed end moment become equal to absolute moments at each ends. Maximum bending moment at the center of beam due to point load = $\frac{FL}{4}$ = 87 kN-m

Step-3: Bending moment diagram

From bending moment diagram (Fig.3.8b), the critical bending moment is 43kN-m

From bending equation,

Required section modulus($Z_{required}$) = $\frac{M}{\sigma}$ = (43 X10^6)/165 = 260606.06mm^3 (3.10)

Adopting two ISMC (Indian Standard Medium Weight Channel) 350 coupled flange to flange with welding joint as shown in Fig.3.8c.

Properties of ISMC 350: Area and Depth of section is 53.66 cm^2 and 350 mm respectively.

Thickness of Flange and web is 13.5 mm and 8.10 mm respectively.

Moment of Inertia; I_{xx} = 1008 **X** 10^4 mm^4; I_{yy} = 430.60 **X** 10^4 mm^4 for individual channel section

Second moment of inertia for built-up section: I_{xx}= 198438210.45 mm^4; I_{yy}= 66202030.96 mm^4

Vertical distance from the neutral axis for built-up section (Y) = 168.25 mm

Section modulus for built-up section: Z_{xx} =1179424.727 mm^3 and Z_{yy} = 393474.18 mm^3

Sectional area found more in xx- direction, so adopting Z_{xx}.

Hence, provided section modulus for built-up section $Z_{provided}$ = 1179424.727 mm^3

Hence, $Z_{provided} > Z_{required}$ which is adequate.

Now, from Hooke's Law; Stress (σ) = E **X** Strain (ϵ); E = 2**X** 10^5 N/mm^2

Again, from bending equation; maximum stress (σ) for provided section during worst load is

$\sigma = \frac{M}{Z} = \frac{43\ X10^6}{1179424.727}$ = 36.46N/mm^2.

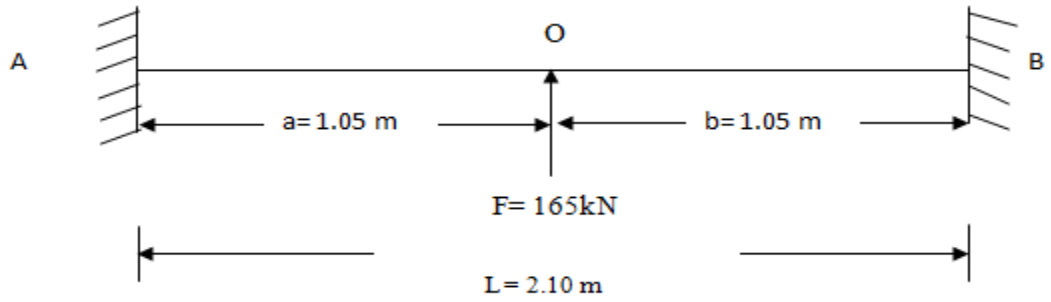

(a)

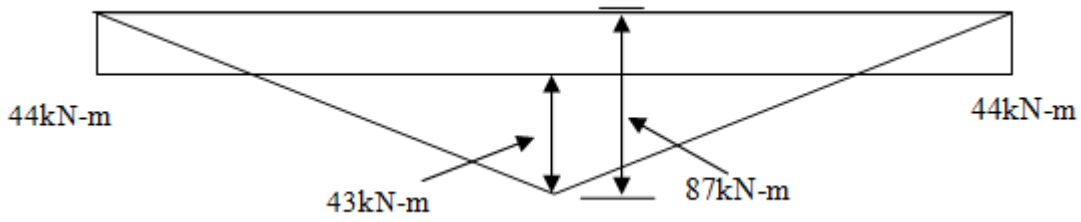

(b)

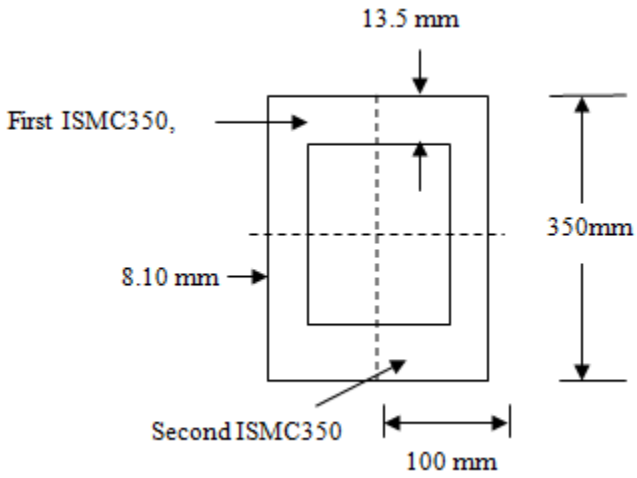

(c)

Fig.3. 8 (a) Fixed beam AB with point load of 165 kN at the center **(b)** Bending moment diagram (**c)** Two ISMC350 connected flange to flange with welding joint

Using Hooke's Law, ***Strain (ϵ) = 0.00018***

In addition,

The ***deflection*** for fixed beam (δ) $= \frac{Fa^3b^3}{3EIL^3} = \frac{165\ X\ 10^3(1.05X10^3)^3(1.05X10^3)^3}{3(2X\ 10^5)(198438210.45)(2.1\ X\ 10^3)^3}$ = ***0.19 mm*** (3.11)

Allowable value of deflection = span/250 = 2100mm/250 = 8.4 mm >> 0.19 mm

Both strain and deflection are negligible for factored load. Moreover, deflection is in allowable limit. Thus, the applied pressure will transmit uniformly from top to bottom without any disturbance.

3.5.3 Test Tank

To minimize the ***boundary effect***, the least tank dimension (1100 m) of tank was selected as ten times greater than the bigger helical plate diameter (96 mm) [57-81]. Similarly, each dimensions of tank were adopted in such a way that there is no boundary effect on the model testing. The size of test tank was adopted as 2 m long x 1.1 m wide x 1.1 m high, while thickness of each plate was adopted 10 mm. For the installation and pullout of helical soil nail, a spherical opening of 160 mm was located at the center of the front plate of the test tank.

For ***group pullout*** and installation of helical soil nail, two more arrangement (center to center uniform and staggered spacing) was made for the front plate of the test tank as shown in Fig. 3.6 (b and c). Evident from the Fig. 3.6 (b and c), the model installation zone is numbered from 1 to 9 for recognition purpose of Helical soil nail for both uniform and staggered spacing. Junaideen et al. [53] and FSI [8] suggested that the *center to center spacing* between helical elements should be in range *1.5D_h to 4.5D_h (D_h = helical diameter of bigger most helix)* in order to avoid the boundary effect. The center to center spacing adopted in present study is greater than 1.5D_h, where $D_h$is bigger most diameter of helix. Thus, influence zone of one nail will not affect the influence zone of other soil nail. The arrangements were attached to front section of tank by using bolted connection one by one as per the test requirement. For group arrangements, there are total nine holes in the front wall for allowing helical nail installation and nail pullout. The width of each circular opening was 140 mm to facilitate installation and pullout of different shaft diameter nail at different inclination angle. Before placing soil samples, the container walls were greased throughout. Moreover, Mittal and Mukherjee [117] also elaborated on adopting tank dimensions in excess of 2.5 times the helical diameter for negligible boundary effects. Based on this, for a maximum D_h = 90 mm (present study), any boundary beyond 3 times the helix diameter (i.e. 270 mm in present case) for single helical nail will treated as free of boundary effects. Simultaneously, as previously mentioned, the suggested centre – to – centre spacing of 1.5D_h is also recommended for avoiding the interference of neighboring nails. Keeping in line with this norm, the centre – to – centre spacing greater than 3D_h (i.e 275 mm) is adopted. This enables to achieve a clear distance of 2.5D_h (i.e 225 mm) for nails located nearest to the tank boundaries during group installation. Hence, the effect from tank boundaries on evaluated parameters is negligible. Hence, the effect of tank boundaries on evaluated parameters is negligible as shown in Table 3.5.

Table 3. 5 Recommendations for no boundaries effect during group pullout

Spacing between Helical nails (mm) ($3D_h$) in (present study)		**No. of nails**	**Group Arrangement**	**Influence zone of each nail ($1.5D_h$)**	**Number of Helices**	**Clear edge distance (mm) (>1.5 D_h = 135)**	
Vertical (S_V)	Horizontal (S_H)					From vertical edge	From horizontal edge
275	275	9	Uniform	96 to 135	2	262	262
275	550	9	staggered	96 to 135	2	412.5	550

3.5.4 UNIVERSAL DATA ACQUISITION SYSTEM

Fig.3. 9 Universal Data Acquisition System

The Universal Data Acquisition System (UDAS) of 30-channel was assembled at Ideal Integrated Technology, Jaipur (Rajasthan), India to record the real-time data as shown in Fig.3.9. The series no. of UDAS was DLX-U-RS 232-USB. The system is entirely instrumented for recording real-time data of vertical as well as horizontal displacement (i.e., pullout) using linear variable differential transformers (LVDTs). The surcharge pressure and pullout force were measured using calibrated load cells, while the stresses developed during installation and

pullouts were measured using earth pressure cells and stored in UDAS. Moreover, UDAS measures the real-time axial and torsional strain during installation and pullout of the helical soil nail. UDAS display the recorded data on liquid crystal display (LCD) and import it into pen drive.

3.6 Instrumentation and specifications

Various types of instrumentation were used in laboratory tests for the measurement of strain, displacement, load, and vertical stresses are shown in Fig.3.10.

3.6.1 Strain Gauges and LVDTs

The Strain Gauges were used to measure the axial and torsional strain, while linear variable differential transformers (LVDTs) were used to measure vertical and horizontal displacement (Fig.3.10 (a & b)).

3.6.2 Adapters

The adapters were used to hold different diameters of the helical soil nail. These are attached to the pullout machine during laboratory experiments to hold different nails (Fig.3.10c).

3.6.3 Earth Pressure Cell

In the present study, earth pressure cells were used to record the real-time data of change in-situ stresses. To closely monitor the in-situ stresses, piezo-resistive type pressure transducers were used during model testing (Fig.3.10d). The detailed specifications of the gadget are given in Table 3.6

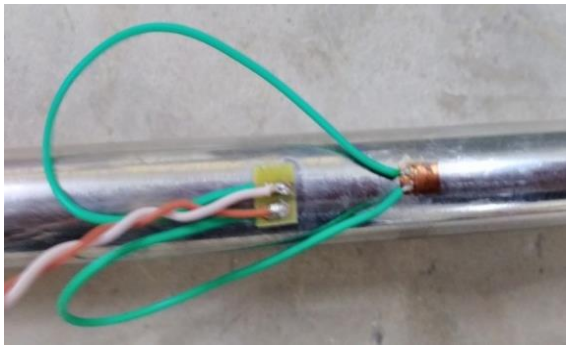

(a) Strain gauge pasted over the nail

(b) Linear variable differential transformer (LVDT)

(c) Adapters

(d) Earth pressure cell

Fig.3. 10 Gadget used in measurements

Table 3. 6 Details specifications of instrumentations

Instrumentation	Specifications
Strain Gauge	• Gauge type: Resistance type • Electrical resistance: 350Ω • Temperature: -269 ˚C to 260 ˚C
Linear variable differential transformer (LVDT)	• Least Count: 0.01 mm • Measurement range: 0.1 mm to 100 mm
Adapters	• Diameter range: 10 mm to 30 mm • Material: Stainless steel
Earth pressure cell	• Capacity: 3 MPa • Sensitivity: 0.01 MPa • Pressure transducers: Piezo-resistive type

3.7 Experimental program

The experimental program has been divided into *seven different groups*:

The *group first* includes hollow and solid shaft nails of different shaft diameters varying from 12 to 18 mm with a single helix. The helical diameter was considered four times the shaft diameter [8] and a constant pitch of 24.5 mm. From the first group, the helical soil nail shaft diameter was optimized for model testing.

In the *second group*, operations were made over the optimized nails achieved from the first group. To fix helical pitch, model nails were tested for different helical pitches ranging from 23 to 41 mm.

In the *third group*, the effect of double-helices nails was investigated for the smooth and rough surface at constant shaft diameter and helical pitch.

In the *fourth group*, tests were conducted to investigate the effect of multi-helices helical soil nails by keeping the other parameters constant.

The *fifth group* includes a pullout study of the optimized shaft without helices.

Based on the results obtained from the five groups, the helical soil nail with the best performance was tested for a different inclination that varies from 0˚ to 30˚, which is term as the *sixth group*.

In the last group, the nails were inspected in the group of nine nails with uniform and staggered spacing at best performing inclination. To simulate actual field conditions of various forces acting during the movement of soil, the group action of helical soil nails with different arrangements (i.e. uniform or staggered) was carried out. For the group of helical soil nails, each nail acting in individual bearing leads to the formation of a cylindrical surface extending from the penetrating nail head and touching the outer edges of the helical plates. Thus, the resistance against pullout for the helical soil nail group depends upon the mobilized shear stress acting along this enlarged cylindrical surface (Fig.3.11a). For helical plates of equal diameter, the formation of a cylindrical surface is obvious. However, the transition of the surface from cylindrical to the conical (tapered) surface is observed for helical nails with increasing helix diameter. The bond stress acting is therefore mobilized along this conical failure surface. Ideally, the conical failure surface is complex and can be mapped using log-spiral lines, but for simplification, straight lines are considered in the present analysis called idealized failure surface. Fig.3.11a shows that in a group action, instead of individual bearing resistance through helical plates, bearing resistance is majorly dependent on the truncated cone that extends beyond the last helix. The bearing offered by the enlarged diameter can thus be given by taking into consideration the increased volume of soil within the truncated soil cone. In this context, it is important to study the group action of helical soil nails with different arrangements (i.e. uniform or staggered) (Fig.3.11 (b) and (c)). Due to movement in soil mass helical nails are subjected to various tensile and compressive forces. The amount of disturbing forces can be too large for a single helical soil nail to resist pullout forces and a group of HN would be suggested to simulate actual field conditions. All tests of single nail were conducted under the different surcharge pressure of 5 kPa, 12.5 kPa, 25 kPa, and 50 kPa respectively, while group pullout of nails was conducted under 5kPa only. The details of different helical soil nail specimens used in study are given in Table 3.7.

Table 3. 7 Scheme of Helical soil nails specimens for laboratory testing.

Sample Identification	Shaft Type (mm)	Shaft Diameter (mm)	Number of Helices	Helix Diameter, (D_h) (mm)	Pitch of helix (mm)	Embedment Ratio (Z/D)
First group:						
A	Solid	12	1	48	24.5	10.4
B	Solid	14	1	56	24.5	8.92
C	Solid	16	1	64	24.5	7.8
D	Solid	18	1	72	24.5	6.9
E	Hollow	12	1	48	24.5	10.4
F	Hollow	14	1	56	24.5	8.92
G	Hollow	16	1	64	24.5	7.8
H	Hollow	18	1	72	24.5	6.9
Second group:						
C1,C2,C3	Solid	16	1	64	30, 35.5, 41	7.8
G1,G2,G3	Hollow	16	1	64	30, 35.5, 41	7.8
Third group:						
I	Solid	16	2	64 and 64	30	7.8
J	Solid	16	2	90 and 90	30	5.55
K	Solid	16	2	64 and 90	30	5.55
L-rough	Solid	16	2	64 and 90	30	5.55
M	Hollow	16	2	64 and 90	30	5.55
Fourth group:						
N	Solid	16	3	64,90 and 96	30	5.2
O	Hollow	16	3	64,90 and 96	30	5.2

N-Rough	Solid	16	3	64,90 and 96	30	5.2
N-4	Solid	16	4	64,90,92, and 96	30	5.2
O-4	Hollow	16	4	64,90,92, and 96	30	5.2
Fifth group:						
P	Solid	16	0	-	-	-
Q	Hollow	16	0	-	-	-
Sixth group: *Helical soil nail was tested for inclinations varies from 0˚ to 30˚*						
Seventh group: *Group of nine helical soil nail with uniform and staggered spacing was investigated*						

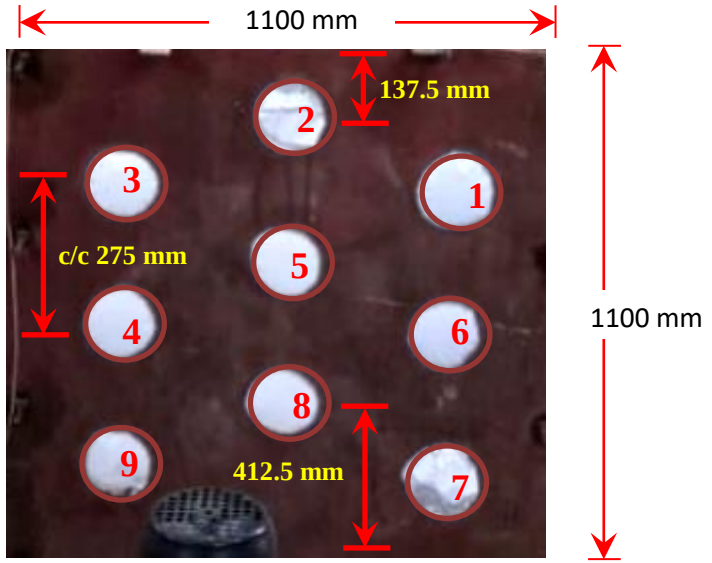

(b)

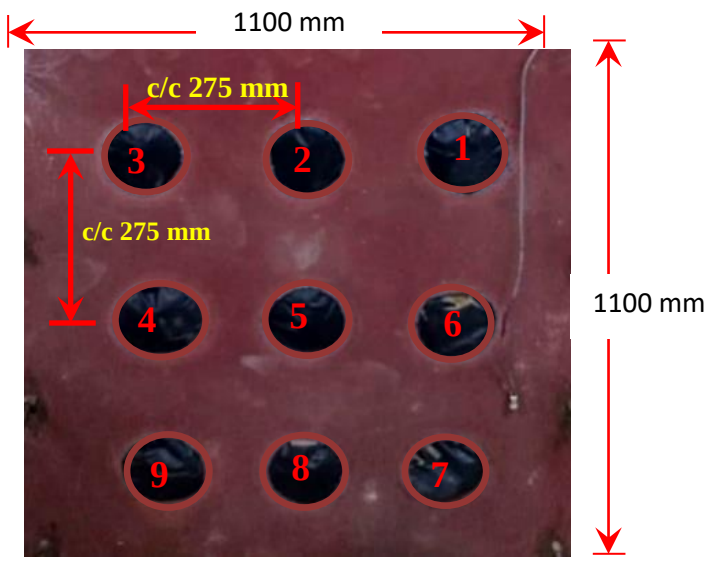

(c)

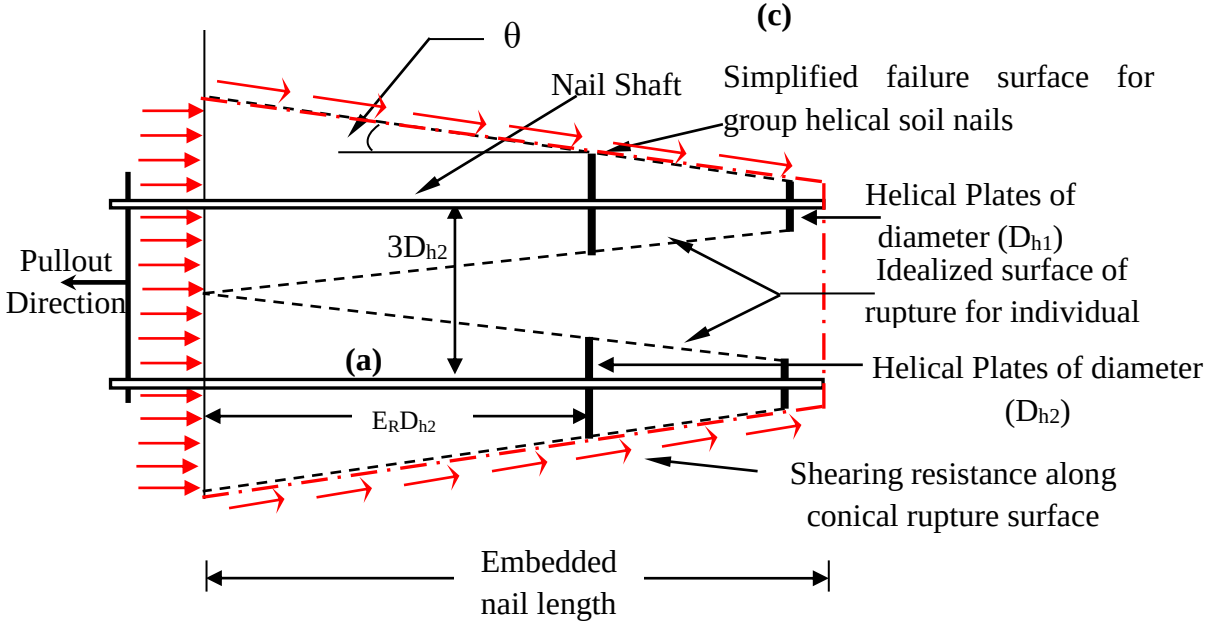

(a)

Fig.3. 11 (a) Idealized failure surface for of helical soil nail **(b)** Group arrangement with staggered centre to centre spacing.**(c)** Group arrangement with uniform centre to centre spacing

3.7.1 SAMPLE PREPARATIONS

The test tank was filled to the tank using sand pluviation technique [118-120]. According to the pluviation technique, the sand sample was equipped to free fall from an elevation (i.e. 108cm in present study) to reach required relative density (Rd) (i.e. 86.4% in present study) and the soil sample was filled up to a height of 1000 mm. The Rd of the prepared sample was checked at different depths using the sand replacement method. The soil sample was then tested under homogeneous overburden pressure of 5kPa, 12.5kPa, 25kPa, and 50kPa using a hydraulic jack. The soil sample was then left undisturbed for 24hr such that it can achieve initial stresses after primary consolidation.

3.7.2 TESTING PROCEDURE FOR SINGLE NAIL FROM 0^0 TO 30^0

The HNs were installed up to effective depth using the drive head at a rate of 10 rpm (revolutions per minute) along with the crowd force. The crowd force helps in the penetration of soil mass with the rate of penetration of one helical pitch in one revolution [114-115]. As the HN begins revolutions and penetration of soil mass, the torque during installation of the nail starts recording real-time installation torque using a torque meter. The helical soil nail specimens were then again left for 24 hours after installation into the soil mass. Afterward, an external displacement controlled pullout force was applied to the embedded nail specimen in the reverse direction at a rate of 1 mm/ min. Zhang et al [61] recommend that the peak pullout force can be taken as either the maximum value or the position where an increase in force per 1 mm displacement is less than 1% or a position where displacement reaches 30 mm. Keeping the suggestion in mind, the helical soil nail sample was pullout out until the pullout displacement of 90 mm was achieved. To install a nail at various inclinations, an arrangement is provided at the tail of the pullout machine. The inclination unit of the machine makes it possible to install and conduct pullout tests on soil nails at different downward inclination angles ranging from 0° to 40° with the horizontal. The unit consists of a manual handle and a clamping screw (in Fig. 3.12). A movable circular pipe is used in the inclination unit to adjust the inclination angle with the horizontal. The angle can be adjustable manually by clamping and unclamping the pin at marked angle positions.

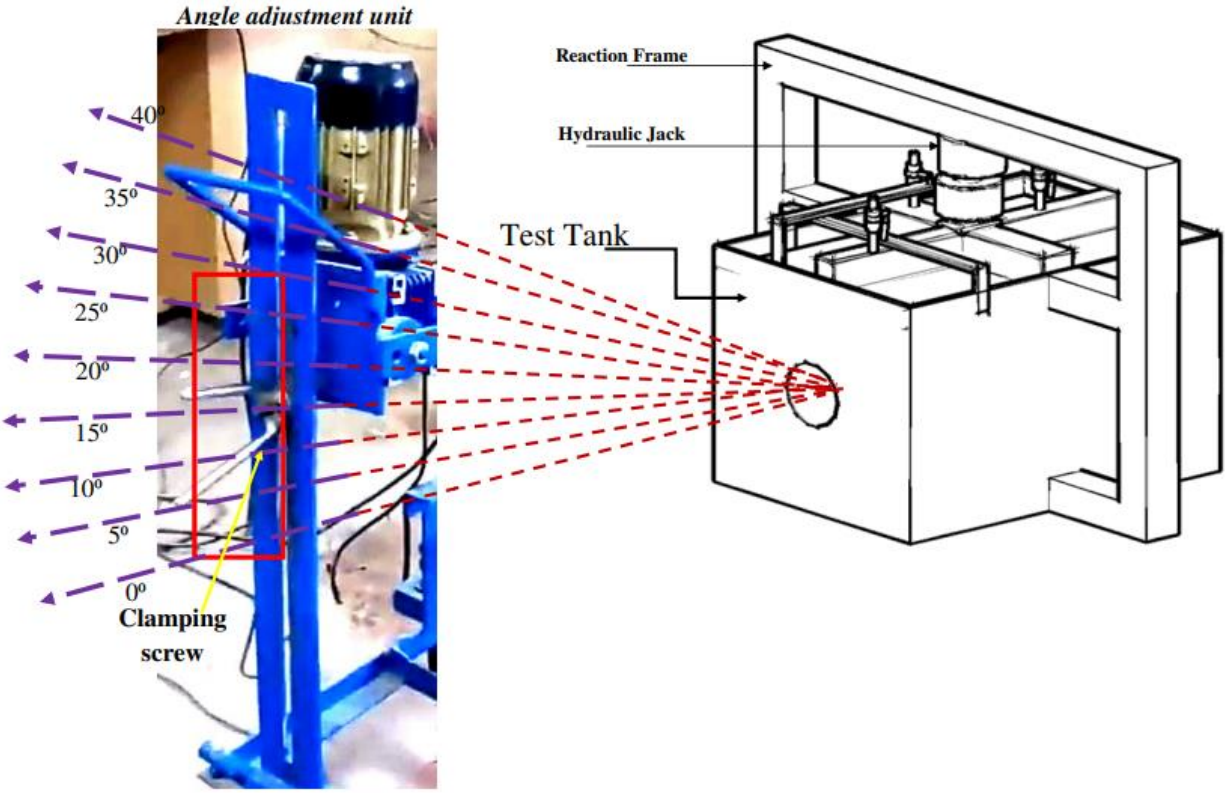

Fig.3. 12 Inclination unit of the pullout machine

3.7.3 TESTING PROCEDURE FOR GROUP OF NAIL

For *group installation* of helical soil nails, a "top-down" construction sequence was employed to simulate the actual site condition. The tank openings were followed with an installation motor and install helical nails from top to down one by one. With the change in soil bed height, the pullout device can also be altered its height using 4 lead screws attached to the base frame of the device.

The *group pullout* of helical soil nails was performed after welding a hook over the tail of each nail. To perform a group-pullout operation, the clutch wires were connected to the hook and then attached to the adapter hook of the pullout machine. The displacement of the individual HN in the group was not measured separately, however, the nail hook can be considered rigid so that all HN can be assumed to have equal displacement during the pullout. The helical soil nails

were installed at desired depth using a drive head rotating at a rate of 10 rpm with a crowd force supporting a rate of penetration of one helix pitch in one revolution. The maximum and minimum pullout displacement rate that can be achieved is 10 mm/ min and 1 mm/min, respectively.

3.7.4 SUMMARY

The chapter includes fabrication of displacement-controlled laboratory setup, nail, and instrumentation used during the testing. The laboratory test apparatus comprises four main units: Installation and pullout device, surcharge application system, test tank, and Universal Data Acquisition System (UDAS). Moreover, chapter includes scheme of laboratory testing and testing procedure in the detail. Further, to compare the model tests results of installation torque and pullout various theoretical models are discussed in next chapter.

CHAPTER-4

THEORETICAL MODELING

CHAPTER 4
THEORETICAL MODELING

4.1 General

The chapter includes the details theoretical modeling of installation torque and pullout of helical soil nail using different mathematical model. The chapter contains theoretical installation torque and pullout of single and group helical soil nail. The theoretical modeling was totally based upon the soil-nail interaction mechanisms of helical element, which is adopted for the validations of experimental result.

4.2 Theoretical installation torque

The installation torque of helical element depends upon various factors like diameter of helical plate, pitch of helix, helical angle, shaft diameter, number of helices, thickness of helix, geometric configurations etc. Fig.4.1 demonstrates the various torque exerted on helical nail during the installation. The theoretical torque includes bearing resistance and skin friction of helices and shaft of helical element respectively [79-89]. For the calculation of theoretical installation torque the torque was calculated by summation of applied torque up to a particular point yields the force that create the moment acting against the applied installation torque. In other word, torque will be considered up to the embedded length of helical element due to torsional moment. The installation of helical soil nail accomplishes of bearing and frictional resistances on helical plate and nail shaft. The precise analysis is very tricky though installation torque was planned by approximate methods. Moreover, different assumptions that are taken into considerations for the proposal of torque are as follow:

- The theoretical analysis is considered independent to installations speed, rotation per minute (RPM), applied crowd force and not able to simulate in the analysis.
- The soil conditions were assumed isotropic and homogenous in all directions in the analysis.

For the calculations of theoretical torque different models were developed thus, the applied torque during the installation of the helical soil nail (HN) are given as follow:

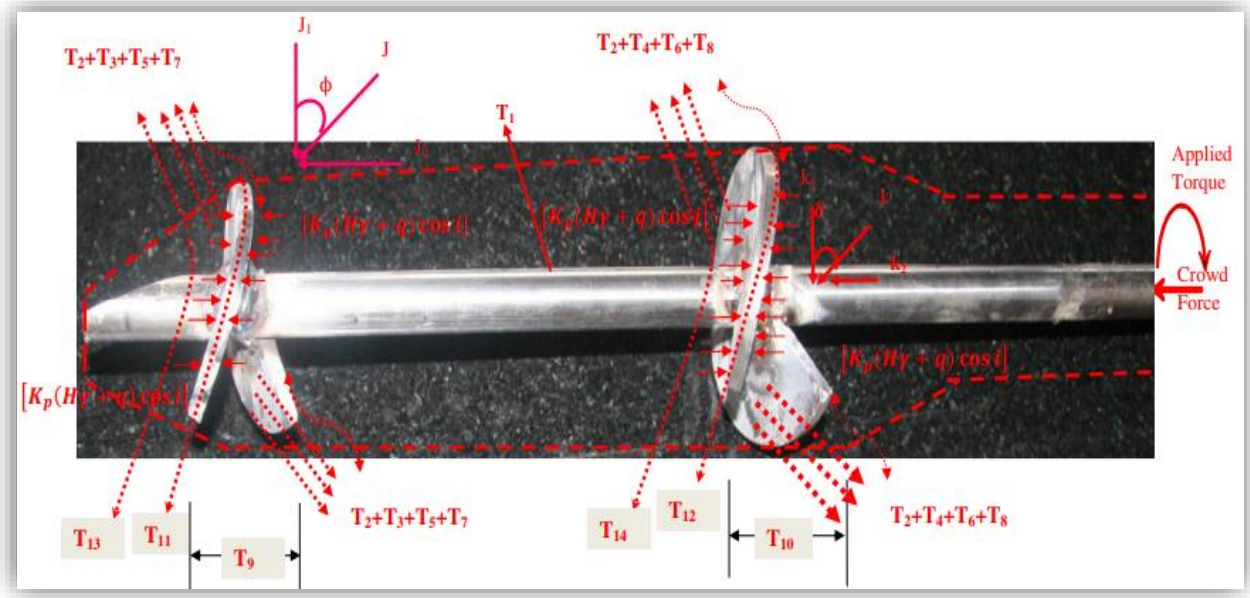

Fig.4. 1 Anticipated Theoretical Torque acting during installation

The exerted installation torque during driving of helical soil nail (T) may be given by the following equations

$$T = T_1 + T_2 + T_3 + T_4 + T_5 + T_6 + T_7 + T_8 + T_9 + T_{10} + T_{11} + T_{12} + T_{13} + T_{14}$$

T_1 and T_2 is the resisting moment acting on the HN's shaft and helices due to the force k_1 and k_2 respectively

$$T_1 = \left[[(\sigma'_{vs} + q) l \cos i] \tan(\delta) \cos\delta \, \pi \frac{d^2}{2} \right] \quad (4.1)$$

$$T_2 = \left[[(\sigma'_{vs} + q) l \cos i] \tan(\delta + ¥) \sin\delta \, \pi \frac{d^2}{2} \right] \quad (4.2)$$

T_3 and T_4 is the resisting moment occurs first and second HN's blade owing to the force J_2

$$T_3 = \left[[(\sigma'_{v} + q) \cos i] \sin\phi \tan(\delta + ¥) [\pi \frac{D^3{}_1}{2}] \right] \quad (4.3)$$

$$T_4 = \left[[(\sigma'_{vx} + q) \cos i] \sin\phi \tan(\delta + ¥) [\pi \frac{D^3{}_2}{2}] \right] \quad (4.4)$$

T_5 and T_6 are the resisting moments acting on the upper surface of the first and second HN's blade respectively due to the acting active earth pressure which develops as a result of the forward movement of the HN's blade.

$$T_5 = \left[[K_a(\gamma Z + q)\cos i]\tan(\delta + ¥)\left[\pi\frac{(D_1 - d)^3}{4}\right]\right] \quad (4.5)$$

$$T_6 = \left[[K_a(\gamma Z_x + q)\cos i]\tan(\delta + ¥)\left[\pi\frac{(D_2 - d)^3}{4}\right]\right] \quad (4.6)$$

T_7 and T_8 is the resisting moment acting on the lower surface of the first and second HN's blade respectively due to the acting passive earth pressure that develops as a result of the applied pushing-down force.

$$T_7 = \left[\left[K_p(\gamma Z + q)\cos i\right]\tan(\delta + ¥)\left[\pi\frac{(D_1 - d)^3}{4}\right]\right] \quad (4.7)$$

$$T_8 = \left[\left[K_p(\gamma Z_x + q)\cos i\right]\tan(\delta + ¥)\left[\pi\frac{(D_2 - d)^3}{4}\right]\right] \quad (4.8)$$

T_9 and T_{10} are the resisting moments due to the bearing force acting on the entire height of the first and second helix's helical pitch respectively.

$$T_9 = \left[F_1\left[\pi\frac{D^2{}_1}{2}\right]\right] \quad (4.9)$$

$$T_{10} = \left[F_2\left[\pi\frac{D^2{}_2}{2}\right]\right] \quad (4.10)$$

Where $F_1 = [(1 + K^*)(\gamma Z + q)]\,\mathrm{pcos}\,i$

$F_2 = [(1 + K_x{}^*)(\gamma Z_X + q)]\,\mathrm{pcos}\,i$

T_{11} and T_{12} is the resisting moment acting on the outer perimeter of the first and second helices thickness of the helix.

$$T_{11} = [(\sigma'_v + q)\cos i]\tan(\delta)\,t_h\left[[\pi\frac{D^2{}_1}{2}]\right] \quad (4.11)$$

$$T_{12} = [(\sigma'_{vx} + q)\cos i]\tan(\delta)\;t_h\left[[\pi\frac{D^2{}_2}{2}]\right] \quad (4.12)$$

T_{13} and T_{14} are moments due to the top periphery first and the second helix penetrating the soil.

$T_{13} = (\sigma'_v + q)(D_1 - d)N_q\ t_h \frac{(D_1+d)}{4}\cos i$ (4.13)

$T_{14} = (\sigma'_{vx} + q)(D_2 - d)N_q\ t_h \frac{(D_2+d)}{4}\cos i$ (4.14)

$\sigma'_v = \frac{1}{2}[(1 + K^*)\gamma\ Z]$;

$\sigma'_{vx} = \frac{1}{2}[(1 + K^*)\gamma\ Z_x]$;

$\sigma'_{vs} = \frac{1}{2}[(1 + K^*)\gamma\ Z_s]$;

σ'_v , σ'_{vx} , σ'_{vs}= average effective vertical stress at first helix, second helix and shaft respectively.

$K^*, K_x^*\ K_s^*$ = Modified earth pressure coefficient for first helix, second helix, and shaft respectively.

Z, Z_x, Z_s = Depth of the first helix, second helix, and shaft below the ground surface respectively

$D_1, D_2 \ldots D_n$ is Diameter of helix;

d is the diameter of shaft;

v is Poisson's Ratio = 0.3

$K^* = = C \times K_0 \times \left[\frac{E}{\gamma Z}\right]^{\alpha} \times \left[\frac{\phi}{45}\right]^{\beta} \times \left[\frac{\Delta t}{D_h}\right]^{\theta}$;

$\alpha = 0.38$

$\beta = 1.39$

$\theta = 0.42$

$C = 2.75$

K_0 is the coefficient of earth pressure at rest;

K_a is the coefficient of active earth pressure;

K_p is the coefficient of passive earth pressure;

D_h is the helical diameter

q is uniform surcharge;

γ is the dry unit weight of the soil;

$\boldsymbol{\delta}$ is the angle of friction between the anchor material and the soil;

¥ is helix angle;

Φ is the angle of friction;

tan $\boldsymbol{\delta}$ is the coefficient of friction between the anchor material and the surrounding soil ;

i is the angle of inclination;

F_1 and F_2 are bearing force;

t_h is the thickness of helix;

4.3 Theoretical Pullout of helical soil nail

Fig.4.2 illustrates the helical soil nail with the soil interface model presented in the current study. To assess the interface parameters and its mechanism pullout tests are commonly used. To closely understand the formal case hyperbolic model is used in the passive zone of the helical nail system in terms of mobilized shear stress and nonlinear strains [121-122]

The equilibrium of net axial forces can be expressed as:

$$[F(x) + dF(x)] - F(x) + \tau\,(x)\pi \sum_{i=1}^{n} D_h[dv(x) + dx] = 0 \tag{4.15}$$

where F(x) and F(x)+dF(x) are pullout force at the nail head and tail respectively; D_h is the diameter of helix; $\tau\,(x)$ is mobilized shear stress between the interface; $dv(x)\ and\ dx$ are change in length and a small length of element respectively.

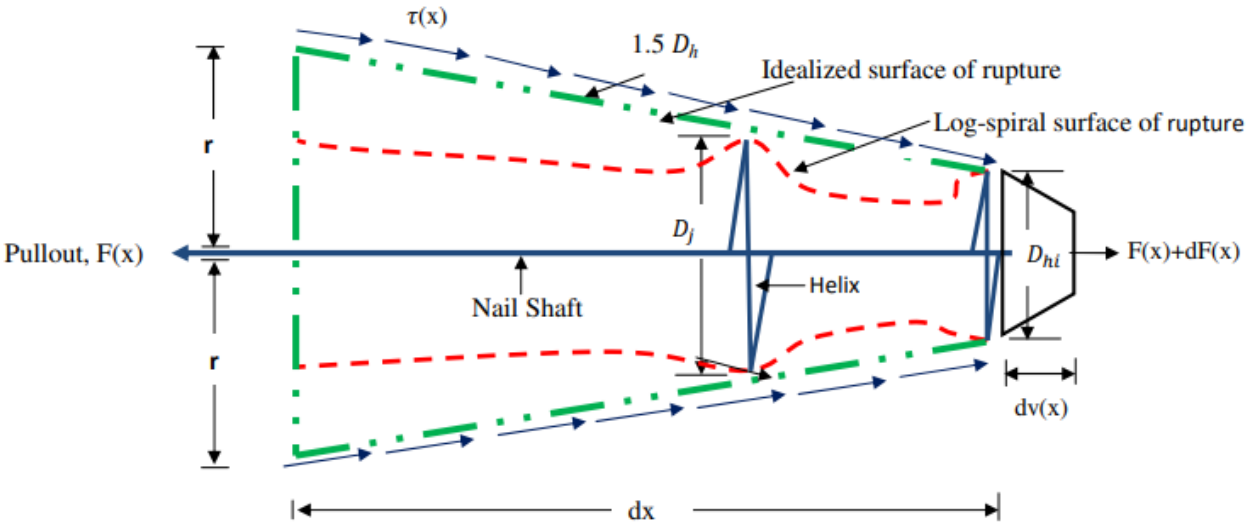

Fig.4. 2 Schematic diagram of helical soil nail subjected to pullout force in soil

Further Eqn. (4.15) can be written as:

$$\frac{dF(x)}{dx} + \tau(x)\pi \sum_{i=1}^{n} D_h \left[\frac{dv(x)}{dx} + 1\right] = 0 \tag{4.16}$$

Compression and tension are assumed to be positive and negative respectively. Due to pullout force acting on nail axial strain develop at x is given as

$$\epsilon(x) = -\frac{F(x)}{EA} = \frac{dv(x)}{dx} \tag{4.17}$$

$$\frac{dF(x)}{dx} = -EA\frac{d^2v(x)}{dx^2} \tag{4.18}$$

By using Eqn. (4.16), (4.17) and (4.18), after re-arranging yields Eqn.(19)

$$EA\frac{d^2v(x)}{dx^2} - \tau(x)\pi\sum_{i=1}^{n} D_h\left(1+\epsilon(x)\right) = 0 \tag{4.19}$$

The pullout strain $\epsilon(x)$ is very-very small and hence for calculation simplification Eqn. (4.19) is approximate equals

$$EA\frac{d^2v(x)}{dx^2} - \tau(x)\pi\sum_{i=1}^{n} D_h = 0 \tag{4.20}$$

The load transfer model expresses the correlation between shear stress ($\tau(x)$) and displacement u(x). The load transfer model is divided into three phases i.e. pure-elastic, elastic-plastic, and pure-plastic. In the pure-elastic phase shear stress varies linearly with the pullout displacement of nail whereas, with further increases in pullout force approach peak level, the increment in shear-stress with nail displacement raise inadequate or become steady called elastic-plastic phase. In the final segment, the nail is out from the passive zone of slope and consider as a critical state of the former case. The pure plastic state is not relevant for design purposes and hence ignored in the analysis [121].

4.3.1. PURE-ELASTIC BEHAVIOR

For external or pullout loading subjected to pile and nail following derivation is presented by [121-123] respectively, given as in Eqn.(4.21):

$$\iint\left[\frac{d^2v(x)}{dx^2} - \frac{k\pi\sum_{i=1}^{n} D_h}{EA}v_e(x)\right]dxdx = 0 \tag{4.21}$$

$v_e(x)$ is nail displacement when pullout forces are subjected to the nail head in the pure-elastic segment.

Let's suppose

$$\frac{d^2}{dx^2} = D^2 \tag{4.22}$$

$$\frac{k\pi \sum_{i=1}^{n} D_h}{EA} = \psi^2 \tag{4.23}$$

Hence from Eqn. (4.21), solution of differential equation can be evaluated as in Eqn.(4.24) and Eqn.(4.25):

$$[D^2 - \psi^2\,]v_e(x) = 0 \tag{4.24}$$

$$D = \pm\boldsymbol{\psi} \;\; \Xi \;\; v_e(x) = \; C_1 e^{\psi x} + \; C_2 e^{-\psi x} \tag{4.25}$$

where C_1 and C_2 are arbitrary constants.

Using Eqn. (4.25) in Eqn. (4.17), yields Eqn. (4.26) and Eqn. (4.27)

$$-\frac{F_e(x)}{EA} = \frac{d\,(\,C_1 e^{\psi x} + \; C_2 e^{-\psi x})}{dx} \tag{4.26}$$

$$F_e(x) \; = -EA\psi\left[C_1 e^{\psi x} - \; C_2 e^{-\psi x}\right] \tag{4.27}$$

Applying boundary condition for pure-elastic phase

$$x = 0, F_e(0) = 0 \tag{4.28}$$

$$x = l, F_e(l) = F \tag{4.29}$$

Using Eqn.(4.28) in (4.27) yields

$$C_1 = C_2 \tag{4.30}$$

Using Eqn. (4.27), (4.29), and (4.30):

$$C_1 \; = \; C_2 = \; \frac{F}{-\,2EA\psi Sinh\psi l} \tag{4.31}$$

By Eqn. (4.25) and (4.31)

$$v_e(x) = \; \frac{F}{(-\,EA\psi Sinh\psi l)} \frac{\left[e^{\psi x} + \; e^{-\psi x}\right]}{2} \tag{4.32}$$

Using EA value from Eqn. (4.23) and simplifying Eqn.(4.32), yield :

$$v_e(x) = \frac{-F\psi\, Cosh\psi x}{(k\pi \sum_{i=1}^{n} D_h\, Sinh\psi l)} \tag{4.33}$$

Eqn.(4.33) is the governing equation for the pure-elastic stage between the load-displacement relationship of the helical soil nail.

At x=l, Eqn.(4.33) can be written as:

$$F = \frac{v_e(x) k\pi \sum_{i=1}^{n} D_h\, tanh\psi l}{\psi} \tag{4.34}$$

The critical pullout force of soil-nail interface may be given as:

$$F_c = -\tau_C \pi \sum_{i=1}^{n} D_h l = ((\gamma z+q)\, tan\delta)\pi \sum_{i=1}^{n} D_h l = -k\,\pi \sum_{i=1}^{n} D_h l \tag{4.35}$$

k is a stiffness factor that can be calculated from the direct shear test or pullout shear test. The ratio of Eqn. (4.34) to (4.35) allocates the normalized pullout force ratio$\left[\frac{F}{F_c}\right]$.

4.3.2 ELASTIC-PLASTIC BEHAVIOR

For the transition phase, the pullout displacement is continuous from the former case. The boundary conditions for the elastic-plastic segment are as follows:

$$x = 0, F_e(0) = 0 \tag{4.36}$$

$$x = l - l_x,\ v_e(l - l_x) = v_p(l - l_x) = v_c \tag{4.37}$$

$$x = l - l_x, \qquad F_e(l - l_x) = F_P\,(l - l_x) \tag{4.38}$$

where $v_p(x)$ and $P_p(x)$ are displacement and pullout force at transition phase respectively. The final point of the pure-elastic stage is the initial point for the elastic-plastic segment hence on integrating Eqn. (4.20), a similar solution to the equation has been developed.

$$v_e(x) = D_1 e^{\psi x} + D_2 e^{-\psi x} \quad ; \quad (l - l_x \geq x \geq 0) \tag{4.39}$$

To solve the load-displacement correlation for plastic section τ(x) = $\tau_c = ku_c$ is substituted in Eqn. (4.20) and double integrating with respect to displacement and yields

$$v_p(x) = \iint \frac{\tau_c \pi \sum_{i=1}^{n} D_h}{EA} dxdx = \frac{\tau_c \pi \sum_{i=1}^{n} D_h\ (x^2 + j_1 x + j_2)}{2EA} \ ;\ (l \geq x \geq l - l_x) \tag{4.40}$$

j_1 and j_2 are arbitrary constant. By applying boundary conditions from Eqn.36 to 38 and substituting the arbitrary constant to Eqn. (4.39) and (4.40) provide the displacement equation for both elastic and plastic zone during pullout in Eqn.(4.41) and (4.42) respectively.

$$v_e(x) = \frac{v_c \cosh(\psi x)}{\cosh(\psi(l - l_x)} \tag{4.41}$$

$$v_p(x) = \frac{\psi^2 u_c}{2}[x - (l - l_x)]^2 + \psi\, v_c tanh(\psi(l - l_x)[x - (l - l_x)] + u_c \tag{4.42}$$

The applied pullout in the elastic-plastic section is due to both resistances offered by elastic and plastic phase, given as:

$$F = -\left[\int_0^{l-l_p} \pi \sum_{i=1}^{n} D_h\, \tau_e(x)dx + \int_{l-l_p}^{l} \pi \sum_{i=1}^{n} D_h\, \tau_p(x)dx\right] \tag{4.43}$$

$$F = -\left[\frac{\pi \sum_{i=1}^{n} D_h\, \tau_e(x)\tanh(\psi l_e)}{\psi} + \pi \sum_{i=1}^{n} D_h\, \tau_c l_p\right] \tag{4.44}$$

where $\tau_e(x)$ = k$v_e(x)$ and $\tau_p(x)$ = kv_c is shear stress mobilized in the elastic and plastic segment respectively. Similar to the pure-elastic segment ratio of pullout force to the critical pullout force determine the normalized pullout force ratio$\left[\frac{F}{F_c}\right]$.

4.3.3 PULLOUT CAPACITY OF INCLINED HELICAL SOIL NAIL

The peak pullout capacity of inclined helical soil nail has vertical (F_v) and horizontal (F_h) two components as estimated in Eqn.4.45 and Eqn.4.46:

$$F_v = F_i \sin i \tag{4.45}$$

$$F_h = F_i \cos i \tag{4.46}$$

The vertical force component is responsible for the extension of failure surface in pullout direction. The horizontal component is responsible for the pullout displacement of helical soil nail and the soil sample deformation. Due to these two components the failure surface 1-2-3-4-5 formed with axis 7-3 of failure surface as shown in Fig. 4.3. The idea is modified after Ghaly et al. 1998 in terms of helical soil nail. Further to investigate the effect of inclined soil nails the theory of conjugate helical soil nail and auxiliary failure surface were established. The idea is

based on the hypothesis that the intersection with soil sample of axis of failure surface 1-2-3-4-5 due to pullout of actual soil nails, reveals that the failure surface of actual and imaginary (conjugate) nail follows the same pattern. Thus, the axis of failure surface 1-2-3-4-5 of imaginary (conjugate) nail is 7-3. Also, it is essential to clear that the peak pullout capacity of the imaginary (conjugate) helical soil nail F_{oc} is not the same the peak pullout capacity of inclined soil nail F_i even both follow the same failure surface. The reason is that both helical soil nail with different inclinations contributing by means of different weight of sand and shearing resistance to the pullout capacity of helical soil nail. For peak pullout capacity (F_o) of helical soil nail installed at 0º with horizontal up to embedded length of l_o, the failure surface will surely pass through the point '1' and '5' respectively. This is due to installation of identical embedded length of similar helical soil nail sample, which generate equal deformations. Thus, the shape of rupture is to be accomplished is 1-10-9-8-5. The required failure surface is thus function of F_i in terms of F_o due passing through the point '1' and '5' respectively. Now as per Riemann's mapping theorem (1953) that a function maps every spot of a section (i.e.f_r) into a equivalent point of random region (i.e.f_r'), and each point (i.e.f_p) on the boundary of the region f_r to a corresponding point $f_p{}'$ on the boundary of the region f_r'. However, Riemann's mapping theorem that mapping function does not generated by this function, it is already in the existence [83]. Nevertheless, locus of both actual and auxiliary failure surfaces through two known point 1 and 5 coincides each other. To achieve this state the conjugate soil nail required to rotate counterclockwise about point 7 at an angle $\frac{i}{3}$ (Fig.4.3).

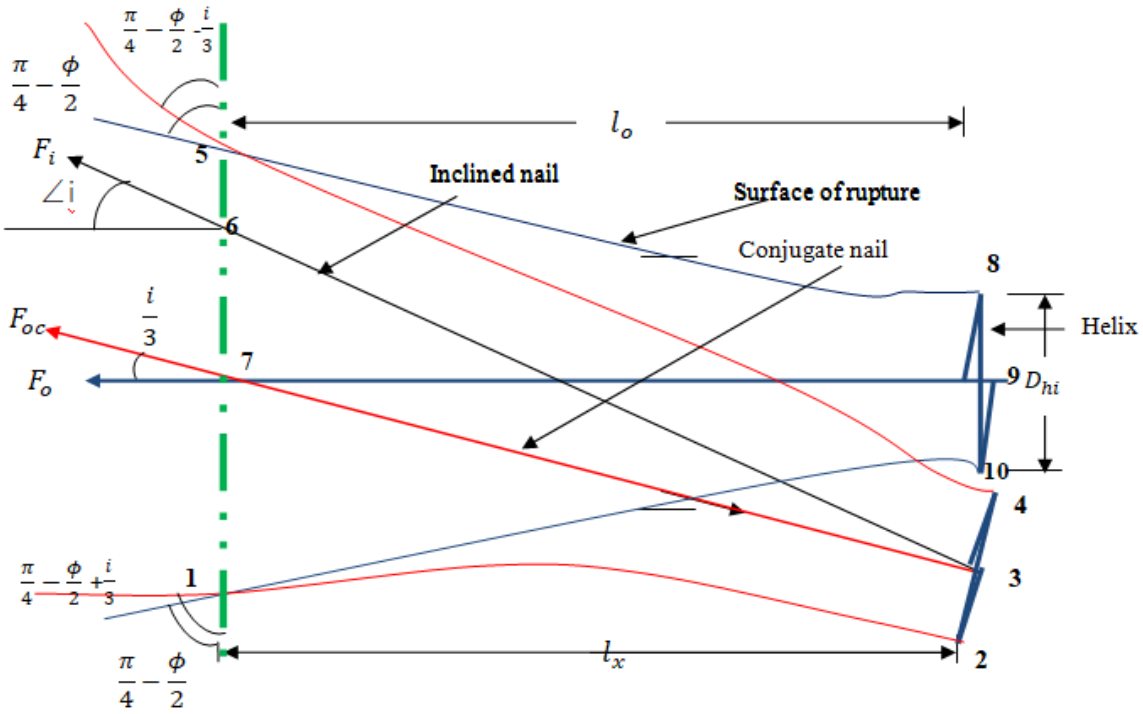

Fig.4. 3 Correlation between actual failure surface of inclined helical soil nail and auxiliary failure surface of rotated conjugate helical soil nail.

To overcome the effect of rotation of estimated pullout capacity of inclined helical nail (F_i), it is also important to the inclined nail to rotate with the rotation of failure surface. Due to which the failure surface 1-2-3-4-5 generates. Therefore, the angle of inclined soil nail becomes equal to $\frac{2i}{3}$ with respect to the horizontal as shown in Fig.4.4. From the simple geometry of Fig.4.4, evident that pullout capacity of inclined helical nail (F_i) is given as in Eqn.4.47

$$F_i = \frac{F_o}{\cos\frac{2i}{3}} \qquad 4.47$$

The Eqn.4.47 is true for the nail installed at different installation length, while for nail installed to similar embedded length the correlation modified to Eqn.4.48

$$F_i = k_i \frac{F_o}{\cos\frac{2i}{3}} \qquad 4.48$$

where F_o = peak pullout capacity of helical soil nail having equal embedded length to that of inclined soil nail;

k_i = coefficient of embedded length;

The co-efficient k_i is expressed in terms of i and $\frac{H}{D_h}$ and ∠i:

$$k_i = 1.015 - 0.002\left[\frac{H}{D_h \cos\frac{i}{3}}\right] \quad 4.49$$

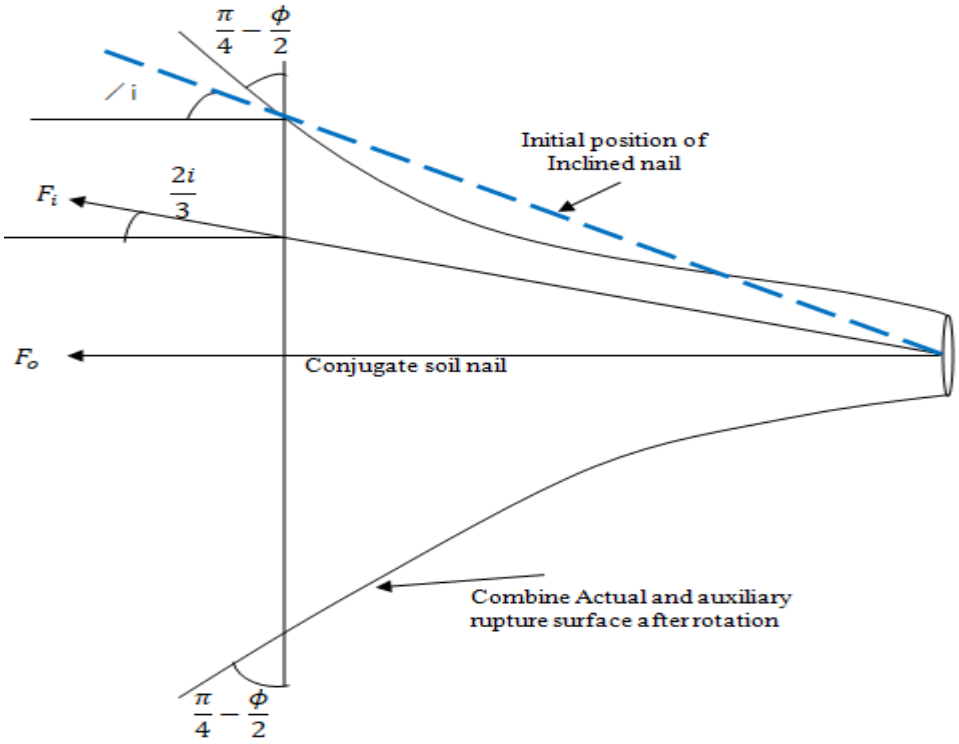

Fig.4. 4 Geometry of failure surface and helical soil nail inclination after rotation

4.3.4 DERIVATION FOR GROUP PULLOUT OF HELICAL NAIL

The group pullout capacity of the helical nail can be analyzed on the basis centre to centre spacing between the adjacent nails which is modified after Chattopadhyay And Pise [124] Shanker et al. [125] The group pullout capacity may be calculated in two different cases, as follow:

Case-1(Spacing ≥ 2 times influence zone)

For this case, the influence circle does not intersect resulting in each nail acts independently. Hence the net pullout capacity of the group (F_g) helical nail becomes equal to the product of a number of the nail (n) and pullout capacity of the single nail (F_s) as given in Eqn. (45)

$$F_g = nF_s \tag{4.45}$$

From Eqn. (45), the effect of the various arrangement of the placement of nails cannot be revealed and the result for the pullout of different group arrangement of the nail will appear the same.

Case-2 (Spacing ≤ 2 times influence zone)

For the case where influence circles overlap each other and to incorporate the effect of various group arrangements, the analysis has been done in another way. Tokhi [14] observed soil mass around a helical nail fail as a curved conical failure. Based on this observation, the group of helical nails is assumed to fails as a conical failure. For a soil-nail slope, the slip surface depends upon interface friction angle. In the present study, the soil nail wall is approximately vertical and the nature of the soil is frictional, hence the planar slip surface is assumed in the analysis. Moreover, the hypothesis of linear slip surface simplifies the study. In the limit equilibrium method (LEM), the pullout capacity of soil nail is attained by mobilized shear strength between interfaces which is balanced by an applied force. Considered a small element of soil with thickness dz at a distance of z from the free and the slip arise from the toe and expand toward the ground surface by intersecting the soil nail as shown in Fig.4.5a. At any length of Δl of failure surface, the mobilized shear resistance $\Delta\tau$ is$\Delta\sigma_n \tan\phi$.

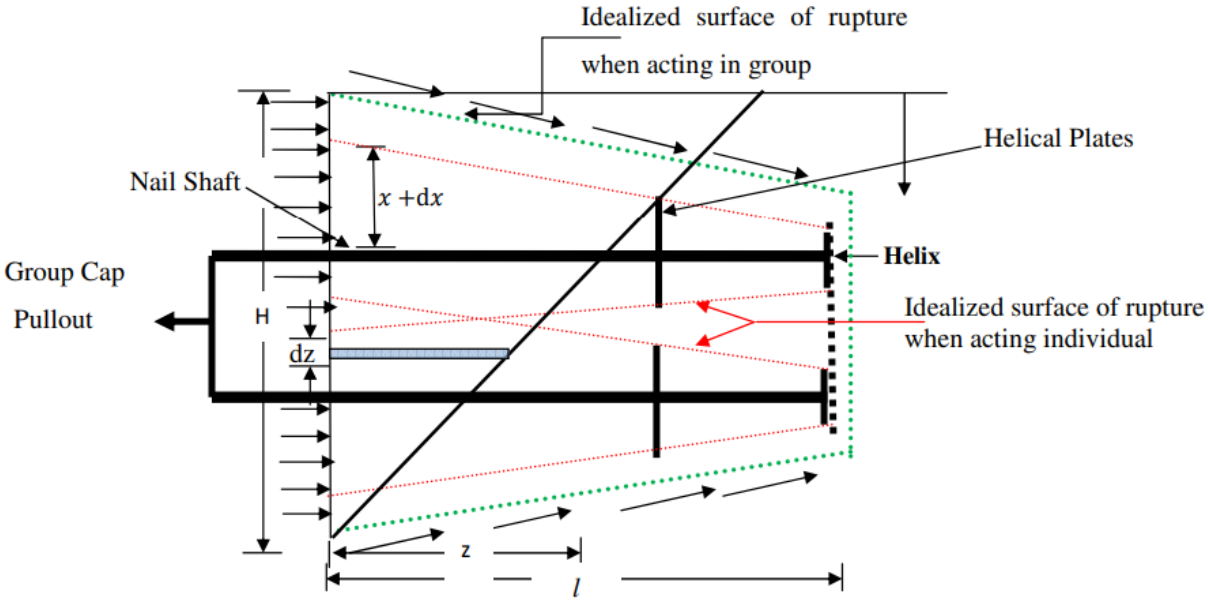

(a)

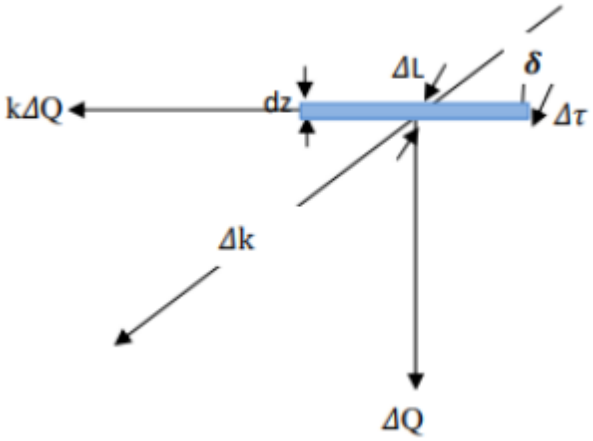
ΔL
δ
kΔQ
dz
Δτ
Δk
ΔQ

(b)

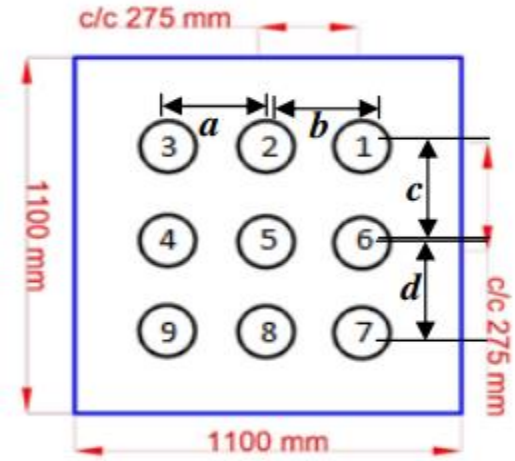
c/c 275 mm
a
b
3
2
1
c
4
5
6
d
9
8
7
1100 mm
c/c 275 mm
1100 mm

(c)

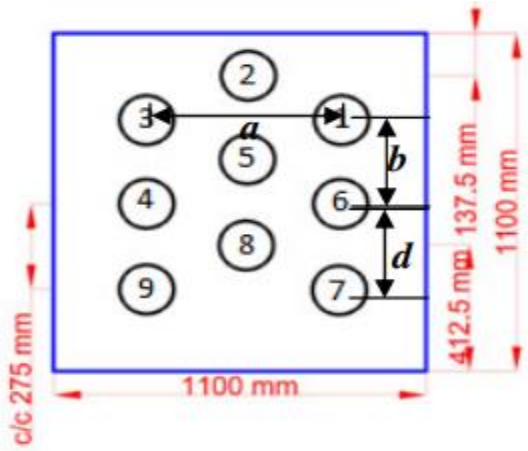
2
3
1
a
b
5
4
6
8
d
9
7
137.5 mm
412.5 mm
1100 mm
c/c 275 mm
1100 mm

(d)

Fig.4. 5 Geometry of rupture mechanism for group of helical soil nail **(b)** Free body diagram of wedge. **(c)** Group cap with uniform centre to centre distance. **(d)** Group cap with staggered centre to centre distance.

$$\Delta\sigma_n = \text{normal force on the failure surface} = \gamma(H)dz\,(k_o cos\delta + sin\delta) \quad (4.46)$$

k_o is coefficient of earth pressure at rest condition

Δl is the length of the failure surface

$\boldsymbol{\delta}$ is $\tan^{-1}\frac{dx}{dy}$

$$\Delta\tau = \gamma(H)dz\,(k_o cos\delta + sin\delta)tan\phi \quad (4.47)$$

Considering the equilibrium of wedge and assuming that weight of soil nail group having length l is equal to the weight of soil corresponding to volume occupied by each soil nail. The equilibrium of net group axial forces can be expressed similar to single nail element as follows:

$$[F + dF] - F + q(a + b + 2x)(c + d + 2x) - (q + dq)(a + b + 2x + 2dx\,)(c + d + 2x + 2dx) - dW - 2(a + b + c + d + 4x + 2dx)\Delta\tau \sin\delta = 0 \quad (4.48)$$

where F and F+dF are pullout force at the nail head (at group cap) and tail respectively.

a,b,c, and d is inter-nail spacing during group installation;

q = is surcharge load= (γH+applied overburden);

dW is change in weight of soil;

$x\ and\ dx$ is the distance from the center of the nail to the outermost periphery and small change in distance concerning ground surface respectively.

Using Eqn.(47) in Eqn.(48) and solving yields:

$$\frac{dF}{dz} = 2q(a + b + 2x)\frac{dx}{dz} + 2q(b + c + 2x)\frac{dx}{dz} + (a + b + 2x)(b + c + 2x)\frac{dq}{dz} + \frac{dw}{dz} + 2(a + b + c + d + 4x)\gamma H(k_o cos\delta + sin\delta)tan\phi \quad (4.49)$$

From Fig.4.5b, the subsequent relations are accomplished:

$$\frac{dx}{dz} = \tan\delta\,; x = z\ \tan\delta$$

$$q = \gamma H + \text{constant overburden } (o)\ ;\ \frac{dq}{dz} = -\gamma$$

Using above relationship in Eqn. (49):

$$\frac{dF}{dz} = 2q(a+b+2z\tan\delta)\tan\delta + 2q(c+d+2z\tan\delta)\tan\delta + (a+b+2z\tan\delta)(c+d+2z\tan\delta)(-\gamma) + \frac{dw}{dz} + 2(a+b+c+d+4z\tan\delta)\gamma H(k_o cos\delta + sin\delta)tan\phi \quad (4.50)$$

where,

$$\frac{dw}{dz} = (a+b+2x)(c+d+2x)\gamma \quad (4.51)$$

Using Eqn.(51) in Eqn.(50), also putting a+b+c+d = C_X and q = $(\gamma H + o)$, yields

$$\frac{dF}{dz} = 2(\gamma H + o)C_X\tan\boldsymbol{\delta} + 8(\gamma H + o)z\tan\delta^2 - 2\gamma z C_X\tan\delta - 8\gamma z^2\tan\delta^2 + 2C_X(\gamma H + o)(k_o cos\delta + sin\delta)tan\phi - 2C_X\gamma z(k_o cos\delta + sin\delta)tan\phi + 8\gamma H z k_o\tan\delta + 8\gamma z^2\tan\delta\,(k_o cos\delta + sin\delta)tan\phi \quad (4.52)$$

Integrating concerning 'z' within limit 0 to l Eqn. (4.52) and simplifying yield ultimate group pullout capacity of soil nail:

$$F = C_X(\gamma H + o)(\tan\delta + (k_o cos\delta + sin\delta)tan\phi)l + \frac{4}{3}\gamma l^3\tan\delta\,(\tan\delta + (k_o cos\delta + sin\delta)tan\phi) \quad (4.53)$$

In present study the nail groups were experimentally tested using different arrangement is shown in Fig.4.5 (c and d), which is further validated using theoretical model as discussed earlier for single and group of helical nails.

4.4 SUMMARY

The installation torque and pullout load are considered as the most important parameters in the design of a helical soil nail wall. In this chapter the theoretical equations for installation torque and pullout capacity of helical soil nails are presented. The proposed theoretical models investigating the pullout behavior of a soil nail in the passive zone based on a simple load transfer model of the nail-soil interface. An extensive parametric study was performed to examine the effects of key model factors on the pullout response of soil nails in different pullout phases (pure-elastic and elastic-plastic).

CHAPTER-5

RESULTS AND DISCUSSIONS

CHAPTER 5
RESULTS AND DISCUSSIONS

5.1 GENERAL

This section contains the detailed laboratory test results of different single and a group of helical soil nail specimens. Further, the installation torque and pullout test results are also estimated and validated for a similar test scheme using a different theoretical model. Based on experimental and theoretical results evaluations regarding the important observations are also revealed in the present section.

5.2 EFFECT ON INSTALLATION TORQUE

The installation of the helical element under torque head is influenced by different parameters which include angle of internal friction of soil, interface friction angle, adhesion, unit weight of soil and nail, relative density, and grain size of soil [96-100]. For installation of helical soil nail the shaft type, shape, shaft diameter, shaft roughness, helix diameter, helix thickness, number of helices, helices pitch, and methods of installation also influences the torque during installation. The installation torque of the helical element influences the pullout capacity of the different helical elements [79-89]

Hoyt and Clemence [12] suggested a relationship between pullout capacity and installation torque for vertically installed helical elements as given by Eqn. (5.1)

$$Q_u = K_t T \tag{5.1}$$

where K_t = empirical factor;

Q_u= Pullout capacity (kN);

T = Average installation torque (kN-m)

Different design manuals for earth retaining systems using helical nailing also adopted Eqn. (5.1) [114-115]. However, for the helical soil nail author was unable to find any published study for the helical soil nails. Thus, based on the testing result of installation torque and pullout capacity of helical soil nail under varying pressure the relationship has been established.

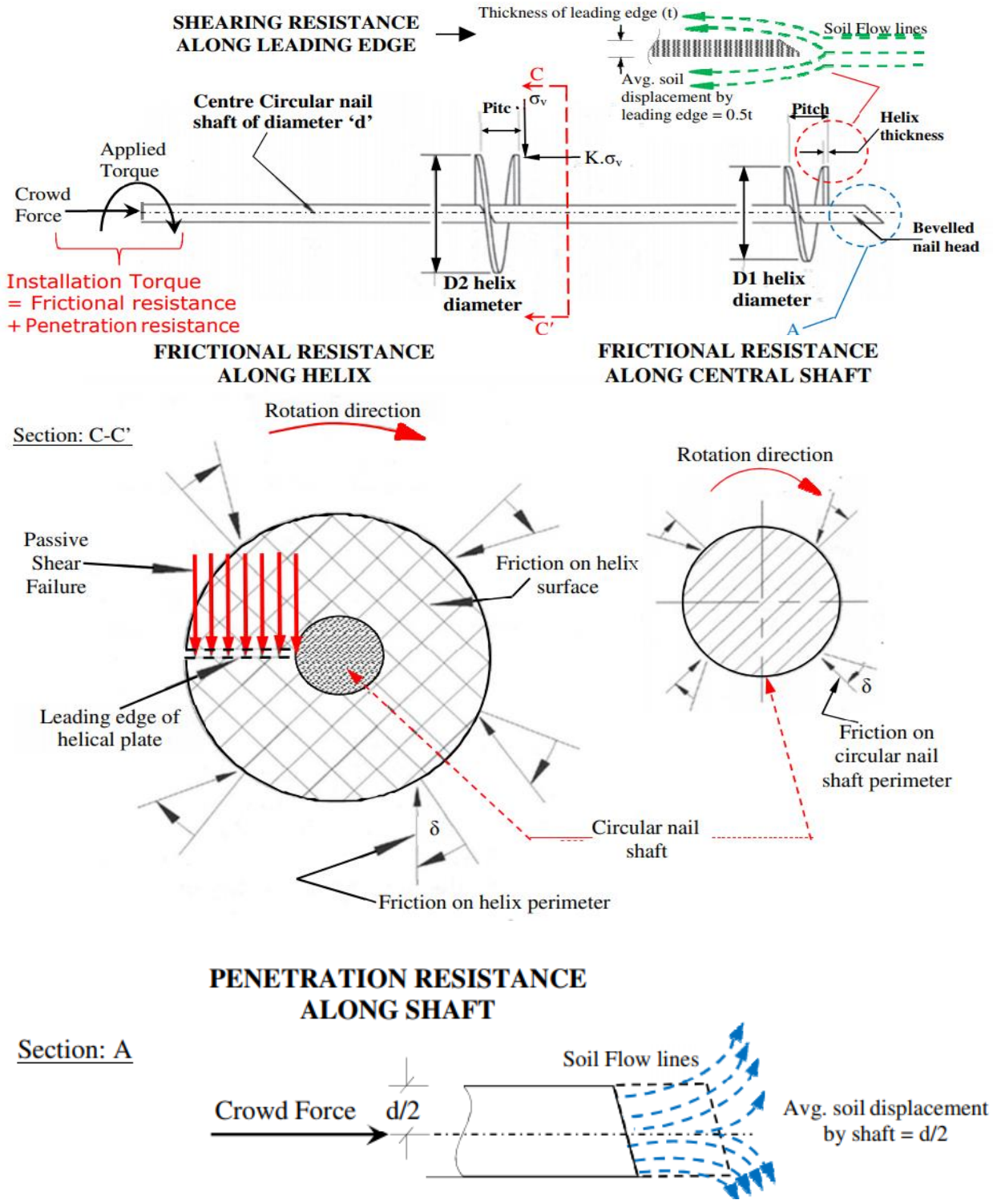

Fig.5. 1 Forces acting during installation of helical soil nail

The installation of helical soil nail undergoes frictional and penetration resistance on a helical plate and nail shaft against the lateral pressure ($K\sigma_v$). Evident from Fig. 5.1 (Section C-C'), the

frictional resistance that occurs on the helices plate increases with the square of helices diameter [115]. Additionally, the perimeter of the helical plate governed by the thickness also imparts frictional resistance. The helical pitch also plays a significant role to change the frictional resistance. As the pitch of helices is larger pitches had to slice against a bulky amount of soil and the resulting increase in work done by friction resistance against the soil friction. The friction resistance also weakly depends on shaft friction during installation. Thus, the allover frictional resistance of helical soil nails is equal to the resistance offered by the net surface area of helical soil nails inside a soil mass. For high efficiency of installation torque of circular nail, shaft requires considerable energy for the installation of circular shaft helical soil nail. Therefore, the total work or frictional energy or energy loss that occurs at the stage of installation depends on the nail shaft and helices as sum up in Eqn. (5.2):

$$Energy\ Loss_{(Friction)} = \sum Energy\ loss\ of\ Individual\ helix\ _{(Friction)} + L\ _{(shaft\ in\ friction)} \tag{5.2}$$

Simultaneously, penetration resistance offered by the beveled nail head and the edge of helices act on the leading edge of the nail. The size of the leading edge includes the diameter and thickness of helices. As the leading edge slash through soil mass, the passive resistance due to shearing starts mobilizing As the installation length of the helical nail increases into the soil mass, it displaces the amount of soil equal to half of the helix thickness [115]. This reveals that as lesser the thickness of helices, the minimum will be the disturbances during installation. Another component of penetration resistance occurs at the center of the shaft area of the nail head. With the increase in the shaft diameter, the net surface area of the nail head rises as well, resulting in increases in overall penetration resistance. Evident from Fig.5.1 (Section: A), the amount of soil displaces by the nail head is equal to the half shaft diameter. Thus, more the shaft diameter more will be the displacement of soil correspondingly more works to be done. Thus, total penetration energy per rotation is expressed as in Eqn.5.3:

$$Energy_{(Penetration)} = \sum Soil\ volume\ displaced\ by\ each\ helix + Soil\ volume\ displaced\ by\ nail\ head \tag{5.3}$$

Thus, the installation energy is desirable to beat the resistance offered by friction and penetration.

Thus, the drive head of the device offers desirable rotational energy and crowd force. The 'installation torque' is therefore defined as the energy generates during the rotation of the nail to overcome the frictional and penetration resistances. The main contribution of crowd force is usually during the beginning of installation and also penetration purpose of soft to hard soil strata. As reported in the literature, for vertically installed helical element the installation torque for the estimation of uplift force is taken the last value of torque or the average value at depth of three times the mean helix diameter [9]. The explanation for adopting this installation torque is that the vertical helical element shift soft to hard soil stratum at greater depth, thus vertical stress is directly proportional to the installation depth of vertical installed helical element and thus raise the lateral pressure on the helical plates. Hence, for vertically installed helical elements the installation torque required at the final stage of installation is significantly high. To balance the variation of installation torque due to change in soil stratum the installation torque is adopted as an average value. However, as per FSI [8] suggests the last installation torque is debatably and hence installation torque during the entire path should be measured

In the current study, the installation torque was measured throughout the installation length to identify the peak installation torque value (T_{max}). Since a homogeneous soil excluding any stratification and uniform relative density was adopted for the model testing program, the peak value of installation torque was considered critical. Also, unlike vertical anchors, the constant lateral earth pressure ($K\sigma_v$) practiced by the helical soil nail because of constant vertical stress (σ_v) for a horizontally installed element, which is another reason for adopting T_{max} value as critical. Thus, the Eqn. (5.1) has been modified for determining K_t utilizing peak installation torque (T_{max}) for different nail specimens and relates it to the peak pullout capacity ($Q_{u(max)}$) as given by Eqn. (5.4)

$$Q_{u(max)} = K_t T_{max} \tag{5.4}$$

Where, K_t = empirical factor (m^{-1});

$Q_{u(max)}$ = Peak pullout capacity of (HN) (kN);

T_{max} = Peak installation torque (kN-m).

As per Eqn. (5.4), the Empirical factor (K_t) for helical soil nails with solid and hollow shaft were found in a range of 19 m^{-1} to 61 m^{-1} and 23 m^{-1} to 58 m^{-1} respectively. The empirical factors for various helical soil nail specimens under varying pressure conditions are listed in Table 5.1. The Empirical factor (K_t) or capacity-to-torque ratio for individual solid and hollow shafts is

evaluated on basis of the peak pullout capacities with peak installation torque (Fig.5.2). Also, combined cases of the solid and hollow shaft were presented by linear relationship in Fig.5.2. The Empirical factor (K_t) is the slope of the line between $Q_{u(max)}$ and T_{max} as shown in Fig.5.2. All specimens were installed at the rate of 10 rpm with the rate of penetration equal to one helix pitch in one revolution.

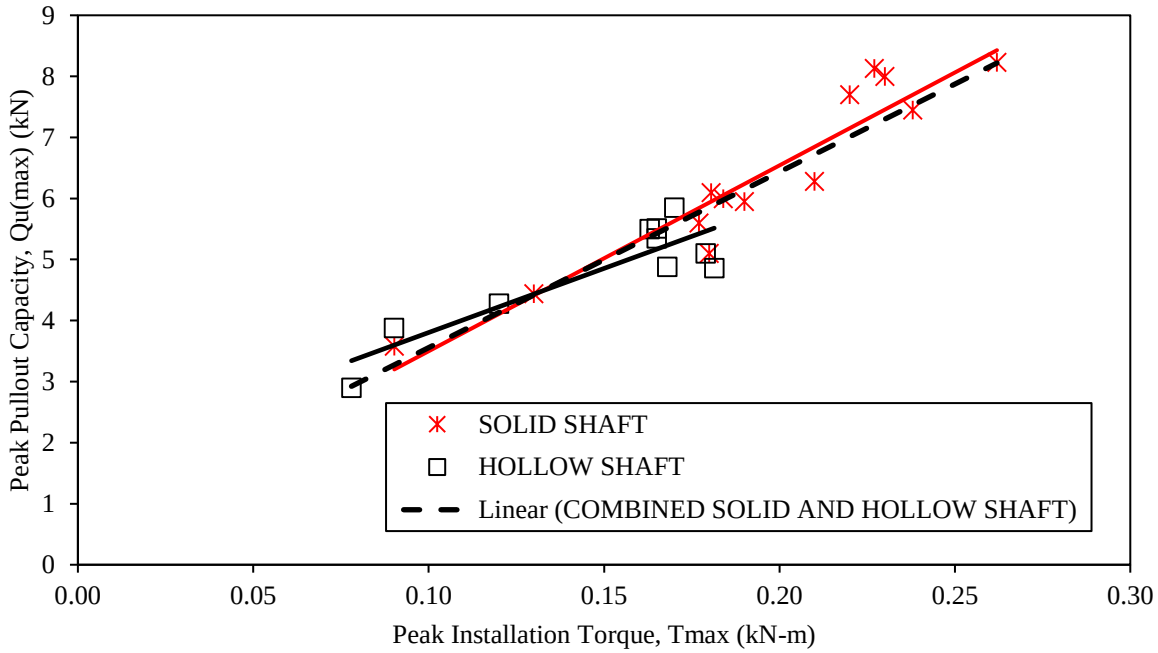

Nail type	**Regression equations**	**R^2 value**
Solid shaft nail	$Q_{u(max)} = 30.4T_{max} + 0.5$	$R^2 = 0.90$
Hollow shaft nail	$Q_{u(max)} = 21T_{max} + 1.7$	$R^2 = 0.78$
Combined solid and hollow shaft	$Q_{u(max)} = 28.8T_{max} + 0.7$	$R^2 = 0.89$

Fig.5. 2 Relationship between peak pullout capacities with peak installation torque

Table 5. 1 Peak installation torque and pull out capacity values for different nail specimens under varying pressure.

Nail Identification	**5kPa**				**12.5kPa**				**25kPa**				**50kPa**				**Shear Stress**	
Solid Shaft helical nail	T_{max} **[kN-m]**	$Q_{u(max)}$ **[kN]**	**K$_t$ =** $\frac{Q_{U(max)}}{T_{max}}$ $[m^{-1}]$	**IF**	T_{max} **[kN-m]**	$Q_{u(max)}$ **[kN]**	**K$_t$ =** $\frac{Q_{U(max)}}{T_{max}}$ $[m^{-1}]$	**IF**	T_{max} **[kN-m]**	$Q_{u(max)}$ **[kN]**	**K$_t$ =** $\frac{Q_{U(max)}}{T_{max}}$ $[m^{-1}]$	**IF**	T_{max} **[kN-m]**	$Q_{u(max)}$ **[kN]**	**K$_t$ =** $\frac{Q_{U(max)}}{T_{max}}$ $[m^{-1}]$	**IF**	tanδ	**c$_a$**
A	0.05	1.92	36.23	14.50	0.06	2.51	41.15	7.58	0.08	2.93	38.15	4.42	0.09	3.58	39.69	2.70	0.75	52.13
B	0.07	2.32	33.62	15.01	0.08	3.04	36.63	7.87	0.12	3.63	31.57	4.70	0.13	4.44	34.15	2.87	0.81	55.32
C	0.09	2.86	31.78	16.20	0.11	3.80	34.55	8.61	0.15	4.65	31.00	5.27	0.18	5.60	31.64	3.17	0.86	62.05
D	0.11	3.30	30.00	16.61	0.14	4.15	29.64	8.36	0.17	5.05	29.71	5.08	0.21	6.28	29.90	3.16	0.92	60
C1	0.07	3.10	43.66	17.55	0.12	4.13	34.42	9.35	0.15	5.00	33.33	5.66	0.18	6.00	32.61	3.40	0.89	71.22
C2	0.07	3.15	43.15	17.84	0.13	4.19	33.52	9.49	0.16	5.09	31.04	5.76	0.18	6.10	33.80	3.45	0.85	68.50
C3	0.08	3.00	38.41	16.99	0.13	3.95	31.32	8.95	0.17	4.70	27.17	5.32	0.19	5.95	31.32	3.37	0.83	69.42
I	0.15	3.42	22.50	19.28	0.22	4.09	18.61	9.23	0.23	5.80	25.22	6.54	0.24	8.45	35.50	4.76	0.82	81.55
J	0.18	3.63	20.74	20.37	0.25	4.75	19.07	10.66	0.27	6.23	23.07	6.99	0.26	9.23	35.23	5.18	0.89	82.12
K	0.15	5.07	33.80	28.52	0.17	7.02	41.29	15.80	0.19	9.68	50.95	10.89	0.22	12.70	57.73	7.14	0.98	106.17
L-Rough	0.16	6.00	37.50	33.75	0.18	8.30	46.11	18.68	0.20	10.63	53.15	11.96	0.23	13.23	58.28	7.44	0.99	109.8
N	.163	6.1	37.42	35	.185	9	48.64	19	.20	11	54	12	.23	13.5	59	7.7	.98	100
N-rough	0.17	6.80	40.00	37.99	0.19	9.20	48.42	20.56	0.21	11.50	54.76	12.85	0.23	14.00	60.87	7.82	0.99	93.45
N-4	0.15	3.5	23.33	18	0.21	4.5	21.42	11	0.17	7	33.33	6	0.19	8	42.1	4.3	0.83	68
P	-	1.20		5.69	-	1.63		3.71	-	1.67		1.90	-	2.10		1.14	0.39	14.52
Hollow Shaft Helical nail																		
E	0.05	1.42	28.40	5.37	0.05	1.87	37.40	2.83	0.07	2.34	33.43	1.77	0.08	2.90	37.18	1.10	0.47	17.68
F	0.06	1.74	31.64	5.64	0.07	2.42	34.57	3.14	0.10	3.00	30.00	1.95	0.13	3.88	29.85	1.26	0.60	22.05
G	0.07	2.00	30.63	5.67	0.09	2.68	29.39	3.04	0.13	3.43	27.01	1.95	0.17	4.28	25.48	1.21	0.72	15.64

H	0.09	2.54	28.22	6.41	0.11	3.32	29.38	3.35	0.15	4.23	28.20	2.13	0.18	5.10	28.49	1.29	0.74	17.89
G1	0.06	2.19	34.22	6.21	0.09	2.87	31.89	3.26	0.13	3.75	29.76	2.13	0.17	4.51	27.33	1.28	0.81	16.28
G2	0.07	1.98	30.46	5.62	0.09	2.76	30.33	3.13	0.13	3.63	28.36	2.06	0.17	4.55	27.58	1.23	0.75	17.98
G3	0.07	1.77	25.65	5.02	0.10	2.51	26.06	2.85	0.13	3.33	24.74	1.89	0.18	4.26	23.48	1.18	0.67	14.74
M	0.10	3.00	30.00	8.48	0.12	4.50	38.79	5.09	0.14	6.40	45.71	3.62	0.17	8.85	52.06	2.50	0.65	25.15
O	0.08	4.00	51.28	11.27	0.10	5.00	49.50	5.64	0.13	7.00	54.26	3.95	0.16	9.50	58.28	2.68	0.60	25.30
O-4	.06	2	33.33	5	0.1	3.5	35	3.11	0.14	3.3	25	2.2	0.17	4.5	26.47	1.2	0.74	18
Q	-	0.87		2.47	-	0.96		1.09	-	1.00		0.57	-	1.28		0.35	0.14	7.55

Empirical factor (K_t) or capacity-to-torque ratio correlation has been revealed in the form of the linear equation for both solid ($R^2 = 0.90$) and hollow ($R^2 = 0.78$) nail specimens as given in Eqn. (5.5) and (5.6):

For hollow soil nail specimens, $Q_{u(max)} = 21T_{max} + 1.7$ (5.5)

For solid soil nail specimens, $Q_{u(max)} = 30.4T_{max} + 0.5$ (5.6)

The equation generated for the combined case (hollow and solid shaft nails) rendering K_t= 28.77 $m^{-1} \approx$ 28.8 m^{-1} with fit line R^2 = 0.89. All the results calculated earlier are under constant overburden pressure of 50kPa.

$$Q_{u(max)} = 28.8T_{max} + 0.7 \quad (5.7)$$

The surface area of helical soil nail is equal to the sum of the area of helices and shaft area respectively and estimated using Eqn. (5.8)

$$A_s = A_{helix} + A_{shaft} \quad (5.8)$$

where, A_{helix} = Surface area of helices plate (mm^2);

A_{shaft} = Surface area of a shaft (mm^2)

The area of helix and shaft is calculated using Eqns. (5.9) and (5.10) as suggested by [79-89] as:

$$A_{helix} = \pi \left[\frac{{D_h}^2 - d^2}{4}\right] \quad (5.9)$$

$$A_{shaft} = \pi d L_s \quad (5.10)$$

where D_h= helix diameter;

d = shaft diameter;

L_s = effective length of the nail;

With an increase in geometric dimension of helical soil nail the area of the nail also increase. The test result reveals that as an area of nail increases, K_t decreases for both helical soil nails.

The capacity-to-torque ratio (K_t) is estimated in terms of shaft diameter for a better understanding of the theory. For helical elements, Hoyt and Clemence [80] suggest that Kt depends primarily on the shaft diameter of the nail. Perko [9] identified the K_t as a function of shaft diameter using

power regression analysis. As per the literature study, the pullout and installation torque as well both are governed by shaft friction significantly.

From the laboratory test results, evident that the diameter of the nail shaft is inversely propositional to the capacity-to-torque ratio (K_t) (Fig.5.3)

$$Kt \quad \propto \frac{1}{d} \tag{5.11}$$

Evident that as the shaft diameter of the different nails is found to increase, the capacity-to-torque ratio (K_t) starts decreasing. The reason for decreasing K_t value is that as the diameter of the shaft increase, equally the helices diameter increases which decrease the contribution of shaft friction (Fig.5.3). However, it does not indicate those bigger shaft diameters are not able to offer high pullout capacity, but it shows that during installation large energy is produced which reduces the shaft friction. Perko, [9] reported a similar kind of observation of vertically installed helical elements. For both hollow and solid shaft, helical soil nail different linear equations have been derived as given in Eqn.5.12 and Eqn.5.13. Clear from Fig.5.3, a linear regression correlation can be established among capacity-to-torque ratio (K_t) and shaft diameter (d) of the hollow and solid shaft with as given in Eqn.5.12 and Eqn.5.13 respectively. In addition, for the combined case Eqn.5.14 presented an average equation for the calculation of capacity-to-torque ratio (K_t).

For hollow shaft, $$K_t = -1.08d + 47 \ , \ R^2 = 0.86 \tag{5.12}$$

For solid shaft, $$K_t = -1.54d + 57 \ , \ R^2 = 0.95 \tag{5.13}$$

For Combine case, $$K_t = -1.3124d + 52 \ , \ R^2 = 0.72 \tag{5.14}$$

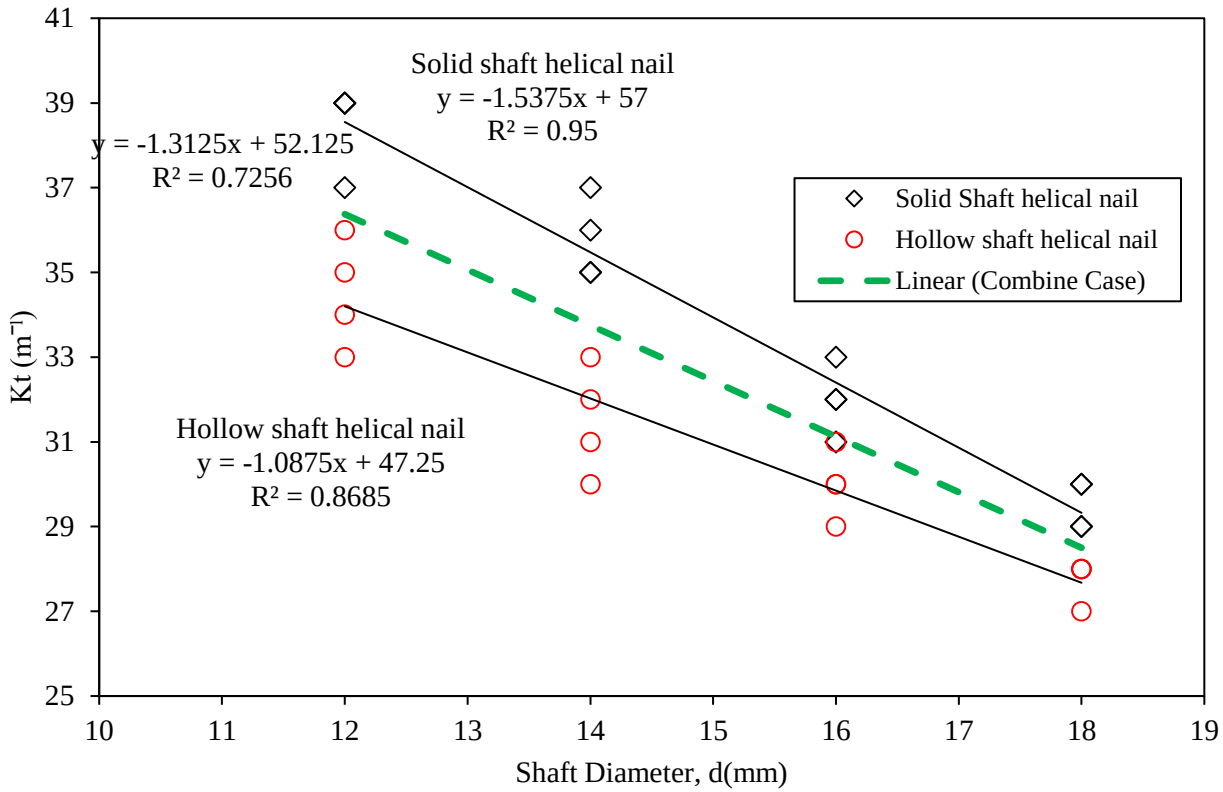

Fig.5. 3 Variation of capacity-to-torque ratio (K_t) with shaft diameter of different helical soil nail

Perko [9] reveals that at bigger shaft diameters both theoretical and empirical values of capacity-to-torque ratio (K_t) are found significantly large due to the occurrence of negligible friction along the shaft. Therefore, as the shaft diameter of helical soil nail changes from 12 to 18 mm the interface friction decreases while due to large plate diameter the friction and resistance increases. Thus, due to the large surface area and greater penetration energy, the shaft friction becomes negligible, and eventually, the capacity-to-torque ratio (K_t) decreases (Fig.5.3).

However, the decrease in K_t for bigger diameter does not represent that bigger shaft diameters are not able to offer high pullout capacity, but it shows that high installation energy is required for the placement of helical soil nails. During the pullout of helical soil nails, the shearing occurs at the edge of the dishes. The external pullout force is governed by the surface area of the helical soil nail, which formed a cylindrical shape of an enlarged diameter. This increment in pullout capacity of HN with a bigger diameter is slight as compared to the increment in installation torque. The difference in increment of required installation torque to pullout capacity is due to factors like crowd force which increases with the ratio of the square of the helical pitch to shaft radius [115], while maintaining a constant rate of installation the large

torque is required for bigger shaft diameter [126]. The relationship between shaft diameter and K_t is weakly correlated using power regression ($R^2 = 0.514$) as shown in Fig.5.4.

Nevertheless, the K_t value is found inversely propositional to shaft diameter has also been observed for a vertically installed helical element by Perko [9]. The relationship was established using power regression between capacity-to-torque ratio (K_t) and shaft diameter (d) as given in Eqn. (5.15)

$$K_t = \frac{140.2}{d^{0.54}} \tag{5.15}$$

Though, the weak correlation ($R^2 = 0.514$) attributed to a small range of shaft diameter (12 mm – 18 mm) adopted in the study.

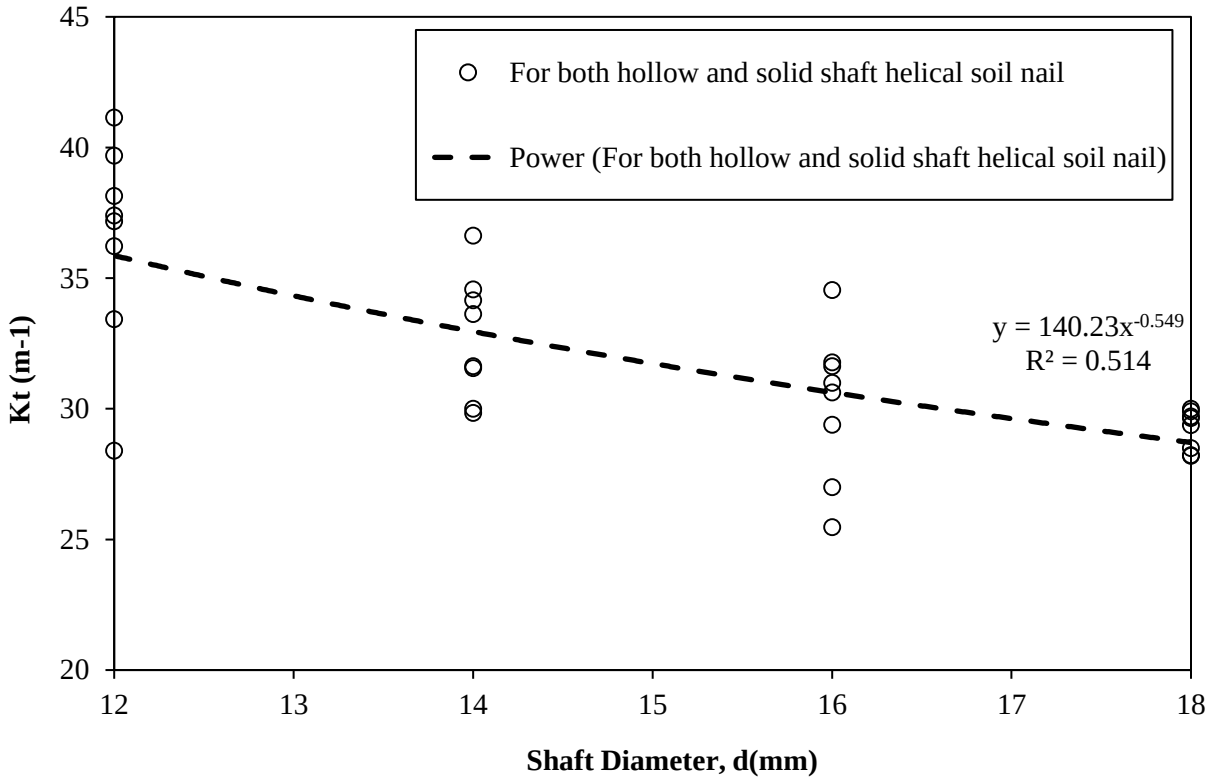

Fig.5. 4 Capacity-to-torque ratio (K_t) with shaft diameter

From Table 5.1, evident that shaft type, helical pitch, surface roughness, surcharge pressure, and a number of helices significantly influence the installation torque. To investigate the installation torque with surcharge pressure of different helical soil nail specimens, dimensional less parameter have been investigated. The Normalized installation torque is thus calculated as the ratio of peak installation torque of different nail specimens to the peak installation of the smallest shaft diameter of hollow and solid shaft helical soil nail (i.e nail A and

E). Thus, the normalized installation torque $\left[\frac{T_{max}}{T_0}\right]$ can be used to estimate the peak installation torque for different model helical soil nails.

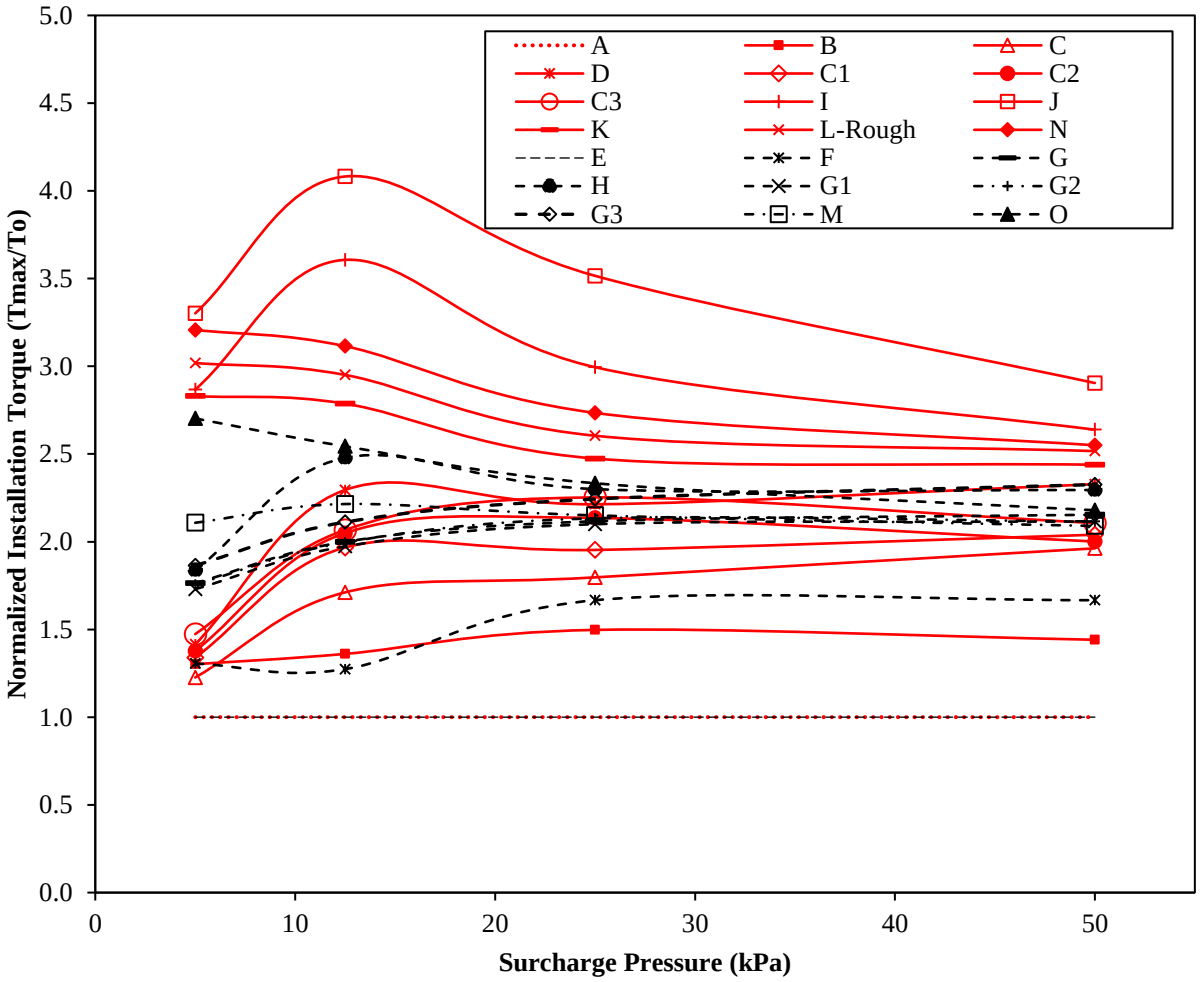

Fig.5. 5 *Normalized installation torque* $\left[\frac{T_{max}}{T_0}\right]$ *with surcharge pressure*

From Fig.5.5, clear that the shaft diameter is directly proportional to $\left[\frac{T_{max}}{T_0}\right]$. A similar type of observation was observed for nails in which the number of helices increases from single to multiple. It is also observed that $\left[\frac{T_{max}}{T_0}\right]$ of the solid shaft is greater than the hollow shaft helical nail. Also, the $\left[\frac{T_{max}}{T_0}\right]$ increases with surcharge pressure from 5to12.5kPa and then start falling gradually as surcharge pressure reaches 50kPa.

In addition, another dimensionless factor $\left[\frac{D_h}{d}\right]$ is term as the ratio of helical plate diameter to shaft diameter is adopted to estimate the torque efficiency of a helical soil nail, observed that increasing$\left[\frac{D_h}{d}\right]$ ratio present good torque efficiency. It is found that peak installation torque is also found to directly proportional to $\frac{D_h}{d}$ ratio for solid shafts helical soil nail comparative to hollow nail, which amplify with the number of helices plates. Thus, it can be concluded that nail with triple helices plates offers the best performance as compared to single, double, and hollow shaft nail. The leading edge of the helical soil nail governs the installation torque depends on the helical size which is the function of shaft diameter. The gap between the leading and trailing edge of helices is called pitch. This intended that the greater the pitch of helices, the larger the distance travel and thus subjected to greater resistance to an external force. The penetration resistance during installation is evaluated in terms of the dimensionless factor of $\left[\frac{D_h}{p}\right]$ which is the ratio of helical diameter to helical pitch. For $\frac{D_h}{p}$ ratio equal to 1.6 found at peak installation torque of a single-plate helical soil nail. The peak installation torque starts decreasing as $\frac{D_h}{p}$ ratio changes from 1.6 to 2.1. Further, peak installation torque decreases beyond $\frac{D_h}{p}$ ratio 2.1. It is explained as that small energy is required for smaller work done against resistance by a small pitch while keeping the helix diameter constant. Keeping the pitch of helices constant with varying or increasing helical diameter offers more frictional resistance from plate helices, which causes more soil displacement. Also, the installation behavior is significantly influenced by the nail depth. The soil disturbance during installation was caused due to the revolution of helical dishes and advancement of shaft respectively. As the helical plate crosses the soil mass that creates coiled shaped cut at pitch distances. Thus, the soil mass is slip and sheared in both horizontal and vertical directions respectively. Due to the passage of helical plate through soil mass, radial displacement at the border of plate occur resulting in decreases in the shear strength of in-situ soil. The helices with similar geometry will not reduce the stiffness and shear strength of soil due to tracing the existing path. However, varying or increasing diameter size of helices causes extra disturbances comparative to the formal case, thus reducing the field properties of soil. Hence, helices with the largest diameter size are considered critical from a disturbances point of view. Keeping this in mind, the $\left[\frac{L}{D_h}\right]$ ratio of the installation depth of horizontally placed

element from the initial position to the bigger helical size is thus used to estimate the incremental shearing strain during the driving process of the nail [127].

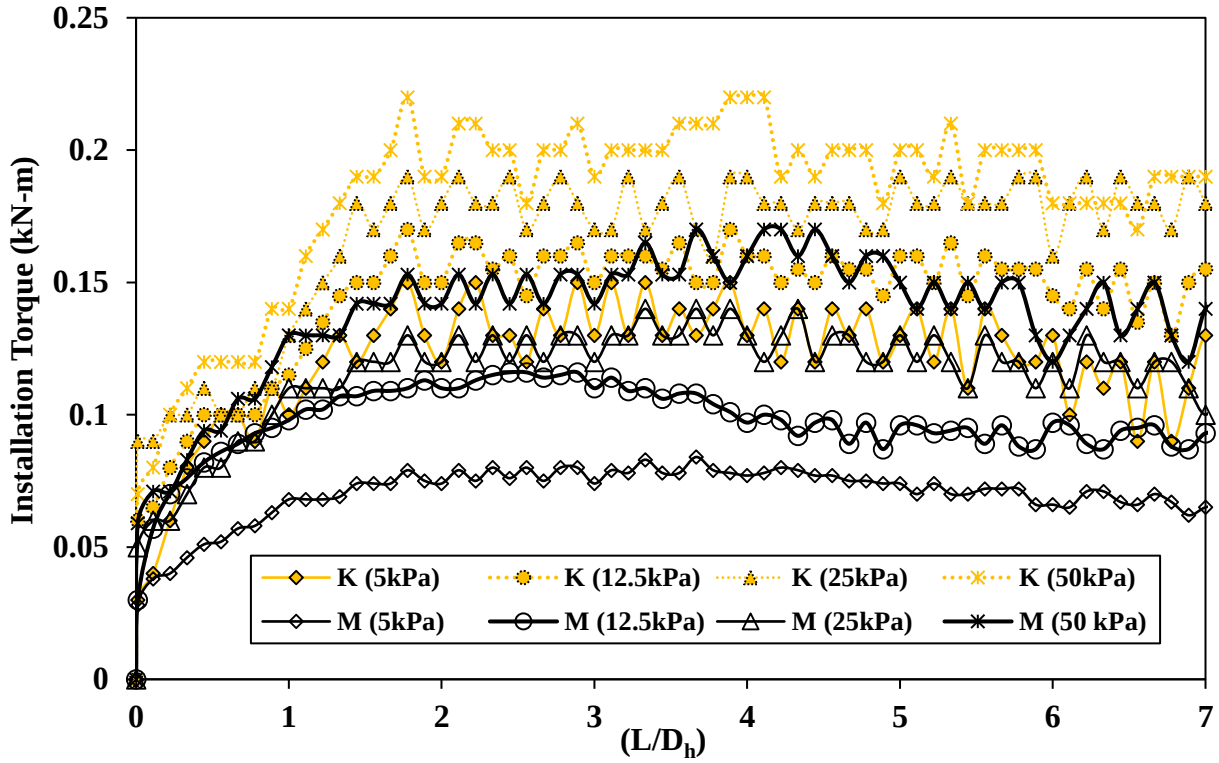

Fig.5. 6 Installation torque with $\frac{L}{D_h}$ ratio

Evident from Fig.5.6, the zig-zag pattern represents the strain-softening behavior taking place inside the soil mass during installation of helical soil nail with hollow and solid shaft. A Strain-softening event is defined as a decrease in resistance with nonstop shearing beyond maximum resistance and represents by the stress-strain behavior of soil.

Concurrently, during the driving of helical soil nails, the torsional shearing stress is accomplished due to the revolving of the helical plate. With the installation progress of the helical soil nail, the turning force achieves a point where the rate of change of ultimate value reallocates from positive to negative with nonstop shearing. The fact is also observed during the recording of installation torque, which is presented as torsional shearing stress (τ_T) as per fundamentals of basic mechanics as shown in Eqn. (5.16)

$$\tau_T = \frac{16T}{\pi D_h^3} \tag{5.16}$$

where, T = Installation torque (kN-m);

D_h = Diameter of the largest helix.

Moreover, change in installation length to original length or normalized embedded length $\left[\frac{\Delta L}{L}\right]$ can able to investigate the incremental shearing strain mobilized during advancement of the nail. Therefore, the stress-strain behavior of soil-nail can be evaluated in terms of torsional stress with normalized embedded length as shown in Fig.5.7. Evident that with an increase in normalized embedded length$\left[\frac{\Delta L}{L}\right]$, the strain-softening event occurs. The presented variation is analogous to the Installation torque with $\frac{L}{D_h}$ ratio.

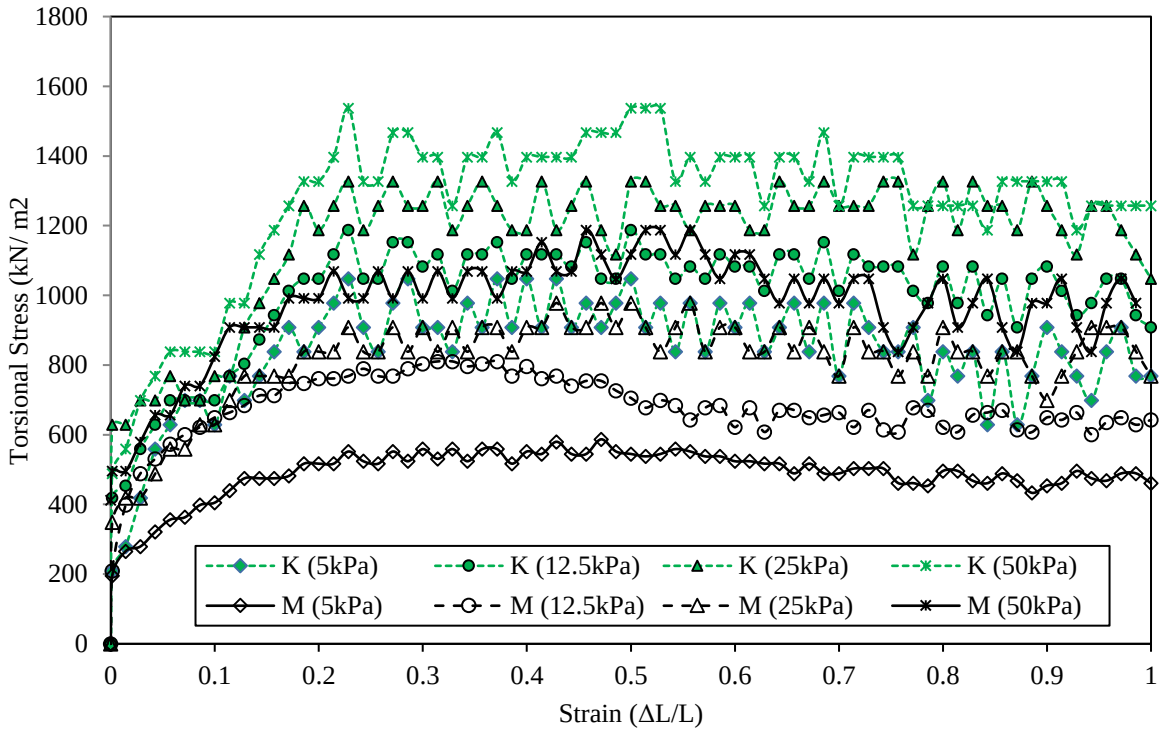

Fig.5. 7 Torsional stress against normalized embedment length

5.3 INSTALLATION TORQUE DURING INSTALLATION

The variation of installation torque capacity with surcharge pressure for different types of helical nail specimens is shown in Fig.5.8 (a) to (i). The test results show that the installation load increases nonlinearly at the initial stage until the peak is reached, and the rate of increase becomes negligible thereafter. As the embedded surface area of the nail increases with the embedded length, there is a proportional increase in the driving resistance acting on the soil nail during installation. Clear from the testing result that installation torque is directly proportional to

overburden pressure. The peak value of installation torque for different nail specimens is reported in Table.5.1. Also, the test result signifies that the helical soil nail geometry significantly influences the installation torque. A similar kind of path has been followed by different nail specimens with varying torque installation value.

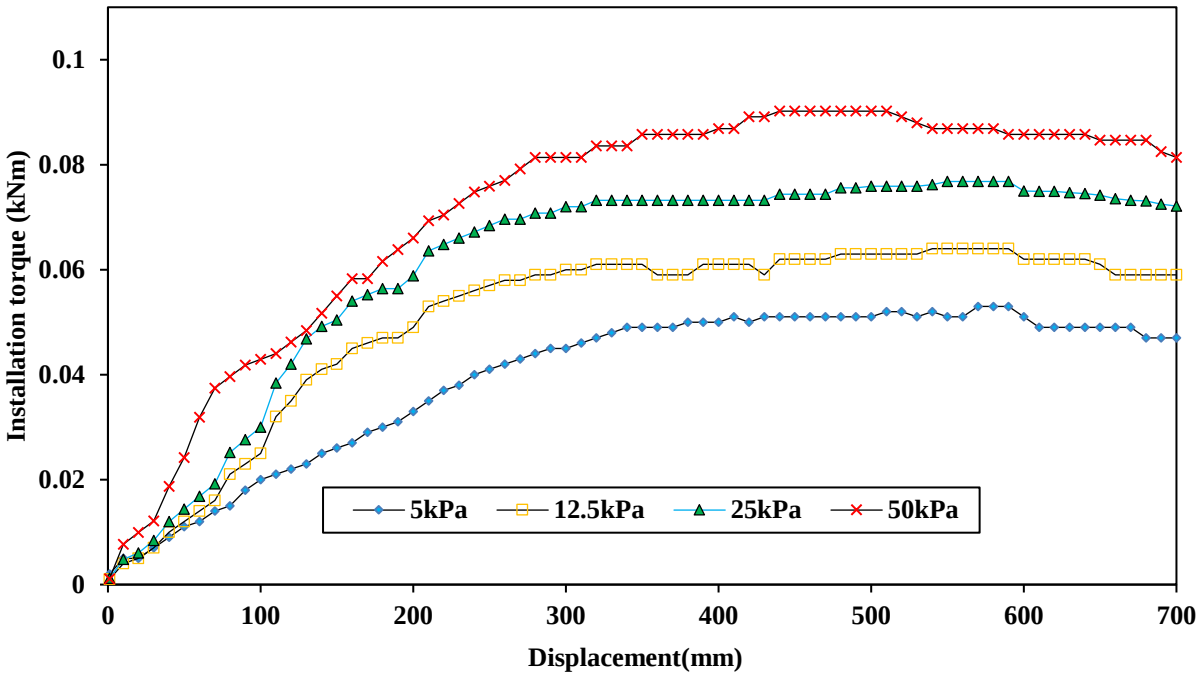

(a) Specimen A

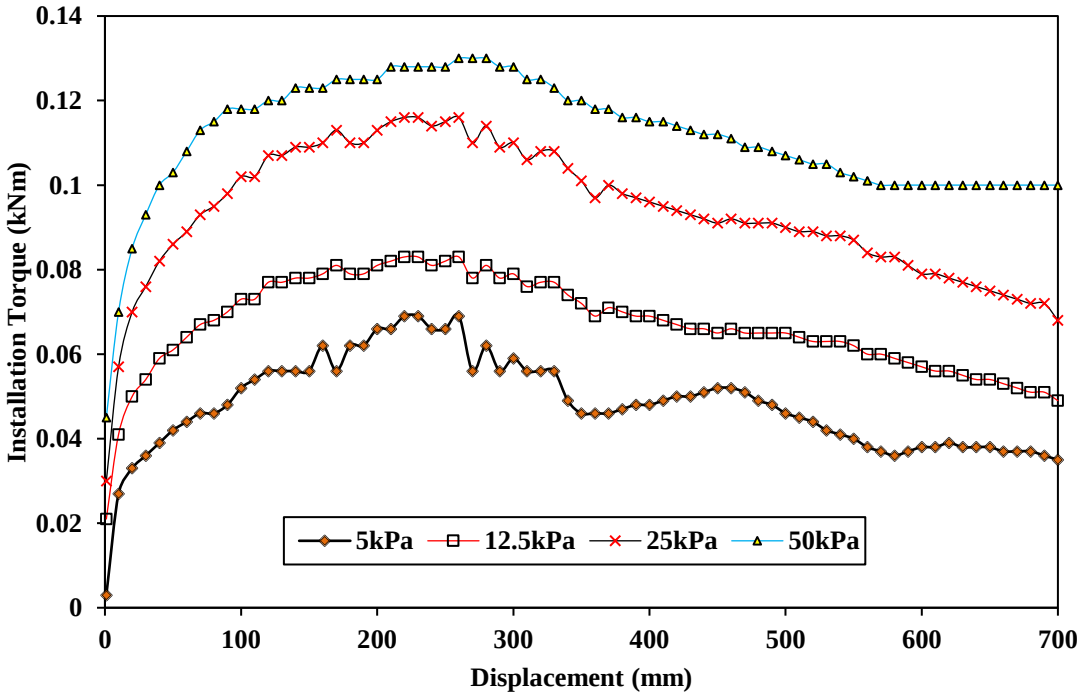

(b) Specimen B

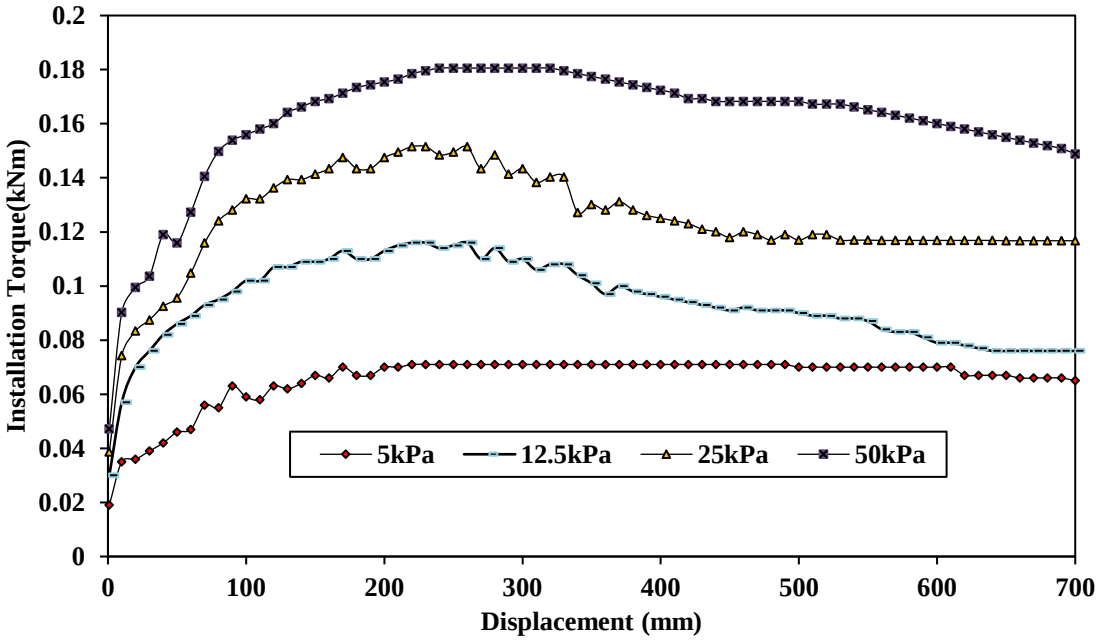

(c) Specimen C

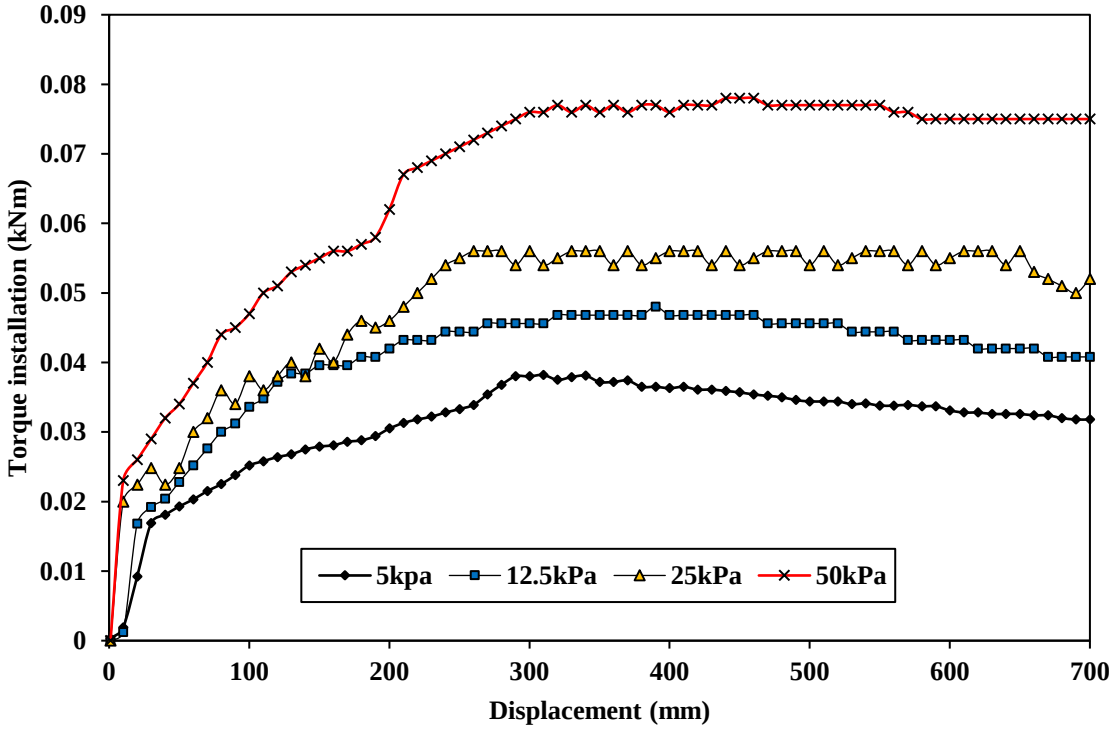

(d) Specimen E

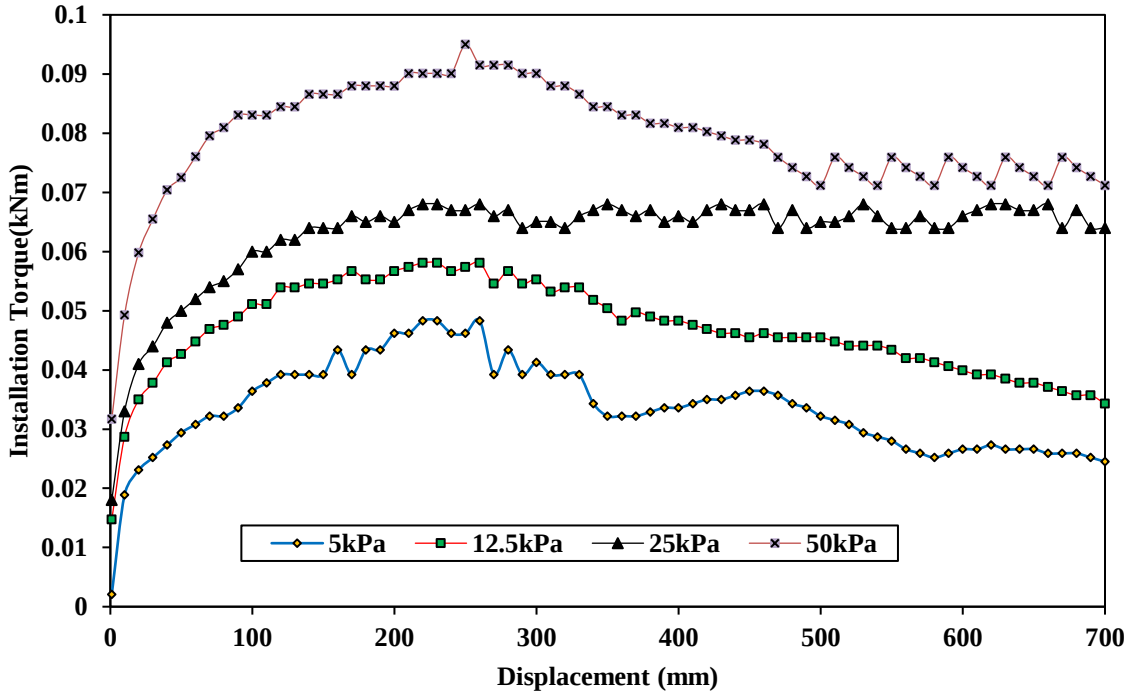

(e) Specimen F

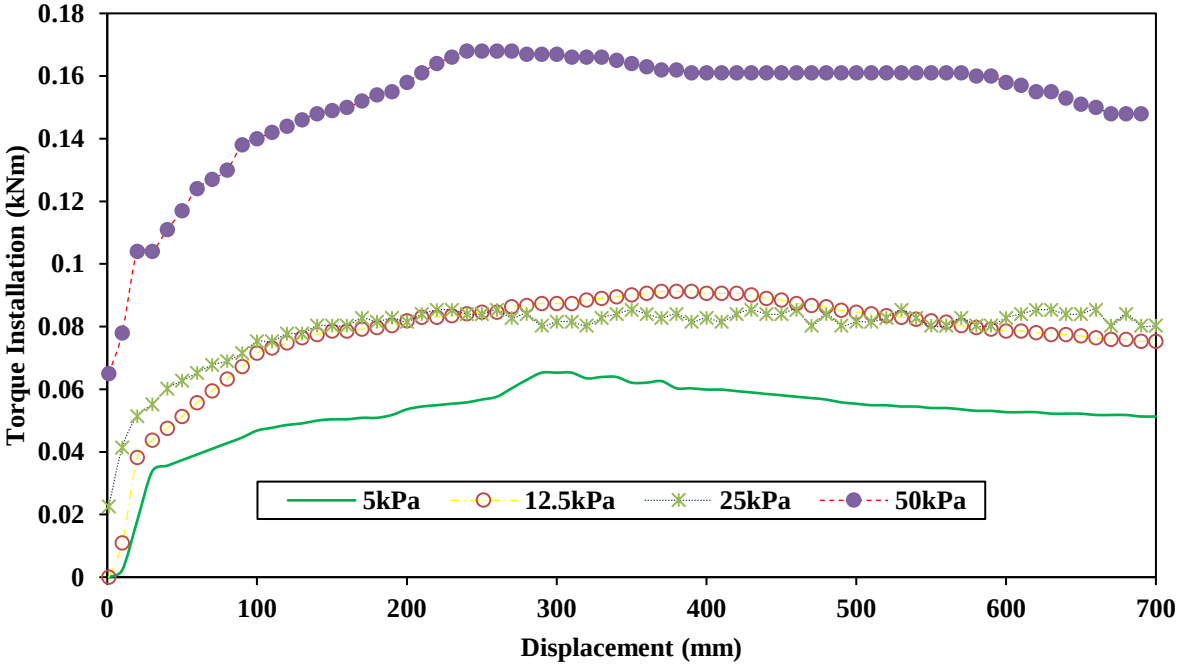

(f) Specimen G

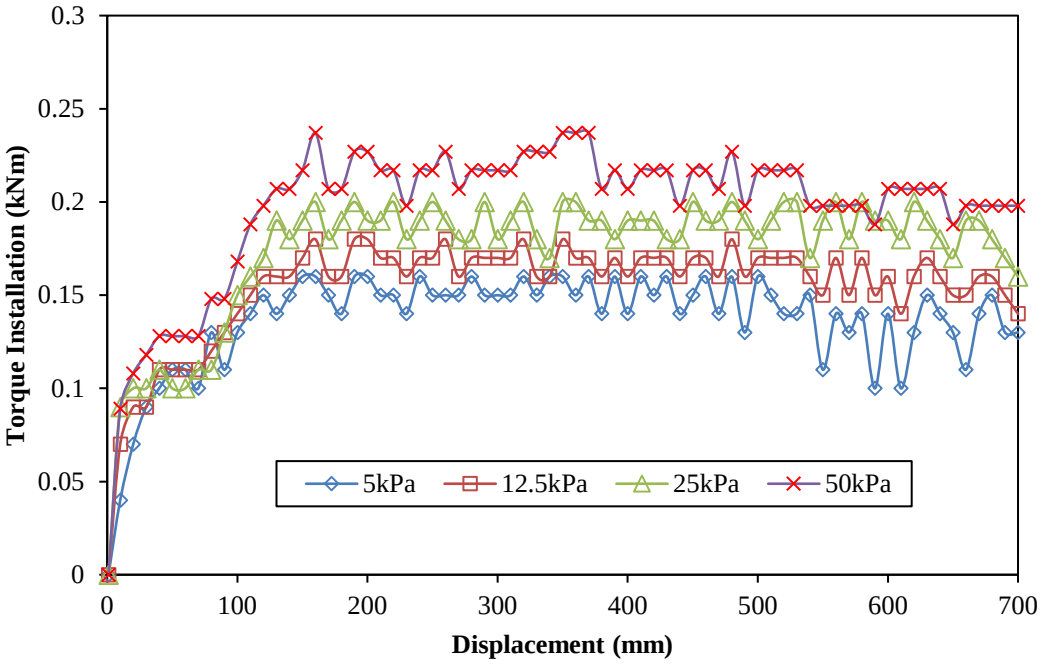

(g) Specimen L-rough

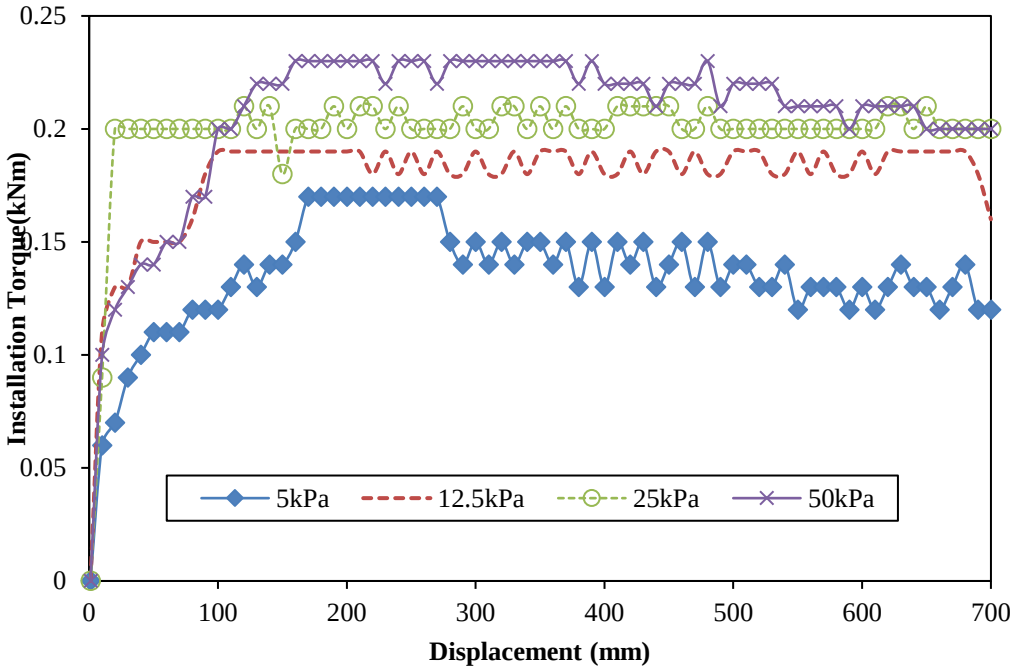

(h) Specimen N

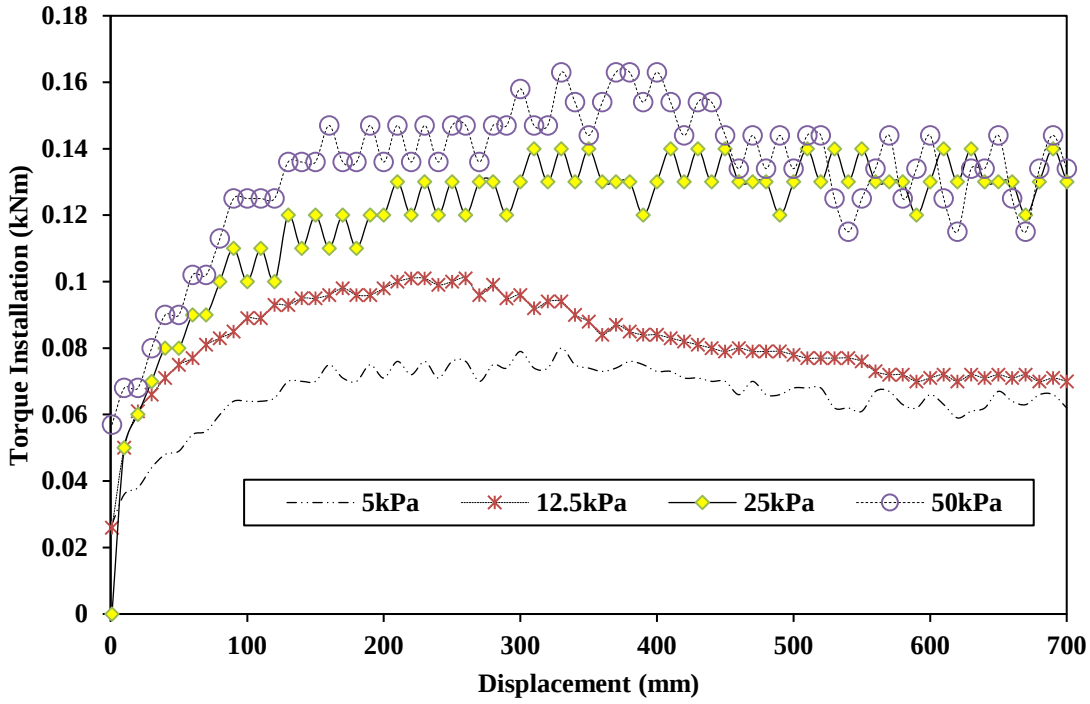

(i) Specimen O

Fig.5. 8 Variation of Installation Torque with Displacement

5.4 PULLOUT STRENGTH

5.4.1 Single helix

Evident from Table 5.1, the pullout strength of hollow shaft helical soil nail is smaller than the solid shaft helical nail specimens. This may due to the weight of hollow nail specimens is approximately 3 times lesser than the weight of solid nail specimens to maintain the constant or equal outer diameter of the hollow nail as that of the solid nail. The average pullout strength for ‘A’ to ‘B’ and ‘B’ to ‘C’ increases by 21% to 24% and 23% to 28% respectively under different overburden pressure. However, the increment in average pullout strength of ‘D’ compared to 'C' is only 9%, which is comparatively less than the formal cases. This shows that as the shaft diameter increase correspondingly the helical diameter also increases, due to which significant disturbances are generated to the adjacent soil. As the disturbances occur to the soil mass the in-situ properties of soil also change [115]. Therefore, specimen 'C' (i.e. 16 mm shaft diameter) was adopted for further geometrical alterations in model helical soil nail. A similar type of observations was also observed for hollow shaft model nail specimens. Also, it is found

that the pullout capacity of 'A' and 'B' was equal to hollow nail specimens 'G' and 'H' respectively. Thus, it can be concluded that solid shaft nails can be partially replaced by 27% to 34% bigger shaft diameter of the hollow nail. Thereby increase in the economy of helical soil nails by saving the material without compromising the pullout strength of soil nails.

5.4.2 EFFECT OF HELICAL PITCH

For the model testing of helical soil nail, Sharma et al. [30] experimented on two different pitches of 23.5 mm and 37 mm in the past literature. The authors [30] reported that maximum pullout capacity improved slightly with increment in pitch. However, in the past literature, no such study mentions the maximum allowable pitch or pitch range on installation torque and pullout strength. Thus, based on two pitches of helices (i.e. 23.5 mm and 37 mm), it becomes complex to understand the pullout and installation torque results. To investigate the influence of pitch two helical nail specimens i.e 'C' and 'G' were selected based on the pullout performance in the first group. The selected nails were investigated with pitch variation of 30 mm, 35.5 mm, and 41 mm respectively.

From Fig.5.9, it is clear that pullout capacity increases with increase in helical pitch. However, beyond a pitch of 35.5 mm, maximum pullout capacity is found to decrease. This can be accounted to the fact that increases in pitch initiates augering effect in the soil. The auguring effect mainly involves crushing of soil grains during rotation and hence leading to high disturbances during installation. Auguring Effect is defined as the rotation of helix without the forward advancement of helical element [96-100]. When a helical nail is rotated during installation the forward movement progress is slowed down or ceases which commonly causes a considerable decrease in the installation torque. The phenomenon is observed with helical plates not conforming to ‘true helical shape’ defined as parallel leading and trailing edges or helical plates perfectly perpendicular to the shaft. It is also observed to occur mostly when helix displaces from a less dense to more dense soil stratum. The rotation of helix with stalled advancement causes significant disturbances to the adjacent soil and under continuous shearing stress crushing of soil grains occurs. In the present study, the auguring effect is related during the nail installation and since pullout capacity is affected by the installation process, it has been related to the decreased pullout capacity of helical nail with large pitch of 35.5 mm. Moreover, auguring effect is also found to effect torque and pullout capacity relationship [114-115]. These

significant disturbances also results in reduction of ϕ, thereby corresponding to decreased pullout strength [97].

The reported literature also depicts same failure bulbs at the helices for different helical pitch suggesting that failure surface created about helices are depends upon helix diameter rather than pitch [98-100]. On the contrary, the present study observed that variation in pitch influences the failure bulb development beyond 35.5 mm thus leading to a decrease in pullout capacity of the nail. For helical nails with shaft diameter of 16 mm and single helix of diameter 64 mm, maximum pullout capacity is found for pitch of 35.5 mm for solid shaft and 30 mm for hollow shaft at overburden pressure of 25kPa. The higher pullout value of hollow shaft at a smaller pitch of 30 mm can be attributed to additional frictional resistance from soil plug formed inside the hollow shaft [97]. It can also be seen from Table 5.1, that percentage increase in maximum pullout capacity of helical nail 'C2' in comparison to 'C' is found to be 10.14%, 10.26%, 9.46%, and 8.93% for overburden pressures of 5 kPa, 12.5 kPa, 25 kPa, and 50 kPa respectively. Similarly, percentage increase in maximum pullout capacity for helical nail 'G1' with respect to 'G' is 9.50%, 7.19%, 9.33% and 5.37% for overburden pressures of 5 kPa, 12.5 kPa, 25 kPa, and 50 kPa respectively. Thus, it can be stated that with increase in overburden pressure and pitch from 24.5 mm to 35.5 mm, pullout capacity is found to increase irrespective of the shaft type i.e. hollow or solid. Thus, a helix pitch of 30 mm is recommended for helical nail configurations for model testing. However, in full-scale practice, the recommended pitch size for helix is 76.2 mm (3 inches ± ¼ inches).

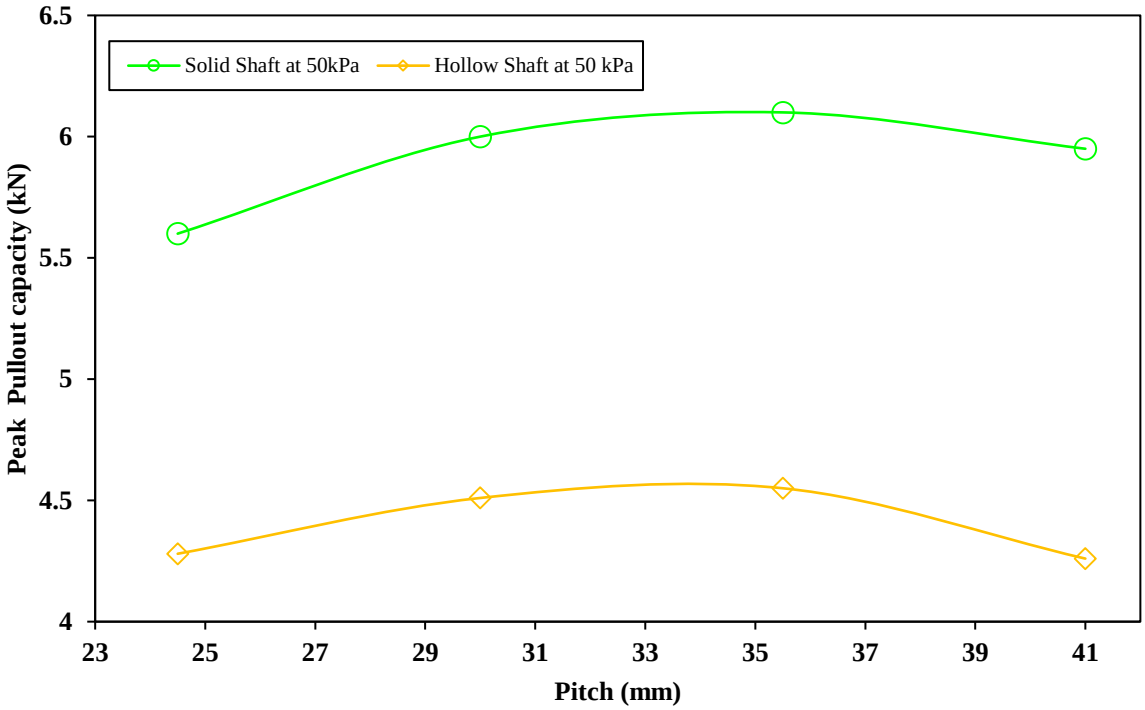

Fig.5. 9 Variation of pullout strength with helical pitch

5.4.3 SOLID AND HOLLOW SHAFT WITH MULTIPLE HELICES

It is observed from Fig.5.10, that maximum pullout capacity increases with increase in overburden pressure from 5kPa to 50kPa for all types of solid and hollow shaft helical nails. This can be accounted to the facts that as overburden increases, large shear stress are generated around the nail shaft. As the pullout progresses, these induced shear stresses along with tensile stresses generated within the bar acts against the pullout force. A multi helical spacing of $3D_h$ (D_h = Helix diameter) based on the concept that the pressure bulbs formed around the helix do not overlap and contribute individually to pullout capacity at helix spacing of $2.5D_h$ to $3.5D_h$ is adopted in the present study [9]. It is observed from Table 5.1 that 'K' yields better pullout capacity in comparison to other solid shaft nails. The peak pullout capacity of 'K' depicts a percentage increase of 39.67%, 47.82%, 55.38%, and 37.59% in comparison to 'J' under varying surcharge. Further, the average pullout capacity of L-rough is found to be 15% greater than 'K'. The increase in pullout capacity can be accounted by additional skin friction by shaft roughness during pullout. Hence, it is suggested that shaft roughness plays an important role in enhancing the pullout capacity of helical soil nails.

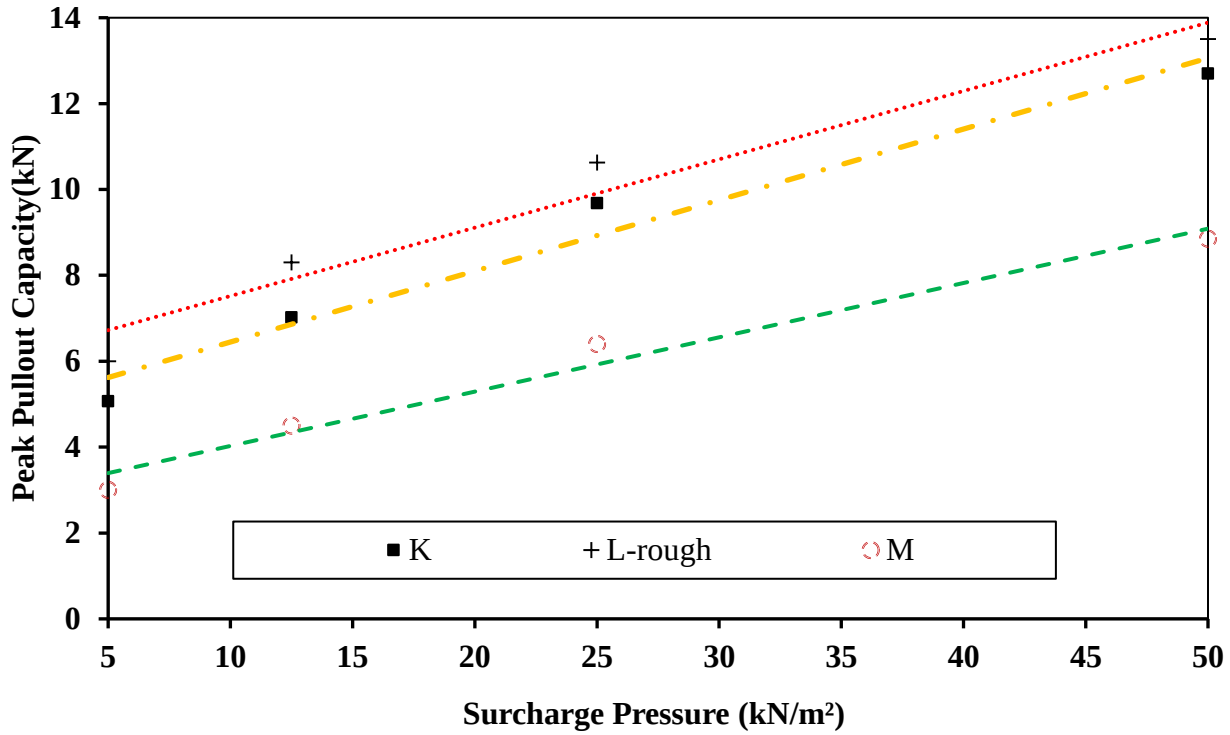

Fig.5. 10 Variation of peak pullout capacity of helical nails under different overburden pressures

The percentage increase in average pullout capacity for nail without helix to nail with single helix is approximately 409.16%. Similarly, an increase of 84.54% is found in average pullout capacity as number of helical plates is increased from single to double helical plates. Alternatively, increase in helical plates from double to triple, an increase of 23% in average pullout capacity is observed. Though, addition of a third helix delivers an increase in pullout capacity but this increase is insignificant in comparison to percentage increase of pullout between helical nail with single helix to double helices. The reason for this insignificant pullout capacity variation can be accounted for the fact that as helices are increases from double to triple, the location of the lowermost helix may lie in zone beyond the collapse mechanism of helix underneath [128]. This would lead to only a small addition of bearing offered by the respective helix and correspondingly small increase in pullout capacity. It is evident from Fig.5.10 that maximum pullout capacity varies linearly with increasing overburden pressure for different helical nails. This is indicative of the fact that pullout behavior of helical soil nail also obeys the Mohr-Coulomb failure envelop. A similar observation was also obtained by Sharma et al. [15]

The pullout resistance behaviour of helical soil nails with tapered multi-helix (‘K’) is better than cylindrical multi-helix (‘J’) at same overburden of 50 kPa. As can be observed from Table.5.1, the peak pullout capacity of tapered multi - helical nail is more as compared to helical

nail with cylindrical multi-helix. The reason can be attributed to the fact that both the helical nail configurations develop a failure surface extending along from the edges of the helix near the nail head to the helix located near the pulled end. In case of cylindrical multi – helix, a soil cylinder is formed around the nail having diameter equivalent to the helices diameter. Thus, during pullout, interface friction acts along the surface of this newly formed enlarged diameter soil tube. Alternatively, when the diameter of helices increase from nail head to nail toe (tapered multi - helix), a conical failure soil region around the nail is developed. Since the interface friction acts along the slanting surface of this conical soil region, both its horizontal and vertical components further increase the size of this conical soil surface. This results in enlarged diameter or out spread of failure soil near the pulled end of nail. Thus, large surface develops more friction against pullout and hence greater pullout capacity for tapered multi – helix nail is attained.

5.4.4 LOAD- DISPLACEMENT BEHAVIOR

The pullout load-displacement responses for 'C', 'G', L-rough, 'N', and 'O' are shown in Fig. 5.11 ((a) to (g)).The pullout load increases nonlinearly in the initial phase and then increases linearly thereafter. The test results show that the pullout resistance of helical soil nails increases rapidly with pullout displacement at the initial stage. However, the rate of increase becomes minimal after the peak pullout load is reached.

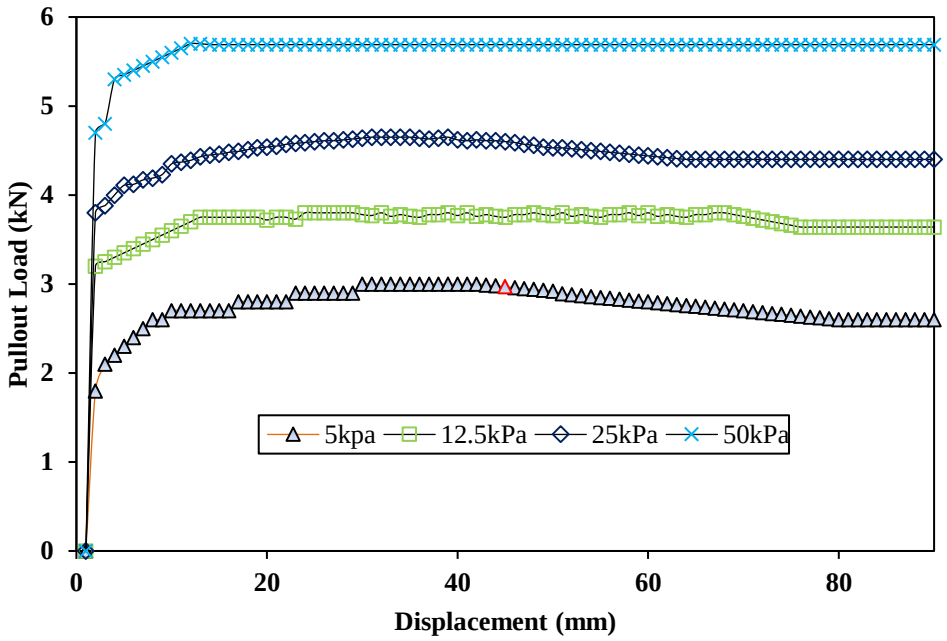

(a) Specimen C

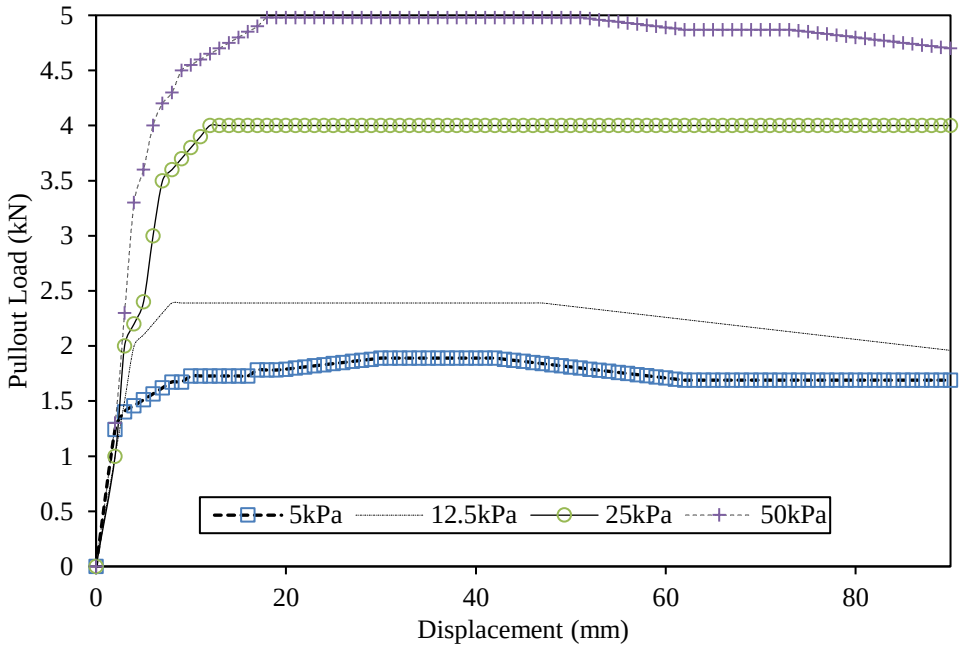

(b) Specimen G

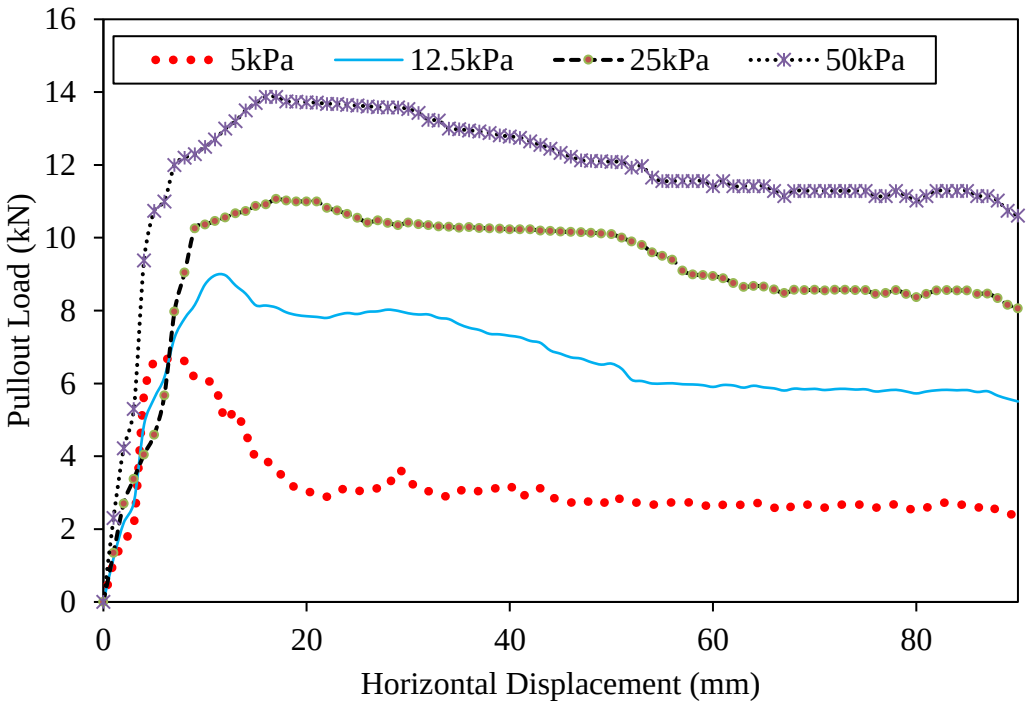

(c) Specimen L-rough

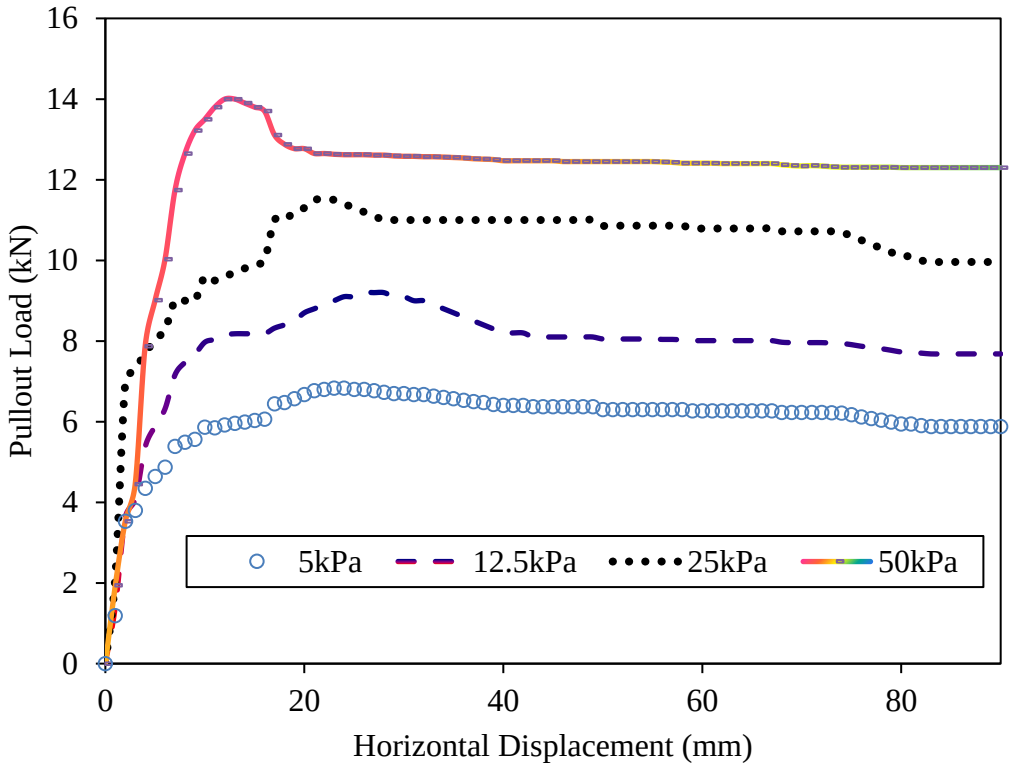

(d) Specimen N

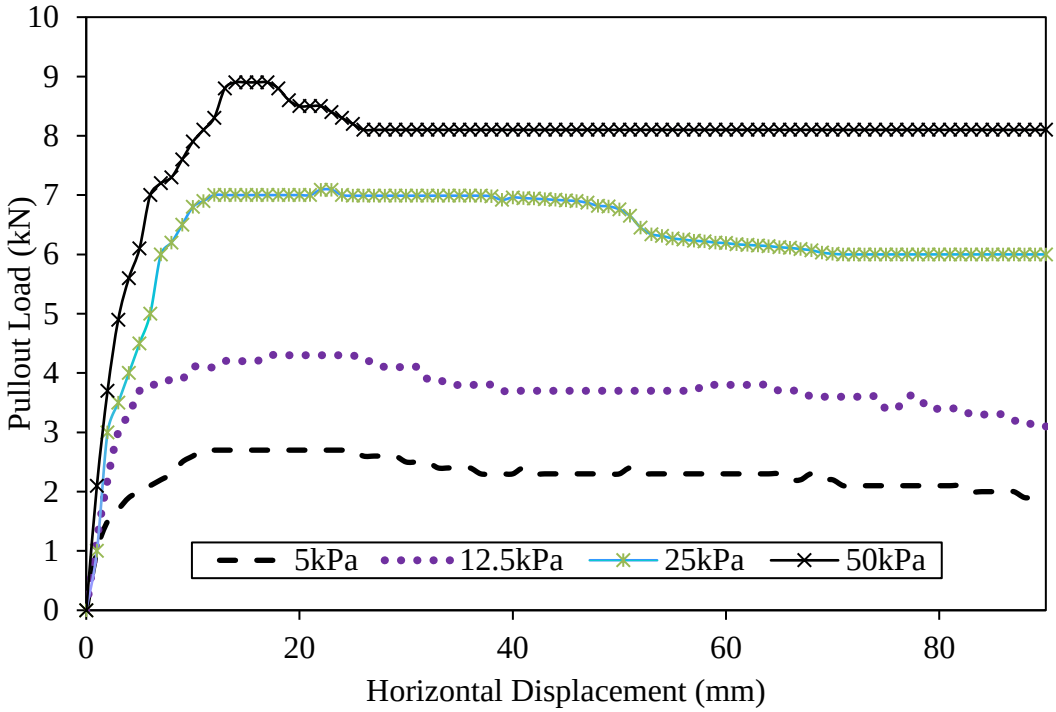

(e) Specimen O

Fig.5. 11 Pullout load–displacement responses for different helical soil nails

5.4.5 EFFECT OF EMBEDMENT DEPTH RATIO (Z/D_H)

The pullout capacity of helical structures has been observed as a function of embedment depth in model tests [79-100]. The embedment depth (Z) for a vertically installed helical structure corresponds to the depth of uppermost helix below the ground surface. As per the reported literature [80-95], failure mechanism of helical anchors is influenced by ratio of embedment depth (Z) of helical anchor to the uppermost helix diameter (D_h). It is observed that as critical embedment depth ratio $Z/D_h > 5$, transition of failure mechanism from shallow failure to deep failure occurs in case of helical anchors and piles. Based on this, transition of failure mechanism for horizontally installed helical nail is evaluated by considering the ratio of embedment depth (Z) taken as the vertical depth of outermost helix from top surface of the test tank to the diameter of outermost helix (D_h) for various adopted helical nail configurations. The variation of embedment depth ratio (Z/D_h) for helical nails is attained by the changing helix diameter only, because embedment depth (Z) is constant for all the helical nails installed horizontally [15].

In the present study, assumption of deep failure mechanism is adopted by considering $Z/D_h > 5$ for each helical soil nail configuration. The impact of Z/D_h on helical nail pullout capacity is studied in terms of a dimensionless parameter called as Normalized Pullout Capacity or Efficiency (η). The Normalized Pullout Capacity or Efficiency (η) is defined as the ratio of pullout capacity of helical nail with different number of helices (Q) to pullout capacity of helical nail without helix (Q_0). It can be seen from Fig. 5.12 that normalized pullout capacity is found to decrease with increase Z/D_h ratio under same overburden pressure for both solid and hollow nail shaft types. The maximum pullout efficiency is obtained for helical nail with three helices for both cases of nail shafts. Using a power regression best fit line ($R^2 = 0.865$), the efficiency (η) of a helical nail can be related to Z/D_h ratio using the relation given by Eqn. (5.17) as:

$$\eta = \frac{125.4}{\left(Z/D_h\right)^{1.8}} \tag{5.17}$$

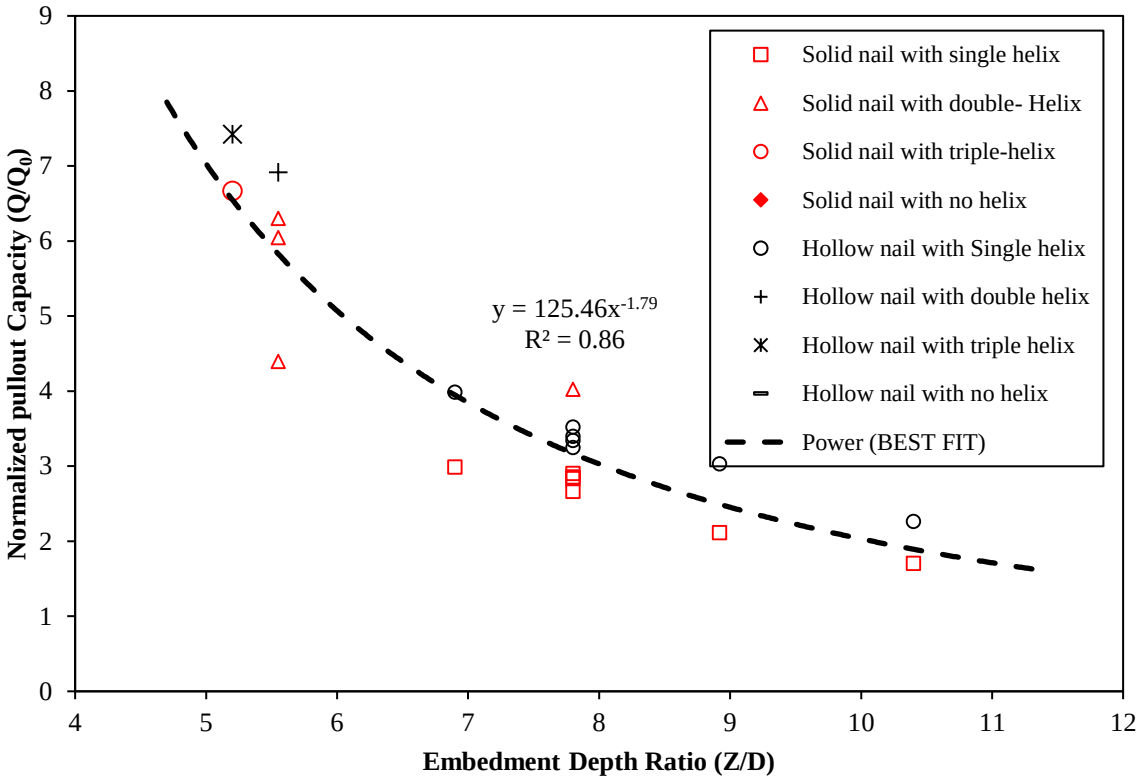

Fig.5. 12 Variation of Normalized pullout capacity with Embedment Depth Ratio

5.4.6 SOIL – HELICAL NAIL INTERACTION

As reported by Jewell and Worth [4], pullout testing enables simulating restrained dilatancy and correspondingly higher bond stress as attained in fields much better than other interface tests. Thus, soil – helical nail interaction during pullout can be studied in terms of mobilized shear stress under varying overburden pressure. The pullout shear stress can be calculated using Eqn. (5.18).

$$Pullout\ shear\ stress = \frac{Maximum\ Pullout\ Force(F_{max})}{Surface\ area\ of\ the\ nail\ (A_s)} \tag{5.18}$$

where, F_{max} = Maximum pullout force obtained from pullout testing of helical nails and A_s is calculated from Eqn. (5.8). The variation of pullout shear stress with normal stress is found to follow the Mohr – Coulomb criteria (Fig.5.13).

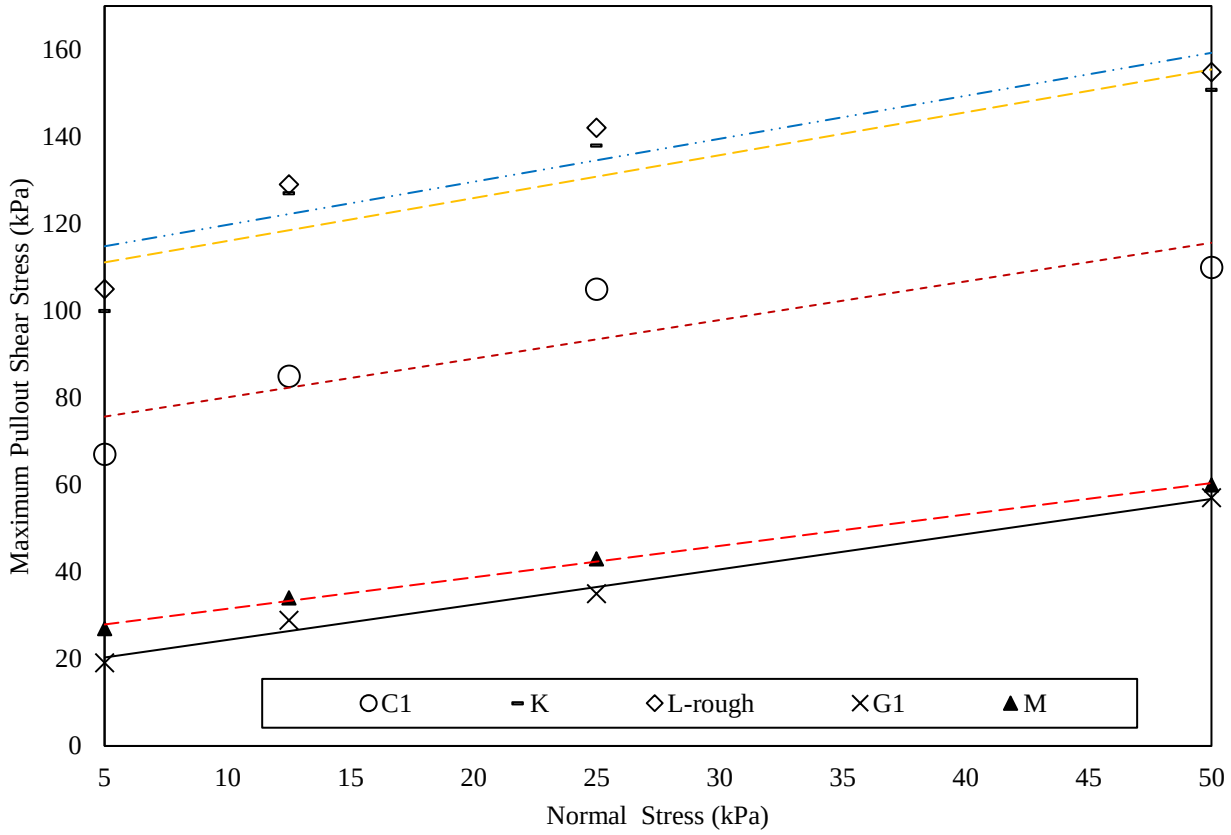

Fig.5. 13 Variations of maximum pullout shear stress and normal stress

It is also observed that maximum pullout shear stress is obtained for 'K' which increases further when smooth solid shaft is replaced with rough solid shaft. However, minimum pullout shear stress is observed for 'P'. In case of hollow shaft, maximum pullout shear stress is obtained for 'M' and minimum for 'Q'. Based on the observations, it can be extrapolated that maximum pullout shear stress will further increase with helical nail having triple helices of equivalent dimensions. Based on the Mohr – Coulomb criterion obtained the shear strength for the soil – helical nail interface (Q_s) can be given by Eqn. (5.19) as:

$$Q_s = c_a + \sigma_n \tan\delta \tag{5.19}$$

where, σ_n = Overburden pressure in kPa;

δ = Interaction friction angle in (°);

and c_a = Adhesion between soil and nail surface.

The interaction between the soil and helical nail primarily involves frictional resistance offered by the shaft and bearing from helices. Thus, to evaluate the influence of both frictional and bearing resistance during pullout, a dimensionless parameter called Interaction Factor (IF) is

used. The Interaction Factor (IF) is defined as the ratio of soil – nails interface shear strength to the applied overburden pressure and is given by Eqn. (5.20) as:

$$IF = \frac{Q_s}{\sigma_n} \tag{5.20}$$

The IF values calculated for both solid and helical nails are summarized in Table 5.1. It can seen from Table 5.1that IF value varies from 2 - 38 for solid helical shaft. The lower boundary of IF = 2 is obtained for 'P', whereas upper boundary of IF = 38 corresponds to 'N'. Similarly for hollow shaft helical nails, IF is found to vary between 0.3 – 11.3. Similar to solid shaft helical nails, 'O' depicts a higher IF = 11.3 and lower IF = 0.3 is obtained for 'Q'. Moreover, higher IF values for solid shaft than hollow shafts signify a better soil – nail interaction. For helical nails of equal shaft and helix diameter with constant pitch, it is found that solid shaft render almost 237% higher interaction than hollow shaft. It is evident from Fig.5.14 that with increase in normal stress, IF for both solid and hollow nails decreases. Likewise, under a constant normal stress, as the number of helices are increased, IF is found to increase. The influence of different nail shaft types, shaft diameter, helical pitch, and number of helices on IF values is assessed by predicting a best fit line using a power regression analysis. For solid shaft, a best fit line with regression value of R^2 = 0.611 is attained, whereas best fit line with R^2 = 0.613 is obtained for hollow shafts. Based on the curve fitting, empirical relationship between IF values and overburden pressure (σ_n) values for different helical soil nails can be derived as given by Eqn. (5.21):

$$IF = \frac{\psi}{{\sigma_n}^{0.7}} \tag{5.21}$$

where, ψ = constant having value of 55 for solid shafts helical nails and 17 for hollow shafts helical nails

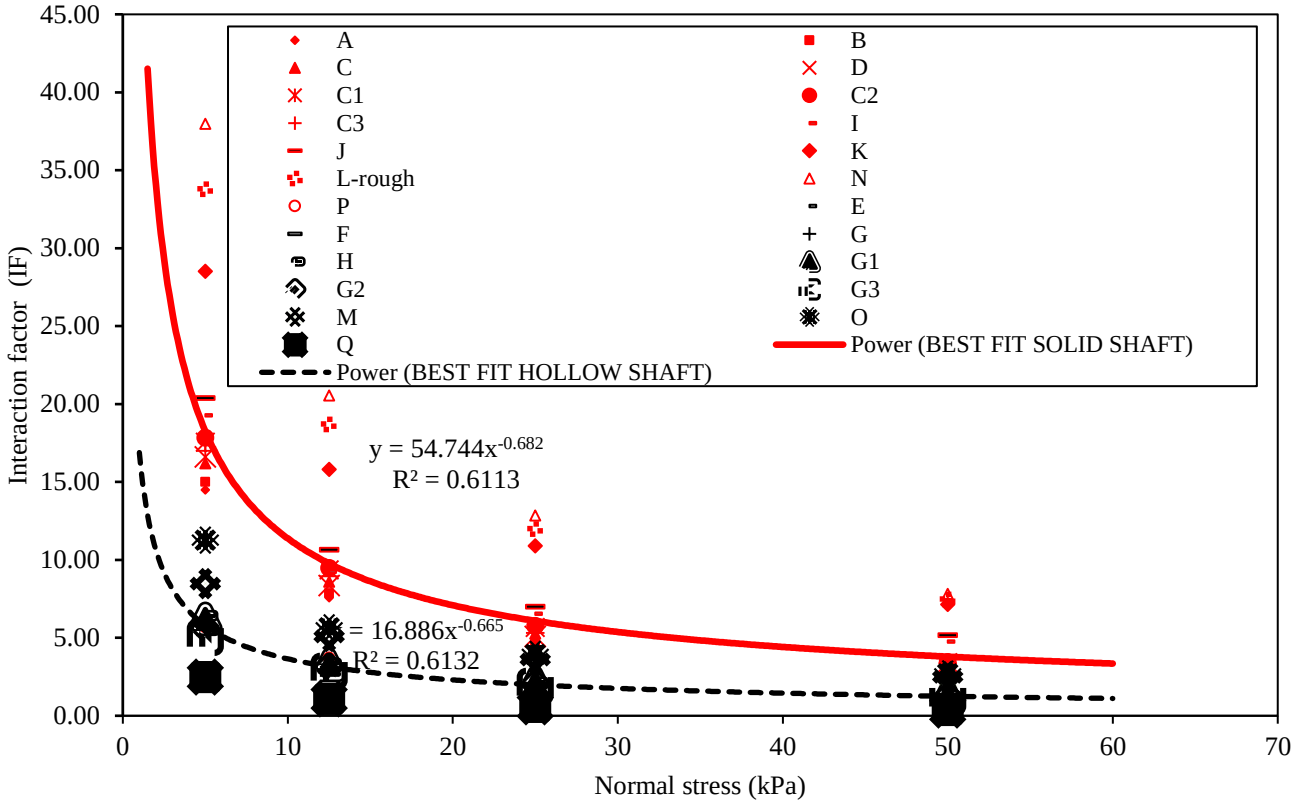

Fig.5. 14 Variation of Interaction factor with normal stress

Further, the interaction factor for different helical soil nail configurations is evaluated as the slope of pullout shear stress–normal stress plot given in Fig.5.13. The interaction factor for all model specimens under different overburden pressure (using Eqn.5.20) is presented in Fig.5.15. As evident from Fig. 5.15, the rough shaft helical soil nail with double helix has a similar interaction factor to smooth and rough shaft helical soil nail with triple helices (i.e. 0.99). This shows that with the addition of the third helix significant disturbance has been recorded and the shaft friction reduces. Thus, the performance of helical soil nails with double helix along with rough shaft is significantly better than nails with triple helix (both rough and smooth shaft) for model testing. However, it does not reflect that triple-helical nails are not capable of producing resistance, but it only means that the pullout capacity also depends on the effective installation length of the nail. Thus, for model testing of helical soil nails with double helix along with rough shaft is recommended.

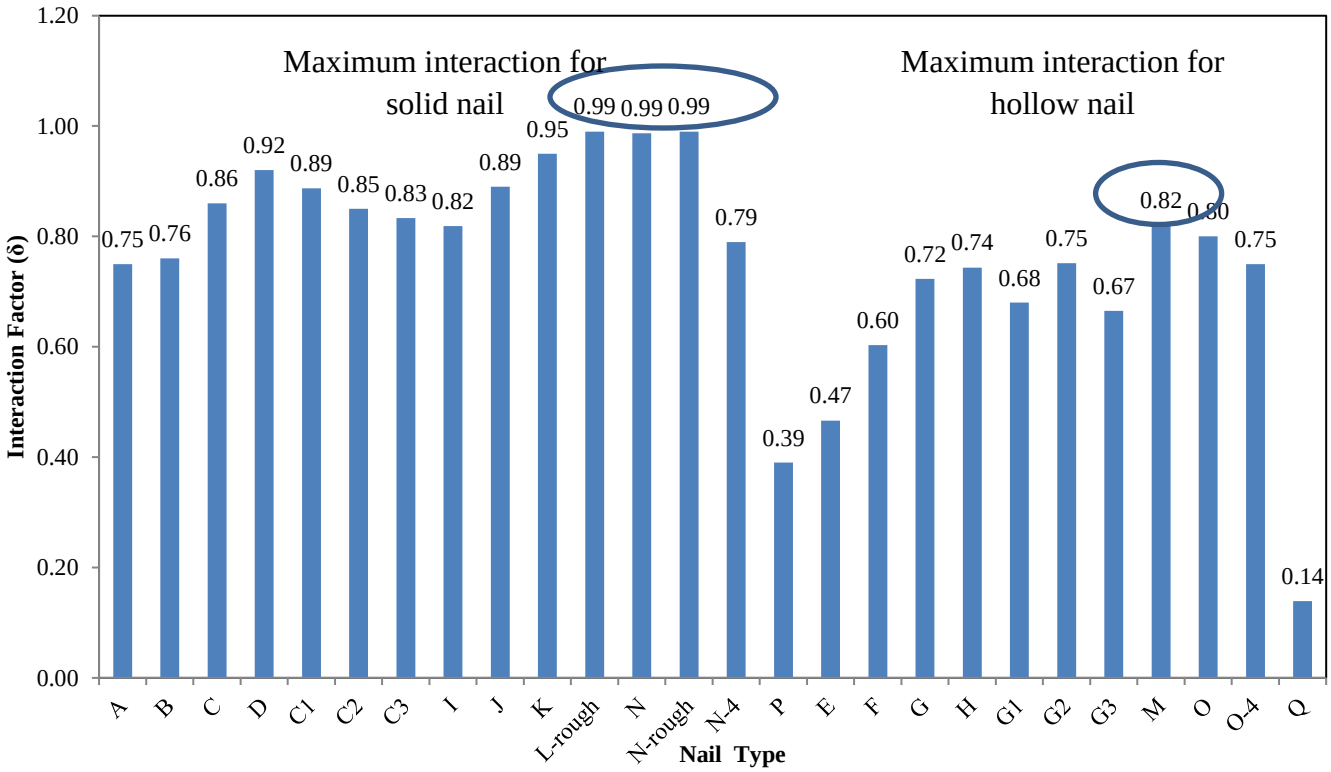

Fig.5. 15 Variation of Interaction factor for different helical nails

5.4.7 IN - SITU STRESS BEHAVIOR DURING INSTALLATION AND PULLOUT

In order to examine the variation of soil stresses during installation and also during pullout of each helical soil nail, four earth pressure cells of capacity 3MPa were placed around the installation location as shown in Fig.5.16. Two earth pressure cells were placed below the nail head, while the other two were situated below the rear end of the nail. All four earth pressure cells lie at a distance of 75 mm below the installed helical soil nail. The reported literature related to investigation of earth pressure variation during helical nail installation and pullout is very limited [12-13]. Moreover, the available literature is confined only to the variation of stress during installation and fails to infer any substantial information regarding the stress variation during pullout. In order to bridge this gap, Fig.5.17 and Fig.5.18 are plotted to depict the variation of earth pressure during installation and pullout of helical soil nail (‘K’ and ‘M’) under 50 kPa, respectively. Cell 1 and 2 test the effect of installation or pullout on vertical and horizontal stresses in initial stage, whereas Cell 3 and 4 measure stresses during final stage. During installation, earth pressure cell 1 and 2 records negligible variations up to installation of 330 mm of embedded nail length. However, beyond 330 mm, a small increment is noted by the

pressure sensors. On the contrary, earth pressure cells 3 and 4 records small decrease in earth pressure as 200 mm of embedded nail length is installed. Between 360 mm to 570 mm embedded nail length earth pressure cells 3 and 4 manifests significant increment in earth pressure. This depicts that small decrease in pressure is accounted to slight disturbances caused in the soil during installation. The increment in earth pressure signifies that increase in confining pressure due to the soil densification also occurs around the nail. This increase in in-situ stresses leads to an increase in pullout resistance also.

In beginning, during pullout the variations in the earth pressure at cell 1 and 2 found nearly unchanged up to 40mm after this there is drops in pressure has been noticed. This scenario represents that during installation of soil nail, the soil around periphery of nail slip out which create a constant gap between nail and soil. So, when nail was pulled out then this nail does not create any disturbance to the periphery on further pulling out soil zone suffer through soil compression. Whereas Cell 3 and 4 shows a constant drop in stress and slight increment for last 10 to 15 mm during the pullout process for both type of nail. The drop in stress represents compression in soil due to pulling force on nail, whereas increment in stress for last 10 to 15 mm signifies that increase in confining pressure due to the soil densification also occurs around the nail after moving 60 to 70 mm of distance from its preliminary position. In addition the earth pressures obtained from each pair of cells were different this represent that stress mobilized around helical soil nail is non-uniform.

As observed from Fig.5.18, during pullout of ‘K’, earth pressure decreases initially, but increasing slightly as the installation progresses. This variation can be credited to the small initial displacement occurring as the helices cut through the soil and then re-densification of soil mass around the helices. Similar, trends were also observed for ‘M’. This indicates that hollow shaft helical nail interacts with surrounding soil on sides of the shaft i.e. the inner side and outer side, thus leading to significant increments in confining pressure during installation. Furthermore, all test results manifests that for each helical nail configurations, minimal stress variations have been observed, whereas for conventional nails large in-situ stress variations are reported due to boring and subsequent grouting [12-13]. Hence, this reveals that helical soil nails generate significantly less disturbances in in-situ soil during installation as compared to grouted soil nails. Moreover, this privilege is offered without any compromises in the pullout capacities.

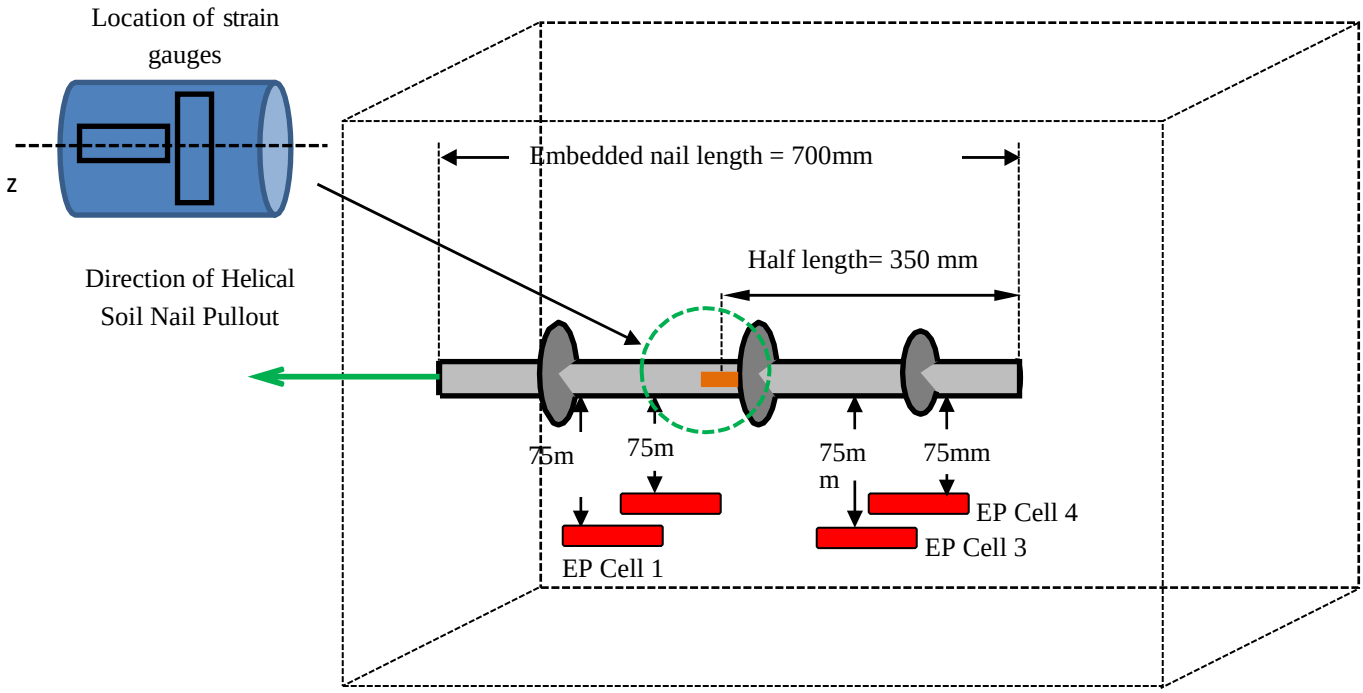

Fig.5. 16 Diagrammatic Representation of the position of the earth Pressure Cell

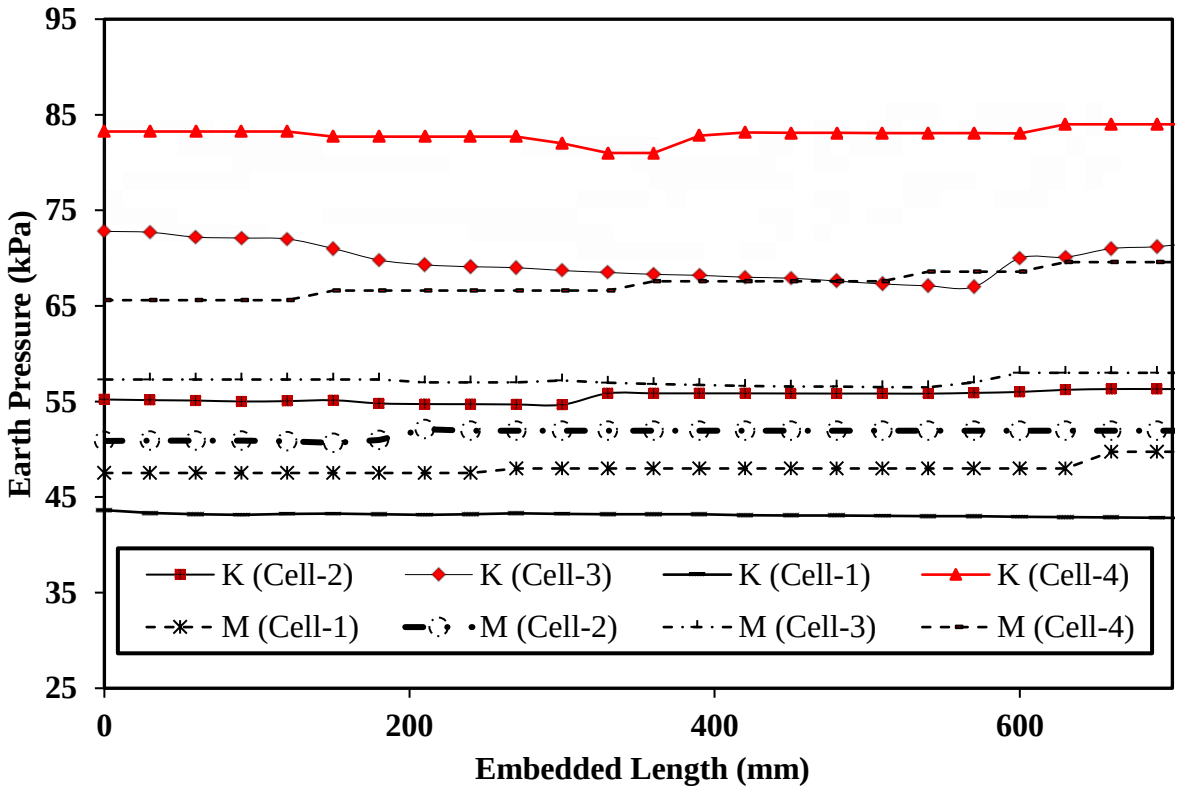

Fig.5. 17 Variation of earth pressure with Installation Length for: K and M

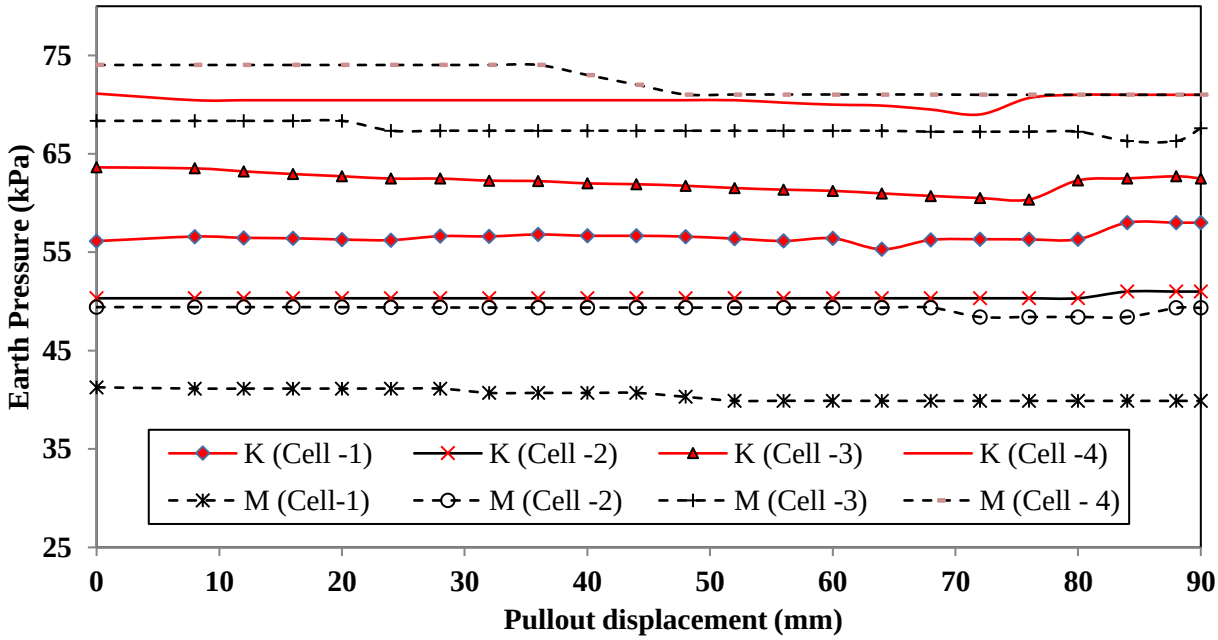

Fig.5. 18 Variation of earth pressure with pullout displacement for**:** K and M

5.4.8 DEVELOPMENT OF AXIAL STRAINS AND SETTLEMENT OF GROUND SURFACE

The axial strains were measured using four strain gauges, located at the 350 mm from the nail head (i.e embedded length (700 mm)/2) on opposite sides of the nail shaft. Two strain gauges were placed along the nail axis while the other two perpendiculars to the nail axis [129].To assure connections remain intact during installation and pullout strain gauges were protected using adhesive tapes. The strain gauge wiring was connected to a terminal pad to increase the safety of connection. Strains are normally taken into account for long-term performance monitoring of a soil nailed structure [5]. As evident from Fig.5.19, hollow shaft helical soil nails develop more axial strains during pullout as compared to solid shaft helical nails. It can also be noted that development of axial strains is also affected by the number of helical plates attached to the shaft. As evident from Fig. 5.19, the axial strains generated in ‘E’ are more than that in ‘O’. With the latter depicting the minimum strain values with pullout slip, it can be deduced that helical nail with hollow shaft and single helix shows maximum axial strain generation whereas with triple helices, strain generation fall off to the lowest. A hollow helical shaft nail with double helices depicts an intermediate effect for axial strain generation. The strain generation behavior can also be used for as a reason for lower pullout resistance offered by ‘E’ in comparison to maximum pullout resistance obtained for ‘O’. In case of solid shaft helical nails, it can be noted that maximum strain generation is observed for ‘A’, which is similar to hollow nails. As the

pullout slip increases, strains generated in both double and triple helices becomes almost same. Additionally, in case of rough solid shaft, lower strain values than helical nail with triple helices are still persistent for large pullout slip. The variation of these strains with pullout slip also satisfies the condition of attaining maximum pullout for solid rough shaft (L-rough) in comparison to smooth shaft. Moreover, pullout capacity of 'K' is found approximately equal to that of 'N'.

Further, it observed that top plate on the soil tank was found to settle during the pullout of helical nails. It was observed that the amount of settlement during pullout of hollow nail shafts was greater than solid shaft. From Fig.5.20, it is evident that settlement value reduces with increase in number of helices for hollow shaft nails. A similar observation can also be made for solid shafts. The soil ahead of the helical plates displaces from its equilibrium condition, thereby creating a momentary void between the nail and soil. As the helix shifts from one position to other, the gap is filled up by the preceding soil displaced from the following helix.

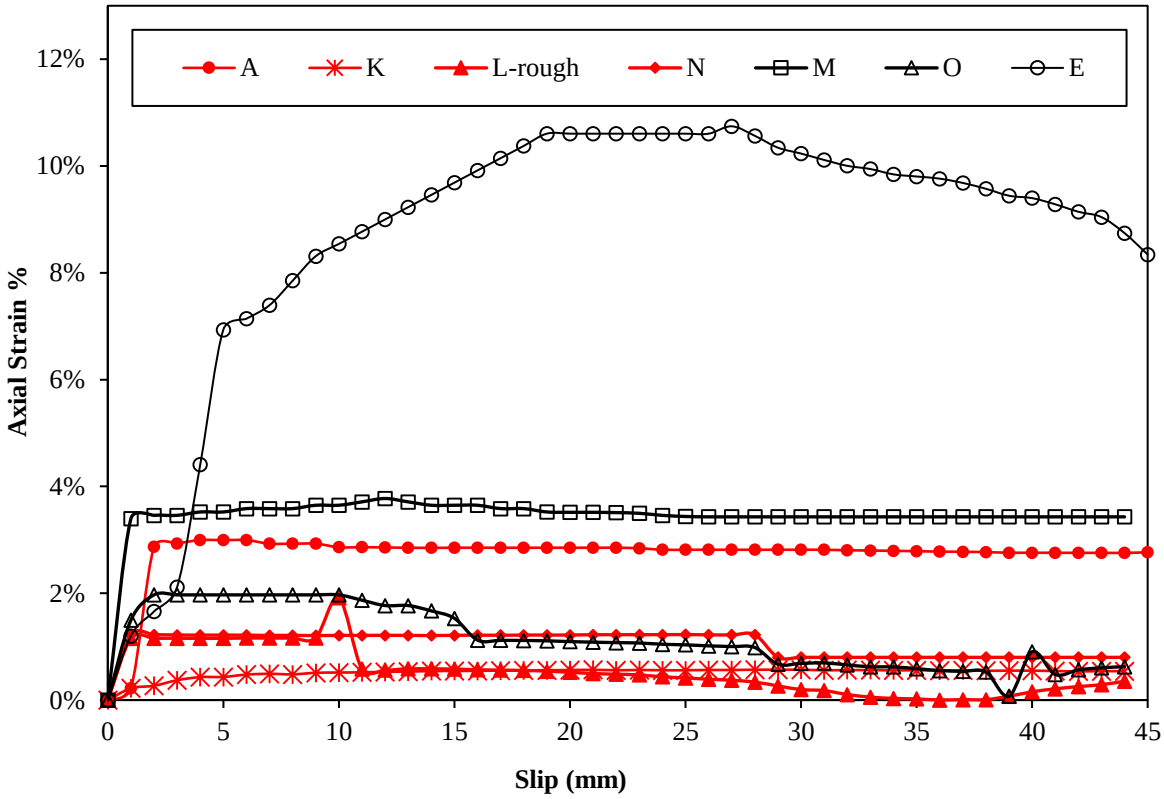

Fig.5. 19 Axial strain % versus horizontal displacement for different helical soil nails

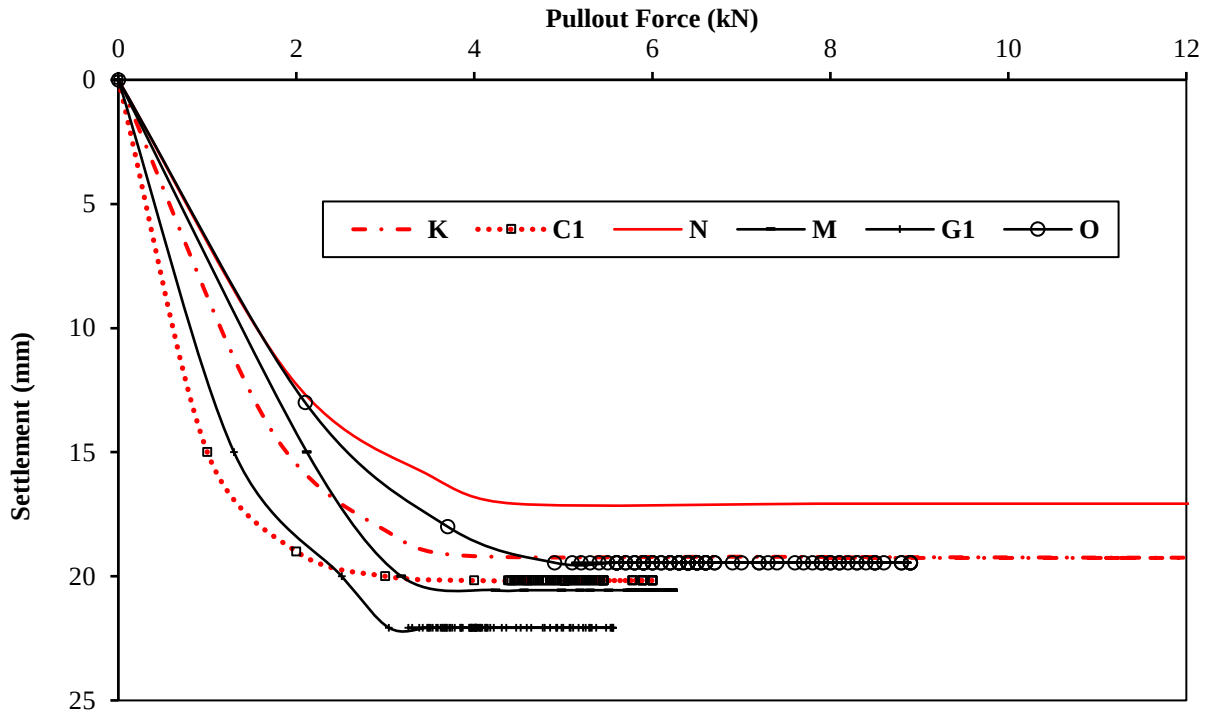

Fig.5. 20 Variation of Pullout force with settlement under surcharge pressure of 50kPa

5.4.9 EFFECT OF SOIL PLUGGING IN HOLLOW OR OPEN-ENDED PIPE HELICAL SOIL NAIL (OPHN)

The review of previous literature reflects that to increase the installation efficiency during piling, use of open-ended pipe piles in comparison to closed end pipe piles in different soil conditions have depicted satisfactory results in terms of bearing and axial load capacity [92-93]. The studies suggested that the phenomenon of soil plugging during driving results in additional internal shaft resistance. Gudavalli et al. [92] suggested that with pile insertion into the soil, an increase in internal shaft friction is observed till complete formation of soil plug is attained. After soil plugging addition soil is not allowed to enter the pipe and thus increases both the internal resistance and bearing resistance is also mobilized.

Thus, to further improve the installation of HN, the present study incorporates the concept of open-ended pipe pile into fabrication of hollow or open-ended pipe helical soil nails (OPHN). The mechanism of load transfer during pullout of OPHN can be understood from Fig.5.21. It can be seen that the pullout force (F) can been equated by three resistance offered from external shaft friction (F_s), internal shaft friction (F_{plug}) due to soil plugging within the hollow pipe and helical bearing resistance (F_b). The relationship between the resistances can be shown by. Eqn. (5.22):

$$\boldsymbol{F = F_s + F_{plug} + F_b} \tag{5.22}$$

In comparison to traditional soil nail where the pullout resistance is governed by resistance from tendon-grout interface (F_{sg}) and grout-soil interface (F_{gs}). Eqn. (5.23), OPHN depicts higher soil – nail interaction than traditional soil nail. However, for solid shaft helical soil nail the is modified as Eqn.5.24

$$F = F_{sg} + F_{gs} \tag{5.23}$$

$$F = F_s + F_b \tag{5.24}$$

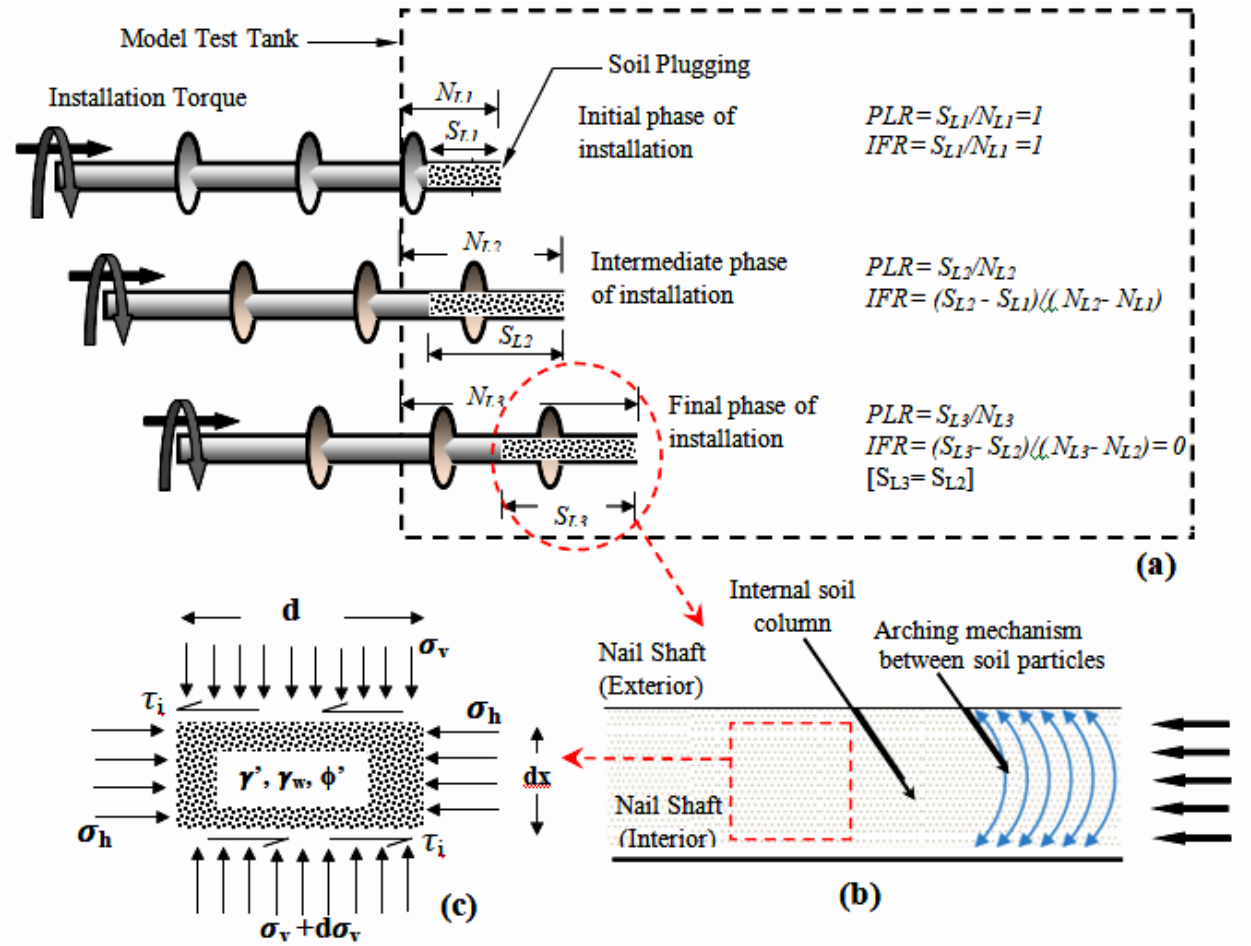

Fig.5. 21 Soil plugging with installation progress (b) Sketch of arching principle (c) Stresses acting on wedge of inner soil

The soil plugging performance was documented by Kishida and Isemoto [130] in context of piles modeled using pipes with open ends. The soil plugging behavior is investigated in terms of plug length ratio (PLR) and incremental filling ratio (IFR) as suggested by [92-95] and is defined by. Eqns. (5.25) and (5.26):

$$Plug\ Length\ Ratio = \frac{S_L}{N_L} \tag{5.25}$$

$$Incremental\ Filling\ Ratio = \frac{\Delta S_L}{\Delta N_L} \tag{5.26}$$

where N_L = nail penetration level;

S_L = soil plug;

ΔN_L = increase in penetration of nail; and ΔS_L = increase in soil plugging with increasing nail penetration (see Fig.5.21a.).

As evident from Fig.5.21a, when nail penetration length becomes equal to soil plug length then plug length ratio and incremental filling ratio becomes equal to 1. In addition, when soil plug length become constant, then IFR equal to 0, whereas plug length ratio is not necessarily 0 at the same level. The mechanism for redistribution of stresses within the soil body during plugging is attributed to arching in cohesionless soils [92-95]. The arching mechanism also governs the pullout behavior of soil in a laterally confined space. During installation of OPHN, soil arching causes concave soil formation at the nail toe level. (Fig.5.21b). Due to this, axial stress acting on the internal soil column at the toe of the nail is transmitted to the nail walls in the form of normal stress and shear stresses, resulting in increased internal shaft friction (Fig.5.21c). Thus, as depicted in Eqn. (5.23), resistance due to soil plug (F_{plug}) is mobilized as pullout progresses in addition to outer shaft friction (F_s) and bearing resistance from helical plates (F_b). During laboratory testing, formation of length of soil plug in all samples of OPHN was recorded after every 50 mm penetration during installation (Table 5.2). A calibrated steel rod of diameter 3 mm is inserted from the nail head into the hollow shaft nail after every 50 mm penetration during installation. From Table 5.2, it is clear that as nail penetration reaches to 0.45 - 0.50 m of nail length, 80 to100 mm length of soil plugging occurs which then becomes constant (at 25kPa) (Fig.5.22) It is observed that soil plugging contributes to the total frictional resistance mobilized during installation which consequently contributes 12% to the total shaft friction (internal) acting during pullout. It is observed that as soil plug length of OPHN increases, the pullout capacity of the nail also increases (Table 5.3). For nail samples ‘G’, ‘M’, and ‘O’, less than 1% increment in soil plug length is recorded which is almost negligible. Based upon this observation, it can be concluded that increase in number of helices does not influence the soil plug length. Moreover, from Table 5.2, it can also be deduced that soil plug length primarily depends upon the shaft diameter and is independent of the number of helix. Fig.5.23 also shows that OPHN with large

diameter incorporates greater soil plug length because of the ease of soil movement into the hollow shaft during nail penetration. The IFR values are found to be varying continuously and after 0.45 to 0.50 m of nail penetration, IFR value becomes equal to zero. This can be accounted to the fact that after 0.45 to 0.50 m of OPHN penetration, soil plug length becomes constant and restrains any further movement of soil into the hollow shaft. Thus, it can be accomplished that incremental filling ratio entirely depends on the soil plug length.

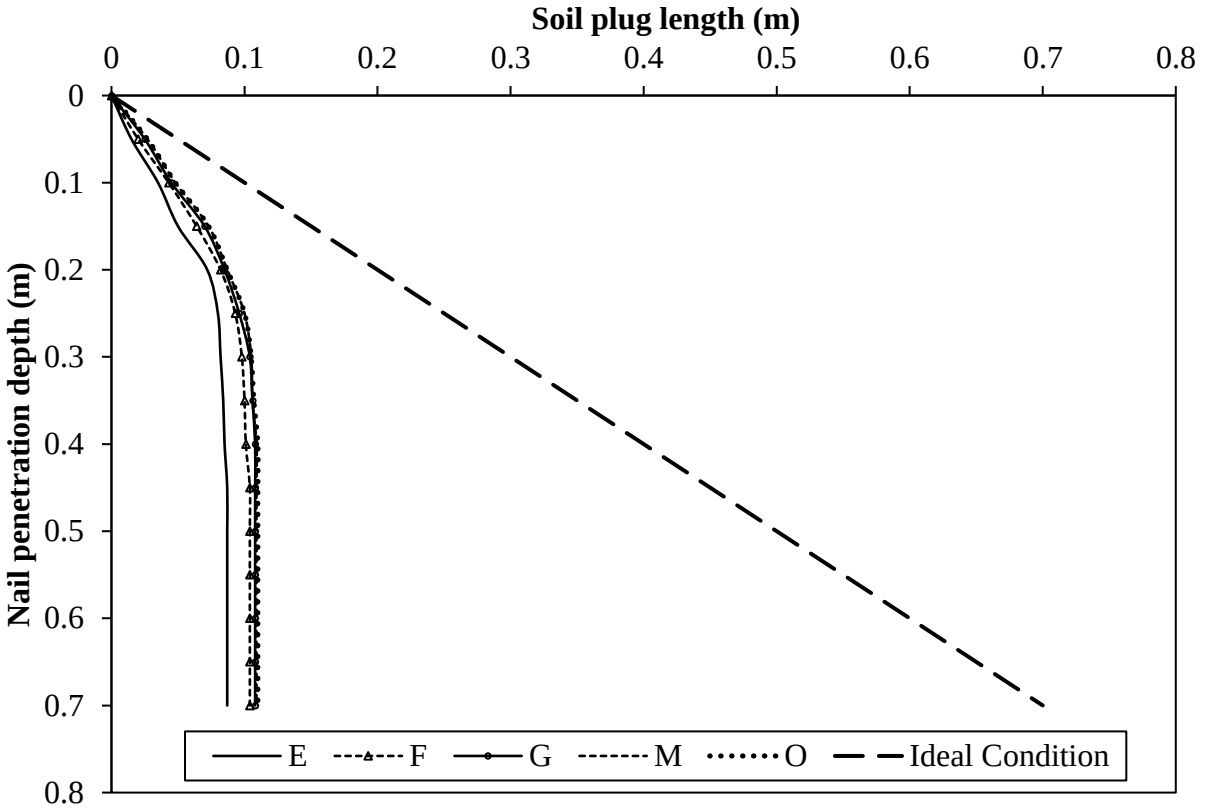

Fig.5. 22 Nail penetration depth versus soil plug depth

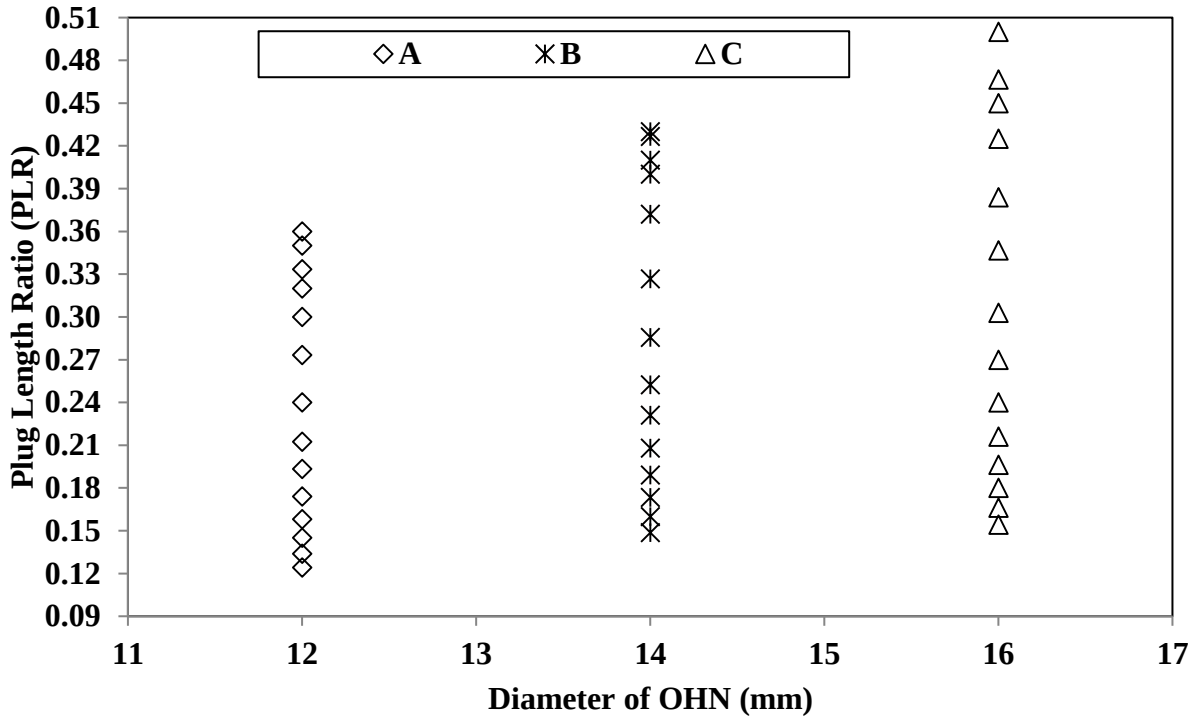

Fig.5. 23 Diameter of Open-Ended Pipe Helical Nail versus measured Plug Length Ratio

Table 5. 2 Summary of experimental result of PLR and IFR (under 25kPa)

Specimens	Length of soil plug (m)	Nail penetration depth(m)	PLR	IFR
	0	0		
E	0.015	0.05	0.30	0.4
	0.035	0.1	0.35	0.3
	0.05	0.15	0.33	0.44
	0.072	0.2	0.36	0.16
	0.08	0.25	0.32	0.04
	0.082	0.3	0.27	0.04
	0.084	0.35	0.24	0.02
	0.085	0.4	0.21	0.04
*	0.087	0.45	0.19	0
	0.087	0.5	0.17	0
	0.087	0.55	0.16	0
	0.087	0.6	0.15	0
	0.087	0.65	0.13	0
	0.087	0.7	0.12	
F	0	0		
	0.02	0.05	0.40	0.46
	0.043	0.1	0.43	0.42

	0.064	0.15	0.43	0.36
	0.082	0.2	0.41	0.22
	0.093	0.25	0.37	0.1
	0.098	0.3	0.33	0.04
	0.1	0.35	0.29	0.02
	0.101	0.4	0.25	0.06
*	0.104	0.45	0.23	0
	0.104	0.5	0.21	0
	0.104	0.55	0.19	0
	0.104	0.6	0.17	0
	0.104	0.65	0.16	0
	0.104	0.7	0.15	
G	0	0		
	0.025	0.05	0.50	0.4
	0.045	0.1	0.45	0.5
	0.07	0.15	0.47	0.3
	0.085	0.2	0.43	0.22
	0.096	0.25	0.38	0.16
	0.104	0.3	0.35	0.04
	0.106	0.35	0.30	0.04
*	0.108	0.4	0.27	0
	0.108	0.45	0.24	0
	0.108	0.5	0.22	0
	0.108	0.55	0.20	0
	0.108	0.6	0.18	0
	0.108	0.65	0.17	0
	0.108	0.7	0.15	
M	0	0		
	0.027	0.05	0.54	0.42
	0.048	0.1	0.48	0.5
	0.073	0.15	0.49	0.28
	0.087	0.2	0.44	0.26
	0.1	0.25	0.40	0.1
	0.105	0.3	0.35	0.02
	0.106	0.35	0.30	0.06
*	0.109	0.4	0.27	0
	0.109	0.45	0.24	0
	0.109	0.5	0.22	0
	0.109	0.55	0.20	0
	0.109	0.6	0.18	0
	0.109	0.65	0.17	0

	0.109	0.7	0.16	
O	0	0		
	0.027	0.05	0.54	0.0042
	0.048	0.1	0.48	0.005
	0.073	0.15	0.49	0.0028
	0.087	0.2	0.44	0.0026
	0.1	0.25	0.40	0.001
	0.105	0.3	0.35	0.0004
	0.107	0.35	0.31	0.0006
*	0.11	0.4	0.28	0
	0.11	0.45	0.24	0
	0.11	0.5	0.22	0
	0.11	0.55	0.20	0
	0.11	0.6	0.18	0
	0.11	0.65	0.17	0
	0.11	0.7	0.16	

* Nail penetration level beyond which, IFR =0.

Table 5. 3 Maximum Plug Length and Maximum Pullout Capacity (under 25kPa)

Test nail	Maximum Plug Length (m)	Maximum Pullout Capacity (kN)
E	0.087	2.34
F	0.104	3
G	0.108	3.43
M	0.109	6.4
O	0.11	7

5.5 Effect of nail Inclination and group performance

5.5.1 Single Helical Nail: Installation and Pullout Behavior at different inclination

Based on experimental results of the first five groups, the helical soil nail with triple helices and rough surface (i.e. N-rough) offers maximum pullout capacity in all model helical soil nail specimens. The percentage increase in average pullout capacity for single to double-helical plates is approximately 85% under different pressure. Further, by changing the shaft of the double-helical nail to a rough shaft (i.e. L-rough) the average pullout capacity increases 10%

than the double-helical nail with a smooth surface. Alternatively, with the increase in helical plates from double to triple, an increase of 23% in average pullout capacity is observed. Though the addition of a third helix delivers an increase in pullout capacity, this increase is insignificant in comparison with the percentage increase in pullout between helical nails with a single helix to double helices. The reason for this insignificant pullout capacity variation can be accounted for by the fact that as helices are increased from double to triple, the location of the lowermost helix may lie in a zone beyond the collapse mechanism of the helix underneath [128]. This would lead to only a small addition of bearing offered by the respective helix and a correspondingly small increase in pullout capacity. With the addition of the fourth helix, the average pullout capacity decreases 40% to the triple-helical nail, due to the generation of a large disturbance in soil mass and the creation of a gap between soil and nail shaft. Also, the pullout strength may depend upon the position or location of the fourth helix, which may offer better results as the installation length or embedment length increases. In the Nutshell, for the present model testing, the difference between the percentage increase of pullout capacity of double and triple-helical soil nail with a rough surface is insignificant. Keeping this thing in mind, further laboratory tests were conducted (i.e. Nail Inclination and group performance) with double-helical soil nail with rough shaft (i.e. L-rough).

To evaluate the effect of inclination on the installation torque and pullout of HN peak corresponding normalized value has been plotted with different inclination angle under different surcharge pressure (Fig.5.24). Peak normalized pullout capacity $\left(\frac{P_{\theta^\circ}}{P_{0^\circ}}\right)$ is defined as the ratio of maximum pullout force at a different inclination to the maximum pullout force at 0˚ inclination, whereas peak normalized installation torque $\left(\frac{T_{\theta^\circ}}{T_{0^\circ}}\right)$ is the ratio maximum installation torque at a different inclination to maximum installation torque at 0˚ inclination [96-100]. From Fig.5.24, it is clear that the installation torque of HN increases significantly with the increases in angle of inclination from 10° to 20° under different surcharge pressure, whereas from 20° to 30° inclination the installation torque falls for HN decreases significantly under different surcharge pressure.

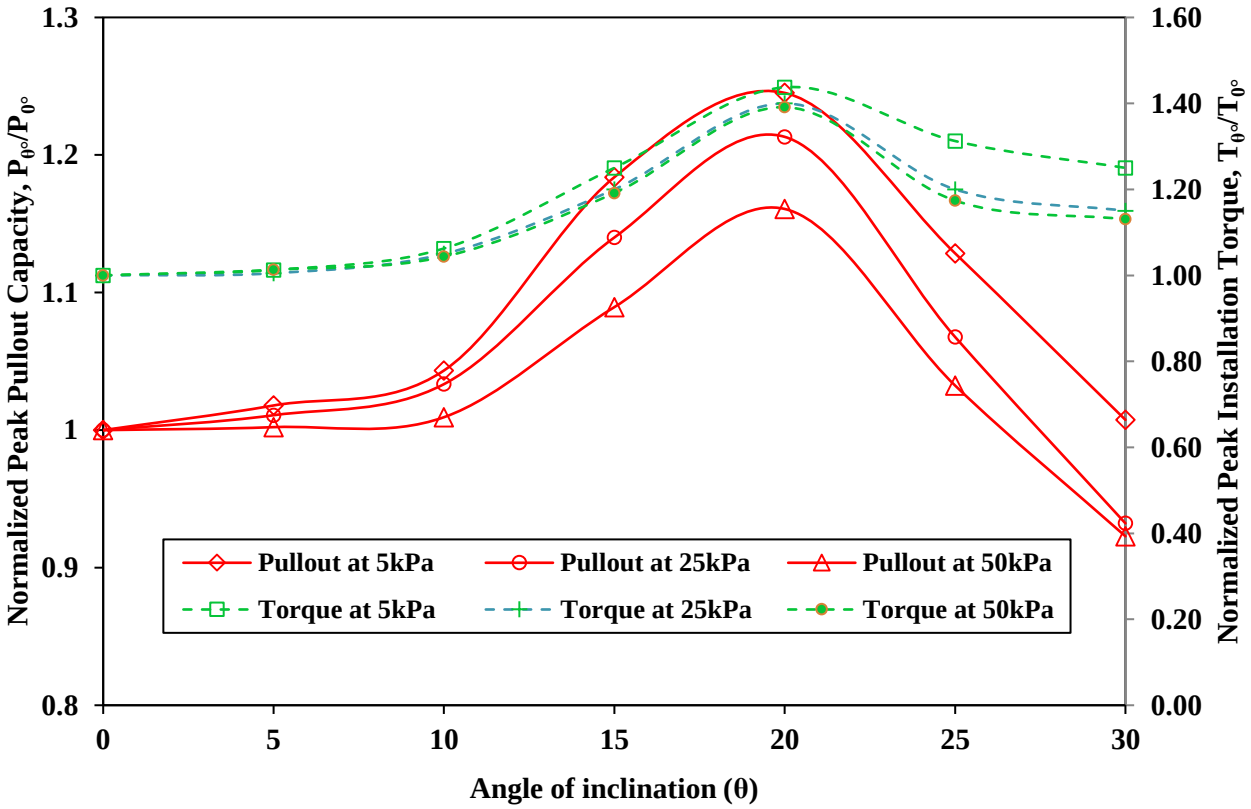

Fig.5. 24 Normalized peak pullout capacity and normalized peak installation torque with different angle of inclination

Similarly, the maximum pullout capacity of helical nail increase significantly with a change in inclination from 10° to 20° and then starts decreasing from 20° to 30°. Also, as evident from Fig.5.24, the maximum pullout capacity and maximum installation torque at 10° and 25° found approximately equal. Thus installation of HN may be suitable from 10° to 25° angle of inclination, whereas 20° inclination is considered as the most favorable angle. Beyond 25° pullout value fall significantly the reason may be due to change in the soil parameters and effective stress acting of the nail. Also, when the inclination angle (angle between HN and horizontal) is less than 25°, then forces mobilized in HN are tensile and HN orientation (angle between HN and the normal to the shearing surface) is all positive. Whereas as the inclination angle changes from 25° onward the forces in the HN changes from tension to compression. Due to which HN orientation changes from positive to negative and HN orientations are close to directions of the compressive strain of the soil [33]. Fig.5.25. shows the variation of pullout capacity (maximum pullout force) with surcharge pressure at different inclination angles. The test results indicate that for different angles of inclination pullout capacity increased linearly with the applied surcharge pressure. The results confirm that even at different inclination pullout

capacity followed the Mohr-Coulomb failure criterion under the applied different surcharge pressure.

However, from Fig.5.24 it is evident that as the surcharge pressure increases from 5kPa to 50kPa the rate of increment in pullout capacity and installation torque decreases with an increase in surcharge pressure. To clearly understand the pullout behavior with surcharge pressure, variation of friction factor ($\boldsymbol{\delta}$) has been presented with σ_0/σ_{max} for the different inclination of the nail under different surcharge pressure. The friction factor ($\boldsymbol{\delta}$) and σ_0/σ_{max} expressed as:

$$\boldsymbol{\delta} = \frac{\tau}{\sigma} \tag{5.27}$$

where τ is peak pullout shear stress which is the ratio of peak pullout capacity to the surface area of HN and σ_0/σ_{max} is the ratio of surcharge pressure to the maximum surcharge pressure. The surface area of HN is calculated as per [79-89]. Fig.5.26 shows the variation of friction factor ($\boldsymbol{\delta}$) with $\boldsymbol{\sigma_0/\sigma_{max}}$ for the different inclination of the nail under different surcharge pressure. It can be observed that the friction factor ($\boldsymbol{\delta}$) decreases with an increase in $\boldsymbol{\sigma_0/\sigma_{max}}$, and this variation presents a maximum value of $\boldsymbol{\delta}$ at 20˚ inclination of HN with horizontal. Also, from Fig.5.25 the regression equation for the inclination of 20˚ shows the maximum value of interface friction in comparison with different inclination. The test result suggests that nail inclination plays an important role in the mobilization of friction factor. Moreover, from experimental test results torque correlation factor (k) was calculated for different inclination, varies from 33.70 m^{-1} to 60.30m^{-1} for HN under different surcharge pressure.

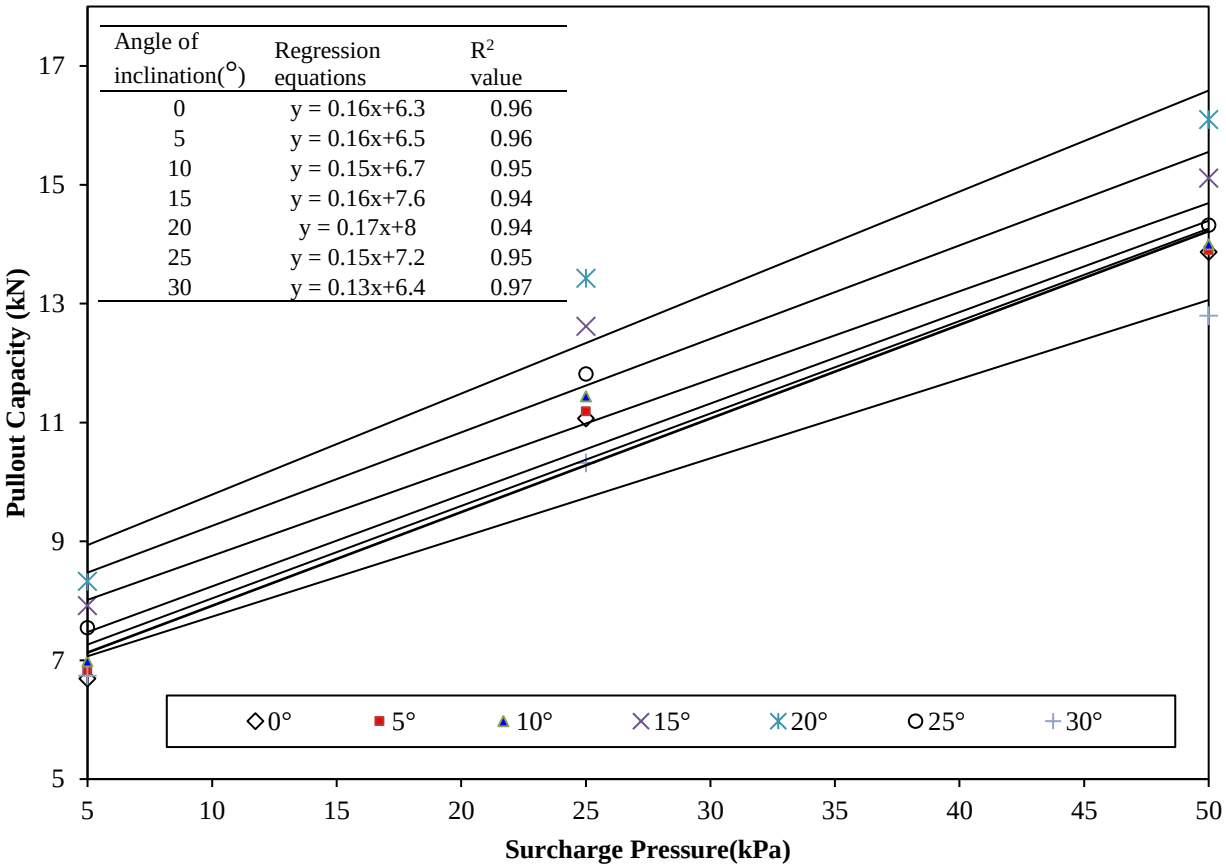

Fig.5. 25 Variation of pullout with surcharge pressure at different inclination angle

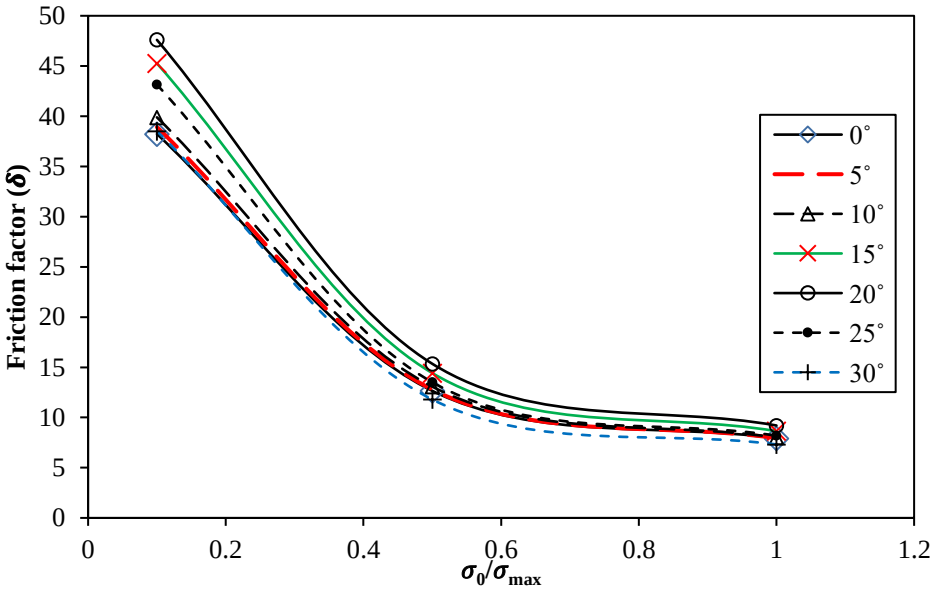

Fig.5. 26 Variation of friction factor (δ) with σ_0/σ_{max} for different inclination of the nail

5.5.2 HELICAL NAILS IN GROUP: INSTALLATION

The installation of HN was done using the top-down approach to simulate the actual field condition. The test was performed in two different arrangements at an angle of 20° with uniform and staggered spacing under overburden pressures 5kPa. The normalized installation torque in group installation is defined as the ratio of installation torque for the n^{th} value to the initial value (T_n/T_i).

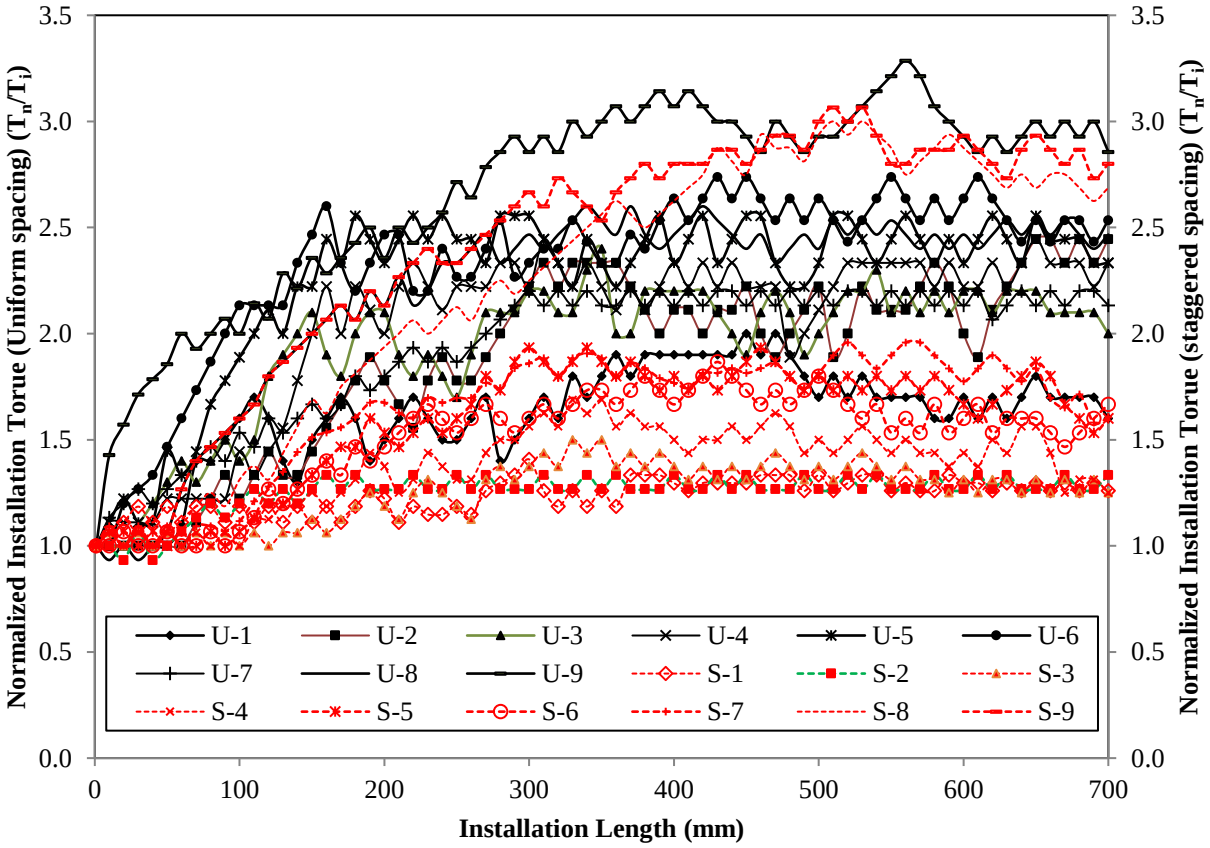

Fig.5. 27 Normalized Installation torque - installation length of HN when install in group with uniform (U) and staggered (S) spacing

Fig.5.27 shows normalized installation torque with installation length of HN when installing in a group with uniform (U) and staggered (S) spacing. As evident from Fig.5.27, during installation of HN in both uniform and staggered arrangement the installation torque increases with installation length. This reflects that stress level increases with installation length resulting in increases in shear strength of soil with the placement of HN. During the installation of every nail, the installation path undergoes various oscillations, reflects the variation in mobilized shear strength of soil due to the installation of HN. Further, the movement of HN

attributes progressive filling of the void that develops below the helix. The installation torque for the case of staggered spacing was found to be increased progressively as the bed height changes from top to bottom. On the contrary, for uniform spacing, the installation torque didn't undergo any definite pattern. For example, the installation torque for HN-6 was found more than the installation torque for HN-7 &8. This reflects that wherewith the change in bed height the installation should have to increase, but it shows a fall in torque value considerably.

5.5.3 HELICAL NAILS IN GROUP: PULLOUT BEHAVIOR

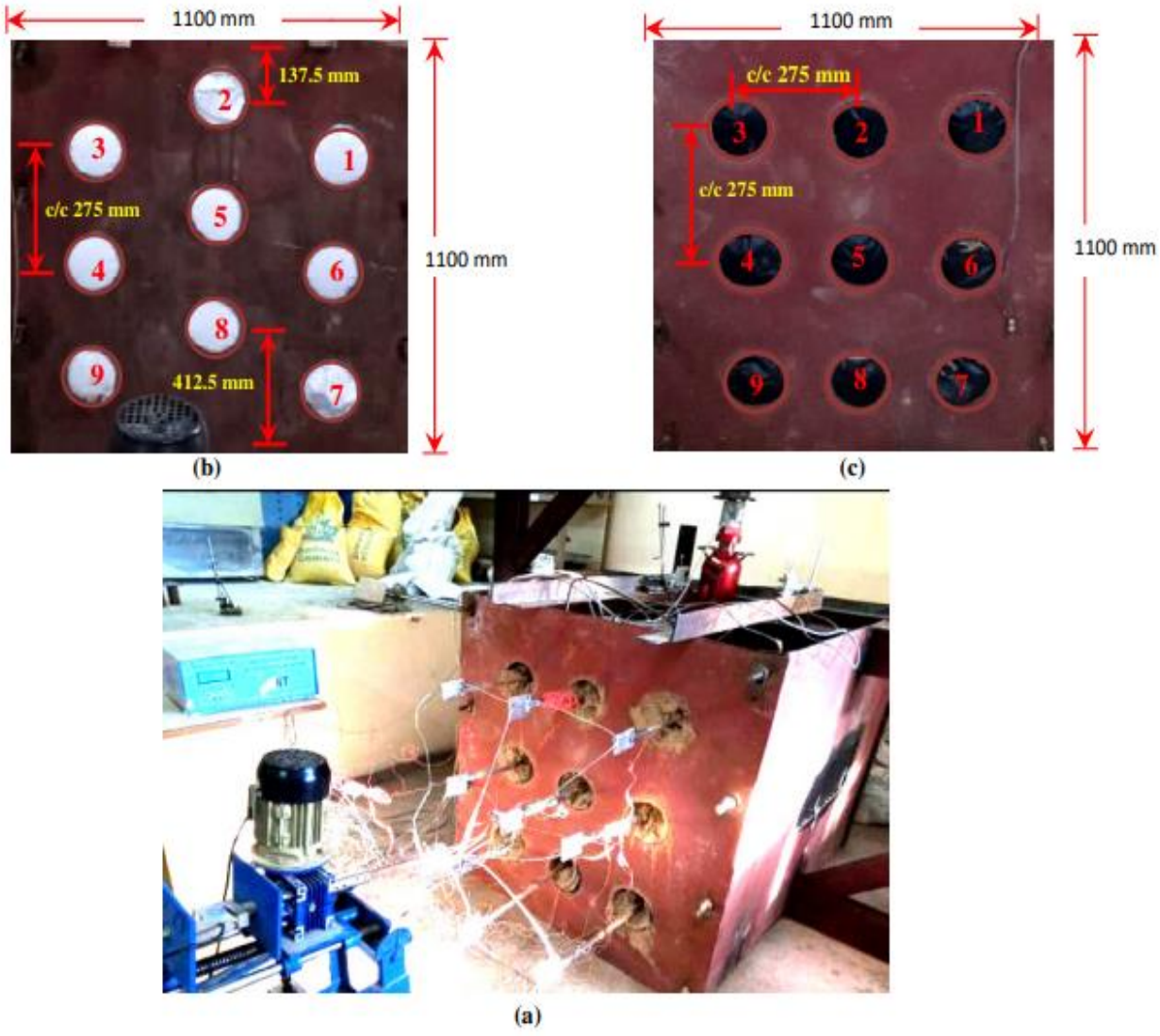

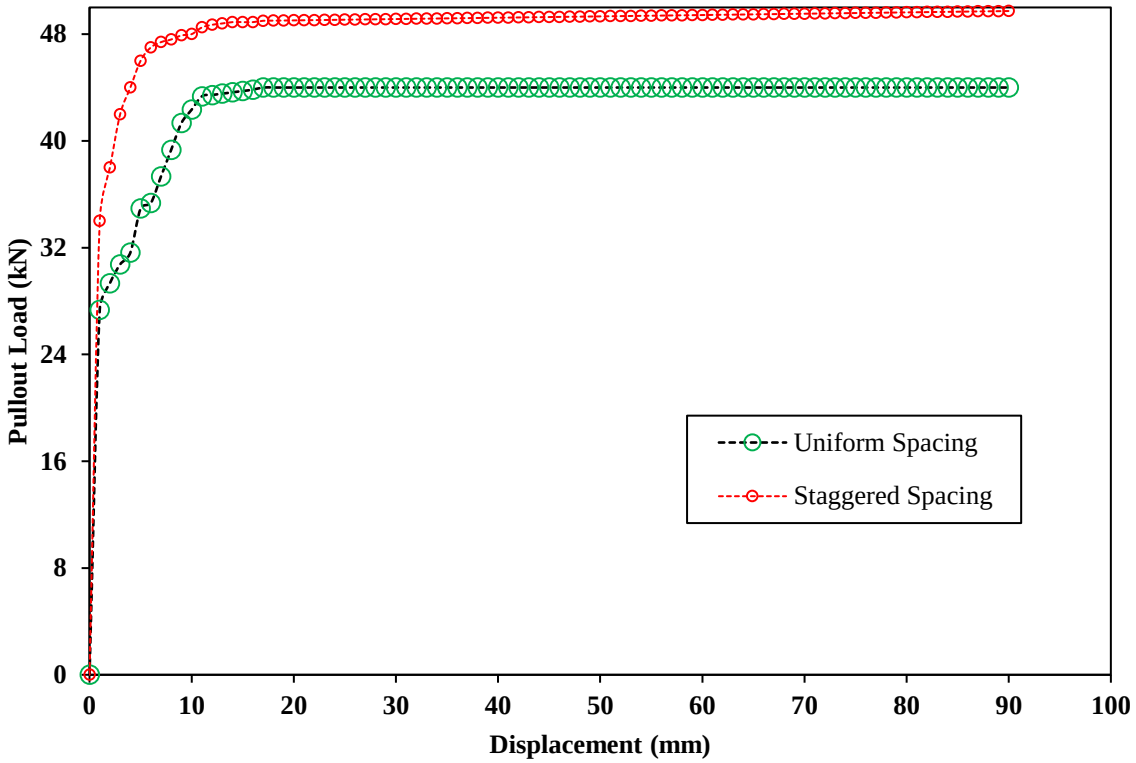

Fig.5. 28 (a) Group pullout in laboratory **(b)** Group arrangement with staggered centre to centre spacing. **(c)** Group arrangement with uniform centre to centre spacing. **(d)** Group pullout load-displacement curve for HN with uniform and staggered spacing

The group pullout of helical soil nail is shown in Fig. 5.28a. Also, Fig.5.28 (b&c) shows the different group arrangements (uniform and staggered), which were used during pullout testing. The displacement of the individual HN in the group was not measured separately, however, the nail hook can be considered rigid so that all HN can be assumed to have equal displacement during the pullout. Fig.5.28 (d) shows the group pullout load-displacement curve for HN with staggered and uniform spacing under imposed pressure of 5kPa. As evident from the test result, the group pullout capacity of HN with staggered spacing was found to be more under surcharge pressure of 5kPa. The friction factor ($\boldsymbol{\delta}$) for the pullout of both uniform and the staggered spacing case has been calculated as per equation (5.27). The friction factor ($\boldsymbol{\delta}$) for HN in a group with staggered and uniform spacing is 31.4 and 27.9 respectively under an overburden pressure of 5kPa. As per (Perko, [9]) the efficiency of an individual double-helical soil nail can be defined as:

$$\eta_i = \frac{Q_D}{nQ_S} \tag{5.28}$$

η_i is the efficiency of the individual nail;

Q_D is peak pullout capacity of HN with double helix;

Q_s is peak pullout capacity of the HN with single helix;

n is a number of helices (for present study n=2).

The efficiency of individual HN is 1.1, whereas group efficiency of HN with staggered and uniform spacing is 0.92 and 0.81 respectively under surcharge of 5kPa. The efficiency of group HN has been calculated using equation (1). From Fig.5.29 and Fig.5.30 it is clear that the vertical distance between influence circles of adjacent HN was the same for both uniform and staggered case, whereas the horizontal distance between influence circles of consecutive HN for the staggered case found to be more i.e. 172.5 mm than uniform case i.e. 140 mm. The small spacing between influence circles of HN causes hindrance in the periphery causes a large change in volume, resulting in decreases in pullout capacity of HN during uniform spacing. As per (Perko, [9]) if η_g is less than 1, the groups' effects of HN will be limiting the pullout capacity. And it is suggested that minimum spacing between helical elements may require to be increased. But due to laboratory constrain the minimum spacing has been adopted 1.5 bigger most diameter. The η_g for both cases is less than 1, however under similar conditions, the group with staggered spacing performing well compared to the uniform spacing. Hence, from the tests result placement of HN with staggered spacing has been suggested for large-scale applications.

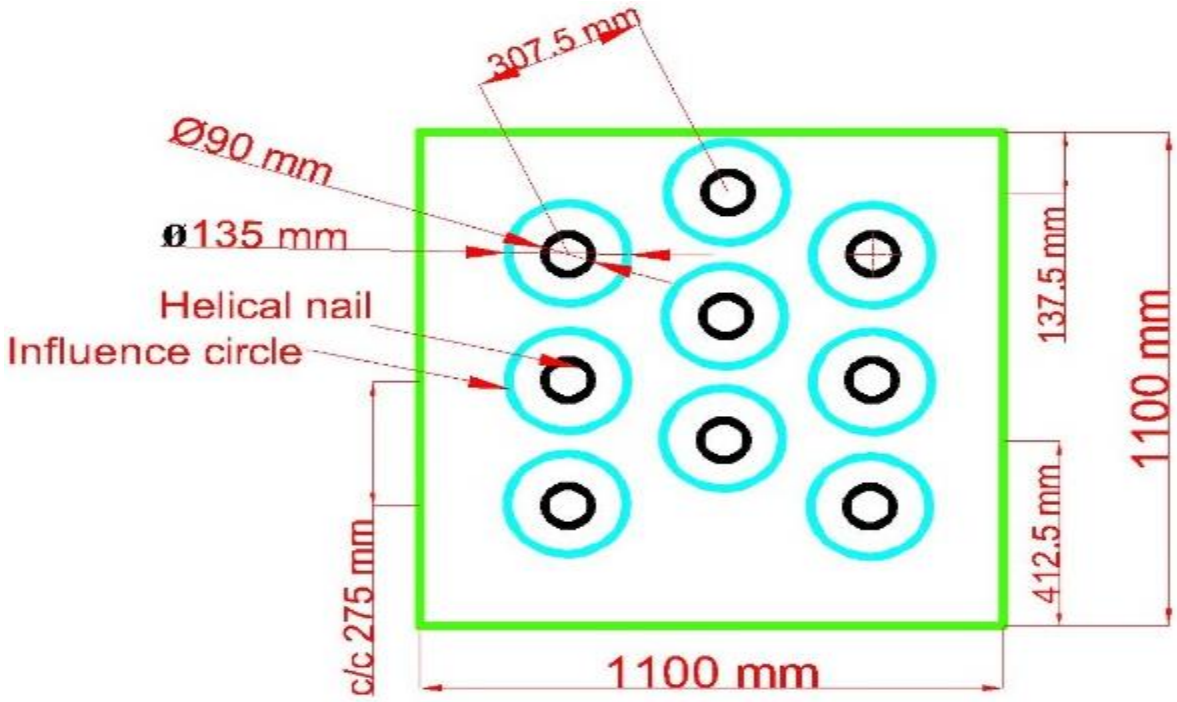

Fig.5. 29 Influence circle of group of nine helical soil nail with staggered spacing

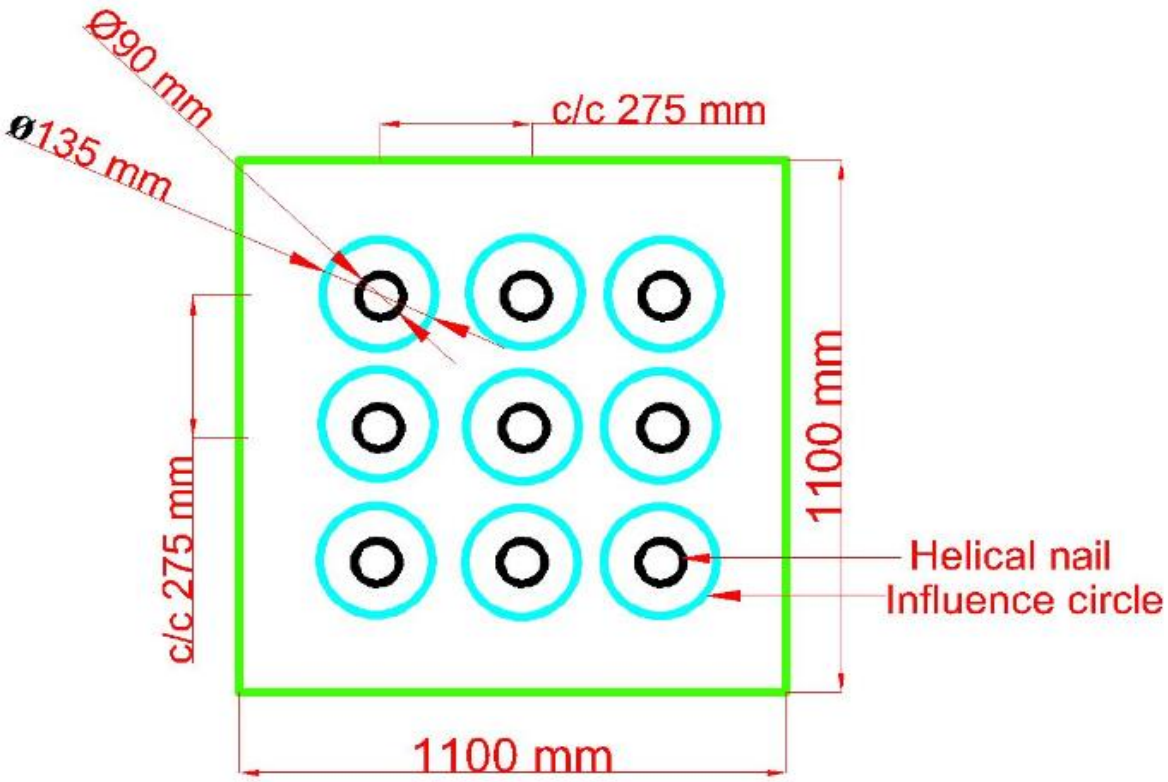

Fig.5. 30 Influence circle of group of nine helical soil nail with uniform spacing

5.5.4 QUANTIFICATION OF SOIL DISTURBANCES DURING SINGLE AND GROUP INSTALLATION

During the installation of the helical element, the helix cuts through the soil and displaces material to allow the movement of helices inside the soil wall. This generates disturbance to the soil, which depends on the soil properties and the installation speed and technique. Soil slopes are most prone to substantial disturbance, even with high-quality installation practice, it is anticipated that nearly all soils undergo some disturbance. To study the installation disturbance factor (IDF) for helical soil nails, a test has been conducted with various inclinations and in-group installation. Further, the authors are of the view that the majority of such analysis results have been carried out for piles and anchors, which are more representative of the selected conditions. To the best of author's knowledge, this is the first study which investigates the installation disturbance factor (IDF) for helical soil nail. As per Lutenegger et al. [87], IDF is defined as the ratio of measured revolutions (MR) per unit of progress to the ideal revolutions (IR) per unit of progress. Further, ideal revolutions (IR) per unit of progress are defined as the ratio of unit progress to the pitch of the helical element. To minimize the disturbance to the soil during the installation of the helical nail as possible for an ideal installation, the values of IDF

should be as close to 1 called perfect installation. On the contrary imperfect installation is interpreted in terms of two different mechanisms: measured revolutions (MR) per unit of progress are greater than the ideal revolutions (IR) per unit of progress and in some cases, it may approach stationary condition. As discussed earlier the installation rate of HN in the present study is 10 rpm, but as helical soil nail enters the soil medium measured rpm was reduced significantly. The pitch used in the present study for the helical nail is 30 mm, resulting in ideal revolutions (IR) for the present study becomes equal to 0.33 (i.e. 10rpm/30mm). In the present study, torque has been measured for every test during the installation of HN using a torque meter. Now measured revolutions (MR) have been calculated from the torque-rpm relation (Source: Engineering Data; Kurz Industrial Solutions). To calculate measured revolutions from torque using relation given in Eqn. (5.29)

$$Measured\ revolutions = \frac{Motor\ Horsepower\ \times 63025 \times Service\ Factor}{Torque} \tag{5.29}$$

In the present study, Motor Horsepower is 0.5; Service Factor is 1.75; Torque is measured during installation of helical soil nail using torque meter. Fig.5.31 shows Installation Disturbance Factors for helical soil nails at a different angle of inclination during installation. As evident from Fig.5.31, for initial 100 mm to 150 mm the IDF is found to be greater than 1 for installation of HN at a different inclination. As the second helix enters into the soil, the IDF varies from 1 to 0.50 at a different inclination and shows little variation at an individual inclination. From the test results, it was observed that during installation of helical soil nail the initial stage (i.e. for 100 mm) shows poor installation, but shows a good installation for remaining length (i.e. for 600 mm). Also, Fig.5.31 shows that the individual average of IDF varies from 0.86 to 0.71 from 0˚ to 30˚ respectively. Moreover, the IDF seems to be constant beyond 20˚ to 30˚. On taking the average of all the tests, it is seen that IDF for helical soil nails is 0.76. Using power regression, a relationship has been developed between IDF and inclination angle (θ) using the average value of different inclination (R^2=0.90) as given in Eqn. (5.30)

$$IDF = \frac{0.87}{(\theta)^{0.12}} \tag{5.30}$$

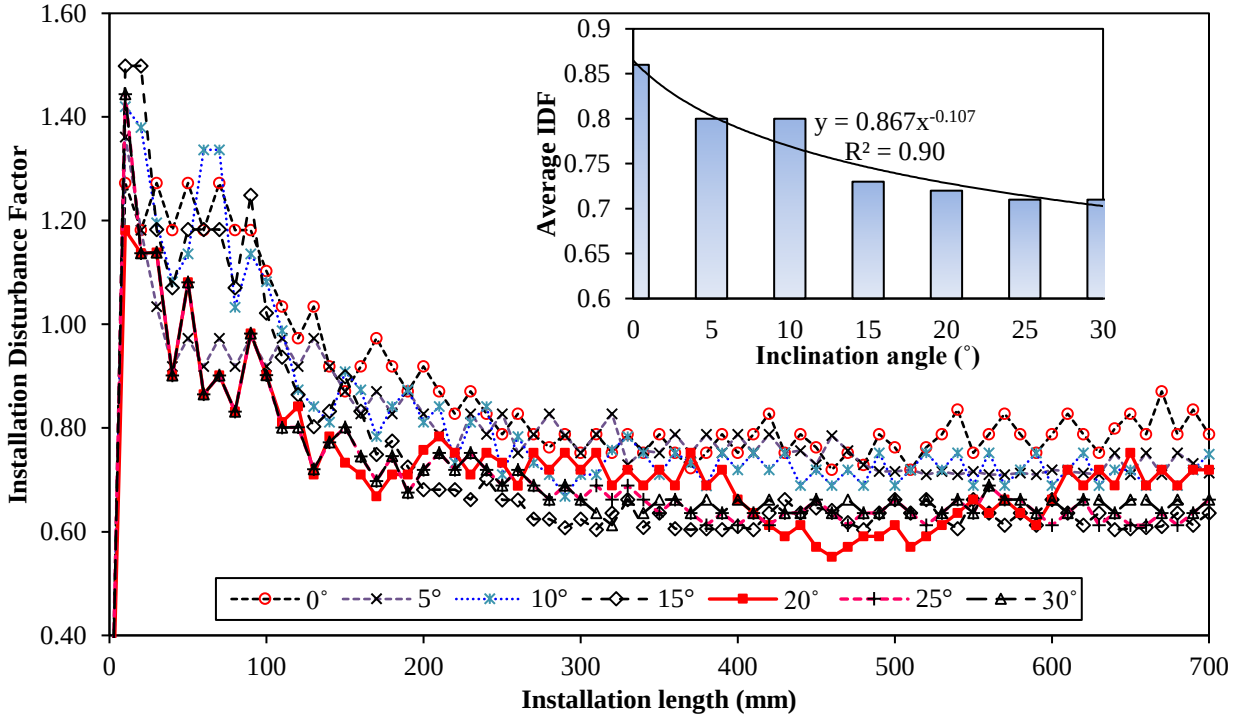

Fig.5. 31 Installation Disturbance Factors for helical soil nail at different angle of inclination during installation.

Fig.5.32 and Fig.5.33 shows installation disturbance factors for helical soil nail installation in a group with uniform and staggered spacing respectively. The IDF for the first six helical nails in a group with uniform spacing was found greater than 1 up to the mid-length, whereas the last three HN shows the least disturbance. On contrary, the group with staggered spacing shows an IDF value of more than 1 for the first HN, the remaining eight nails showed a slight distortion in the beginning and later showed very good installation. In addition to this, it is seen that for both cases that as the bed height change from top to bottom the IDF starts dropping beyond 0.50. The fall in IDF signifies as bed height change from top to bottom the revolution speed of helical nail found is to decreases or approach stationary condition. This decrease in the revolution speed of helical nails is due to the densification of soil with bed height. Moreover, the least IDF for HN in a group with uniform spacing was found to be 0.38, which is shown by nail at ninth position. Whereas the least IDF for HN in a group with staggered spacing was found to be 0.34, which is shown by nail at eighth position. The least IDF found for HN with staggered spacing shows the soil density is the highest for the staggering case.

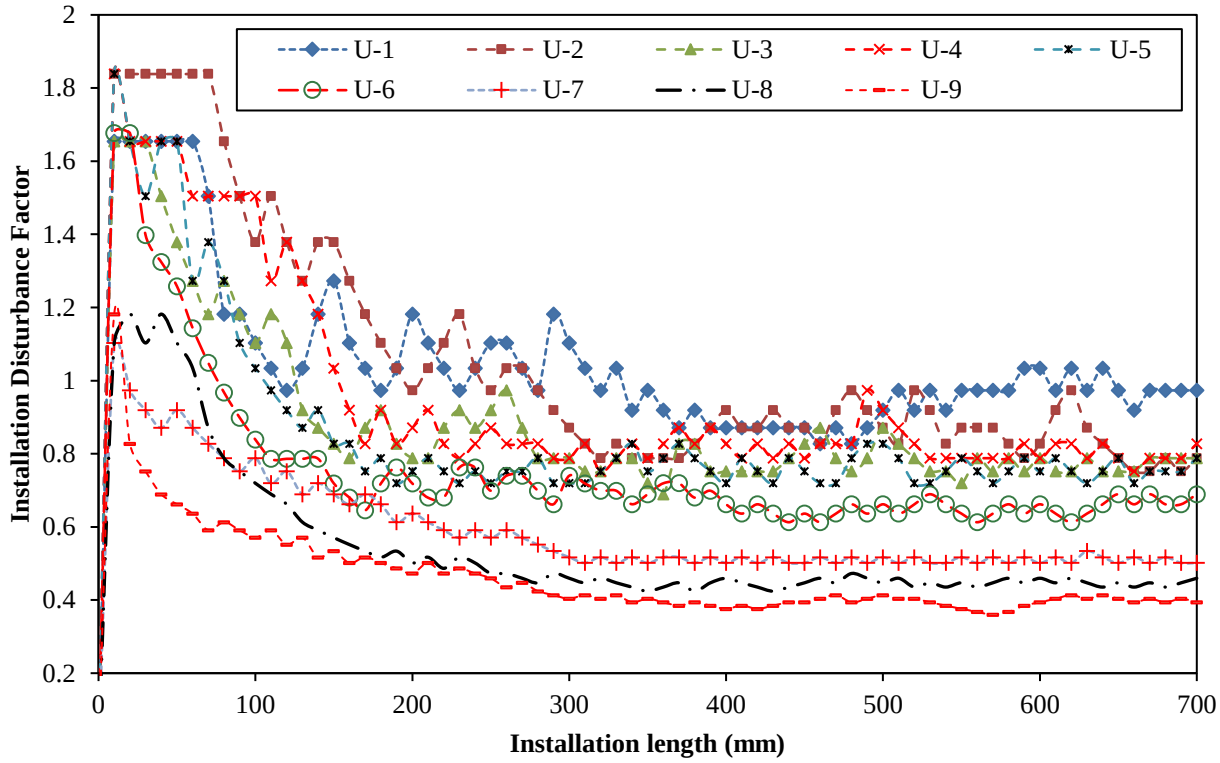

Fig.5. 32 Installation Disturbance Factors for helical soil nail installation in group with uniform spacing.

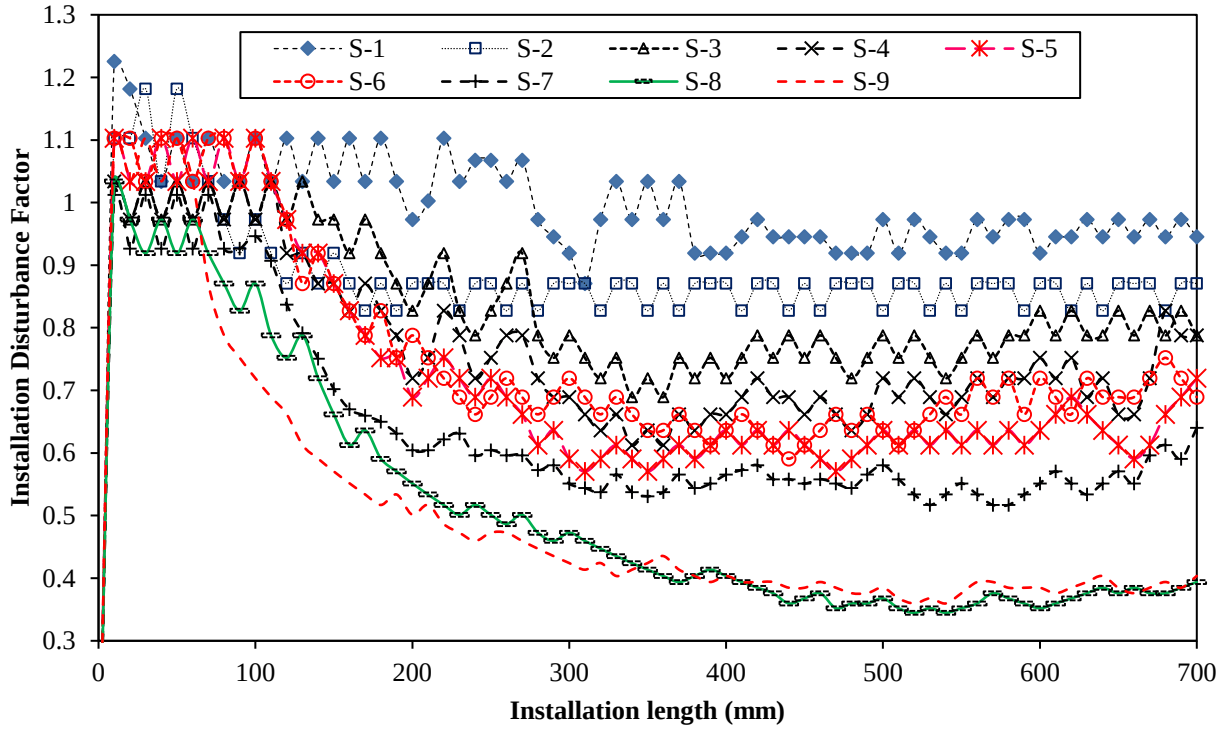

Fig.5. 33 Installation Disturbance Factors for helical soil nail installation in group with staggered spacing.

5.5.5 Earth pressure development during Installation and Pullout

To measure the earth pressure during installation and pullout of group HN six earth pressure cells were used. No such previous attempt has been made to investigate earth pressures during group action of the helical nail. The earth pressure cells were arranged in such a way that cell-1 and cell-2 were placed 70 mm above the topmost phase of HN. The cell-1 was placed 700 mm and cell-2 has placed 500 mm away from the group cap. Cell-3 and Cell-4 were placed on the left and right side of the tank at a depth of 600 mm from the top and 700 mm in length away from the group cap. Cell-5 and cell-6 were placed at the bottom of the tank concurrent to cell-1 and cell-2.

The earth pressures were the same for the installation of the first nail at an angle of 20° during uniform and staggered spacing. This because the bed height and applied surcharge pressure was similar for both the case (i.e. 5kPa) and found to be increasing slightly with an increase in depth. Even every nail showed small disturbances during installation of nail since the last nail is the most significant nail from disturbance and installation point view, so in-situ earth pressures are presented for both uniform and staggered spacing case. The installation of HN in a group with uniform spacing showed a drop in earth pressure throughout the installation process. Also, during installation of HN in one zone showed an increment in confining pressure, on the other zone loss of soil showed a fall in confining pressure. However, loss of soil does not happen in the case of staggered spacing. During the installation of the last nail in uniform spacing, cell-6 revealed negative earth pressure whereas cell-3 revealed zero earth pressure due to the reason that soil is weaker in the tension zone so tension cracks may form hence stresses are negative (Fig.5.34). Consequently, there is the separation of soil and wall due to the formation of tension cracks. Additionally, in the case of staggered spacing, there has been found no negative stresses however, there is slight increment has been observed in these stresses during the installation of the last nail. Hence, it is reported that during the installation of the helical nail with staggered spacing, less disturbance and densification of soil without heaving has been observed.

In the case of group pullout of HN with uniform and staggered spacing (Fig.5.35), the heaving of soil has been observed for both cases whereas in the case of uniform spacing slightly more increment in the tension cracks has been noticed. In the nutshell, staggered spacing has been recommended for the design of a helical soil nail wall.

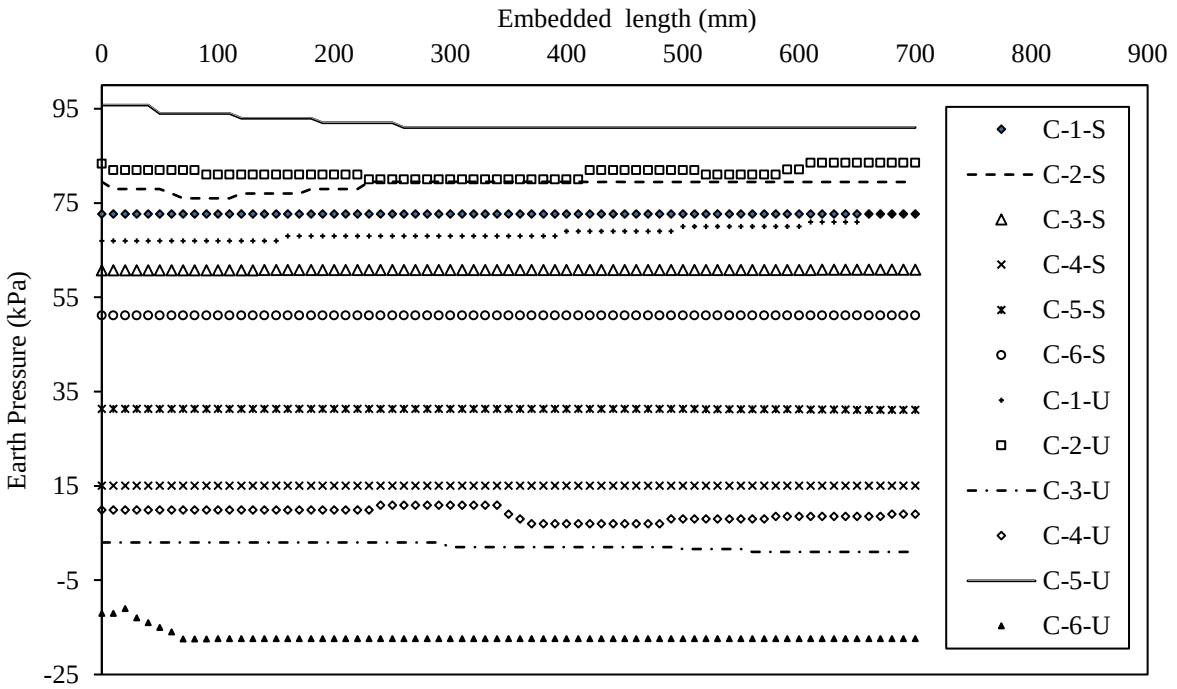

Fig.5. 34Variation of earth pressure during installation of last nail in staggered and uniform spacing

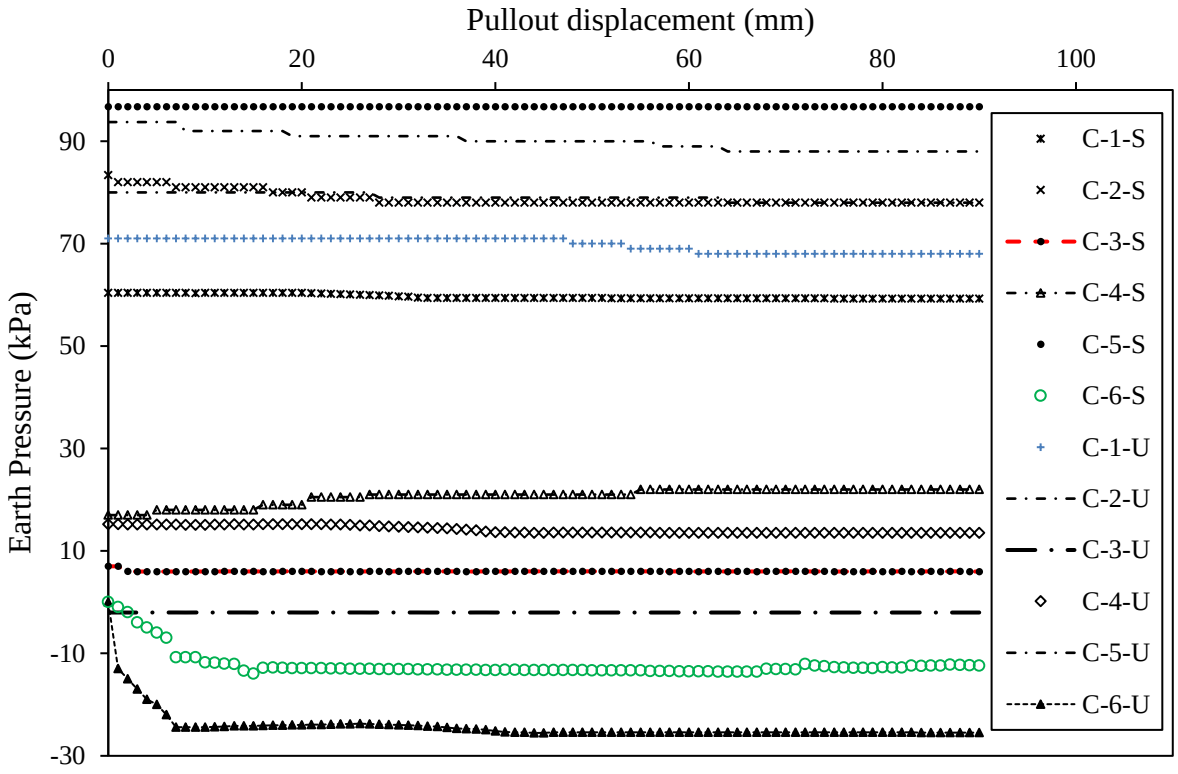

Fig.5. 35 Variation of earth pressure during group pullout of HN with staggered and uniform spacing

Note: C represent cell; S and U represent staggered and uniform spacing.

5.5.6 Evaluation of torsional and axial strains during installation and pullout

Four resistance type strain gauges were used for measured torsional and axial strain pasted at the mid-length of the helical nail. As per Omega, [129] strain gauges were pasted in respective direction to measure both torsional strain and axial strain. The torsional strain presented during installation of HN where axial strain is negligible and axial strain presented during pullout of HN where torsional strain is negligible. Fig.5.36 and Fig.5.37 show variation of cumulative torsional and axial strain with installation length at different inclination angles (under 50kPa). The ultimate value of the torsional and axial strain was found at 15˚ and 20˚ which are overlapping each other. As discussed earlier that the ultimate pullout capacity was observed at 20˚ for HN, this indicates that the pullout capacity is directly propositional to the torsional and axial strain. From the group pullout capacity, the strains presented in the study are only for critical cases during group installation and pullout of HN with uniform and staggered spacing. The torsional and axial strain was observed on the last nail (nail-9) for both uniform and staggered spacing cases. The ultimate torsional and axial strain was found significantly larger for the case of staggered spacing (Fig.5.38 and Fig.5.39). As discussed previously pullout capacity is directly propositional to strain, this indicates that the pullout capacity of a group with staggered spacing impart greater strength in comparison to a group with uniform spacing.

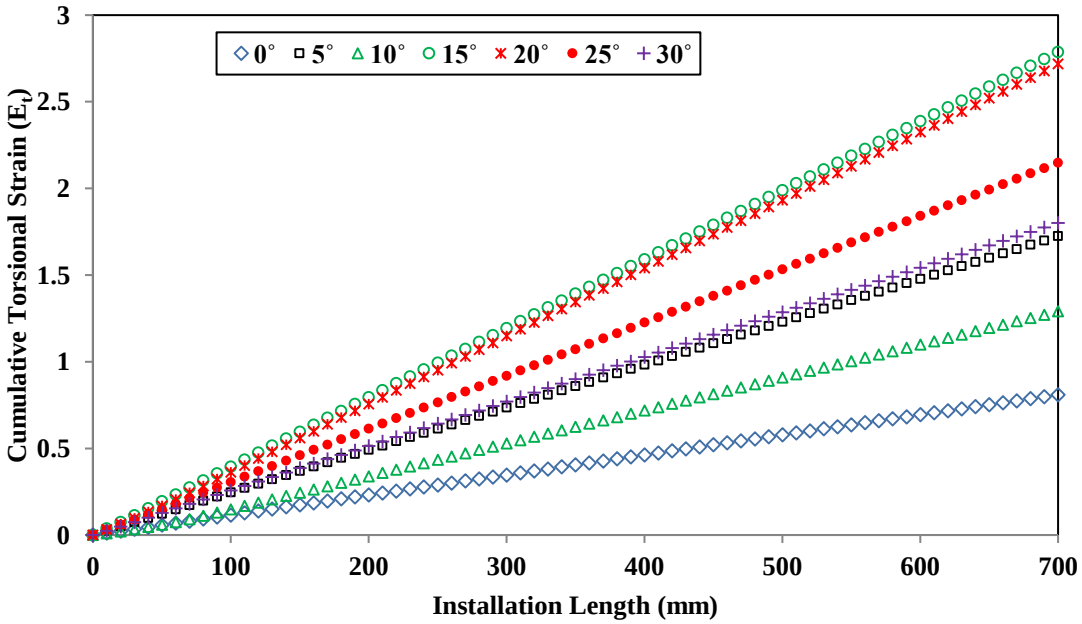

Fig.5. 36 Variation of cumulative torsional strain with installation length at different inclination

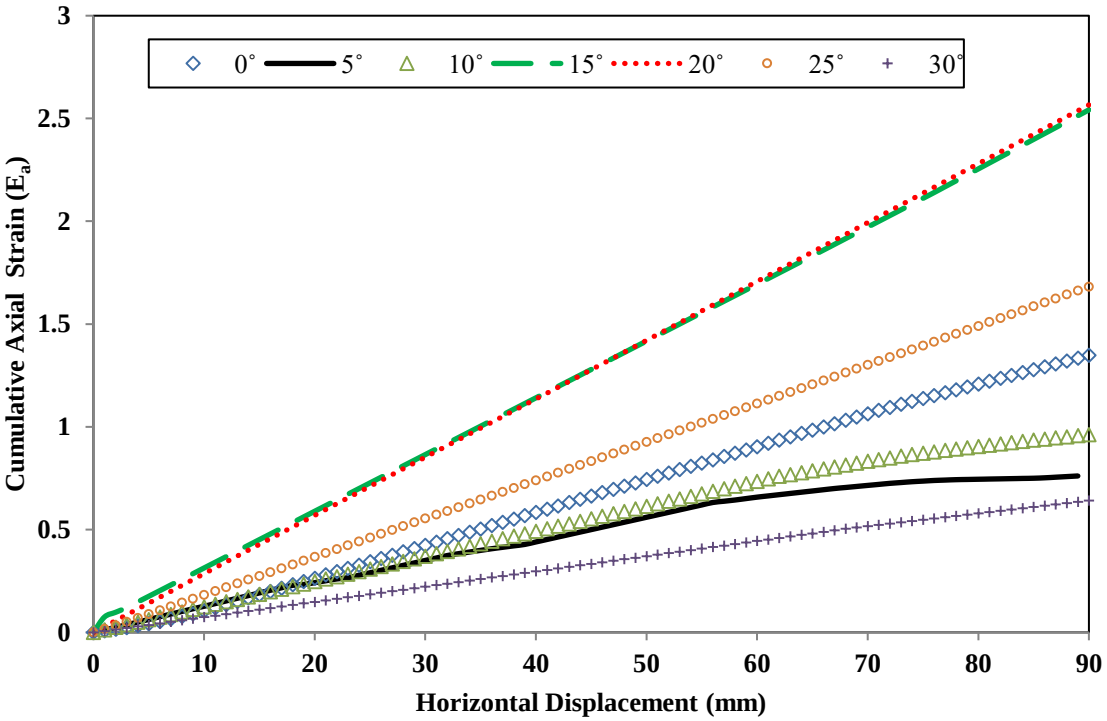

Fig.5. 37 Variation of cumulative axial strain with horizontal displacement at different inclination

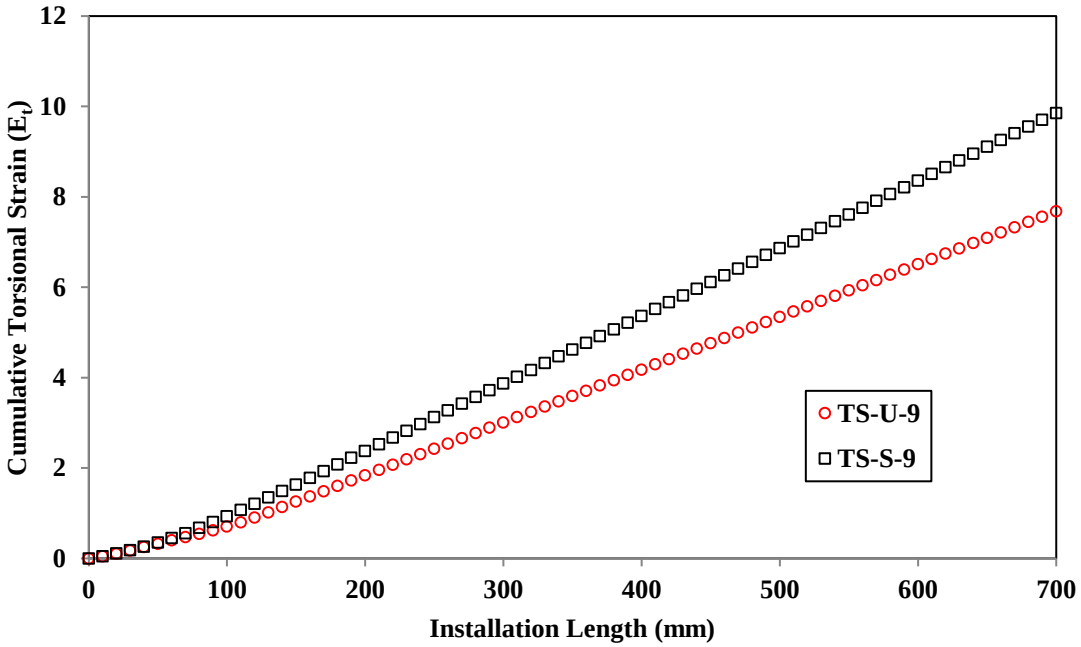

Fig.5. 38 Variation of cumulative torsional strain with installation length for critical nail in group

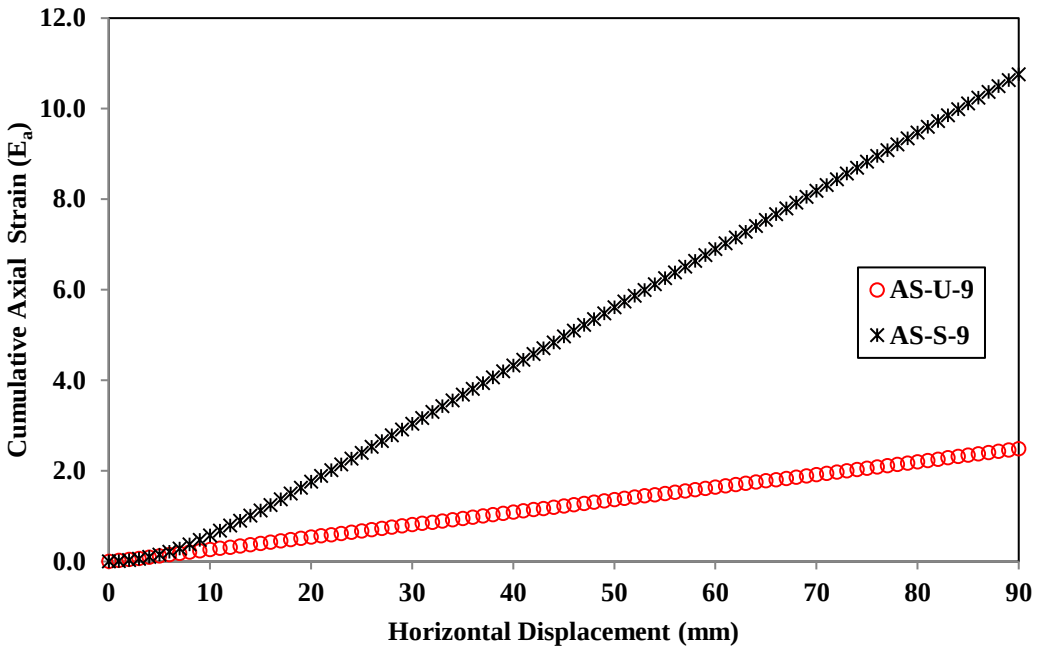

Fig.5. 39 Variation of cumulative axial strain with horizontal displacement for critical nail in group

Note: U represents uniform spacing and S represents staggered spacing.

5.6 Validation

The present study inspects the installation torque and pullout load-displacement behavior of helical soil nails (HNs) in the laboratory under varying parameters like shaft diameter, surcharge pressure, number of helices, and group action in a cohesionless medium. The validation of the laboratory results has been presented using empirical model for installation torque and pullout load-displacement which is already explained chapter 4. The model for installation torque is based on the experimental study and modified for the case of the helical nail [80-90]. Moreover, for the pullout load-displacement behavior, an empirical model has been developed on laboratory results and modified for the case of helical soil nail from existing models for conventional [121-123,131-132]. The predicted results for installation torque and pullout load were then compared with the experimental results. In addition, in the present study, the installation torque and pullout load capacity for a group of helical nails have also been calculated using the theoretical approach and which then validated with experimental results under different surcharge pressure.

5.6.1 Comparison of theoretical and laboratory installation torque and pullout load

The torque and pullout capacity depends on various factors like geometry of helical nail, soil properties, and soil-interaction and installation methods as discussed earlier. The theoretical torque increases consistently with installation length and surcharge pressure. From Fig.5.40 and Fig.5.41, the theoretical and experimental value follows a similar trend and in good agreement between the theoretical and the laboratory results of installation torque and pullout-load for a nail with a rough shaft respectively (L-rough). Although, the experimental value of installation torque shows certain fluctuation during installation exhibit strain softening effect [96-100] and installation disturbance. Whereas theoretical torque not showing any fluctuation reason may be that during experimental testing the soil-nail element undergoes three-dimensional condition, while in theoretical analysis various parameters are under predicted and are a function of friction angle, installation length, and geometry of nail only. But other factors like soil dilatancy, installation method, the 3-D effect of confining pressure, etc may also influence the theoretical installation torque and pullout load respectively. A similar trend was observed for different nail samples.

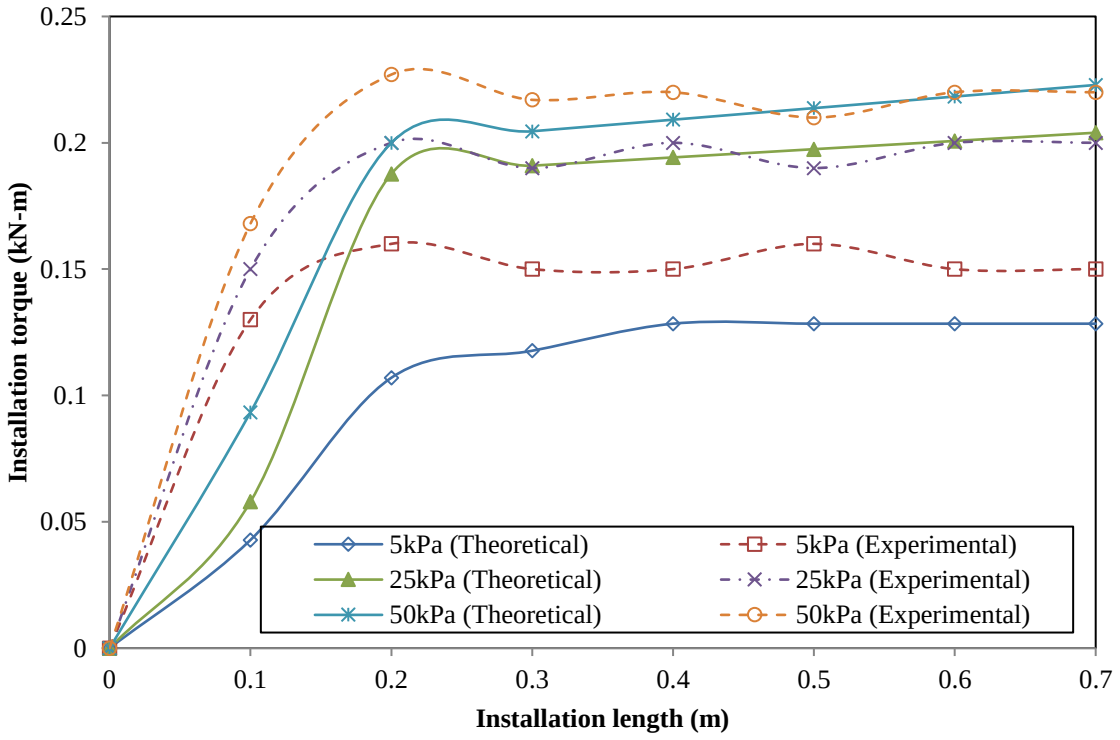

Fig.5. 40 Experimental and predicted installation torque with installation length

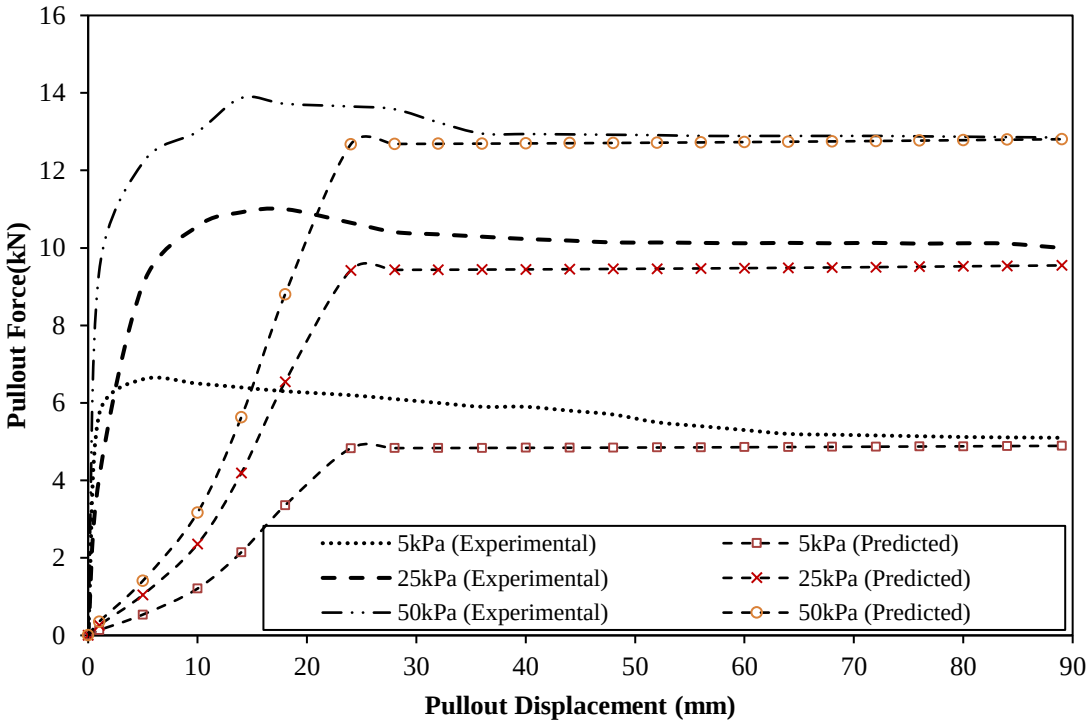

Fig.5. 41 Experimental and predicted load-displacement curve

Figs. 5.42 (a & b) compare the both experimental and theoretical predicted value of peak and residual shear strength for different nail specimens of the helical nail. The model used exclusively for helical soil nails to predict the result, which is modified after Gurung and Iwao [122]; Hong et al.[121]. As evidence that the theoretical and experimental results are in good agreement with each other having (R^2 = 0.97) and (R^2 = 0.99) for peak and residual shear strength respectively. Thus, the model used in the study can calculate the peak and residual shear strength for different helical nail samples under variable parameters and conditions.

From the different helical nail samples, double-helical nails (K) exhibit maximum pullout strength, which further shows an average increase of up to 15-20% under varying surcharge pressure and roughness. The experimental result is further validated with theoretical results and it is observed that the pullout force of different helical nail is directly proportionate to surcharge pressure and roughness of the nail.

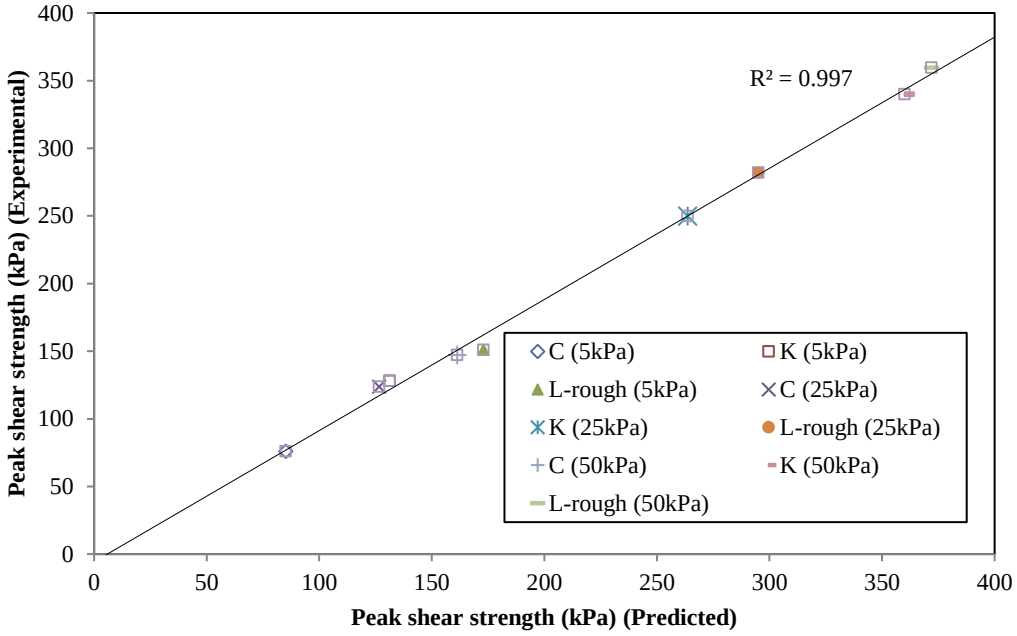

(a)

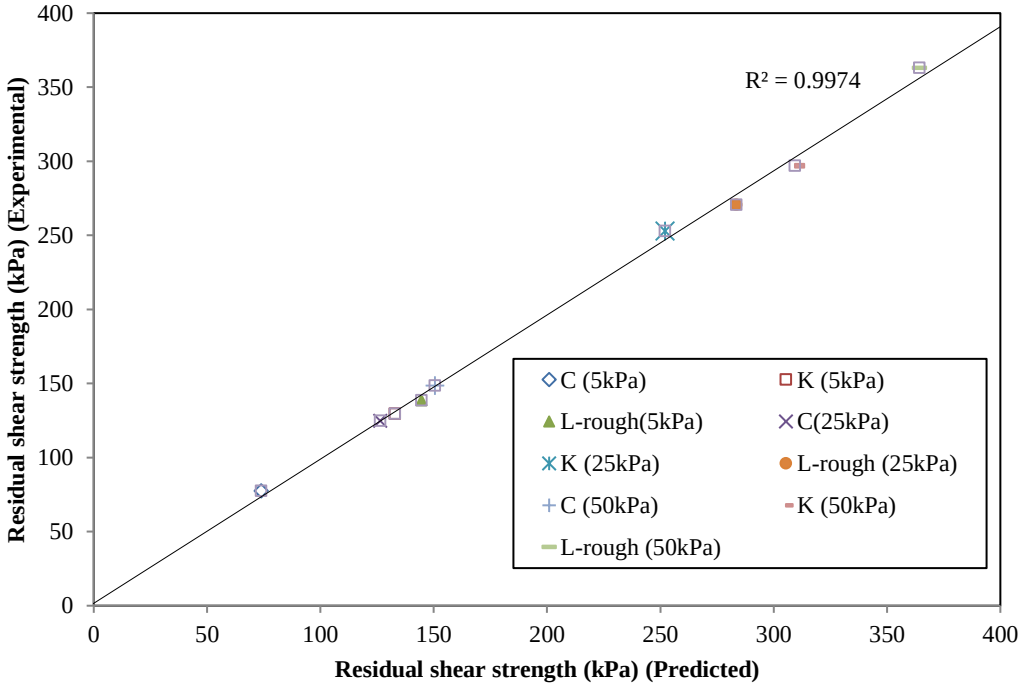

(b)

Fig.5. 42 Comparison of theoretical and experimental values of the nail–soil interface-shear-strength: (a) Peak stage; (b) residual stage

Now, the comparisons between theoretical and experimental values of peak installation torque and peak pullout capacity at different inclinations are found in good agreement with each other.

From Fig.5.43 and Fig.5.44, evident that the installation torque increases slightly increases with an increase in inclinations from 0º to 20º and then starts decreasing and become constant. The torque was recorded maximum for the range from 10º to 20º, corresponding accomplishes peak pullout capacity. Thus, it is evident that the installation torque is directly propositional to the pullout capacity of the helical soil nail. The test result follows a similar trend for different surcharge pressure. Moreover, the theoretical model for installation torque and pullout capacity predicting similar kinds of results to the experimental value.

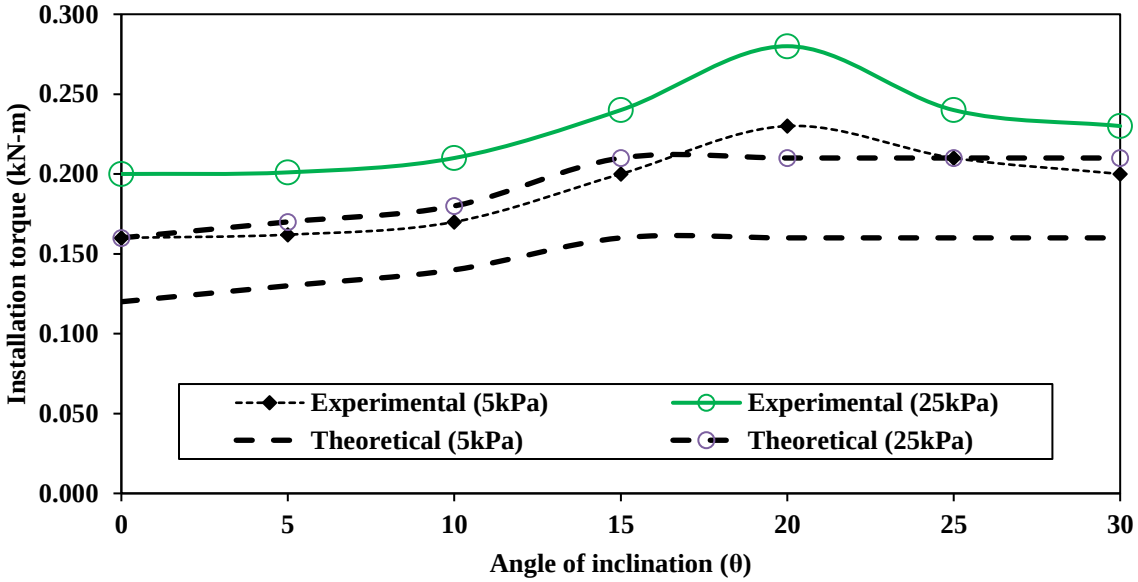

Fig.5. 43 Variation of theoretical and experimental value of peak installation torque with angle of inclination

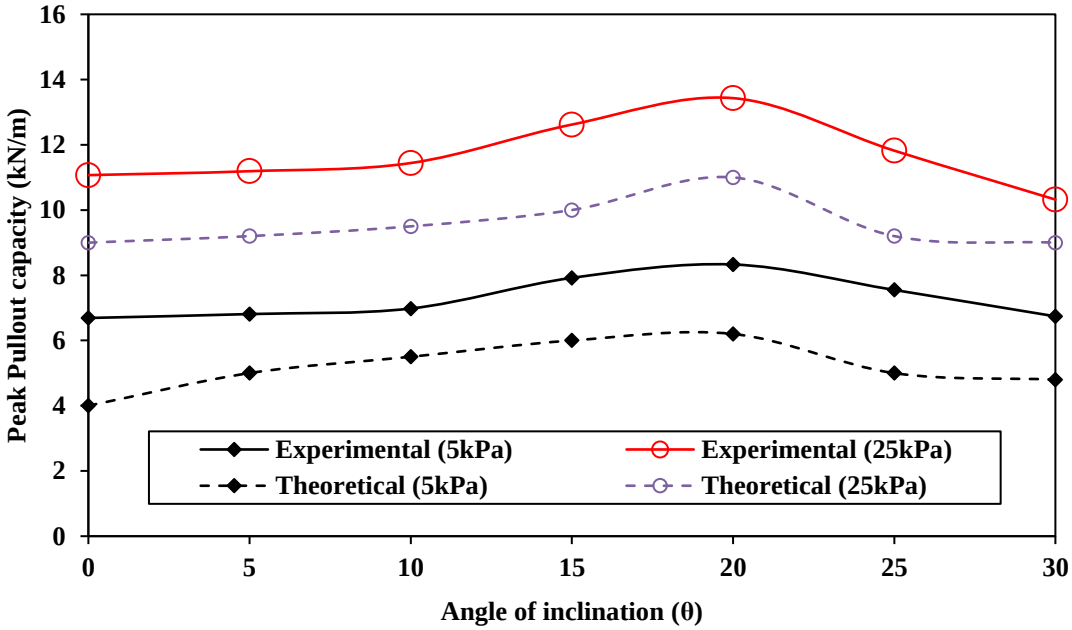

Fig.5. 44 Variation of theoretical and experimental value of peak pullout capacity with angle of inclination

The groups of the helical nail were installed at uniform and staggered spacing group with an angle vary between 15˚-20˚ [5] under 5kPa of overburden pressure. From Fig.5.45a, evident that theoretical installation torque for nails 1, 2, and 3 remains identical because the soil density and height of soil overburden (γh) remains almost the same for all cases. Similarly, for nails 4, 5, and 6 and 7, 8, and 9 the installation torque also remains the same respectively. Whereas experimental results show that helical nail installation torque in increasing order as 1-2-4-3-5-6-7-8-9 (nail number) respectively. Nevertheless, the increment of installation torque is slight but installation torque increase with depth or with an increase in bed height. The trend shows that nail number 4 shows slightly lesser installation torque comparative to helical nail number 3. This is because of volume change observed in cohesionless materials due to over densification of soil around the periphery of helices. The installation torque range for group installation of the nail with uniform spacing varies from 0.12 to 0.43 and 0.15 to 0.43 as calculated theoretically and experimentally respectively.

For group installation with staggered spacing (Fig.5.45b), it is observed that the installation torque recorded experimentally was little on the higher side comparative to the theoretically calculated value but follows a similar trend. Alike to the single nail group installation of nails shows a strain-softening effect [96-100]. Evident from Fig.6b, with change or

increases in bed height the installation also increase, reason may the increase in the soil confining pressure with an increase in surcharge pressure over the nail. Also, the least installation torque (i.e. 0.16kN-m) was observed for a second number of the nail both experimentally and theoretically. The reason may be that the installation of a helical nail was accomplished at shallow depth. The peak installation torque was recorded for helical nail 8 and 9 by both experimentally and theoretically (0.50kN-m) methods respectively. Evident, that the height of bed plays a significant role in the installation of a helical soil nail. The installation torque (IT) for nails 8 and 9 follows turbulence in the path, which means that some part of time nail number 8 show more torque than nail number 9 and vice-versa. This is happening because at different installation depths the soil attaining and loosening the periphery soil and achieve its highly compact state. Due to which re-arranging of soil particle position took place resulting in achieving a highly dense state of the soil mass.

The load-response for the group of the nail with staggered was higher than, the nail with uniform spacing (Fig.5.46). The experimental results are validated with theoretical results, which are in good agreement with each other and follow a similar trend. The predicted (theoretical) results show a relatively lesser value of nails. Alternatively, the model predicts a slightly lesser collapse value of a group of the nail than the actual collapse value. Thus, during the designing of soil nail wall structure, it would be the best fit model which will predict slightly lesser collapse value for a nail structure from the safety point of view. Hence, the used model is best for the collapse assessment of soil nail wall structure.

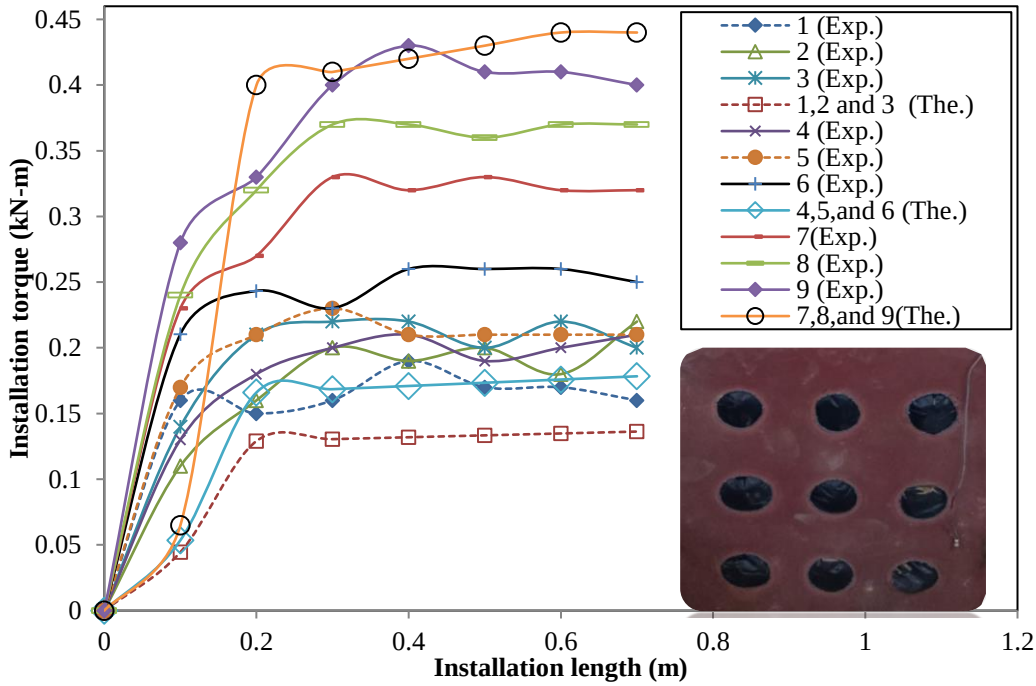

(a) Uniform Spacing

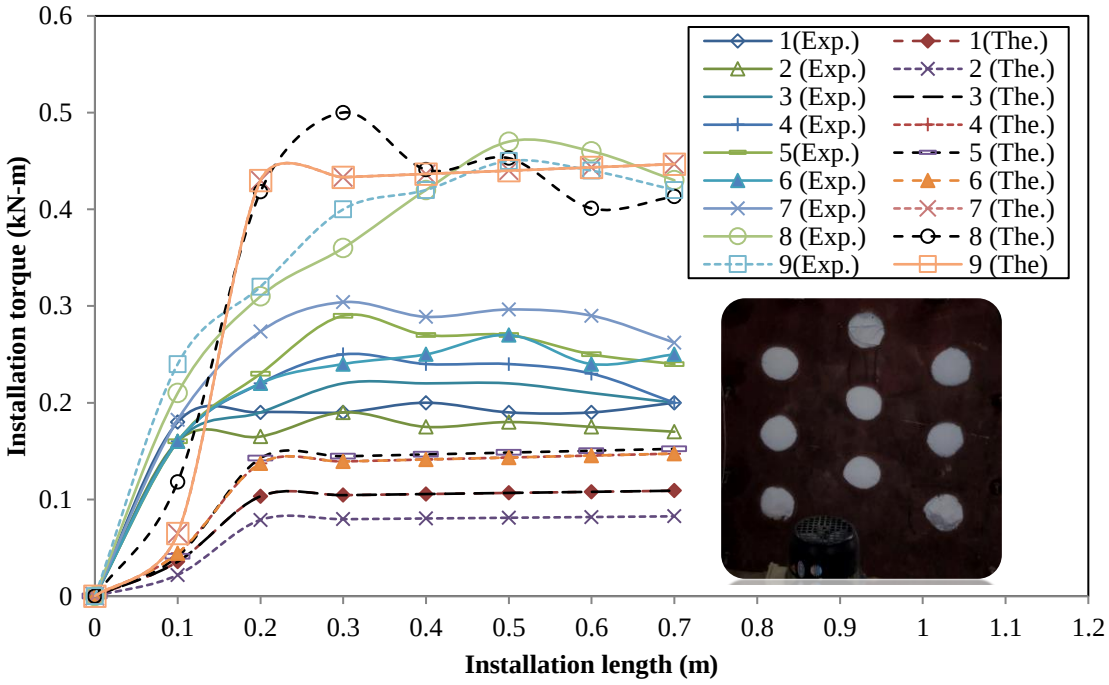

(b) Staggered Spacing

Fig.5. 45 Experimental and predicted installation torque with Installation length for group with (a) Uniform Spacing (b) Staggered Spacing

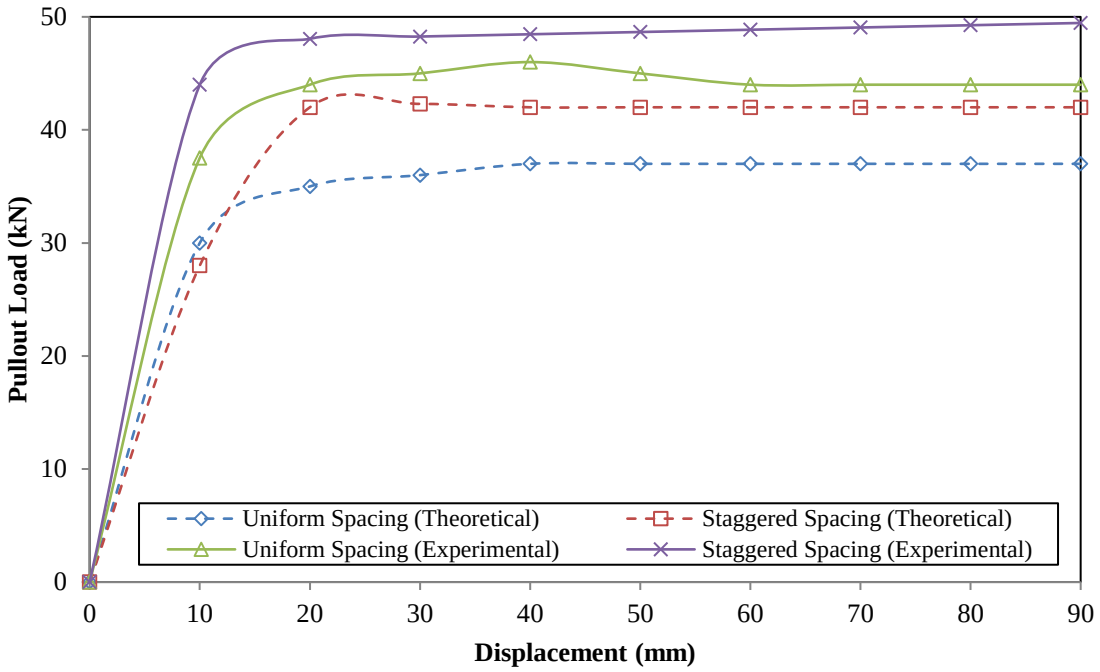

Fig.5. 46 Group pullout-load response for uniform and staggered spacing

5.6.2 Estimation of appropriate Capacity-to-Torque Ratio (K_t)

The capacity-to-torque ratio is considered as the function of the shaft diameter of the helical element [8-9]. As per Hubbell, [115] and Perko, [9] the capacity-to-torque ratio (K_t) is strongly affected by elements shaft diameter and thickness of helix and poorly affected by crowd force number of helices, and helix pitch. Thus in the present study shaft diameter is considered as the predominant factor which affects the (K_t) value. Nevertheless to maintain the uniformity in the results of the nail with a single shaft were only presented in the study. In this context, the experimental and theoretical data of K_t has been plotted with the shaft diameter of HN. As evident from Fig.5.47, the capacity-to-torque ratio (K_t) decreases with an increase in the shaft diameter of HN. The laboratory test results are validated with the theoretical data, which follow the similar trend of K_t with shaft diameter. The K_t value decreases because the helices size increases with increases in shaft diameter of HN resulting in shaft friction becomes equal to negligible (only helices will contribute), which reduces the capacity-to-torque ratio (K_t).Power regression analysis was applied to the experimental and theoretical data individually. The two different equations were generated for experimental and theoretical data with the coefficient of determination ($R^2 = 0.992$) and ($R^2 = 0.995$) respectively. Eqn. 5.31 and 5.32 present the experimental and theoretical equations respectively for capacity-to-torque ratio (K_t) as:

$$K_t = 164.29\ \mathrm{d}^{-0.56}, \qquad (R^2 = 0.992) \tag{5.31}$$

$$K_t = 99.22\ \mathrm{d}^{-0.38}, \qquad (R^2 = 0.995) \tag{5.32}$$

Power regression analysis was also applied for the combined case of experimental and theoretical data and equation (Eqn. 5.33) has been generated with the coefficient of determination ($R^2 = 0.91$).

$$K_t = 127.68\ \mathrm{d}^{-0.47}, \qquad (R^2 = 0.92) \tag{5.33}$$

With the change in soil condition or change in shear strength parameter of soil and resulting in the Eqn. 5.31 may change to some extent or over predict the K_t value, whereas Eqn.5.32 predicts a lesser value of K_t, which looks safer from a safety factor point. Nevertheless, the Eqn.5.33 generated was more appropriate for the estimation of capacity-to-torque ratio(K_t), because neither it under-predict nor over-predict.

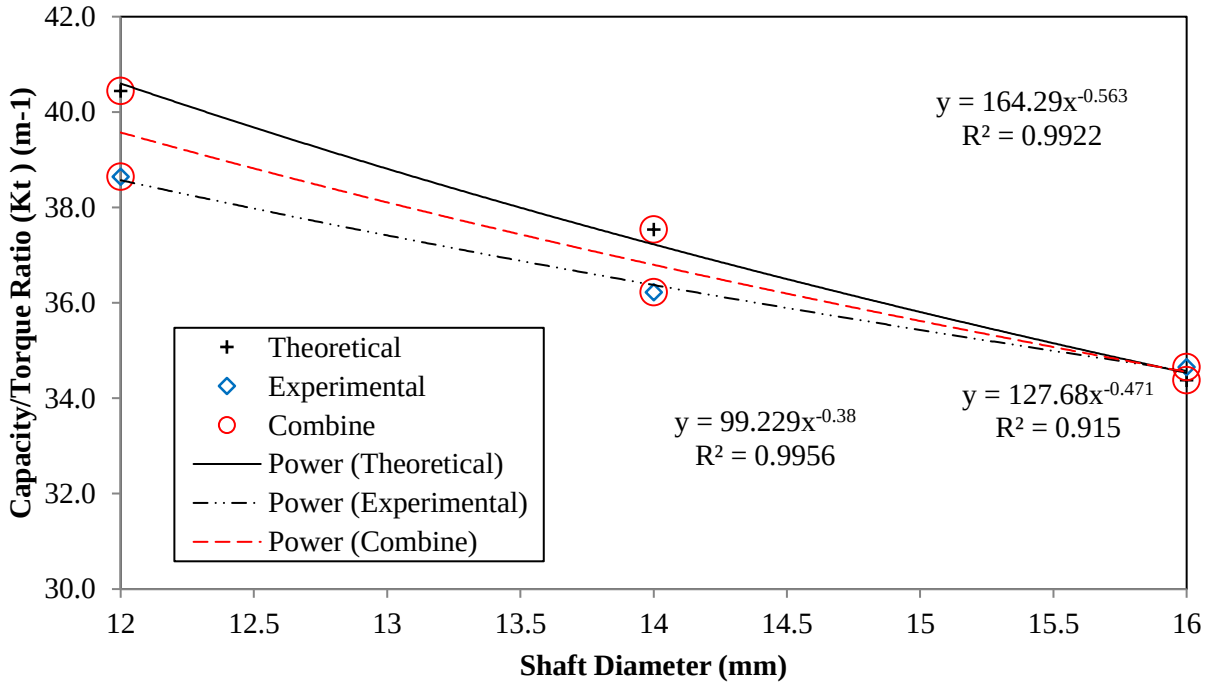

Fig.5. 47 Variations of Capacity/Torque Ratio (K_t) (m^{-1}) with Shaft Diameter

5.6.3 Effect of shaft diameter

Fig.5.48 and Fig.5.49 present the variation of shaft diameter with peak installation torque and peak pullout capacity respectively. The results indicate that the peak installation torque and peak pullout capacity increases with an increase in the shaft diameter of the nail. The average increases in installation torque and pullout capacity with increases in 2mm of diameter is 40%

and 28% under different pressure. This increase in installation torque and pullout capacity was due to an increase in surface area of the nail and resulting increases in the skin friction. The results show that the installation torque and pullout capacity are a linear function of each other. Fig.5.48 and Fig.5.49 also present that with an increase in surcharge pressure the peak installation torque and peak pullout capacity also increases. The theoretical model attributed good agreement with the laboratory results. The result confirms that the pullout capacity followed the Mohr-Coulomb failure criterion under varying pressure. Moreover, the mobilized installation torque and pullout capacity increased considerably with the surface roughness.

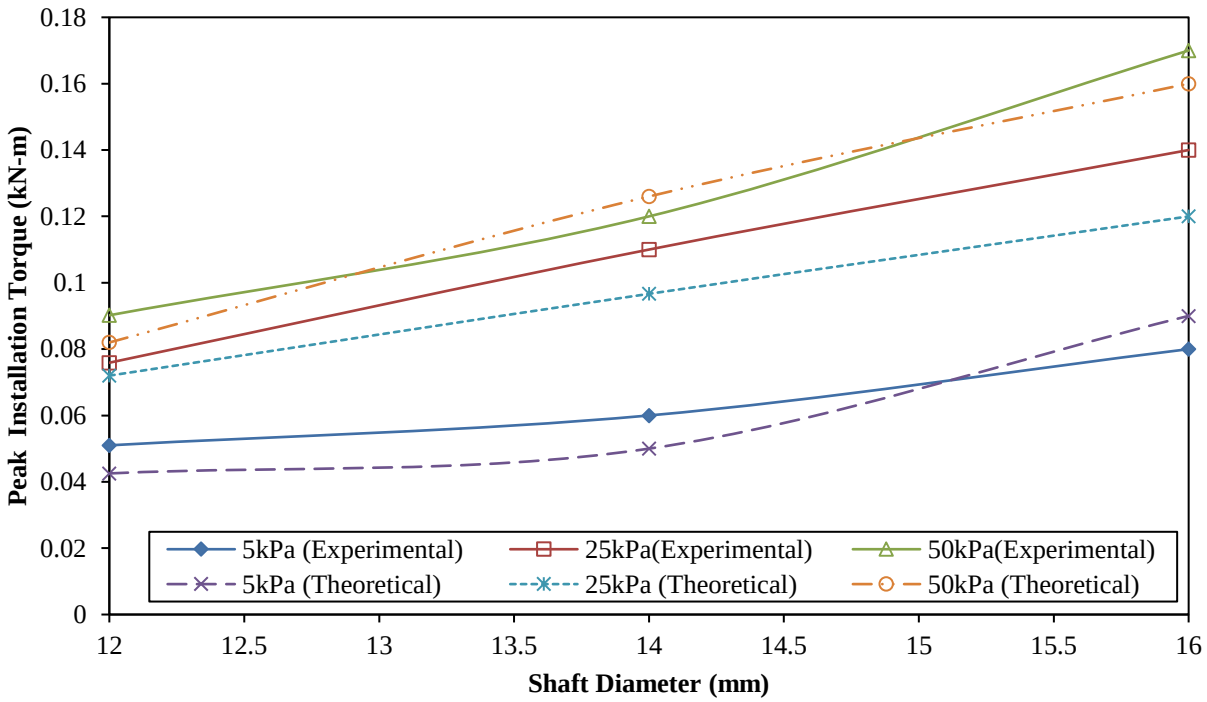

Fig.5. 48 Variation of Peak Installation Torque with Shaft Diameter

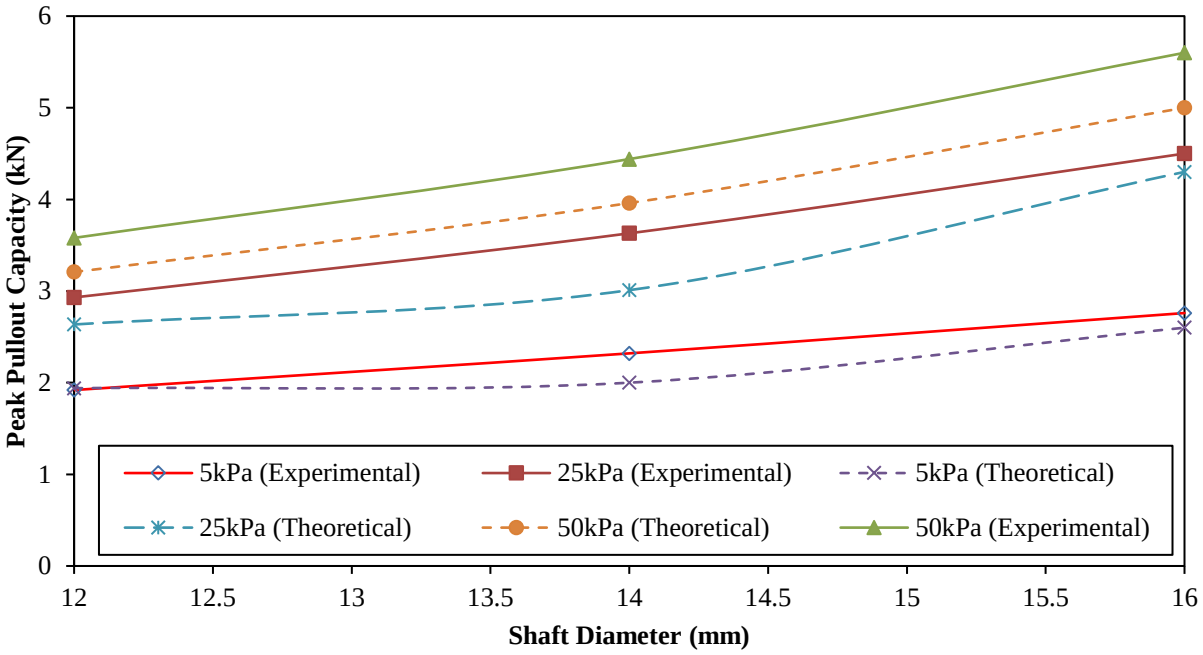

Fig.5. 49 Variation of Peak Pullout Capacity with Shaft Diameter

5.6.4 Applicability of proposed theories

The model proposed in the present study is for the installation torque and pullout resistance capacity of the helical nail. To validate the applicability of proposed theories, the experimental data of previously publish literature have been used in proposed theories for installation torque and pullout capacity. The calculated results are then compared with already published experimental results. For the comparison of installation torque of helical nail, data two experimental studies [15] was used, while for the pullout capacity of helical nail data four laboratory study [14-15] was used in the proposed empirical model. The essential input parameters that were adopted from these studies [14-16,97] are presented in Table 5.4. The investigation of the reported results of helical soil nail, using the projected theories has revealed encouraging results, and the theories have the potential to calculate the installation torque and pullout capacity of helical soil nail (Fig.5.50 and Fig.5.51). A similar trend was observed for installation torque and pullout load-displacement. It can be observed that the installation torque (Fig.5.50) shows slight fluctuations which can be taken into account due to the effect of installation speed, soil conditions, and crowd force during installation, whereas average installation torque remains almost the same. The load-displacement curve shows (Fig.5.51) the pure-elastic and elastic-plastic stage for both predicted results and previously published results

and found in good agreement. The calculated results are for installation torque and pullout-load slightly underestimate the result of the fact that the empirical models adopted the uniform soil density, uniform friction angle, and uniform surcharge pressure have been taken into account throughout the study. However, laboratory studies may not able to maintain the consistency in soil parameters of soil samples. The soil has a very complex nature and thus the soil properties changes with the installation of the helical nail in the field. In that case due to complexities in estimating the changed parameters least value of shear strength parameter is recommended to use the model for estimation of installation torque and pullout resistance capacity.

Table 5. 4 Soil-nail parameter employed in literature

Parameter	**Tokhi,2016**	**Rawat et al. 2016**	**Sharma et al. 2017**	**Sharma et al. 2020**
Helix diameter (mm)	150,150	172.5,172.5	64,96	64, 96
Helix thickness (mm)	5	5	9	10
Helical Spacing (mm)	500	50	192	200
Shaft diameter (mm)	38	15	16	16
Shaft type	Smooth	Smooth	Smooth	Rough
Effective Length (mm)	600	800	900	700
Surcharge (kPa)	75	20	99	50
Surcharge height (z) (mm)	500	500	750	500
Cohesion (c)	0	0	0	0
Friction angle (ϕ°)	40	36.5	38	37
Interface friction ($\boldsymbol{\delta}$)	26	12	16.17	31
Max. dry density (γ) (kN/m^3)	18.15	16.5	16	16.87
Elastic moduli (GPa)	200	200	200	200

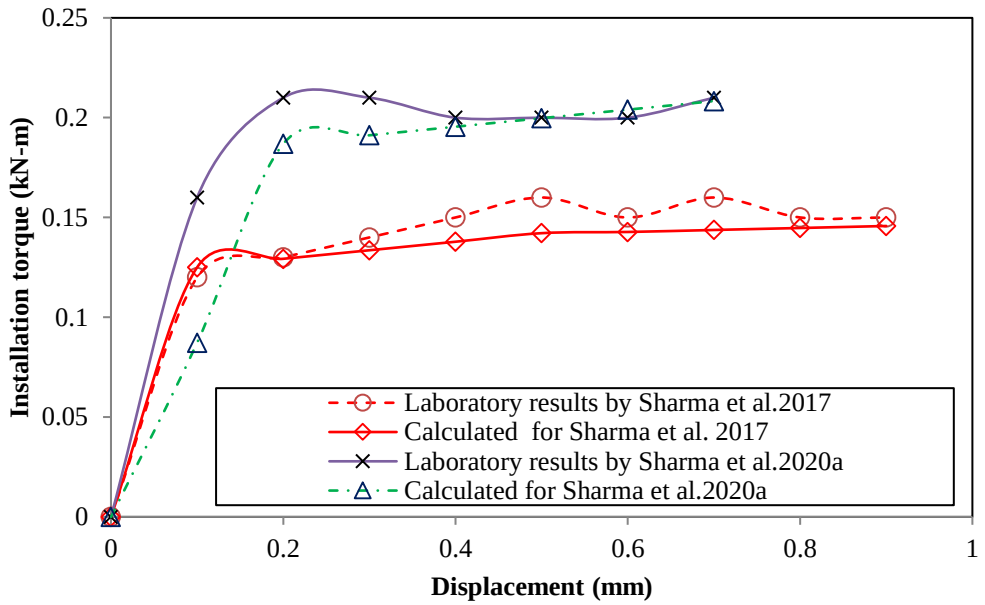

Fig.5. 50 Variation of Installation torque with displacement

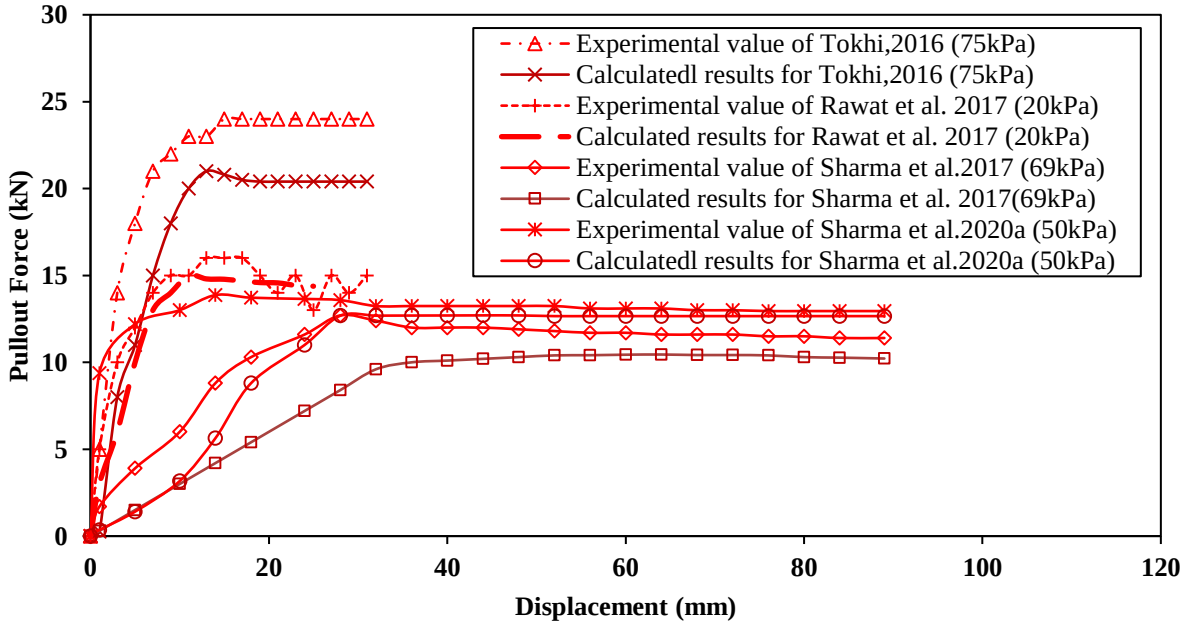

Fig.5. 51 Variation of Pullout load with displacement

5.6.5 RELIABILITY OF THE PRESENT METHOD UNDER DIFFERENT SOIL CONDITIONS

The reliability of the present method can be realized from the comparison of pullout response of helical soil nails under different soil conditions such as c = 0, ϕ = 0 and c– ϕ soil. Figure 5.52 represents the variation between pullout loads with horizontal displacement for helical nails in

different types of soil as observed by different researchers. Tokhi [14] carried out pullout testing in both cohesionless and cohesive soil depicting a nonlinear variation with horizontal nail movement. A similar observation was also made by [15] on the pullout of helical nails in cohesionless soil. In line with reported literature, the pullout response of open-ended helical soil nails using the present method also undergoes three phases from pure elastic to elastic– plastic, and eventually pure plastic. The pullout displacement of the helical soil nail varies linearly in the elastic phase, but after attaining maximum pullout load, the pullout becomes constant in the elastic–plastic region. In the pure-plastic phase pullout load is found to decrease and reach the post ultimate state of elastic–plastic phase [131-132]. Thus, it can be stated that the present methodology will provide a similar pullout trend irrespective of soil types. However, variations in the magnitude of pullout response for different soil types can be attributed to different relative density and overburden used during testing. The pullout response in different soils also reveals that the adopted method works on the basic load transfer mechanism of helical nail pullout governed by bearing resistance from helical plates and shaft skin friction for all types of soils.

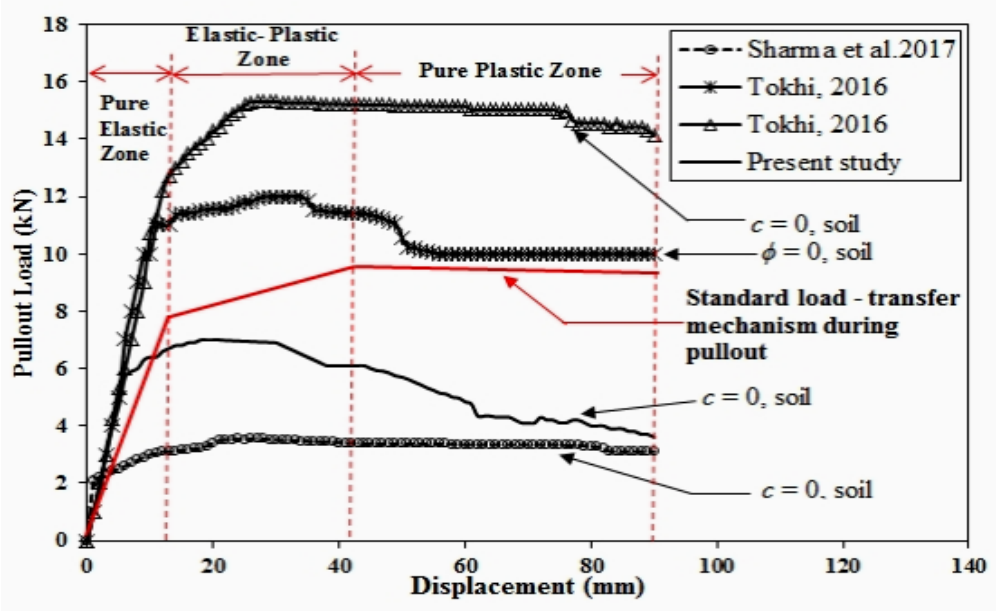

Fig.5. 52 Variation of pullout loads - displacement for helical nails in different types of soil

5.7 SUMMARY

The present study examines the behavior of helical soil nail installed in cohesionless soil subjected to pullout force under varying parameters such as helical nail configuration (shaft diameter, helical diameter, helical pitch, number of helices), nail shaft types (roughness and stiffness), installation torque, and overburden pressure. The installation torque and corresponding nail pullout capacity can be established using a torque correlation factor (K_t). K_t value decreases with increasing embedded nail area and is inversely proportional to the nail shaft diameter. From pullout tests result, it is found that pitch in the range of 24.5–35.5 mm shows better pullout capacity. Also, results show that additional helices will only contribute to pullout capacity if located outside the region of soil mobilized in the failure mechanism of lower helix. Moreover, higher axial strains are found for hollow shaft nail, which alters with the increase in number of helices. The test results indicate that soil plug contributes (open-ended pipe helical soil nail) about 11.5% of the total mobilized skin friction during pullout. The pullout capacity increases with increase in the number of helices and nail shaft diameter. However, soil plug length is independent of number of helices.

CHAPTER-6

PRACTICAL APPLICATION

CHAPTER 6
PRACTICAL APPLICATION

6.1 GENERAL

A debris flow type of landslide is believed to have propagated from existing minor landslides and heavy rainfall on August 13, 2017, near the village of Kotropi (Mandi District, Himachal Pradesh), India. The disastrous landslide swept away two state transport buses causing 47 fatalities [134-135]. A stretch of 300-m on National Highway-154 was completely buried under debris by a massive 1153 m of slope run-out extending over 190 m of slope width. The present research work aims at mitigation of Kotropi slope failure using helical soil nails. The preliminary study involves geotechnical and chemical testing of Kotropi soil. With favorable prevailing soil conditions, helical soil nails with length of 6 m and diameter 20 mm are used for stabilizing the failed slope. The stability of helical soil-nailed slope is determined by calculating factor of safety using limit equilibrium method which is also validated by numerical modeling using finite element subroutine PLAXIS 2D. A factor of safety of 1.54 is achieved by calculations in comparison with 1.67 from numerical modeling. Moreover, a decrease in maximum horizontal slope deformation is also achieved from 0.13 to 0.06 m.

6.2 STUDY AREA

The present study investigates a landslide which occurred near the village of Kotropi, in Mandi District of Himachal Pradesh, India (Fig. 6.1), which is 414 km from New Delhi and 150 km from the capital Shimla. This place is only 90 km from Dharamshala, which is the wettest place in Himachal Pradesh. The Kotropi region is extended between 31.9121° N LATITUDE and 76.8879° E LONGITUDE**.** Geologically, the area is in a thrusted contact between Siwaliks and Shali group of rocks containing mainly of dolomites, brick red shale, micaceous sandstones, purple clay and mudstones [136]. Since these rocks are weak in strength, hence when subjected to displacement by thrust make this area highly prone to landslides.

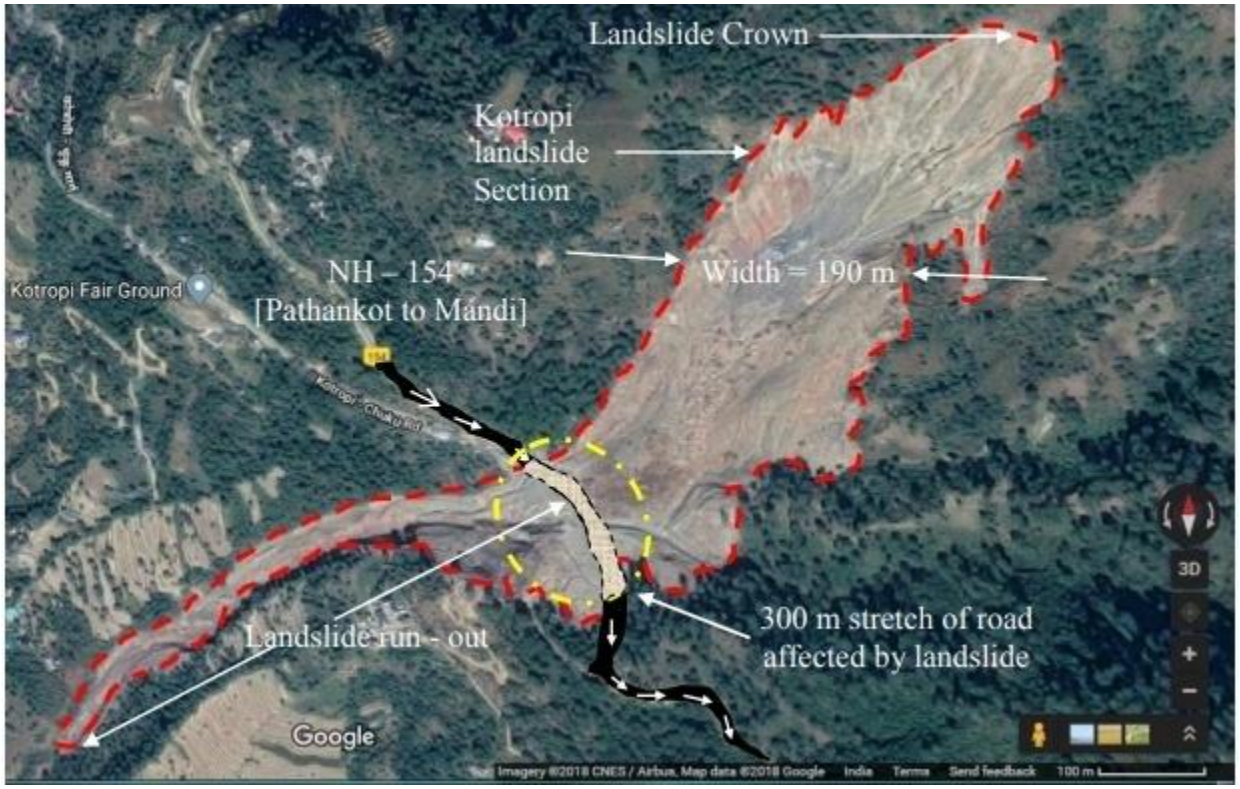

Fig.6. 1 Kotropi Landslide section

6.2.1 LANDSLIDE CLASSIFICATION

Landslides can be classified into various types such as rock compound slide, silt flow slide, clay rotational slide, clay flow slide, earth flow, sand flow, debris flow, mud flow. Fig.6.2 shows that before the actual landslide, Kotropi region had been suffering local landslide scars at the slope crest. The group of these small and old landslide caused occurrence of large landslide in the area [136]. As per the report [136], Kotropi landslide was a 'debris flow' type landslide in which the ‘Debris flow’ occurs along with floods comprising of large amount of soil mass flowing in a steep channel. During intense flooding in this steep channel, the stream bed damages the slope, causing massive movement of sediment. The flow usually initiates with a slide, debris avalanche or rock fall. During Kotropi landslide, the channel created by debris flow is about 1155m from landslide crown. As the soil mass begins to flow under the debris type landslide, change in volume of failing slope is restricted due the movement of soil mass occurring within confined boundaries such as that in a steep channel [137]. Since the movement does not allow for volume change, pore – pressure builds up even in coarse grained – soils, thereby leading to liquefaction of soil mass. This leads to a decrease in soil shear strength which makes the slope

unstable [138]. Moreover, as the flow moves downstream, the slope bed is weakened by erosion which adds up large amount of debris in the flow [139].

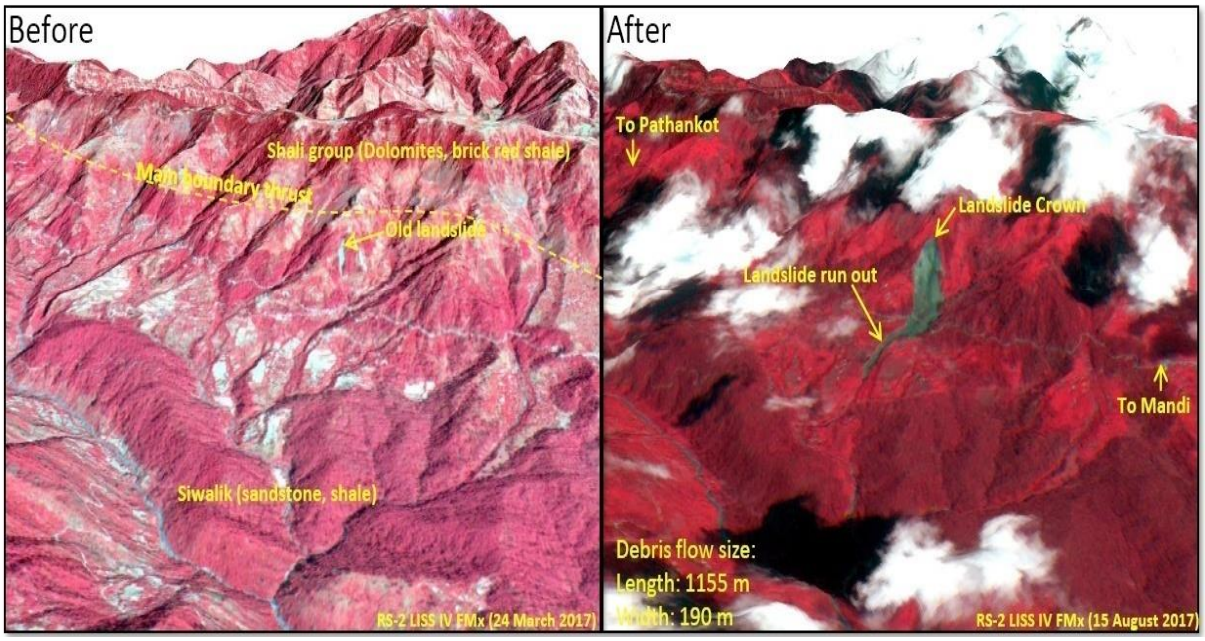

Fig.6. 2 Before and after landslide image of Kotropi landslide [16]

6.2.3 GEOTECHNICAL INVESTIGATION OF KOTROPI SOIL

The investigation of geotechnical properties of Kotropi landslide soil is important so as to identify feasibility of soil for helical soil nailing. The length and breadth of landslide is 1153 m and 300 m, respectively. As reported by PH and PP state unit, Chandigarh [140], failure zone for Kotropi landslide is found to lie between 5 to 8 m. The samples are collected upto a depth of 6 m, however, physical characterization of soil reveals minimal variation beyond 1.5m, and hence results upto 1.5 m depth are only reported. In order to take samples from the site, landslide was equally divided into three sections (uppers section, middle section and lower section) along the landslide slope. Each section upper, middle, and lower is further divided into three sections 80 m apart to cover the maximum horizontal profile of landslide slope. Thus, the entire Kotropi slope is divided into 9 sections i.e. 3 (Horizontal) and 3 (vertical) from where soil sampling is carried out (Fig.6.3). The soil samples from each section are collected using core cutter method in open pits at different depths of 0.5m, 1m, and 1.5m. A total of 27 disturbed soil samples are collected, sealed in plastic bags and were transported to Geotechnical Engineering Laboratory at Jaypee University of Information Technology, Waknaghat, Solan, Himachal Pradesh, India for its

characterization. The sampling procedure carried out is in accordance to IS: code 14680 - 1999 [141].

Fig.6. 3 Sampling point at Kotropi landslide (Mandi, Himachal Pradesh)

For characterization of soil samples grain size analysis, Atterberg's limit, compaction test, direct shear test, triaxial shear test, and chemical analysis are conducted. The results of these parameters are used for determining the feasibility of helical soil nailing at Kotropi and for modeling in FE analysis. The grain size analysis is carried out using sieve analysis and hydrometer analysis on all three section (i.e. top, middle, and bottom) of Kotropi landslide at 1.5m depth (Fig.6.4) as per IS: 2720, Part - 4 [108]. The tests results depict Cu = 9.30 and Cc = 0.24 for top section, for middle section soil value of Cu = 8.33 and Cc = 0.925 and for bottom section soil value of Cu = 8.31 and Cc = 0.68. The particle size distribution also revealed that the fineness modulus between 5 to 12% and hence the soil is classified as SP-SM (i.e. poorly graded sand containing silt.

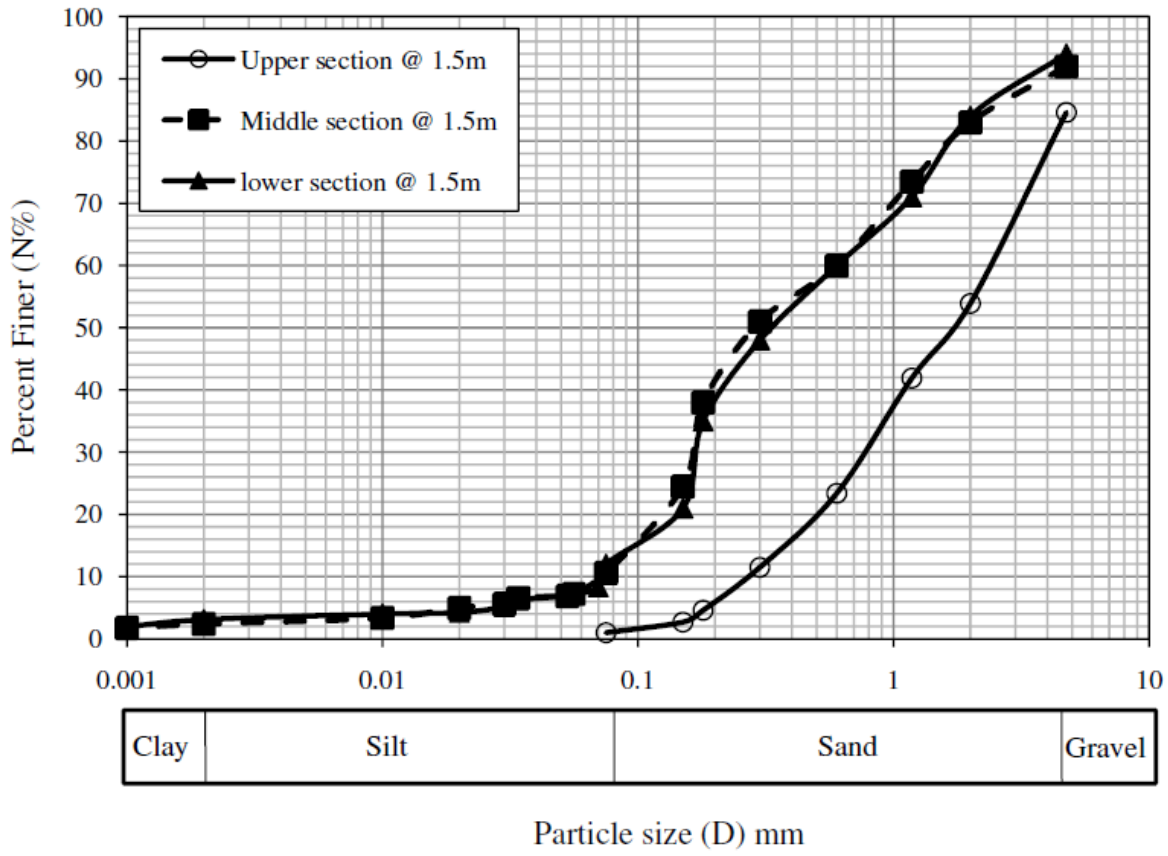

Fig.6. 4 Particle size distribution curve

However, in order to check the feasibility of helical soil nailing for creep condition, determination of Atterberg's limit is required [142]. Creep tends to induce deformation of soil – nailed structures [142]. Atterberg's limit tests are carried out on three different sections (i.e. top, middle and bottom) of landslide at 1.5 m depth as per IS: 2720, Part-5 (Fig. 6.5). The results of Atterberg's limit are summarized in Table 6.1.

Table 6. 1 Atterberg's limit test results

Parameter	Upper	Middle	Lower
Liquid limit (W_L)%	32	33	32
Plastic limit (W_p)%	19	16.6	16.3
Plasticity index (*Ip*)	13	16.4	15.7

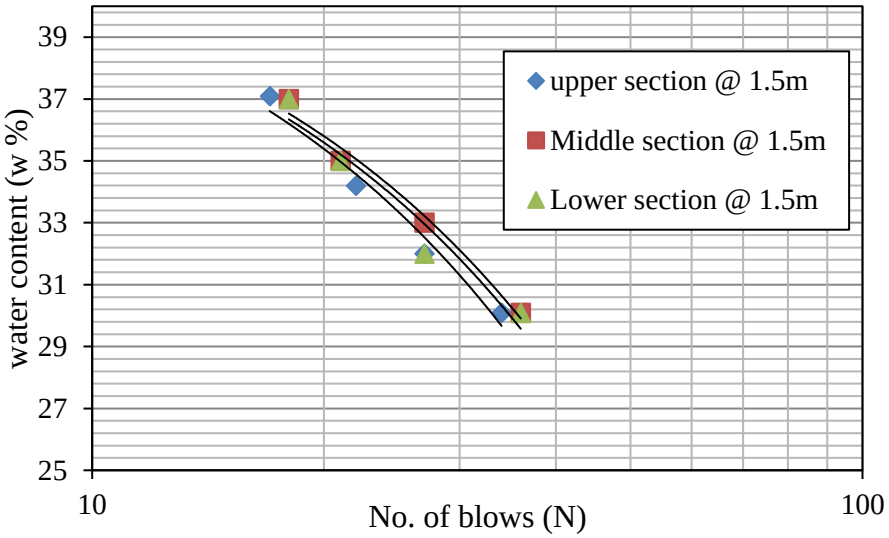

Fig.6. 5 Liquid limit of Kotropi soil

The determination of dry density is done by light compaction tests performed as per IS: 2720, Part-7 [109]. Fig.6.6 represents variation of dry density and water content for different section of soil at 1.5m depth. It is found that the soil samples attain a maximum dry density of 1.69 g/cc at an optimum moisture content of 10%.

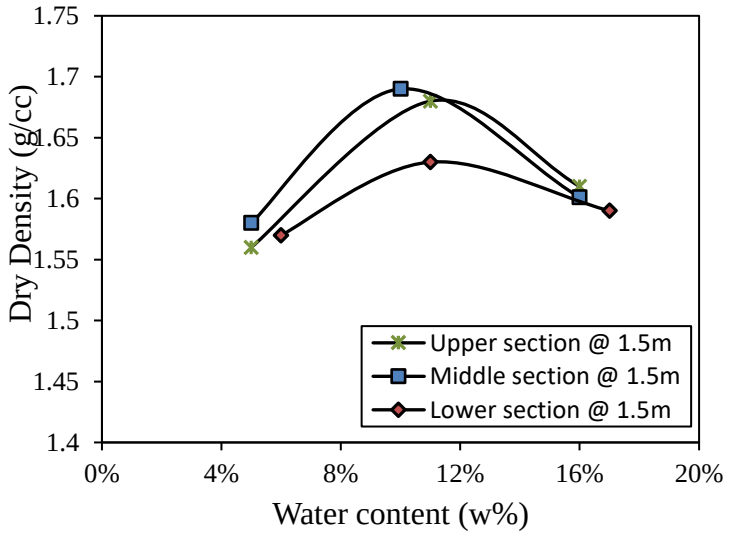

Fig.6. 6 Compaction curves for top, middle, and lower section of slope

During 'debris flow' landslide, soil bed is subjected to rapid impact loading condition which results in significant increase in pore water pressure within the failing soil mass [137-139]. The rapid impact loading is analogous to a short – term loading condition and geotechnical investigation of Kotropi landslide soil reveals the presence of poorly graded sand (SP). In such

condition both drained or un-drained and total or effective stresses are same and hence either of them can be considered to assess the shear strength parameters of the landslide. Based on this knowledge and keeping in mind the presence of small fraction of available silt in the sampled soil, Direct shear test (DST) [111] is employed for determination of shear strength parameters (c_u and ϕ_u). It has been found from the literature that DST test has been suggested for soil characterization in cases of debris type landslide.

The tests are conducted under un-drained condition at normal pressures of 50kPa, 100kPa, 200kPa as per IS: 2720, part-13 [111]. From Table 6.2, it is can be seen that the average value of c and ϕ is 26.66 kN/m^2 and 32.66°, respectively. The value of cohesion 'c = 27.16 kN/m^2 can be attributed to the fact that though Kotropi soil mainly consisted of poorly graded sand (SP), apparent cohesion has developed due to presence of moisture from the infiltration experienced by the slope.

Table 6. 2 Shear Strength parameter for all three sections of landslide by using DST test

Landslide section	***c* (kN/m²)**	***ϕ***
Top	26	32.5°
Middle	26	33°
Bottom	28	32.5°

6.2.4 CHEMICAL PROPERTIES OF KOTROPI SOIL

According to FHWA [5] and Hubble Helical nail manual [115], in – situ soil conditions are required to be checked for safety of soil nails against corrosion and creep for serviceability condition. Hence, in order to check the long-term serviceability of helical soil nails, chemical characterization through pH, chloride, and sulfate content of soil is necessary.

Helical soil nailing is not recommended for acidic soil (pH value less than 5) which contains high level of soluble iron, thereby increasing the corrosion potential. Moreover, soil basic in nature (pH value is greater than 7) is also not suggested suitable as it may contain sodium, calcium and calcium magnesium carbonates which are mildly corrosive. In the present study, pH value of Kotropi soil is found between 6.5 to 7 which signifies the feasibility of helical soil nail with respect to PH.

In addition to pH, soil containing more than 200 ppm of sulphate and 100 ppm of chloride are also categorized as aggressive soils [5] with the view that such soil promotes corrosion of steel at relatively fast rates. Hence, sulphate and chloride content of kotropi soil is also determined to check the thresholds value for non - aggressive soil which implies that the level of corrosion can be tolerated with reasonable confidence. The tests are conducted as per AASHTO290 [143] and AASHTOT291 [144].

From the test results (Table 6.3), it is observed that sulphate and chloride content in Kotropi soil are within permissible limits [5]. According to FHWA [5], if sulphates and chlorides are within permissible limits then only galvanization of soil nails is required without any specific pretreatment of soil.

Table 6. 3 Chemical properties of collected soil samples.

Properties	**Top section**	**Middle section**	**Bottom section**	**Recommendation (as per FHWA [5])**
Chloride content(mg/L)	60	40	80	<100
Sulphate content (mg/L)	66.6	133.3	190	<200
Soil pH	6.5	6.6	6.5	5-10

6.2.5 Feasibility of helical soil nails at Kotropi landslide

The Kotropi soil is classified as poorly graded sand containing silt. The percentage of chloride and sulphates is within the permissible limit and the nails are free from corrosive action of chemical like chloride and sulfates. The obtained test results are compared with favorable soil conditions for soil nailing as shown in Table 6.4, which exhibit the feasibility of helical soil nails at Kotropi landslide.

Table 6. 4 Comparison of obtained test results with reference manual for favorable condition for soil nailing

Properties	Ground condition	Soil creep potential	Soil corrosion potential
Parameter for present work	• **For top section soil** Cu = 9.3 and Cc = 0.24 • **For middle section soil** Cu = 8.33 and Cc = 0.925 • **For bottom section soil** Cu = 8.31 and Cc = 0.68 • It is clear that from C_U and C_C values that the soil can be classified as SP-SM (i.e. poorly graded sand containing silt).	• **For Top section** Liquid limit, W_L=32 Plastic limit, W_p=19 Plasticity Index =13 • **For middle section** Liquid limit, W_L= 33 Plastic limit, W_P =16.6 Plasticity Index, I_P =16.4 • **For bottom section** Liquid limit, W_L=32 Plastic limit,W_P=16.3 Plasticity Index, I_P =15.7	pH = 6.5 (all three section) **Conc. of sulfates (mg/l):** Top = 66.6(mg/L) Middle = 133.3(mg/L) Bottom = 190(mg/L) **Chloride content (mg/l):** Top = 60(mg/L) Middle = 40(mg/L) Bottom = 80(mg/L)
Remark (as per FHWA[14] and Hubble helical nail manual [26])	**(1)** Soil nailing is favorable for dense to very dense granular soil with apparent cohesion, weathered rock with adverse weakness planes, stiff to hard fine grained soils residual soil and glacial fill. **(2)** Favorable for Poorly-graded, cohesion less soil $C_u > 2$	**(1)** If liquid limit $\geq$ 50 and Plasticity index $\geq$ 20, then it is considered that creep may occur in soil, which is not favorable for soil nailing. **(2)** Soil creep is deformation of the wall resulting reduction of the shear strength of the soil. Therefore, liquid limit< 50% and plasticity index < 20 is favourable for soil nailing because soil does not meet the criteria for creep potential.	**(1)** pH should lies between 5<pH<10 **(2)** Sulfates content should be less than 200(mg/L) **(3)** Chloride content should be less than 100 (mg/L)

6.2.6 ADVANTAGES OF HELICAL SOIL NAIL OVER CONVENTIONAL SOIL NAIL

Helical soil nails are beneficial over conventional nail as they provide the opportunity of easy installation without significant soil disturbance and spoil production. The helical plate facilitates ease of penetration by application of torque. Moreover, helical soil nails do not require grouting for establishing interface bond between grout - nail and grout - surrounding soil. The required interaction is provided by the bearing from helical plates and interface friction between shaft and surrounding soil. Thus, using helical soil nails not only reduces the requirement of grout material but also makes installation process economical and quicker. These nails are passive bearing elements, which play the role on movement of soil mass and active earth pressures to mobilize soil shear strength along the nail.

6.2.7 THEORETICAL FACTOR OF SAFETY OF HELICAL SOIL – NAILED SLOPE

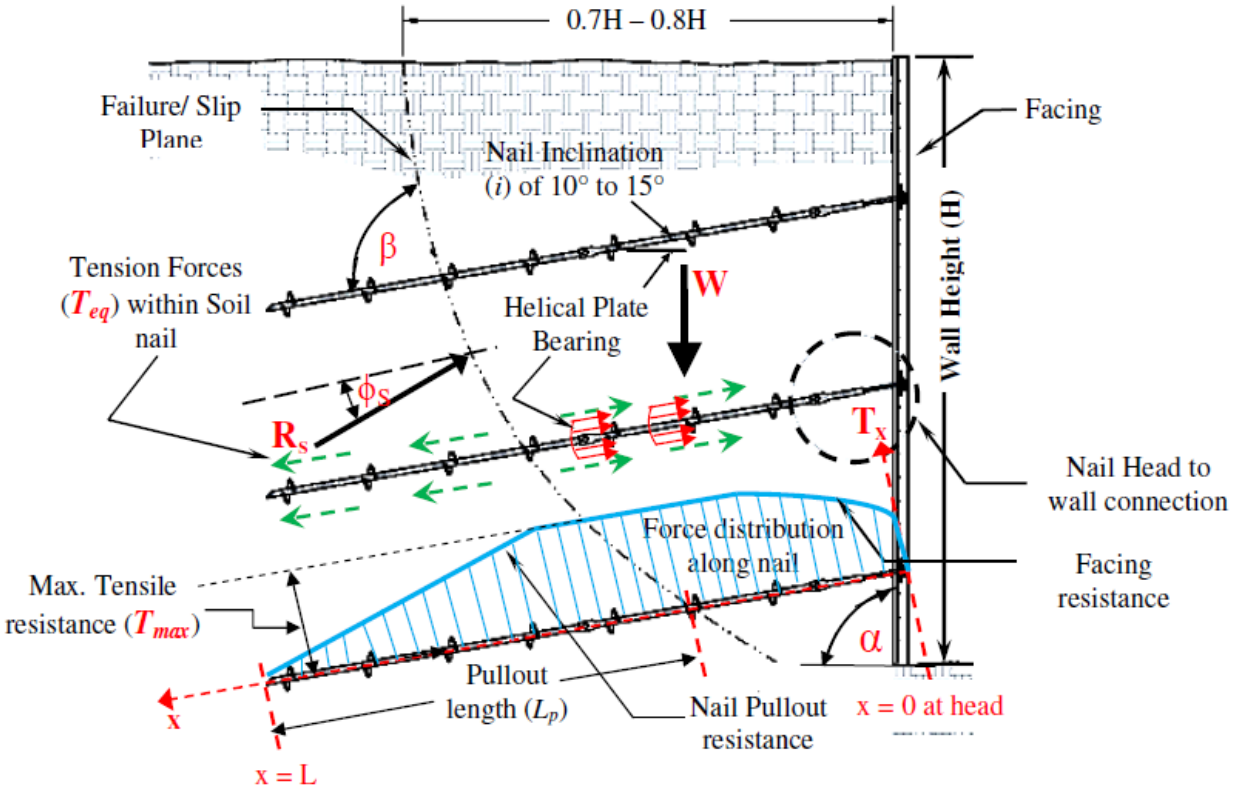

Fig.6. 7 Various forces acting in a helical soil – nailed wall [8-9, 98]

Theoretical factor of safety is used to determine soil - nailed wall stability which include geometry problem, soil properties and nail tension. The analysis is based upon limit equilibrium method (LEM), which presents basic principles for safe design of constructed or natural earth slopes. A detailed sketch of helical soil - nailed slope depicting various forces acting on slope sections, nail location, probable slip surface, and corresponding soil properties is given in

Fig.6.7. The factor of safety using the force equilibrium of different soil wedges as adopted from FHWA [5] is obtained from Equation (6.1).

$$FS = \frac{(T_{EQ}\cos(\Psi - I) + [(W + Q)\cos\Psi + T_{EQ}\sin(\Psi - I)]\tan\emptyset)}{(W + Q)\sin\Psi} \quad (6.1)$$

Where,

$$T_{eq} = \text{equivalent nail force} = \sum_{j=1}^{n}(\mathbf{T_{all}}) \quad (6.2)$$

$$W = \text{weight of the failure wedge} = 0.5\gamma H^2 \cot^{\varphi} = 439\text{kN/m} \quad (6.3)$$

$$K_a = \frac{1 - sin\,\emptyset}{1 + sin\,\emptyset} = 0.301 \quad (6.4)$$

The average maximum tensile force in the upper two thirds of the wall,

$$T_{eq} = \sum T_{all}(U) + \sum T_{all}(L) \quad (6.5)$$

$$T_{all_{(u)}} = 0.75\,K_a\gamma_s HS_v S_H = 0.75 \times 0.301 \times 16 \times 10 \times 1 \times 1 = 36.12\,kN = 36.12\text{kN} \quad (6.6)$$

Upper 2/3 of the 10m high wall contains 7 nails.

$$\sum T_{all_{(u)}} = 7 \times 36.12 = 253\,kN \quad (6.7)$$

$$\text{Maximum tensile forces in the lower one third of the wall} = 0.55\,K_a\gamma_s HS_v S_H \quad (6.8)$$

$$T_{all_{(L)}} = 0.55 \times 0.301 \times 16 \times 10 \times 1 \times 1 = 26.48\,kN \quad (6.9)$$

Lower one third of the wall contains 3 nails

$$\sum T_{all_{(L)}} = 3 \times 26.48 = 79.46\,kN \quad (6.10)$$

$$T_{eq} = 79.46 + 253 = 332.46\,kN \quad (6.11)$$

$$\Psi = 45^{\circ} + \frac{\emptyset}{2} = 61.25° \quad (6.12)$$

i = nail inclination of soil nail wall with horizontal = 15°

Therefore, stability safety factor (FOS) = 1.54 ≥ 1.35

Factor of Safety against Sliding according to Hubble [115]

$$K_a = tan^2\left(45 - \frac{\emptyset}{2}\right) \quad (6.13)$$

$$K_a = tan^2\left(45 - \frac{32.5}{2}\right) = 0.30 \tag{6.14}$$

The horizontal force from the retained soil is determined using Eqn. (6.15) as:

$$F = \frac{1}{2}K_a\gamma H^2 = \frac{1}{2}\,(0.3) \times (16) \times (10^2) = 240.71\ kN/m \tag{6.15}$$

Helical soil nails are installed at 15° angle, adopted length of nail = 0.6H

$$\text{Factor of safety against sliding is determined as follows} = \frac{\gamma HL \tan \emptyset}{F} \tag{6.16}$$

Factor of safety = 2.54; which is $\geq$ 1.5. Hence safe.

6.3 NUMERICAL MODELLING USING FINITE ELEMENT METHOD.

6.3.1 GEOMETRICAL DEFINITIONS OF THE MODEL

Simulation of the actual site condition has been carried out by Finite Element Method (FEM) using PLAXIS 2D. From the length of 1155m of landslide, repairing only height of 60m wall (i.e. 30m above and 30m below from National Highway-154) such that the road section can be constructed and made open to use. The entire height of Kotropi slope is divided into vertical segments of 10 m each. The soil is removed from top 10 m so as to improve the stability of constructed segments. However, FE analysis with top 10 m intact with the slope has also been carried out to check the variation in FOS for restored helical soil nailed Kotropi slope. With removal of top 10 m of slope, the effective slope height is 20 m above the road (NH - 154) as shown in Fig.6.8.

As per IS: code 14680:1999 [145], procedure of benching is required for achieving stability of slopes. The procedure involves dividing the long slope into smaller segments. The geometry of each segment is determined by error trial such that each helical - nailed section is stable against failure with FOS greater than 1.5. In order to achieve this some sections have been assigned vertical slope. Moreover, vertical slope also facilitates easy helical soil nail installation.

Table 6. 5 Helical nails wall geometry and other parameters

Parameters	Parameters adopted in the design
Nail length	6m
Vertical Height of the wall	30m
Vertical Height of each segment	10m

Nail Type	Helical Nail (without grout)
Nail inclination	15°
Nail Spacing(S_h x S_v)	1m x 1m
Elasticity modulus of reinforcement(E_n)	200 (GPa)
Thickness of facing	225mm
Slope angle	65° for upper section and 68° for lower section
Unit weight γ (kN/m³)	16
Diameter of helical nail	20 m

6.3.2 MATERIAL PROPERTIES

The Kotropi soil is modeled using Mohr-Coulomb (MC) model. MC-model is an elasto-plastic model, which combines Hooke's law and the Coulomb's failure criterion. The present helical soil - nailed slope design is primarily based on deformation. As reported in literature [146] for progressive slope failure model to investigate the strain - softening behavior elasto – plastic analysis is required. Moreover, large displacement reinforced slope problems are best evaluated using elasto – plastic analysis. Therefore, helical soil – nailed Kotropi slope is simulated as an elasto – plastic model to overcome the shortcomings involved in Factor of safety prediction of slopes involving large displacement through Limit Equilibrium Method (LEM).

The depth and subsoil properties employed for modeling original Kotropi slope in Plaxis 2D are adopted from the geotechnical investigation carried out on the soil samples collected from the area under study. Care is taken that soil sampling is conducted beyond the failure zone so that the characteristics of original slope are incorporated into the FE analysis. However, among the determined C_u and ϕ_u values at various depths, the minimum values are adopted in FE analysis for worst case scenario. The various soil model parameters adopted are listed in Table 6.6

Table 6. 6 Helical nail modelling parameters in Plaxis 2D

Parameters	**Values (units)**
Helical Soil Nail	
Modelling element	Plate
Modelling type	Elasto- plastic

Modulus of elasticity of helical nails (E_n)	200 GPa
Equivalent modulus of elasticity (E_{eq})	200 GPa
Equivalent axial stiffness (EA)	0.06280 x 10^{-3} kN/m
Equivalent bending stiffness (EI)	2.093 x 10^{-9} kN- m²/ m
Equivalent plate diameter (d_{eq})	20 mm
Kotropi Slope soil	
Cohesion (c)	
Upper slope section	26kN/m²
Middle slope section	26kN/m²
Lower slope section	28kN/m²
Angle of Friction(ϕ)	
Upper slope section	32.5°
Middle slope section	33°
Lower slope section	32.5°
Modulus of Elasticity of soil (E_{soil})	9.6 x 10^3 kN/m^2
Poisson ratio of soil (μ)	0.3
Dilatancy angle of soil (ψ)	0

The entire problem is modeled in plane strain condition and for long - term condition using drained analysis. The prevalent soil conditions at Kotropi landslide found after geotechnical investigation depicted poorly - graded sand containing silt (SP - SM) soil. During debris flow at Kotropi, the in – situ coarse - grained soil is assumed to have not lead to generation of pore – water pressure even under rapid impact loading condition. Since the shear strength parameters for undrained (c_u and ϕ_u) from UU test and drained (c' and ϕ') from CD test conditions for coarse - grained soil is similar, UU test shear strength parameters can be used for assessing long- term behaviour of the slopes also. Consequently, total and effective stresses are also equal for coarse – grained soils, since SP – SM soil will not support generation of any pore – water pressure during failure. Thus, c_u and ϕ_u values determined through UU test have been used

for drained analysis for investigating the long – term behavior of helical soil – nailed Kotropi slope. For modeling helical soil nails, plate elements are used [147-148]. The material parameters used for structural elements simulating soil nails are the axial stiffness *EA* and flexural rigidity *EI*. For helical soil nails, an equivalent modulus of elasticity (*Eeq*) is also determined for accounting the contribution of elastic stiffness of reinforcement bar. As per Babu and Singh [147], equivalent modulus of elasticity (*Eeq*) is calculated from Equation (6.17) as:

$$E_{eq} = E_n\left(\frac{A_n}{A}\right) + E_g\left(\frac{A_g}{A}\right) \tag{6.17}$$

where, E_n is the modulus of elasticity.

A_n is cross-sectional area of helical nail, A is gross area of nail, A_g is cross- sectional area of grouted soil nail, E_g is modulus of elasticity of grout material, E_n is the modulus of elasticity of nail. Since no grouting is done during helical soil nail installation, hence *Ag* = *Eg*= 0. Moreover, the cross - sectional area of nail (A_n) and gross area of nail will also be equal.

$$\therefore Eeq = E_n\left(\frac{A_n}{A}\right) \tag{6.18}$$

$A = 0.25\pi D_n^2$ is the total cross-sectional area of soil nail. If S_h is horizontal, S_v is vertical spacing of soil nails and D_n = diameter of helical nail, then axial and bending stiffness [9] can be obtained by Equations (6.19) and (6.20) as:

Axial stiffness (kN/m)

$$EA = \frac{E_n}{S_h}\left(\frac{\pi D^2{}_n}{4}\right) \tag{6.19}$$

'n' subscript indicate nail

Bending stiffness (kNm²/m)

$$\mathrm{EI} = \frac{\mathrm{E_n}(\pi \mathrm{d}^4{}_\mathrm{n})}{\mathrm{S_h}64} \tag{6.20}$$

Since the helical soil nails have circular shaft as adopted for the present design, plate elements are converted to circular section with equivalent plate diameter of nail using Equation **(**6.21) as:

$$d_{eq} = \sqrt{12\frac{EI}{EA}} \tag{6.21}$$

6.3.3 NUMERICAL ANALYSIS OF HELICAL SOIL – NAILED SLOPE

Once the material properties of soil and helical soil nails are defined, boundary conditions are modeled using standard fixities available in PLAXIS 2D package. The base of slope is fixed in x-y direction with the back of the slope being restricted only in the x-direction. The slope face is free to move in both x and y directions, respectively. The top of the slope is also free to move in vertical direction [147-148].

The modeling of soil-nail interface is done by using a strength reduction factor (R_{inter}) value. To assure appropriate soil nail interaction, an interface of virtual thickness factor ($\Delta = 0.1$) is used. This factor (Δ) is multiplied by the thickness of element in mesh generation procedure. The interface is allotted similar properties to that of corresponding soil section. As per Brinkgreve [149], strength reduction factor (R_{inter}) is used to model the interface friction between nail and soil during failure. The R_{inter} refers to shear strength parameters of soil with joint strength as:

$$R_{inter} = \frac{\tan\phi_{interface}}{\tan\phi_{soil}} \tag{6.22}$$

$$R_{inter} = \frac{c_{interface}}{c_{soil}} \tag{6.23}$$

As can been seen from Eqn. (6.22), R_{inter} value models the interface friction that will be mobilized between soil and nail in case of granular soil and similarly for fine – grained soil, where cohesion predominates , Eqn. (6.23) is used. The discretization of modeled slope is carried out by using medium size mesh for soil domain with fine meshing in regions around helical nails to accurately model the interaction between soil and nails. To model equilibrium conditions for Kotropi helical nailed slope, initial stress are generated using K_0- procedure through Janbu's relation. This procedure simulates the earth pressure at - rest condition.

The modeled slope is then analyzed using staged construction for the fact that soil nailing installation is carried out in stages. The 10 m top soil of slope is removed by deactivating its cluster. Since installation of helical soil nails is carried out after every 1m, excavation depth of 1m is simulated by deactivating the corresponding soil cluster in every calculation stage. A total

of 8 calculations stages are defined for the entire Kotropi slope of 30 m. The reinforced Kotropi slope is also provided with a concrete facing, which is also modeled using plate elements with properties of concrete.

Finally the helical – nailed Kotropi slope is analyzed for safety and plastic deformation. In Plaxis 2D, safety factor for slopes is determined using strength – reduction method [147-149]. The shear strength parameters of the soil are continuously reduced until slope failure. The strength of plate and anchors is not influenced by Phi/c reduction. A factor known as total multiplier $\sum Msf$ is used to define the value of soil strength parameters [149] at a given stage of analysis as given in Equation (6.24).

$$\sum Msf = \frac{\tan \emptyset_{input}}{\tan \emptyset_{reduced}} = \frac{c_{input}}{c_{reduced}} \tag{6.24}$$

The slope deformation behavior is attained from its plastic analysis. The complete FE model of reinforced Kotropi slope with helical soil nails is shown in Fig. 6.8.

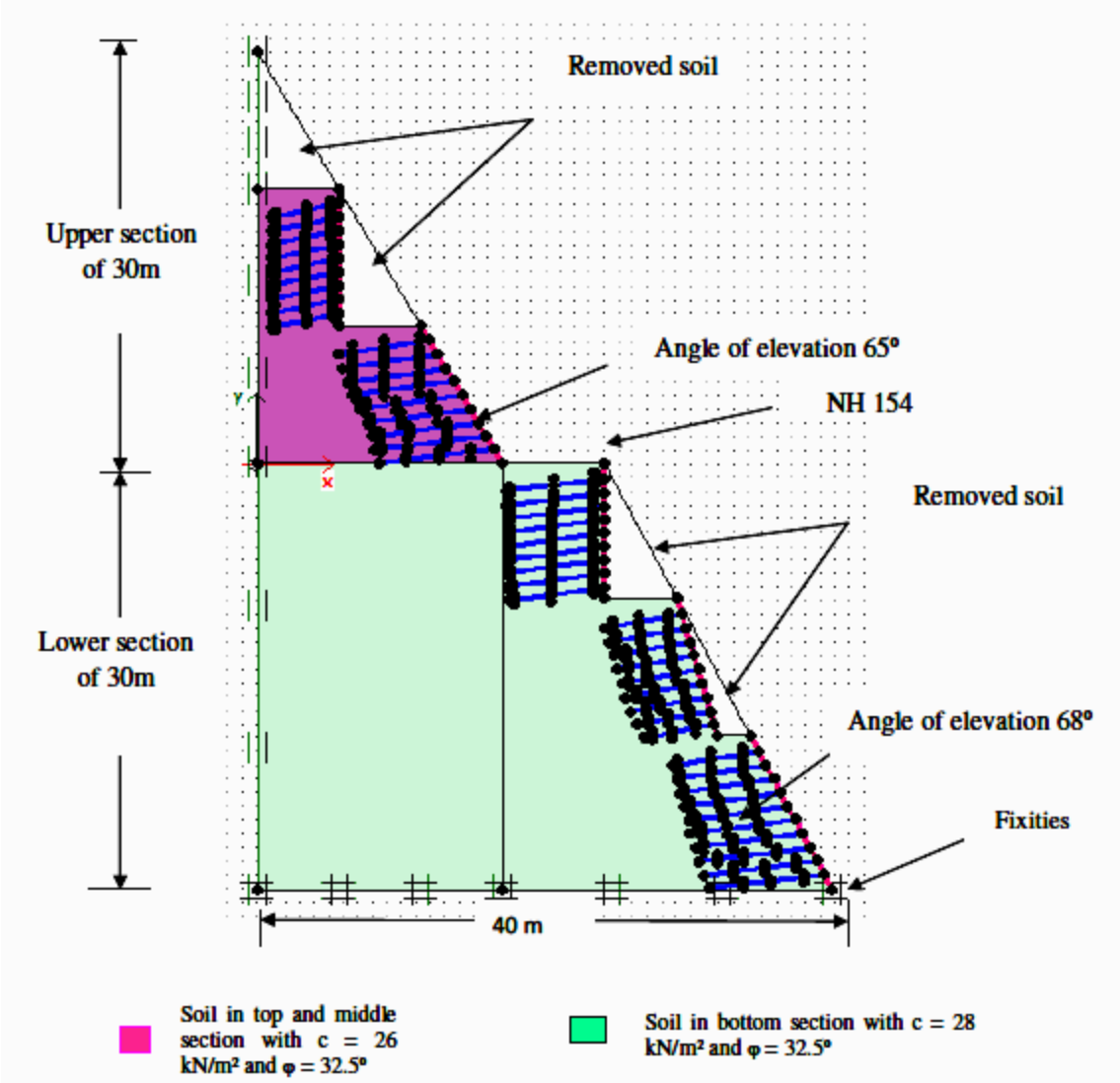

Fig.6. 8 Geometrical Configuration of Finite Element model of Kotropi slope

6.3.4 FINITE ELEMENT RESULTS FOR FACTOR OF SAFETY

The factor of safety (FOS) calculation yields a value of incremental multiplier $\sum$Msf which is found to become concurrent at failure. According to Brinkgreve et al. [149], value of $\sum$Msf represents the factor of safety, which is plotted against Cartesian displacement ($\left| U \right|$ m) of slope. However, the Cartesian displacements are not relevant for factor of safety, it only indicates whether or not a failure mechanism has developed.

The analysis of original unreinforced Kotopi slope reveals that as deformation occurs, the soil tends to detach itself from the slope. The analysis terminates with a result that 'soil body seems to collapse'. This clearly signifies the occurrence of landslide due to transition of soil into

its plastic state. A similar observation is also made while locating the plastic zones during failure. It is observed that top of the slope is found to detach itself as it cuts - off from the remaining slope under tension. The slip failure occurs along the zone where the soil has moved into plastic deformation. Hence factor of safety for unreinforced Kotropi slope cannot be determined as it fails which reflects a FOS<1. However, after installation of helical soil nails, an increase in factor of safety is obtained. The reinforced Kotropi slope is analyzed for both cases of with and without the top 10m of soil. It is observed that factor of safety of 1.57 is obtained with top 10 m of soil as shown in Fig.6.9.

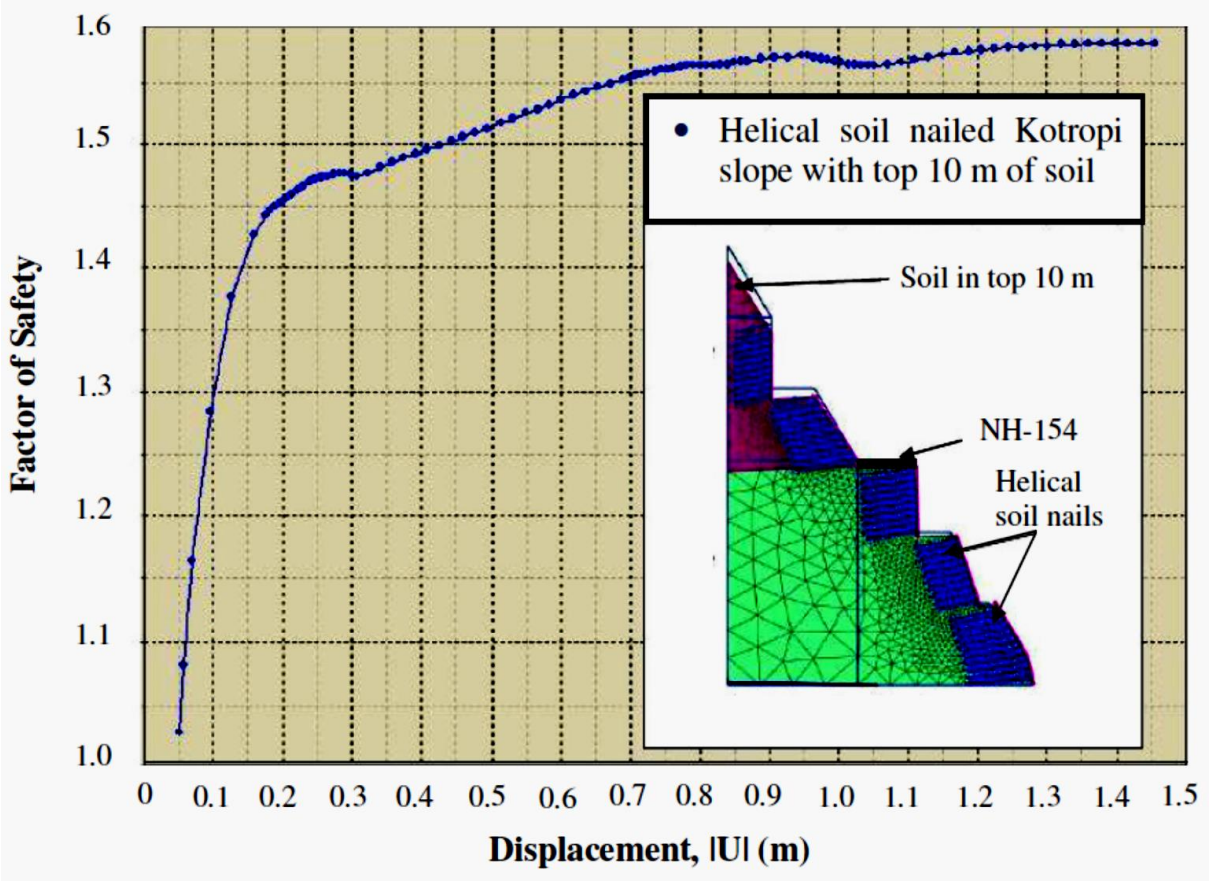

Fig.6. 9 Factor of Safety for reinforced slope with top 10m soil

However, from Fig.6.10, it can be observed that the factor of safety is found to increases to 1.67 with removal of 10 m of slope at the top. The percentage increase in factor of safety is found to be 6.4% with soil removal at top 10m of slope. Hence, during restoration of slope it is recommended that top 10 m of soil should be removed to achieve a better FOS. It is found that factor of safety obtained after nailing is greater than 1.5 which is the permissible value for global

factor of safety of soil – nailed structures [5]. Therefore, it can be stated that the designed helical soil nails can render stability to the Kotropi slope against failure.

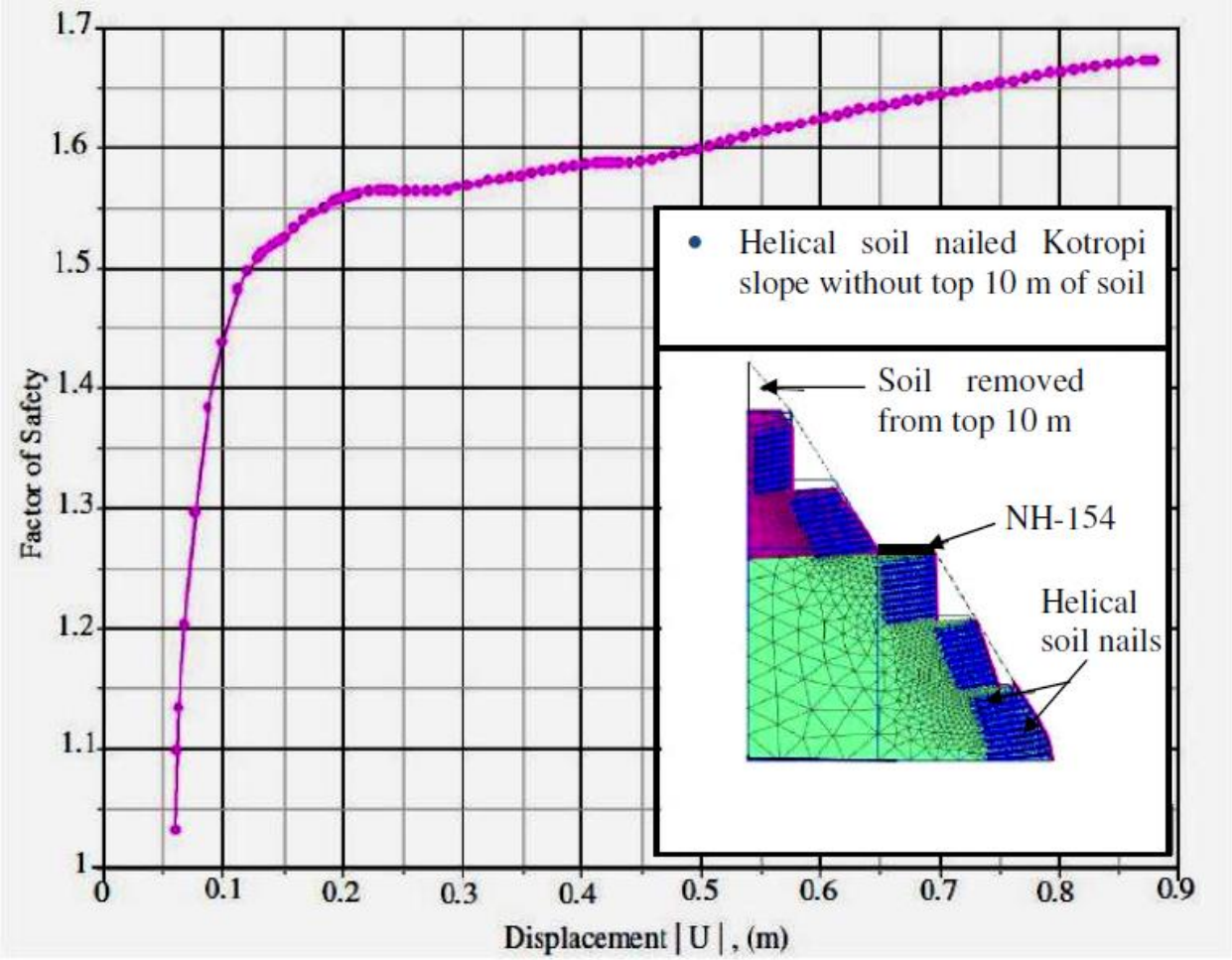

Fig.6. 10 Factor of Safety for reinforced slope without top 10m soil

6.3.5 VALIDATION OF FACTOR OF SAFETY

It is observed from both theoretical calculations (LEM) and numerical method (FEM) that factor of safety are higher than overall stability (FS=1.5). The LEM gives a FOS of 1.54 whereas FOS of 1.67 is achieved from PLAXIS 2D. The difference in LEM factor of safety and factor of safety obtained from FEM may be due to fact that LEM primarily involves equilibrium of forces acting on soil wedge whereas FEM based PLAXIS 2D considers elastic – plastic deformation of nodes. The latter being more accurate as it takes into consideration of helical soil nail – soil interaction while nails are only considered as stabilizing force in LEM.

6.3 Finite Element Results for Failure Surface

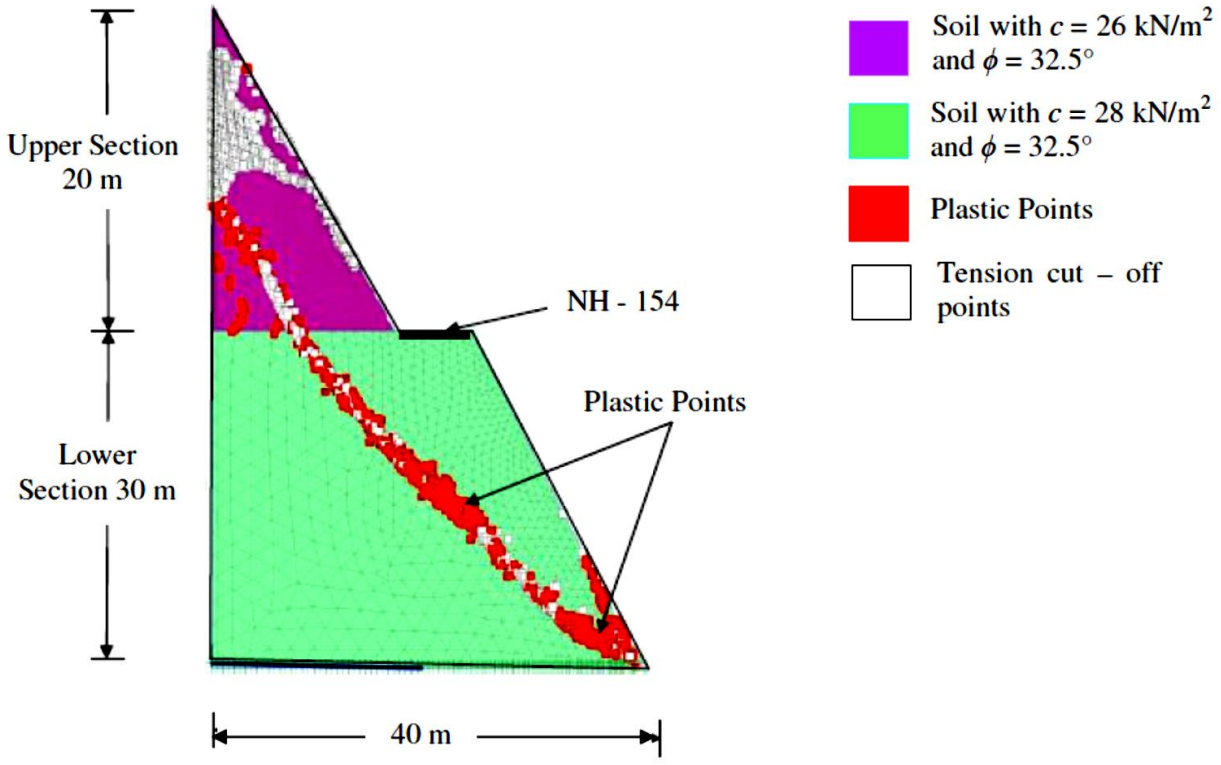

Fig.6. 11 Plastic Point of unreinforced slope

Fig.6.11 depicts critical slip failure for original unreinforced Kotropi slope corresponding to a factor of safety (FOS) which is found to be less than 1. During the finite element modeling in Plaxis 2D, the soil body is found to have collapsed reflecting to the failure of original slope during landslide. The top of Kotropi slope is found to have undergone tension cut-off depicted by white zone. The soil lying in this zone is found to have detached itself from the original slope and moved down the slope face in the form of a debris flow. The red zone reveals the regions on the slope where permanent deformation of soil has occurred. This zone is also the probable slip surface during Kotropi landslide. Fig.6.12 also reveals that tension cut- off points and plastic points lie along similar soil failure zones which further strengthen the discussion over the movement of slope.

The depth of failure surface during landslide mainly depends upon the properties of soil and its thickness. In case of slope being in homogeneous soil condition, depth of failure surface is the height of slope and the bottom soil is stiffer than top soil. In non - homogeneous soil, it depends purely on the type of soil and its thickness. In the present study the soil type is found to be homogeneous but anisotropic. From Plaxis 2D by using distance measurement feature depth

of failure surface was 3m from the top, 8m at the center and 0 m at the bottom. Similar results are also reported by GIS team after preliminary assessment of Kotropi landslide [150], where the depth of failure surface was found to be 5 – 8 m.

Though the entire slope comprises of poorly graded sand, properties are found to be different for slope top, middle, and bottom. The critical slip surface is obtained by investigation the failed region which has undergone plastic deformation during slope failure. Plaxis 2D provides the opportunity to located these plastic points as shown in Fig.6.12. It is also observed from Fig.6.12 that the slip surface has moved to a deeper zone with nailing of different slope sections as compared to unreinforced slope. With the transition of failure surface to a deeper zone, shear resistance along the failure surface increases, thereby yielding a factor of safety greater than 1.

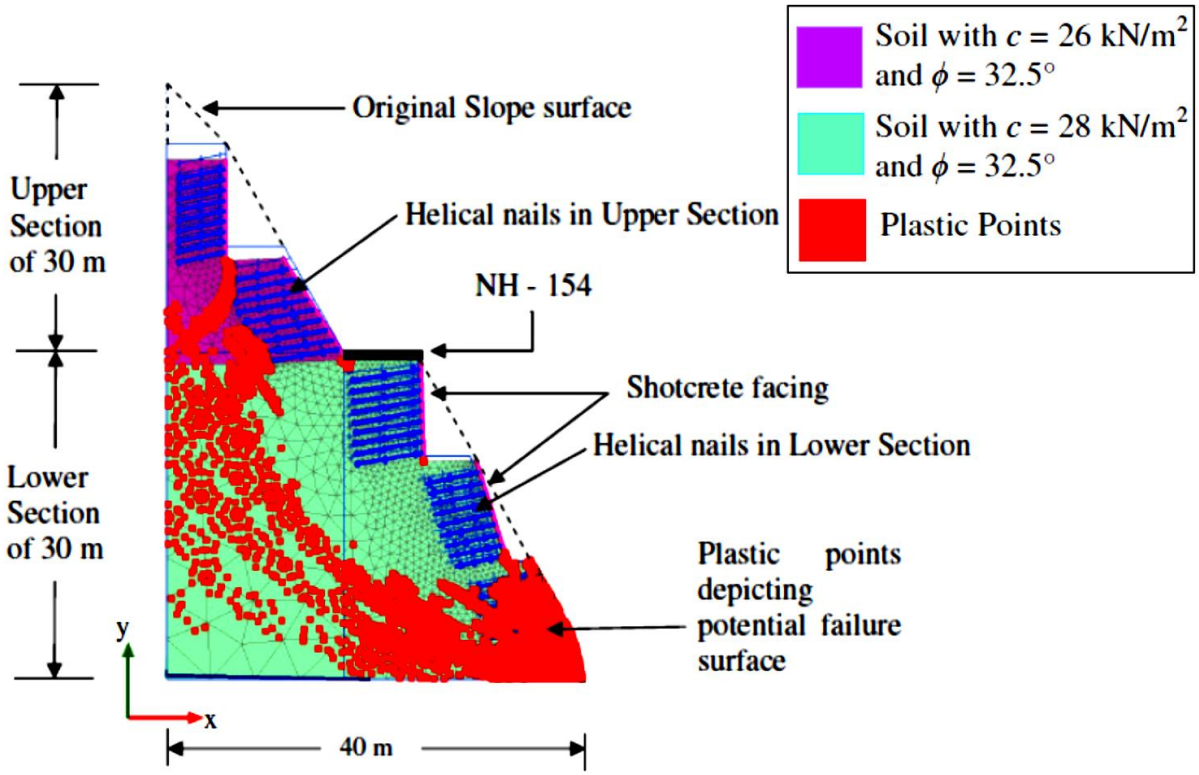

Fig.6. 12 Plastic Point of slope after nailing

The plastic zone for reinforced slope in comparison to unreinforced slope shows absence of tension cut – off zone. Moreover, no clearly defined slip surface is obtained for reinforced slope as compared to unreinforced slope where plastic points accompanied with tension cut – off points contributes towards development of landslide. Due to interaction of helical soil nails,

interface friction increases between soil and nail. As the soil deformations, the interface friction increases with respect to time due to increased soil settlement and consequently increased shearing resistance along helical nails. The strains generated around helical soil nails helps in resisting the destabilizing force resulting in stabilized slope. The helical soil nails are also found to provide additional resistance due to bearing from helical plates. The diameter of helical plates allows large volume of soil to interact with helical nail, which creates helical soil nails acting as large diameter nails [96-100].

The stability of a soil - nailed system primarily depends upon its internal stability and general global stability. The internal stability corresponds to stability contribution from nails whereas general global stability reflects stability with no contribution from nails. The nails are found to contribute towards stabilization through mobilization of its tensile, pullout and facing resistance. Among this tensile strength and facing resistance are mobilized whether or not the slip surface is intersecting with the nails. If the slip surface is found to intersect with the nails, the pullout resistance is mobilized and contributes towards internal stability [5,151]. The soil nails in sections A, B, C and D (Fig.6.13a) reflects to a similar condition where only the tensile strength of helical nails and facing resistance are found to render stability during slope deformation. Thus, it can be stated that sections A, B, C and D are stabilized by only by tensile resistance and facing resistance of the corresponding helical nails in their respective locations. Moreover, the general global stability is also found to have been achieved as depicted by a FOS>1.5 [14] for helical soil nailed Kotropi slope.

6.3.6 NAIL FORCES

The nail forces developed in the helical nails are found to be compressive and tensile in nature. As can be seen in Fig. 6.13, the top section (i.e. slope above NH- 154), all helical nails are found to be under tensile forces. This reflects to the fact that reinforcing action due to nail is significantly achieved for the upper portion of the Kotropi helical – nailed slope.

However, nail forces in lower portion of rectified slope are found to be both tensile and compressive. The last row of nails in the lower 10 m below the highway is found to depict compressive forces (Fig.6.13 (b). Any stabilization measure like soil nails, rock bolts etc are found to be effective if they are located in the zones of tensile strains generated during deformation. Thus, location and orientation of nails plays a vital role in the type of forces that will be mobilized during failure. It is also observed that the nail forces tends to undergo

transition from tension to compression if the angle between the normal to the slip surface and nail is found to change from positive to negative [33-34] .

As observed from Figs.6.13(a) and 6.13(b), most of the helical nails are found to act under tension since they do not intersect with the failure surface. This clearly reflects that nail inclination of 15° with horizontal is effective in rendering the reinforcing action to respective sections. However, it can be observed from Fig.6.13(b), bottom two rows of helical soil nails in section ‘c’ and last four rows of helical soil nails in section ‘d’ depicts helical nails under compression. The reason for this variation can be contributed to the fact that for these sections the local failure slip surface must have been terminating at toe of the section, thereby intersecting through the lower rows of helical nails. The orientation of these rows of nails must have changed the angle between slip surface normal and nail inclination from positive to negative. Thus, making the nails lie in zones of compressive strains instead of tensile strains and hence compressive forces are found to have mobilized.

The axial forces of helical soil nails are affected due to inclination. Due to increase in nail inclination, reinforcing forces decreases in nails. The force in some nails shift from tension to compression due to variation of angle between nail inclination and normal to failure surface from positive to negative which makes the nails location close to direction of compressive strain developed during failure instead of tensile strains [33-34]. Moreover, location of plastic point as given in Fig.6.12, shows higher concentration of failure points at toe of slope which can be attributed to mobilization of only tension forces in the last 10 m portion of helical soil – nailed slope.

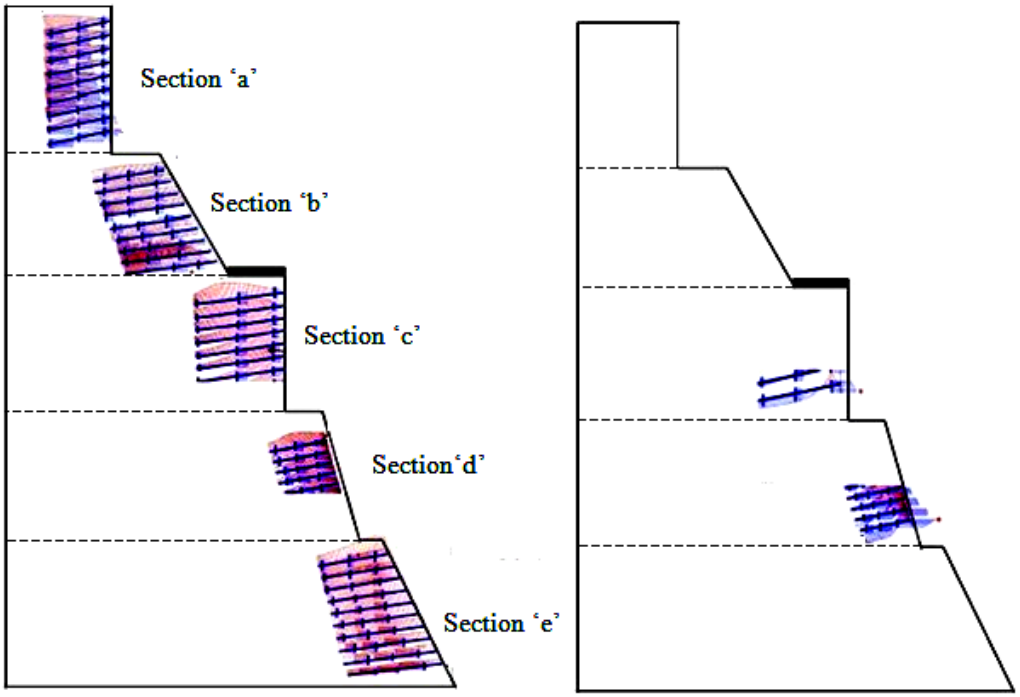

Fig.6. 13(a) Tensile forces in helical nails **(b)** Compressive forces in helical nails

The maximum force in soil nails was observed 8.16 x 10^{-6}kN/m. This force was tensile in nature and observed at the bottommost section (e) of the slope. Maximum axial forces in each section are listed in Table 6.7.

Table 6. 7 Maximum axial forces in section

Section	Maximum Nail force	Nature of force
a	0.14 x 10^{-6}kN/m	Tension
b	0.40 x 10^{-6}kN/m	Tension
c	0.11 x 10^{-6}kN/m	Tension
d	0.16 x 10^{-6}kN/m	Tension
e	**8.16 x 10^{-6}kN/m**	Tension

6.3.7 Assessment of Lateral Displacement

In Kotropi slope, decrease in shear strength of soil is due to heavy rainfall, which led to displacement in slope [114-115]. The lateral displacement can be predicted well for unreinforced slope from Fig.6.14. It is clear that there is large displacement occurring over the unreinforced

slope due to decreases in shear strength of soil. The unreinforced slope is found to have undergone a total deformation of 13 cm predominantly at the crest of the slope.

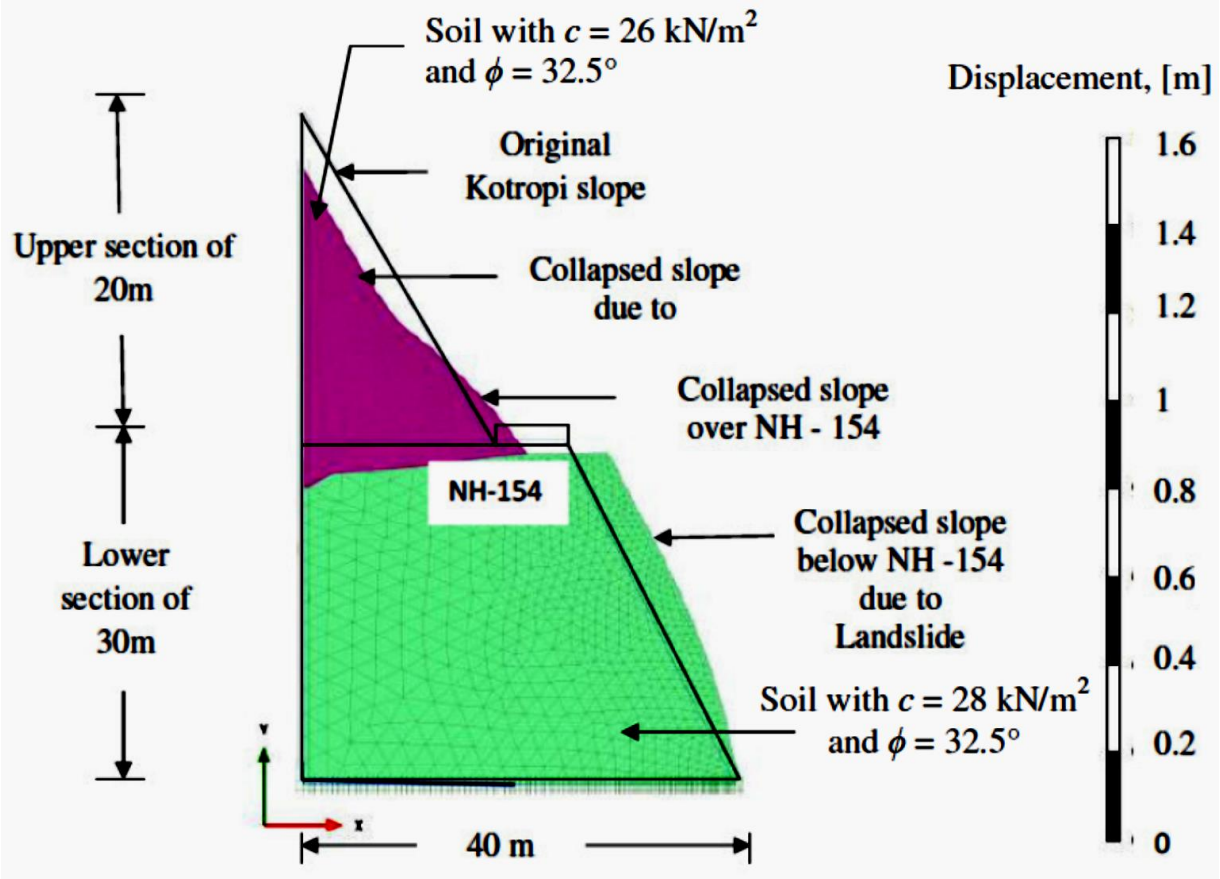

Fig.6. 14 Slope deformation of unreinforced Kotropi slope

According to FHWA [5], maximum long-term horizontal displacements at the top of the wall can be estimated for poorly graded sand by Eqn. (6.25)

$$\Delta h = \Delta V = \left(\frac{\Delta h}{H}\right) X\, H \tag{6.25}$$

And also,

Maximum lateral displacement = 0.2% of vertical height [14]

Here total height of slope = 60m

$$\frac{\Delta h}{H} = \frac{1}{500}\ , for\ c - \Phi\ soil \tag{6.26}$$

Thus, permissible slope displacement for helical soil-nailed slope as obtained from Equation (6.25) and (6.26) is found to be 0.12 m. Moreover, FE analysis of rectified helical soil nailed Kotropi slope shown in Fig.6.15 yields maximum displacement of 0.06 m. Thus, stabilization of Kotropi slope using helical nails is found satisfactory for serviceability condition also i.e. displacement of helical soil nailed Kotropi slope < 0.12 m (permissible limit). Hence, it can be stated that suggested helical soil nail design for restoring slope stability is satisfactory.

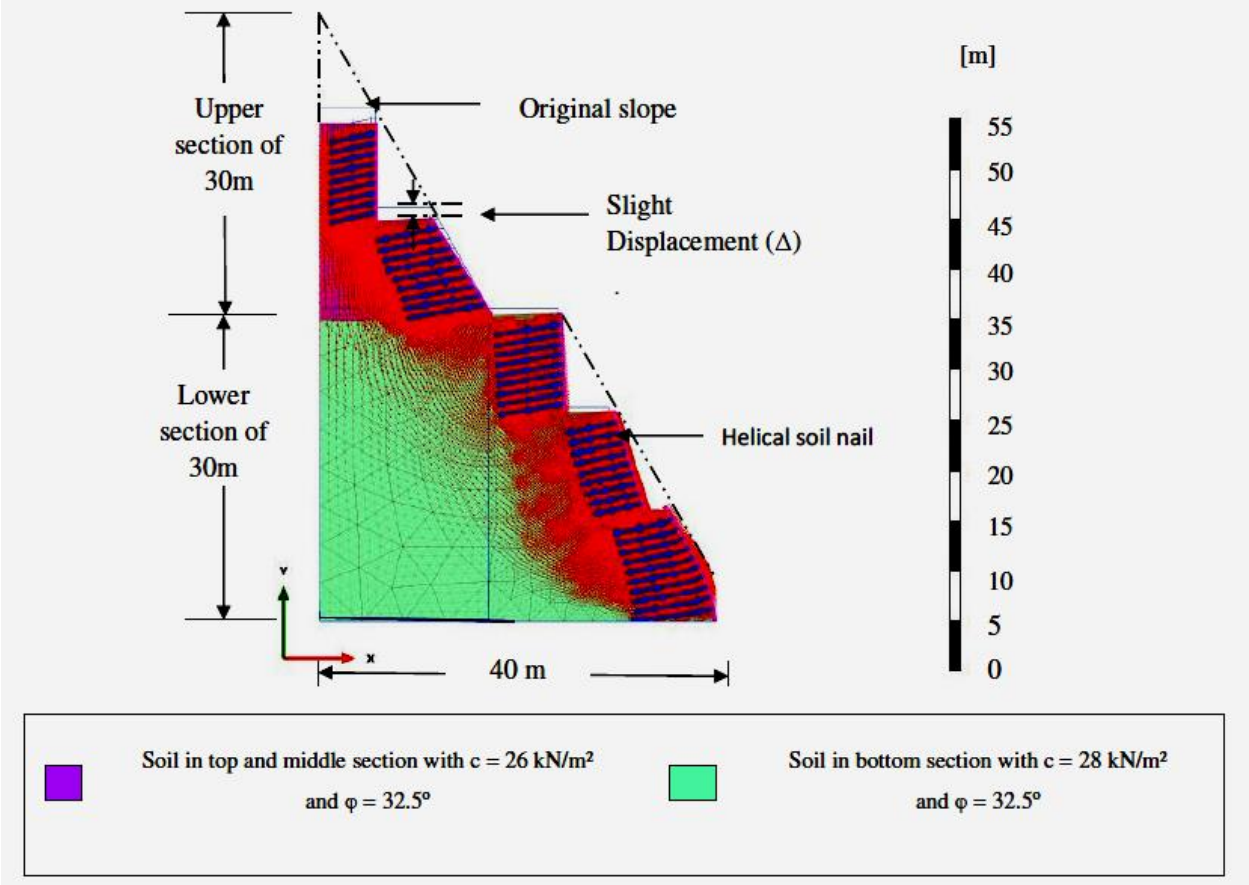

Fig.6. 15 Deformation of helical – nailed Kotropi slope

6.4 Summary

The present chapter includes the geotechnical and chemical soil investigation of Kotropi landslide. In addition to evaluation of factor of safety from LEM, the FEM analysis of stabilized Kotropi landslide slope is also carried out using helical soil nails. The factor of safety, deformation, and nail forces of unreinforced and reinforced Kotropi slope has been presented and compared. Based on the results obtained, it can be raveled that Kotropi slope without soil nail is

found to collapse reflecting to a FOS (factor of safety) <1. The factor of safety is found to increase to 1.67 by using helical soil nails for restoring the Kotropi slope which is greater than global safety factor 1.5. It can be concluded that slope stabilization can be achieved from the given helical soil nail design. The deformation of original Kotropi slope is found to reduce from 0.13 m to 0.06m for unreinforced and reinforced slopes, respectively. Also, the numerical analysis of helical soil nailed Kotropi slope depicted that slope displacements are within permissible limits which is conclusive for assessing the feasibility of helical soil nail performance under serviceability condition. From the nail force distribution, it can be concluded that nail forces are found to develop tensile forces which signifies efficient reinforcing action of installed helical nails.

CHAPTER-7

Conclusion and Future Scope

CHAPTER 7
CONCLUSIONS AND FUTURE SCOPE

7.1 GENERAL

The chapter enlists the conclusions derived from the results of model testing and theoretical modeling of soil–nail with different types of helical soil nails specimens. It also incorporates some major conclusions based on comparison of results between model testing and theoretical modeling.

7.2 CONCLUSIONS

The present study evaluates the experimental results on single and multi helical soilnails with smooth solid, smooth hollow or open-ended pipe and rough solid shafts under variation of parameters such as installation torque, pullout behavior, pitch variation, embedment ratios, soil-nail interaction, in-situ stresses, axial strain variation and ground settlement. The study also investigates the installation and pullout behavior of single helical soil nail at different inclinations and surcharge pressures. The optimum inclination determined for single nail is used for group installation and pullout test. Group of 9 helical soil nails with two different arrangements of staggered and uniform spacing are investigated for installation torque, installation disturbance factor, pullout force, earth pressures and strains developed. Further, theoretical models were proposed for the estimation of installation torque and pullout load-displacement of single and group of the helical soil nail. The theoretical models for installation torque and pullout force were based on the various resisting moment and force acts during the operation. The theoretical model was used to predict the installation torque at different positions of the helical nail in terms of torsional resistance. Another empirical model was presented to predict the pure-elastic and elastic-plastic stage for helical soil nails under different pressure and different shaft diameter. Based on the outcomes achieved, following conclusions are drawn:

1. The installation torque to pullout capacity of helical soil nails can also be correlated using an empirical factor K_t as for the case of helical anchors and helical piles. However, K_t for helical soil nails with solid shaft range from 19 m^{-1} to 61 m^{-1} and 23 m^{-1} to 58 m^{-1} for helical soil nails with hollow shafts. K_t decreases with increase in embedded helical nail area and

exponential of nail shaft diameter ($d^{0.54}$). During helical nail installation, strain softening phenomenon is observed for both cases of hollow and solid shafts.

2. The installation torque increases with shaft and helix diameter, number of helices, overburden pressure from 5 kPa to 12.5 kPa and falls off gradually till 50 kPa. The solid shaft nails depict higher installation torque in comparison to hollow shaft nails for all D_h/d and D_h/P ratio. Thus, it can be concluded that helical soil nails having solid shaft require greater installation torque for all variations of shaft diameter, helix diameter, pitch and number of helices.
3. The variation of maximum pullout under increasing overburden pressure follows Mohr-Coulomb failure criteria. Similar results were also obtained from direct shear test for different interfaces. The failure envelops for soil–rough surface solid shaft interface depicts maximum interface friction angle in comparison to soil–smooth hollow shaft interface and soil–smooth solid shafts interface. Higher interaction factor (IF) values in the range of 2–38 are obtained for solid shafts as compared to hollow shafts with IF values in range of 0.3 to 11.3. The IF values increases as the number of helices increases along the nail shaft for both solid and hollow nails. In addition, the nail with rough shaft contributes significantly to IF and pullout capacity.
4. Significant increment in the pullout capacity is obtained with increase in number of helical plates from single to multi-helix. The maximum pullout capacity is attained for a pitch of 30 mm and is thus recommended for model testing purposes. However, addition of a third helix brings only a small increment in pullout capacity under increasing overburden pressure for both hollow and solid shafts. The normalized pullout capacity is found to decrease with increasing Z/D_h under same overburden pressure. However, beyond Z/D_h = 10.4, pullout efficiency of both multi–helix and helical nail without helix is same.
5. The variation of in-situ stresses developed during installation and pullout of multi–helix nail are lower than helical nail without helix or conventional soil nails. Thus, it can be concluded that helical soilnails exhibit significantly lesser disturbances during installation and pullout in comparison to conventional soil nails.
6. The axial strain for smaller diameter shafts (both solid and hollow shafts) is more than for equivalent large diameter shafts. Helical nail with more number of helical plates depict lower axial strains, higher pullout and consequently higher installation torque as compared to helical

nails with less helical plates. The settlement of ground surface reduces as number of helices is increases.

7. The pullout capacity of hollow shaft helical nail increases with an increase in plug length which correspondingly increases with an increase in nail diameter. However, plug length only contributes to 11.5% of total internal skin friction with remaining achieved from the helical bearing. The soil plug length is independent of the number of the helix.
8. The test results concluded that pullout capacity and installation torque helical soil nail significantly influenced with angle of inclination. The pullout capacity of helical soil nail significantly increases from 10° to 20° with horizontal and then decreases, Thus, angle of inclination of 20° is considered as most favorable angle. Moreover, the average installation disturbance factor for single helical soil nail at different inclination between 0˚ to 30˚ varies from 0.86 to 0.71. Hence the average installation disturbance factor for single helical soil nail is considered as 0.76. With increasing surcharge pressures, installation torque and pullout capacity of single helical soil nail increases, but the rate of increment reduces considerably.
9. For group of helical soil nails, staggered configuration performs significantly better as compared to uniform configuration. The low IDF value and installation torque values suggest improved installation of helical nails over uniform arrangement. Staggered arrangement also renders higher pullout capacity, low torsional strains, and low axial strains. Moreover, negative earth pressures indicative of soil expansion is observed for uniform configuration depicting its low efficiency during both installation and pullout.
10. The theoretical model was used to predict the installation torque at different positions of the helical nail in terms of torsional resistance. Another empirical model was presented to predict the pure-elastic and elastic-plastic stage for helical soil nails under different pressure and different shaft diameter. The installation torque of helical soil nail depends upon nail geometry, soil parameters, embedded length and surcharge height of soil mass, thus the theoretical model proposed based on these parameters, predict the results are in very good agreement with laboratory result and with reported in the literature as well.
11. The Pullout of helical nail possesses mainly two phases of resistance comprises of pure elastic-phase and elastic-plastic phase, the maximum pullout load of different helical soil increases nail diameter. The proposed empirical models accurately reproduced the installation torque, pullout load of single and group of the helical soil nail. The model for

pullout force replicates the identical value of peak and residual shear strength of interface from experimental results for the variable condition of soil and nail. The installation torque and resistance force offers by helical nail increase with depth or with an increase in bed height. Two different equations were developed based on theoretical and experimental results to calculate the capacity-to-torque Ratio (K_t) for the diameter of nails. To predict the more precise result for K_t, combine the result from theoretical and experimental data was plotted to develop a more precise correlation to estimate the appropriate capacity-to-torque Ratio (K_t) for different diameters of the helical nail with $R^2 = 0.92$.

The theoretical and experimental results confirm that the empirical models are able to estimate the peak resistant value of different helical nails. The reported theories may be doubtless can be used as a reference by field engineers. In addition, the present study allocates the reader to understand the effects of several key parameters of the pullout-load response of a helical soil nail.

7.3 SCOPE FOR FUTURE WORK

The present research work has been limited to static conditions of soil–nailed slopes which leave a research gap for dynamic analysis of soil slopes using smooth, hollow, rough types of shaft. Moreover, soil nailing has been carried out in uniform soil conditions of drained cohesionless soil has been used for all model testing and theoretical modeling which can be further looked into by using a different type of soil such as cohesive soil or a c – ϕ soil. Further validation of this research work can be done by carrying out large scale field studies using similar types of soil nails as helical soil nail with smooth, hollow, rough types of shaft.

LIST OF PUBLICATIONS

JOURNALS

1. Sharma P, Rawat S, Gupta AK (2020a) Laboratory investigation of Pullout Behavior of Hollow and Solid shaft Helical Nail in Frictional Soil. Acta Geotechnica. https://doi.org/10.1007/s11440-020-01069-6

(IF 5.8, SCI and Scopus indexed)

2. Sharma P, Rawat S, Gupta AK (2020b) Horizontal Pullout Behavior of Novel Open-Ended Pipe Helical Soil Nail in Frictional Soil. International Journal of Civil Engineering. https://doi.org/10.1007/s40999-020-00535-2

(IF 1.5, SCI and Scopus indexed)

3. Sharma P, Rawat S, Gupta AK (2018) Study and Remedy of Kotropi Landslide in Himachal Pradesh, India. Indian Geotechnical Journal DOI 10.1007/s40098-018-0343-1

(**Scopus indexed)**

4. Sharma P, Rawat S, Gupta AK (2021a) Laboratory Investigation of Pullout Behavior of OpenEnded Pipe Helical Soil Nail in Frictional Soil. Geotechnical and Geological Engineering *DOI: 10.1007/s10706-020-01666-y*

(**Scopus indexed**)

5. Sharma P, Rawat S, Gupta AK (2021b) Force–Displacement Characteristics of Helical Soil Nail under Monotonic Pullout Loading: Experimental and Theoretical Study. Indian Geotechnical Journal DOI: 10.1007/s40098-021-00515-w

(**Scopus indexed)**

6. Sharma P, Rawat S, Gupta AK (2021c) Experimental investigation of pullout behaviour of open-ended pipe helical soil nail in frictional soil. https://doi.org/10.1080/17486025.2021.1903088

(**Scopus indexed, ESCI)**

7. Sharma P, Rawat S, Gupta AK (2021d) Laboratory Investigation of Hollow and Solid Shaft Helical Soil Nail by Displacement Controlled Pullout Testing. Geotech Geol Eng https://doi.org/10.1007/s10706-021-01832-w

(**Scopus indexed**)

8. Sharma P, Rawat S, Gupta AK (2021) Experimental investigation of helical soilnail group behavior under torque installation and monotonic pullout loading. Arabian Journal of Geoscience

(SCI indexed, Scopus, IF 1.54)

CONFERENCES

1. Sharma P, Rawat S, Gupta AK (2018) Comparative study between factor of safety of a slope using conventional soil nail and helical soil nail. 3rd Himachal PradeshScience Congress 2018, held at IIT Mandi on 22nd -23rd October 2018
2. Sharma P, Rawat S, Gupta AK (2018) Remedy Measure for the Kotropi Landslide (Mandi, H.P.) India: A Case Study. ***International on Innovative trends in engineering***, (MECIT-2018). Journal of Civil Engineering and Environmental Technology p-ISSN: 2349-8404; e-ISSN: 2349-879X; Vol. 5(3) pp. 125-128

COMMUNICATED PAPER ENTITLED

1. Experimental and Theoretical approach on installation torque with pullout load-displacement of Helical Soil Nail. **(Under review)**

REFERENCES

REFERENCES

[1] French National Project CLOUTERRE, "*Recommendations CLOUTERRE: Soil nailing recommendations for designing, calculating, constructing, and inspecting earth support systems using soil nailing*", Rep. No. FHwA-SA-93-026, Federal Highway Administration, Washington, D.C. English translation. 1991

[2] Rabejac S, Toudic P, "*Construction d'un mur de soutènement entre Versailles-Chantiers et Versailles-Matelots*", (Trans: Construction of a retaining wall between Versailles-Chantiers and Versailles-Matelots), Revue générale des chemins de fer, Vol. 93, Paris, France, 232-237,1974

[3] Gassler G, Gudehus G, "*Soil Nailing-Some Aspects of a New Technique*", in Proceedings of the 10th International Conference on Soil Mechanics and Foundation Engineering, Vol. 3., Session 12, Stockholm, Sweden, 665-670, 1981

[4] Jewell RA, Wroth CP, "*Direct shear tests on reinforced sand*", Géotechnique, 37(1), 53–68, (1987).doi:10.1680/geot.1987.37.1.53

[5] FHWA, "*Geotechnical engineering circular No. 7: Soil nail walls – reference manual*", FHWA, Washington, D.C. Rep. No. FHWA-NHI-14-007, 2015.

[6] Aziz E, Stephens T, "*Cost and schedule savings from directly-driven soil nail and innovative fascia systems*", GeoCongress 2013:1704–1718.https://doi.org/10.1061/9780784412787.171

[7] Lindsay FM, Mickovski SB, Smith MJ, "*Testing of self drilled hollow bar soil nails. In: Geotechnical engineering for infrastructure and development*", 2015, pp 2969–2974

[8] FSI, "*Technical manual: helical piles and anchors, hydraulically driven push piers, polyurethane injection& supplemental support systems*", 2nd ed. Foundation Support Works, Omaha. 2014, pp. 33–39

[9] Perko HA, "*Helical Piles: A Practical Guide to Design and Installation*", 2009, John Wiley and Sons, Hoboken

[10] Junaideen SM, Tham LG, Law KT, Lee CF, Yue ZQ, "*Laboratory study of soil–nail interaction in loose, completely decomposed granite*", Canadian Geotechnical Journal 2004 vol.41:Issue.2, 274-286, https://doi.org/10.1139/t03-094

[11] Su LJ, Chan TCF, Shiu YK, Cheung T, Yin JH, "*Influence of degree of saturation on soil nail pullout resistance in compacted completely decomposed granite fill"*, Can. Geotech. J., 2007, 44(11), 1314–1328. https://doi.org/10.1139/T07-056

[12] Su LJ, Chan TCF, Yin JH, Shiu HYK, Chiu SL, *"Influence of overburden pressure on soil nails pull-out resistance in a compacted fill",* J. Geotech. Geoenviron. Eng., 134(9), 2008, 1339–1347. https://doi.org/10.1061/(ASCE)1090-0241(2008)134:9(1339)

[13] Zhou W, *"Experimental and theoretical study on pullout resistance of grouted soil nails",* 2008 (Doctoral dissertation, The Hong Kong Polytechnic University).

[14] Tokhi H, *"A study of new screw soil nail",* Dissertation, 2016, RMIT University, Melbourne.

[15] Sharma M, Samanta M, Sarkar, *"A laboratory study on pullout capacity of helical soil nail in cohesionless soil",* Canadian Geotechnical Journal, 2017, 54(10):1482-1495 dx.doi.org/10.1139/cgj-2016-0243

[16] Rawat S, *"Testing and Modeling of soil–nailed slopes",* Dissertation, Jaypee University of Information Technology, Waknaghat, Solan, Himachal Pradesh, India, 2017

[17] Rabcewicz L, *"The new Austrian tunnelling method",* Part I, Water Power 16 (11):453–457 17. 1964a

[18] Rabcewicz L, *"The new Austrian tunnelling method",* Part II, Water Power 16 (12):511–515 1964b

[19] Lazarte, C.A., Elias, V., Espinoza, R.D., and Sabatini, P.J, *"Soil Nail Walls, Geotechnical Engineering Circular No. 7",* Report No. FHWA-IF-03-017, Federal Highway Administration, Washington, DC. (2003)

[20] Juran I. and Elias V, *"Soil nailed retaining structures: Analysis of case histories",* Soil Improvements: A Ten Year Update, ASCE Geotechnical Special Publication No.12, p232-244. (1987)

[21] Juran I, George B, Khalid F, Elias V, *"Kinematical limit analysis approach for the design of nailed soil retaining structures",* In: Proceedings of the geotechnical symposium on theory and practice of earth reinforcement, Japan. AA Balkema, Rotterdam, pp 301–306. (1988)

[22] Juran, I., G. Baudrand, K. Farrag and V. Elias, *"Design of soil nailed retaining structures",* Geotechnical Special Publication. (1990)

[23] Stocker MF, Korber GW, Gassler G, et al, *"Soil nailing"*, C.R. Col. Int. Reinforced des. Sols. Paris, pp 469–474. (1979)

[24] Gassler G, Gudehus G, *"Soil nailing-some aspects of new technique",* In: Proceedings of tenth ICSMFE. Balk-ema, Stockholm, pp 943–962. (1981)

[25] Stocker MN, Riedinger G, *"The bearing behaviour of nailed retaining structures"*, In: Lambe PC, Hansen LA (eds) Proceedings of design and performance of earth retaining structures, Geotechnical Special Publication, vol 25. ASCE, New York, pp 612–628. (1990)

[26] IRC: SP: 102-2014, *"Guidelines Design And Construction Of Reinforced Soil Walls",* Indian Roads Congress (2014)

[27] Potyondy, J.G, "*Skin friction between various soils and construction materials*", Géotechnique, 11(4): 339–353. (1961) doi:10.1680/geot.1961.11.4.339

[28] L. Borana; Jian-Hua Yin; D. N. Singh; S. K. Shukla; and F. Tong, "*Direct Shear Testing Study of the Interface Behavior between Steel Plate and Compacted Completely Decomposed Granite under Different Vertical Stresses and Suctions*", . J. Eng. Mech., 2018, 144(1): 04017148-1-13 DOI: 10.1061/(ASCE)EM.1943-7889.0001352.

[29] Wang, Z., and Richwien, W, "*A study of soil-reinforcement interfaces friction*", Journal of Geotechnical and Geoenvironmental Engineering,(2002) 128(1): 92–94. doi:10.1061/(ASCE)1090-0241(2002)128:1(92) (2002)

[30] S.H. Liu, D. Sun, H. Matsuoka, "*On the interface friction in direct shear test*", Computers and Geotechnics 32 (2005) 317–325. doi:10.1016/j.compgeo.2005.05.002

[31] Jewell RA, Pedley MJ, "*Soil nailing design: the role of bending stiffness*", Ground Eng 23(2) (1990).

[32] Jewell RA, Pedley MJ, "*Analysis For Soil Reinforcement with Bending Stiffness*", J. Geotech. Engrg. 1992, 118(10): 1505-1528

[33] Shiu Y, Chang G, "*Effects of inclination, length pattern and bending stiffness of soil nails on behavior of nailed structures*", GEO Report No. 197. Geotechnical Engineering Office, Hong Kong (2006)

[34] GEO (Geotechnical Engineering Office), "*Geoguide 7: Guide to Soil Nail Design and Construction",* The Government of the Hong Kong Special Administrative Region, Hong Kong. (2008)

[35] Ranjan G, Rao A, "*Basic and Applied Soil Mechanics*", New Age International, (2007)

[36] Schlosser F, Guilloux A, *"Le frottement dens les sols*", Revue Francaise de Geotechnique 16:65–77, (1981)

[37] Heymann G, Rohde AW, Schwartz K et al*, "Soil nail pullout resistance in residual soils",* In: Proceedings of the international symposium on earth reinforcement practice, Kyushu, Japan, vol 1, pp 487–492 (1992)

[38] Mecsi J, *"Some practical and theoretical aspects of grouted soil anchors*", In Ground anchorages and anchored structures: Proceedings of the international conference organized by the Institution of Civil Engineers and held in London, UK, on 20–21 March 1997, Thomas Telford Publishing, p 119–130 (1997)

[39] Sharma M, Samanta M, Punetha P, "*Analysis of helical soil nailed walls under static and seismic conditions*",Canadian Geotechnical Journal 57(6):04019002-1–04019002-16. https://doi.org/10.1139/cgj-2019-0240. (2019b)

[40] Luo SQ, Tan SA, Yong KY, "*Pull-out resistance mechanism of a soil nail reinforcement in dilative soils"*, Soils Found 40(1):47–56, (2000)

[41] Luo SQ, TANT S, Cheang W et al, "*Elasto-plastic analysis of pull-out resistance of soil*", Ground Improvement 6(4):153–161,(2002)

[42] Pedley MJ, "*The performance of soil reinforcement in bending and shear*", Ph.D. Thesis, University of Oxford, 1990.

[43] Zhang, C.-C., Q. Xu, H.-H. Zhu, B. Shi, and J.-H. Yin, "*Evaluations of load-deformation behavior of soil nail using hyperbolic pullout model*", Geomech. Eng. 6 (3): 277–292. https://doi.org/10.12989/gae .2014.6.3.277. (2014)

[44] Kondner, R.L., "*Hyperbolic stress-strain response: Cohesive soils*", J. Soil Mech. Found. Div., 89(1), 115-144. (1963)

[45] Gomez, J.E., Filz, G.M. and Ebeling, R.M, "*Extended hyperbolic model for sand-to-concrete interfaces*", J. Geotech. Geoenviron. Eng., ASCE, 129(11), 993-1000. (2003)

[46] Chu, L.M. and Yin, J.H, "*A laboratory device to test the pull-out behavior of soil nails*", Geotech. Test. J., ASTM, 28(5), 499-513. (2005a)

[47] Chu, L.M. and Yin, J.H., "*Comparison of interface shear strength of soil nails measured by both direct shear box tests and pullout tests*", J. Geotech. Geoenviron. Eng., ASCE, 131(9), 1097-1107. (2005b)

[48] Sharma M, Samanta M, Punetha P, "*Experimental investigation and modeling of pullout response of soil nails in cohesionless medium*", Int J Geomech ASCE 19(3):04019002-1–04019002-16. doi: 10.1061/(ASCE)GM.1943-5622.0001372. (2019a)

[49] Srivastav, A., and P. K. Basudhar, "*Modeling of soil–woven geotextile interface behavior from direct shear test results*", Geotext. Geomembr. 28 (4): 403–408 (2010)

[50] Tei K, "*A Study of soil nailing in sand*", PhD thesis, University of Oxford, London. (1993)

[51] Milligan GWE, Tei K, "*The pull-out resistance of model soil nails*", Soils Found 38 (2):179–190 (1998)

[52] Franzen G, "*A laboratory and field study of pullout capacity*, "Doctoral thesis, Chalmers Univ. of Technology, Göteborg, Sweden (1998)

[53] Junaideen SM, Tham LG, Law KT, "*Laboratory study of soil-nail interaction in loose, completely decomposed granite*", Can Geotech J 41(2):274–286 (2004)

[54] Hsu, S.T., and Liao, H.J., "*Uplift behaviour of cylindrical anchors in sand*", Canadian Geotechnical Journal, 35: 70–80. (1998)

[55] Yin JH, Su LJ, "*An innovative laboratory box for testing nail pull-out resistance in soil*", ASTM Geotech Test J 29:451 (2006)

[56] Yin JH, Zhou WH, "*Influence of Grouting Pressure and Overburden Stress on the Interface Resistance of a Soil Nail*", J. Geotech. Geoenviron. Eng. (2009).135:1198-1208 *DOI: 10.1061/(ASCE)GT.1943-5606.0000045*

[57] Gurpersaud N, Vanapalli SK, Sivathayalan S, "*Semi-empirical method for estimation of pull-out capacity of grouted soil nails in saturated and unsaturated soil environments*", J Geotech Geo-environ Eng (ASCE), 139(11): 1934–1943.(2013) *https://doi.org/10.1061/(ASCE)GT.1943-5606.0000883*

[58] Stephens TJ, Holtz RD, Aziz ES, "*Construction and Initial Performance of a Full-Scale Excavation Supported by SpiralnailGroutless Soil Nails*" Geo-Congress 2013**https://doi.org/10.1061/9780784412770.035**

[59] Xinyu Ye, Shanyong Wang, Qiong Wang, Scott William Sloan, Daichao Sheng, "*Numerical and experimental studies of the mechanical behaviour for compaction grouted soil nails in sandy soil*", Computers and Geotechnics 90 (2017) 202–214 **https://doi.org/10.1016/j.compgeo.2017.06.011**

[60] Kwong, A. K. L. and Lee, C. F., "*A Field Test Study on Instrumented Soil Nail Installed in Cut Slope*" (2008). International Conference on Case Histories in Geotechnical Engineering. 2. https://scholarsmine.mst.edu/icchge/6icchge/session02/2

[61] Zhang LL, Zhang ML,Tang WH, Hon M, "*Uncertainties of Field Pullout Resistance of Soil Nails*", J. Geotech. Geoenviron. Eng. 2009.135:966-972. *DOI: 10.1061/ (ASCE) GT.1943-5606.0000014*

[62] G.L. SivakumarBabu, "*Case Studies in Soil Nailing*", IGC 2009, Guntur, INDIA

[63] G. Babu&Vikas Singh, "*Soil nails field pullout testing: evaluation and applications*", International Journal of Geotechnical Engineering (2010) 4: (13-21) http://dx.doi.org/10.3328/IJGE.2010.04.01.13-21

[64] Zhu HH, Yin JH, Yeung AT, Jin W, "*Field Pullout Testing and Performance Evaluation of GFRP Soil Nails",* J. Geotech. Geoenviron. Eng 2011. 137(7), 633–642.

[65] Cheng YM, Au SK, Yeung AT, "*Laboratory and Field Evaluation of Several Types of Soil Nails for Different Geological Conditions*" Canadian Geotechnical Journal; 2016 53(4), https://doi.org/10.1139/cgj-2015-0267

[66] Yu JD, Kim NY, Lee JS, "*Nondestructive Integrity Evaluation of Soil Nails Using Longitudinal Waves*", J. Geotech. Geoenviron. Eng., 2018, 144(11): 04018080-1-14. **https://doi.org/10.1061/(ASCE)GT.1943-5606.0001976**

[67] Ye X, Wang S, Li Q, Zhang S, Sheng D, "*Negative Effect of Installation on Performance of a Compaction-Grouted Soil Nail in Poorly Graded Stockton Beach Sand*", J. Geotech. Geoenviron. Eng., 2020, 146(8): 04020061(1-10) **https://doi.org/10.1061/(ASCE)GT.1943-5606.0002301**

[68] Moayed RZ, Namaei A, "*Evaluation of the Pullout Resistance of Soil Nails in Tehran Alluvium by Considering the Overburden Pressure Effect*", GeotechGeolEng (2019) https://doi.org/10.1007/s10706-019-01063-0

[69] H. Bayesteh, M. Sabermahani, H. R. Elahi, "*Comparison of the Performance of Self-Drilled Hollow Bar and Strand Anchors in Soft Soil: A field Study*", GeotechGeol Eng. (2020) https://doi.org/10.1007/s10706-020-01403-5

[70] Pradhan B, Tham LG, YueZQ, Junaideen SM, and Lee CF, "*Soil–Nail Pullout Interaction in Loose Fill Materials*", International Journal of Geomechanics. vol.6, Issue 4, 238-247, DOI:10.1061/(ASCE)1532-3641(2006)6:4(238) (2006)

[71] ShafieeS, "*Numerical simulation of the behaviour of soil nailing. Interaction of soil nail and behaviour of the structure",* PhD Thesis, Paris (1986)

[72] Smith IM, Su N, "*Three-dimensional FE analysis of a nailed soil wall curved in plan*", Int J Numer Anal Methods Geomech (1997) 21(9):583–597

[73] Babu GLS, BRS M, Srinivas A, "*Analysis of construction factors influencing the behavior of soil nailed earth retaining walls*", Ground Improv 6(3):137–143 (2002)

[74] Babu GS, Singh VP, *"Simulation of soil nail structures using PLAXIS 2D*", PLAXIS Bull 25:16–21, (2009)

[75] Singh VP, Babu GS, *"2D numerical simulations of soil nails walls*",GeotechGeolEng 28:299–309, (2010)

[76] Zhou YD, Cheuk CY, Tham LG, "*Numerical modelling of soil nails in loose fill slope under surcharge loading"*, Computers and Geotechnics 36 (2009) 837–850. doi:10.1016/j.compgeo.2009.01.010

[77] Su LJ, Yin JH, Zhou WH, *"Influences of overburden pressure and soil dilation on soil nail pull-out resistance",* ComputGeotech 37(4):555–564 (2010)

[78] Sharma A,Ramkrishnan R, "*Parametric Optimization and Multi-regression Analysis for Soil Nailing Using Numerical Approaches*", GeotechGeolEng (2020). https://doi.org/10.1007/s10706-020-01230-8

[79] Mitsch, M.P., and Clemence, S.P., "*The uplift capacity of helix anchors in sand", In* Proceedings of the Uplift Behavior of Anchor Foundations in Soil, Detroit, Mich., (1985) *Edited by* S.P. Clemence. American Society of Civil Engineers. pp. 2647.

[80] Hoyt RM, Clemence SP, "*Uplift capacity of helical anchors in soil*", Proceedings 12th international conf. on soil Mech. And Fodn. Engg., Brasil,Vol.2, pp. 1019-1022,(1989)

[81] Ghaly A, Hanna A, Hanna M, "*Installation torque of screw anchors in sand"*, Soils and Foundations, 31(2): 77–92. (1991) doi:10.3208/sandf1972.31.2_77.

[82] Ghaly A, Hanna A, "*Experimental and theoretical studies on installation torque of screw anchors",* Can. Geotech. J. 28, 353-364 (1991)

[83] GhalyA andClemence SP, "*Pullout performance of inclined helical screw anchors in sand",* J. Geotech. Geoenviron. Eng. 1998.124:617-627.

[84] Tsuha CHC, Aoki N, Rault G, Thorel L, Garnier J, "*Physical modeling of helical pile anchors",* International Journal of Physical Modelling in Geotechnics, 7(4): 1–12. (2007) doi:10.1680/ ijpmg.2007.7.4.01.

[85] Tsuha, C. de H.C., and Aoki N, *"Relationship between installation torque and uplift capacity of deep helical piles in sand",* Canadian Geotechnical Journal, 47(6): 635–647, (2010)doi: 10.1139/T09- 128.

[86] Tsuha CHC, "*Theoretical model to control on site the uplift capacity of helical screw piles embedded in sandy soil",* Ph.D. thesis, Department of Geotechnics, São Carlos School of Engineering, University of São Paulo, São Carlos, Brazil. [In Portuguese.] (2007)

[87] Lutenegger AJ, Erickson J, Williams N, *"Evaluating installation disturbance of helical anchors in clay from field vane tests",* In: Proceedings of DFI annual meeting 2014

[88] Sakr M, "*Relationship between installationstorques and axial capacities of helical piles in cohesionless soils",* Canadian Geotechnical Journal. 52(6): 747-759, (2015) https://doi.org/10.1139/cgj-2013-0395

[89] Schiavon, J.A., Tsuha, C.D.H.C., and Thorel, L, *"Scale effect in centrifuge tests of helical anchors in sand*", International Journal of Physical Modelling in Geotechnics, 16(4): 185–196. (2016) doi:10.1680/jphmg.15.00047

[90] Kwona O, Leeb J, Kimb G, Kimb I, Lee J, "*Investigation of pullout load capacity for helical anchors subjected to inclined loading conditions using coupled Eulerian-Lagrangian analyses",* Computers and Geotechnics 111 (2019) 66–75. https://doi.org/10.1016/j.compgeo.2019.03.007

[91] Akhil Pandey and VinayBhushanChauhan, "*Evaluation of Pull-Out Capacity of Helical Anchors in Clay Using Finite Element Analysis*", Geo-Congress 2020 GSP 317. **https://doi.org/10.1061/9780784482803.007**

[92] Gudavalli SR, Safaqah O, Seo H, "*Effect of soil plugging on axial capacity of open-ended pipe piles in sands",* In: Proceedings of 18th international conference on soil mechanics

and geotechnical engineering, Paris, pp 1487–1490. http://www.cfms-sols.org/sites/default/files/Actes/1487-1490.pdf (2013)

[93] J. Ko and S. Jeong., *"Plugging effect of open-ended piles in sandy soil*", Can. Geotech. J. 52: 535–547 (2015) dx.doi.org/10.1139/cgj-2014-0041

[94] Han F, Ganju E, Salgado R, Prezzi M, "*Comparison of the load response of closed-ended and open-ended pipe piles driven in gravelly sand",* ActaGeotech. (2019a) https://doi.org/10.1007/s11440- 019-00863-1

[95] Han F, Ganju E, Salgado R, Zaheer M, *"Axial resistance of open-ended pipe pile driven in gravelly sand",* (2019b) Geotechnique. https://doi.org/10.1680/jgeot.18.P.117

[96] Sharma P, Rawat S, Gupta AK, *"Horizontal Pullout Behavior of Novel Open-Ended Pipe Helical Soil Nail in Frictional Soil",* International Journal of Civil Engineering. (2020a) https://doi.org/10.1007/s40999-020-00535-2

[97] Sharma P, Rawat S, Gupta AK, *"Laboratory investigation of pullout behavior of hollow and solid shaft helical nail in frictional soil",* Acta Geotechnica (2020b) https://doi.org/10.1007/s11440-020-01069-6

[98] Sharma P, Rawat S, Gupta AK, *"Study and Remedy of Kotropi Landslide in Himachal Pradesh, India",* Indian Geotechnical Journal. (2018) Vol. 48(4), 1-17. DOI: 10.1007/s40098-018-0343-1

[99] Sharma P, Rawat S, Gupta AK, *"Laboratory Investigation of Pullout Behavior of Open-ended Pipe Helical Soil Nail in Frictional Soil"*, Geotechnical and Geological Engineering, (2021a) DOI: 10.1007/s10706-020-01666-y

[100] Sharma P, Rawat S, Gupta AK, *"Force–Displacement Characteristics of Helical Soil Nail under Monotonic Pullout Loading: Experimental and Theoretical Study",* Indian Geotechnical Journal (2021b) DOI: 10.1007/s40098-021-00515-w

[101] Sharma P, Rawat S, Gupta AK, *"Experimental investigation of pullout behaviour of open-ended pipe helical soil nail in frictional soil"*, Geomechanics and Geoengineering(2021c) https://doi.org/10.1080/17486025.2021.1903088

[102] Sharma P, Rawat S, Gupta AK, *"Laboratory Investigation of Hollow and Solid Shaft Helical Soil Nail by Displacement Controlled Pullout Testing*", Geotech Geol Eng. (2021d) https://doi.org/10.1007/s10706-021-01832-w

[103] Rawat S, Gupta AK, *"Analysis of nailed soil slope using limit equilibrium and finite element methods",* Int J Geosynth Ground Eng(2016a) 2(4):34. https://doi.org/10.1007/s40891-016-0076-0

[104] Rawat S, Gupta AK, "*An experimental and analytical study of slope stability by soil nailing"*, Electron J GeotechEng 21(17):5577–5597. Int. J. of Geosynth. and Ground Eng. (2016b) 2:34 DOI 10.1007/s40891-016-0076-0

[105] Rawat S, Gupta AK, "*Testing and modeling of screw nailed soil slopes*", Indian Geotech J (2017a) 48(1):52–71. https://doi.org/10. 1007/s40098-017-0229-7

[106] Rawat S, Gupta AK, Kumar A, "*Pullout of soil nail with circular discs: a three-dimensional finite element analysis*",J Rock MechGeotechnEng 9:967–980. https://doi.org/10.1016/j.jrmge. 2017.05.003 (2017)

[107] Rawat S, Gupta AK, "*Numerical modellingof pullout of helical soil nail*", J Rock MechGeotechnEng(2017b) 9(4):648–658. https://doi.org/10.1016/j.jrmge.2017.01.007

[108] BIS (Bureau of Indian Standards), "*Methods of test for soils: Grain size analysis*", IS 2720-4. New Delhi, India: BIS (1985)

[109] BIS (Bureau of Indian Standards), "*Methods of test for soils: Determination of water content–dry density relation using light compaction*", IS 2720-7. New Delhi, India: BIS (1983)

[110] BIS (Bureau of Indian Standards), *"Determination of dry density of soil in-place by the core-cutter method"*, IS 2720-1975/88 (Part XXIX)

[111] BIS (Bureau of Indian Standards), *"Methods of test for soils: Direct shear test*", IS 2720-13. New Delhi, India: BIS. (1986a)

[112] Deardorff, D., Moeller, M., and Walt, E, "*Results of an instrumented helical soil nail wall"*, In Proceedings of the Earth Retention Conference, ASCE. (2010) pp. 262–269. doi:10.1061/41128(384)24.

[113] Rotte VM, Viswanadham BVS, *"Influence of nail inclination and facing material type on soil-nailed slopes",* Proc ICE Ground Improve(2013) 166(2):86–107. https://doi.org/10.1680/grim.11. 00026

[114] Hubbell Power Systems Inc, "*Screw nailing retention earth structures*" design manual, Chance USA. (2015)

[115] Hubbell Power Systems, *"Inc.,HUBBELL Technical Design Manual"* Edition 4. Chance Atlas. (2018)

[116] BIS (Bureau of Indian Standards), "*General Construction In Steel – Code of Practice (Third Revision)",* IS 800:2007.New Delhi, India: BIS.(2007).

[117] Mittal S and Mukherjee S, "*Behaviour of group of helical screw anchors under compressive loads*", *Geotechnical and Geological Engineering, 33*(3), pp.575-592. (2015)

[118] Vaid, Y.P. and Negussey, D, "*Relative density of pluviated sand samples*", Soils Found Japanese Soc. Soil Mech. Found. Engrg., 24:101–105 (1984)

[119] El Sawwaf, M, and Nazir, A, "*The effect of soil reinforcement on pullout resistance of an existing vertical anchor plate in sand*", Computers and Geotechnics, 33(3): 167–176. (2006) doi:10.1016/j.compgeo.2006.04.001.

[120] Ibrahim S.F., Hasan H.F. Fadnil AI, "*Evaluation of Bearing Capacity for Model Piles Driven in Sandy Soil*", Journal of engineering and development vol. 18 No.3, (2014) ISSN- 1813-7822

[121] Hong CY, Yin JH, Zhou WH, Pei HF, "*Analytical study on progressive pullout behavior of a soil nail"* J GeotechGeoenvironEng 138(4):500–507. (2012) https://doi.org/10.1061/(ASCE)GT.1943- 5606.0000610

[122] Gurung, N, and Iwao Y, "*Analytical pull-out model for extensible soil-reinforcements*", Proc. JSCE, 624, 11–20 (1999).

[123] Misra, A., and Chen, C. H., "*Analytical solution for micropile design under tension and compression"*, Geotech. Geol. Eng., 22(2), 199–255(2004).

[124] Chattopadhyay BC, And Pise PJ, "*Uplift Capacity of Piles in Sand*", J. Geotech. Engrg.112:888-904 (1985).

[125] Shanker K, Basudhar PK, Patra NR, "*Uplift Capacity of Pile Groups Embedded in Sand*", IGC(2009)

[126] Bowen G, "*A static based theory for the capacity to torque factor for helical piers in compression*", In: Proceedings of helical foundations and tie-backs seminar, deep foundation institute, University of Alberta, Canada, June (2009)

[127] Liu J, Liu M, Zhu Z, "*Sand deformation around an uplift plate anchor*", J Geotechn Geo-Environ Eng 138(6):728–737. (2012)

[128] Hao D, Wang D, Loughlin C, Gaudin C, "*Tensile monotonic capacity of helical anchors in sand: interaction between helices",* Can Geotech J. (2018) https://doi.org/10.1139/cgj-2018-0202

[129] Omega.co.uk (Strain gages manual), *"Positioning strain gages to monitor bending, axial, shear, and torsional loads: a guide to installation (E56)",* http://www.personal.umich.edu/*bkerkez/ courses/cee575/Handouts/2strainpositioning.pdf. Accessed 2019

[130] Kishida H, Isemoto N, "*Behaviour of sand plugs in openend steel pipe piles*", In: Proceedings of the 9th international conference on soil mechanics and foundation engineering, (1977) Tokyo, pp 605–608

[131] Yin, J.-H., C.-Y. Hong, and W.-H. Zhou, "*Simplified analytical method for calculating the maximum shear stress of nail-soil interface*", Int. J. Geomech. 12 (3): 309–317. https://doi.org/10.1061/(ASCE)GM .1943-5622.0000151. (2012)

[132] Zhang, C.-C., Q. Xu, H.-H. Zhu, B. Shi, and J.-H. Yin, "*Evaluations of load-deformation behavior of soil nail using hyperbolic pullout model.*" Geomech. Eng. 6 (3): 277–292. (2014) https://doi.org/10.12989/gae .2014.6.3.277

[133] Wan-Huan Zhou, Jian-Hua Yin, Cheng-Yu Hong, "*Finite element modelling of pullout testing on a soil nail in a pullout box under different overburden and grouting pressures*" , Canadian Geotechnical Journal, 2011

[134] Kanwar Y, "*46 Killed as massive landslip buries vehicles in Himachal Pradesh*", https://www.thehindu.com/news/national/other-states/many-killed-as-cloudburst-triggers-landslip-in-himachal-pradesh/article19485223.ece accessed on August 14 2017

[135] Kumar J, "46 dead as landslide buries two buses in Mandi, rescue ops to resume tomorrow", https://www.tribuneindia.com/news/himachal/46-dead-as-landslide-buries-two-buses-in-mandi-rescue-ops-to-resume-tomorrow/451552.htmlaccessed on August 14,2017

[136] Version-2, *"Kotropi landslide, Mandi district, Himachal Pradesh (a preliminary report)",* National remote sensing Centre/ISRO, Hyderabad, https://nrsc.gov.in/sites/all/pdf/KotropiLandslid13aug2017_Final_Ver2_15aug2017.pdfaccessed on 15 Aug. 2017

[137] Sassa K, "*The mechanism of debris flows. In: Proceedings, 11th International Conference on Soil Mechanics and Foundation Engineering*", San Francisco, 1, pp. 73–1176. (1985)

[138] Shanmugam G, "*The landslide problem*", Journal of Palaegeoography, 4 (2): 109-166. (2015)

[139] Hungr O, Leroueil S, Picarelli L, "*The Varnes classification of landslide types, an update*", Landslides, 11:167–194. (2013)

[140] Sarkar R, Kurar R, ZangmoS, Dema UG, Subba SJ, Sharma DK, "*Application of soil nailing for landslide mitigation in Bhutan: A Case study at Sorchen Bypass*", Electronic J. GeotechEng, 22 (13): 4963-4980. (2017)

[141] IS: code 1892-1979, "*Indian standard code of practice for subsurface investigation for foundation*",Bureau of Indian Standard (BIS) New Delhi.

[142] IS: 2720 – 5, "*Atterberg limit test*",Bureau of Indian Standard (BIS) New Delhi, (1985)

[143] AASHTO291, "Standard method of test for determining water – soluble chloride ion content in soil"

[144] AASHTO T 290, "Water Soluble Sulfate Content in Soil"

[145] IS: code 14680: "*Landslide Control Guidelines*", Bureau of Indian Standard (BIS) New Delhi. (1999)

[146] Snitbhan N, Chen WF, "*Elastic–plastic large deformation analysis of soil slopes*", Comput Struct 9(6):567–577 (1978) https://doi.org/10.1016/0045-7949(78)90006-8

[147] Singh VP, Babu GS, "*2D numerical simulations of soil nails walls*", Geotech Geol Eng 28:299–309 9. (2010)

[148] Babu GS, Singh VP, "*Simulation of soil nail structures using PLAXIS 2D*", PLAXIS Bull 25:16–21(2009)

[149] Brinkgreve RBJ, Engin E, and Swolfs WM, "*Plaxis 2D 2012 Manual Plaxis*", The Netherlands.

[150] PH and HP State Unit, Chandigarh, "*Report on preliminary assessment of the landslide, team of GSI office",* https://employee. gsi.gov.in/cs/groups/public/documents/document/b3zp/mtyx/*edi sp/dcport1gsigovi161798.pdf. Accessed 1 Nov 2017

[151] M.kulczykawski P, Jaraslaw K, Boguslaw, "*Application of soil nailing technique for protection and preservation Historical building"*, IOP conf. series: Materials Science& Engineering, 245. (2017), DOI 10.108811757-899X/245/2/022055.